Performance Analysis of Spatially Distributed MIMO Mode Division Multiplexed Fibers For Sensing Application

A Thesis

Submitted in fulfillment of the requirement for the award of degree

of

DOCTOR OF PHILOSOPHY

Submitted by

Rajan Gupta

Registration No. 901406008

Supervisor

Dr. R.S. Kaler

Senior Professor

THAPAR INSTITUTE
OF ENGINEERING & TECHNOLOGY
(Deemed to be University)

Department of Electronics & Communication Engineering,

Thapar Institute of Engineering and Technology

(Deemed to be University),

Patiala-147004, Punjab, India

Certificate

I, Rajan Gupta hereby certify that the work which is being presented in this thesis entitled "Performance analysis of Spatially Distributed MIMO Mode Division Multiplexed Fibers for sensing applications" in partial fulfillment of requirements for the award of degree of the Doctor of Philosophy in Electronics and Communication Engineering from Thapar University, Patiala, is an authentic record of my own work carried under the supervision of **Dr. R.S. Kaler.**

The matter presented in this thesis has not been submitted in any other University/Institute for the award of any degree or diploma.

Date: 29 July, 2019

(Rajan Gupta)

Signature of candidate

This is certified that the above statement made by the candidate is correct to the best of my knowledge.

Date: 29 July, 2019

Dr. R. S. Kaler

Senior Professor

Department of ECE

Thapar Institute of Engineering and Technology

ABSTRACT

The internet traffic is continuously growing at a faster rate to fulfill the demand of diverse services such as high-definition video streaming, multimedia, smart phone users, online shopping, cloud computing, online gaming etc. The optical fiber is the heart of networking architectures supporting extremely high data rate and capacity. In order to cope up with an exponential growth in internet traffic and to fulfil the demand of users worldwide, there emerges a vital requirement for high-capacity optical networks. Great challenges exist in both long-haul and short-reach optical networks when upgrading the capacities. Earlier, the electrical multiplexing techniques were utilized to increase the capacity but support lower rate in Gbps. With the advent of WDM technology and support of optical amplification, capacity started increasing from 100 Gb/channel to 400 Gb/channel but with the progress in DWDM this capacity rate further reaches to 8Tb/fiber and then digital coherent techniques also came into picture offering capacity of 24Tb/fiber. A significant capacity increase has been witnessed during the last decade with the revival of the coherent optical techniques, which makes full utilization of the available degrees of modulation in single-mode fiber (SMF).

With the development of hybrid WDM technologies (combination of WDM/OTDM/OCDM), the capacity of the long-haul optical networks rapidly approaches the Shannon limit, which imposes an upper limit for the channel capacity in SMF. To support a sustainable capacity increase, the long-haul optical networks are faced with the challenge to achieve a capacity beyond the Shannon limit. From here arises the need for such a system that can overcome Shannon limit and further fulfil the increasing demand of capacity. Thus, SDM (Spatial Division Multiplexing) transmission is thought to be best alternate for growing capacity of optical fiber communication technologies. SDM including MDM (mode-division multiplexing) utilizing MMFs or FMFs (few-mode fibers) and multiplexing of core employing multi core fibers (MCFs), has caught up interest from last few years to boost internet data capacity of optical fiber communication. Data transmission throughout fiber modes or cores simultaneously is an adequate and efficient system of communication but its development poses challenges.

Optical Mode division multiplexing (OMDM) is a promising technology that supports forthcoming capacity demand of internet worldwide. The multiplexing of spatial

domain with fibers capable of supporting multiple modes is an efficient way as transmission capacity scales with number of modes. MIMO concept is based on installation of multiple antennas at transmitter and receiver end. Different MIMO algorithms have been developed as it provides increase coverage, higher data rate and achieves better BER as compared to SISO. Spatial Multiplexing employ MIMO system that offers higher data rate as multiple data symbols are transmitted simultaneously using multiple antennas. This thesis deals with the performance investigation and design of Optical MIMO Mode division multiplexed transmission system for high capacity long haul multichannel transmission to efficiently utilize the fiber bandwidth.

Less development in this area poses different challenges as there is simultaneous transmission of signals through multiple modes of fiber. Emerging MDM systems need improvement in mode MUX and DEMUX supporting multiple modes, fibers that support multiple spatial modes, optical amplifiers with less number of components capable of operating on several modes. In Graded-index MMF the index gradient causes rays propagating at steeper angles to catch up with rays propagating at shallow angles in the fiber. Due to this feature of graded-index fiber, it provides less pulse dispersion than step-index fiber and therefore, superior bandwidth performance.

The optical fiber technology is dominating the field of communication as well as progressing in the field of sensing. Optical fiber sensors offer the option of measurement in harsh surroundings where conventional electrical and electronic sensors perform with difficulty. The advantages of fiber optical sensor include light weight, small size, resistant to electromagnetic interference, more sensitive, low power and adequately long lifetime. Every country depends on network of pipelines (like transportation of oil, natural gas, gasoline, liquid petroleum; chemical storage tankers, Oxygen and LPG cylinders, reservoirs, hot boiling furnaces, water pipelines in buildings, sewer lines, telephone lines, electric lines etc.) to safely transport energy resources to fuel their countries economic engine. Leakage is the major risk that might take place in pipelines due to failures like cracks, bursting, corrosion, drilling, manufacturing flaws, earthquakes and heavy loads put additional stress).

Different technologies including microwave wireless sensors, visual inspections, ultrasonic, acoustic emission, radiography, multimode sensing, eddy current and magnetic flux have been developed over the past few decades but these lack portability, constant monitoring and susceptibility to electromagnetic interference. Thus, there

exists the need to develop methods with an efficient and reliable non-destructive in-situ periodic monitoring technique for pipeline structures. Optical Bragg grating multimode fiber based sensor is proposed for leakage detection in underground energy storage pipelines. This thesis also addresses the issues discussed above by experimentally monitoring the variation in pipeline parameters (like strain and thickness reduction due to corrosion) utilizing surface mounted Fibre Bragg Grating Optic Sensors.

Initially, the nonlinear propagation in mode division multiplexed multimode fiber link is investigated. The impact of Nonlinear Kerr effect, inter-modal (IMFWM) and intramodal FWM for waves with different spatial modes (LP_{01}, LP_{02} and LP_{11} and LP_{12}) over MMF has been analyzed with the help of optical spectrum analyzer using VPI Photonics/ VPI transmission Maker™ Version 9.7 simulator.It has been concluded that nonlinear interaction between modes resulted into interference that degraded the performance of multichannel mode division multiplexed system. To achieve full phase matching and reduce the effect of IMFWM, chromatic dispersion has been increased in each spatial mode throughout the link.

The mode division multiplexed transmission system is proposed for transmission of 9 independent signals superimposed over 9 different LP_{lm} modes through MMF (multimode fiber) link at 1550 nm wavelength with low input power. In order to check the performance of system different MIMO configurations (4×4, 6×6 and 9×9) have been investigated for different LP_{lm} (linearly polarized) modes such as LP_{01}, LP_{02}, LP_{11}, LP_{12}, LP_{03}, LP_{04}, LP_{13}, LP_{21} and LP_{22}. The bit error rate and quality factor is measured for different MIMO configurations over different modes with different transmission distances. It is found that maximum transmission distance covered by modes (LP_{01}, LP_{02}, LP_{11} and LP_{12}) is 90 km and provided acceptable bit error rate of 2.6×10^{-9} and Quality factor (>8 dB) for 4×4, 6×6 and 9×9 MIMO MDM system.Further, this thesis deals with different LP mode grouping combinations for four cases (Even, Odd, Random Even+Odd and Symmetric Even+Odd with mode gap) to investigate the performance of 3×3, 4×4, 5×5, 6×6, 7×7, 8×8 and 9×9 OMIMO MDM configurations to enhance the transmission quality of the system.The optimization of system is done by utilizing LMS adaptive MIMO signal processing algorithm to minimize the mean-squared error at the output signal in order to avoid mode group coupling in MDM based system.The main challenge lies in designing the mode division multiplexed transmission system as it needs improvement in multiple modes supporting

fibers, optical amplifiers with less number of components that can function with various modes, mode multiplexer capable of generating different linearly polarized modes as well as capable of multiplexing *N* independent mode signals into one unit and a demultiplexer compatible with MDM. Then, the MM-EDFA (Multimode Erbium doped fiber amplifier) is designed in three configurations (pre-, boost- and inline-) to investigate the performance of Multi input multi output MDM system. It is concluded that inline-MM EDFA configuration outcomes better results in terms of bit error rate $\leq 10^{-9}$, quality factor more than 10.2 dB covering a maximum of 100 km transmission distance for considered MIMO configurations. Further, this thesis deals with multi-modal domain to design hybrid 10 Tb/s LP-WDM-MDM (Linearly Polarized Mode Division Multiplexed-Wavelength Division Multiplexed) system for transmission of 25 independent channels over 25 LP modes through multimode fiber link and thus, contributes in providing high capacity with minimum use of bandwidth for upcoming optical communication at reduced channel spacing. The effect of parameters like channel index spacing of LP modes, different input power and different data rates for different number of users is observed in terms of BER and quality-factor at different lengths of multimode fiber.

The optical Bragg grating multimode fiber based sensor is proposed for leakage detection in underground energy storage pipelines. The concept of mode coupling between core and cladding modes and the effect of fluctuations in temperature and strain on fiber Bragg grating is theoretically analyzed. The simulation results reported that the proposed sensor achieved a wavelength shift of (0.07 μm towards higher wavelength and 0.003 μm towards lower wavelength) for strain and temperature sensor with applied strain of 2000 με and at temperature of 50^{o}C respectively. By varying claddings thermo-optic coefficient (ζ_{clad}) from 7.8 x10^{-6} to 9.12x10^{-6} temperature sensitivity of sensor is enhanced to14 nm/^{o}C. The detection of leakage in different pipeline structures is done by performing experiments to evaluate the performance of Optical Bragg grating strain sensor. It is reported that the optical Bragg grating strain sensor achieved a wavelength shift of 3.2 nm with applied load of 65 kN resulting into strain of 2495με. The strain is applied on both closed energy storage pipeline structures and open pipeline structures and it is examined that the experimental outcomes hold good for different network of pipelines. Further, two Optical FBG strain sensors (S1 and

S2) are connected using one optical fiber and it is found that both sensors (S1 and S2) provides better sensitivity in terms of wavelength shift (2.4 nm and 1.89 nm).

Featuring distinctive simplicity with reduced interference, the proposed MIMO MDM design is ideal to cope up with the reliable and error free transmission with minimum use of bandwidth for upcoming optical communication. This analysis can further be used for mode group division multiplexingto increase the capacity of high speed transmission over multimode fiber link.Thus, research work presented in this thesis relate the concept of mode coupling in MMF to mode division multiplexing technique for enhancing capacity of an optical communication network as well as mode coupling in gratings inscribed inside MMF to optical in-grating fiber sensor for monitoring underground energy storage pipelines.The investigative study of optical Bragg grating inscribed in MMF can be used for developing low cost sensing systems and provides great scope in chemical industries, power plants, commercial transportation, energy storage reservoirs where leakage is the major issue. Most of the research outcomes of the thesis have been published in different SCI journals as listed in beginning.

List of Publications

The thesis includes following research papers:

SCI Publications:

[1] R. Gupta, R.S. Kaler, "Performance comparison of pre-, boost-, and inline-multimode erbium-doped fiber amplifier configurations to boost mode-division multiplexed multimode fiber link", SPIE:Optical Engineering, vol. 55, no. 5, pp. 056102-1 to 056102-6, 2016. (I.F: 1.082)

[2] R. Gupta, R.S. Kaler, "Performance Investigation of LP modes over MMF link to boost MIMO Mode Division Multiplexing", Optoelectronics and advanced materials-Rapid Communications, vol. 11, no. 11-12, pp. 643-647, 2017. (I.F: 0.412)

[3] R. Gupta, R.S. Kaler, "Performance Investigation of high capacity 10 Tb/s LP-MDM-WDM over multimode fiber link for short reach applications", Optoelectronics and advanced materials- Rapid Communications, vol. 12, no. 7-8, pp. 441 - 446, 2018. (I.F: 0.412)

[4] R. Gupta and R. S. Kaler, "Nonlinear Kerr and Inter-modal four wave mixing effect in mode division multiplexed multimode fiber link", SPIE:Optical Engineering, vol. 58, no. 3, pp. 036108-1 to 036108-8, 2019. (I.F: 1.082)

International Conference Publications:

[1] R. Gupta and R. S. Kaler, Investigation of hybrid Linearly Polarized Mode Division Multiplexed-WDM system over MMF to enhance system capacity, Proceedings of IASTEM-292nd International Conference on Recent Advances in Engineering and Technology (ICRAET), pp. 55-60, 10th -11th Dec 2017, Bangkok, Thailand. (DOIONLINE- IASTEM.06112017.6089). (Also published in International Journal of Electrical, Electronics and Data Communication (IJEEDC), vol. 6, no.2, pp. 57-62, 2018).

[2] R. Gupta and R. S. Kaler, "Development of fiber optic sensors for leak detection in underground energy storage pipelines", IEEE International Conference WECON 2018, Chitkara University, 16th -17th Nov, 2018. (Presented and in press).

Communicated:

[1] R. Gupta and R. S. Kaler, "Investigation of linearly polarized mode index grouping combinations over MMF to boost OMIMO-mode division multiplexing", Optoelectronics and advanced materials- Rapid Communications, 2019.

[2] R. Gupta and R. S. Kaler, "Investigation of Bragg grating inscribed inside MMF based sensor for temperature and strain monitoring of energy storage pipelines", Optik, 2019.

ACKNOWLEDGEMENT

I would like to offer my heartiest salutation to the Almighty for unbroken health and courage bestowed upon me in all the adversities at every step and at every moment throughout the entire span of my studies and in every aspect of my life. My deep sense of appreciation due to my second God, my parents, ***Mrs.NirmalaGarg***and ***Mr.Jeevan Kumar Garg***, for their continuous affection and encouragement.

The completion of any academic work is inconceivable without the expert guidance of a mentor. I acknowledge and extend my deepest gratitude to my respected guide ***Dr. R.S. Kaler***, Senior Professor, Department of Electronics and Communication Engineering, Thapar University, Patiala, whose indispensable tutelage and wise counsel at every step of my work enabled me to complete the work without obstruction. Despite his various academic and official assignments, he spread his precious time and took great pains in discussing even in minute details of this work.

I would like to thank the education hub Thapar University, Patiala who gives me a lot in my life. Out of deep sense of gratefulness, I express my sincere thanks to ***Dr.RafatSiddique***, Dean (RSP), ***Dr.AlpanaAgarwal***, Head ECE and members of **doctorate committee** for continuous appreciation and support.

I am thankful to the various International Journals (published by SPIE, OSA, OAMRC etc.) who examined my research papers. Their suggestions and comments have really helped me in bringing this thesis to the present shape.

Once again, I acknowledge my deepest debt of gratitude to ***Dr. R.S. Kaler***, who was kind enough even to go through the final manuscript and without whose valuable guidance, active encouragement and constant supervision; this study could not have been completed and presented in present form.

Finally, words are not adequate to express my special gratitude to my brother ***'Hitesh Goel',*** my husband ***'RiteshGoel',*** and my familyfor their patience, support and active assistance in many ways.

Rajan Gupta

LIST OF CONTENTS

Dedicated to

my

Father

List of Figures

List of Tables

List of Acronyms

FOC	:	Fiber Optic Communication
SMF	:	Single Mode Fiber
TMF	:	Two Mode Fiber
FMF	:	Few Mode Fiber
MMF	:	Multi-Mode Fiber
MCF	:	Multi Core Fiber
PCF	:	Photonic Crystal Fiber
CMF	:	Coupled Mode Fiber
UMF	:	Uncoupled Mode Fiber
CMT	:	Coupled Mode Theory
WDM	:	Wavelegth Division Multiplexing
OTDM	:	Optical Time Division Multiplexing
OCDM	:	Optical Code Division Multiplexing
SDM	:	Spatial Division Multiplexing
OMDM	:	Optical Mode Division Multiplexing
MIMO	:	Multi Input Multi Output
MM	:	Multi-mode
FM	:	Few-mode
LP	:	Linearly Polarized
MM-Tx	:	Multi-mode Transmitter
MM-Rx	:	Multi-mode Receiver
IM-FWM	:	Inter-modal Four Wave Mixing
NLSE	:	Nonlinear Schrodinger Equation
FSO	:	Free Space Optics
DSP	:	Digital Signal Processing
LMS	:	Least Mean Square
OAM	:	Orbital Angular Momentum
FPI	:	Fabry Perot Etalon
OTDR	:	Optical Time Domain Reflectometry
ROTDR	:	Raman Optical Time Domain Reflectometry
BOTDR	:	Brillouin Optical Time Domain Reflectometry
FBG	:	Fiber Bragg Grating

NDE	:	Non-Destructive Evaluation
LPG	:	Long Period Grating
O_2	:	Oxygen
SiO_2	:	Silicon Dioxide

CHAPTER 1
INTRODUCTION

1.1 Introduction and motivation

Optical fiber technology has been the matter of extensive research and development to the concept that light wave communication systems today emerges as the most preferred method to transmit versatile data and information. Fiber optic field has undergone remarkable expansion and advancement over last 25 years. Optical fiber communication is the spinal cord of the telecommunication network which supports internet.The optical communication system comprises of a transmitter that encodes data, superimpose data onto light, optical fibre as a transmission medium that carries the optical information signal to destination and a receiver that recovers the information from the received optical signal.

Optical fiber serves as central part of networking architectures supporting extremely high data rate.Optical fiber is the transmission channel that offers large bandwidth [1], offers low loss links compared to electrical cables or radio, comparatively light in weight and cheap as compared to copper cables needed to carry the same amount of information. Over the past decades, the telecommunication services have installed optical fiber links on the land, underseas, cable T.V systems, in terrestrial and oceans for trunk traffic [1]. Optical fiber links are suitable for fixed user locations and having capability to support potential applications due to inherently large capacity. These links are more reliable and require specialized tools for installation and maintenance. Further, the technology used in optical devices comprising of components (optical sources and detectors) is still developing to fulfill the system requirements. Thus, due to above features fibers acts as an essential part of networking architectures supporting extremely high data rate.

Optical networks traffic has been progressively increasing every decade with a factor value of 100 and capacity of SMF rising 10,000 times from previous three decades[2]. The quick increase in data traffic with smart phones and multimedia are raising the requirement for higher capacity. The capacity offered by fiber optic communication technology always exceeds the increasing demand by orders of magnitude as shown in Fig. 1.1.However, the margin between capacity and increasing demand starts to shrink in recent years. The capacity of a communication channel is bounded by Shannon's limit expressed as C = B log(1+SNR)where B indicates the channel bandwidth and SNR

denotes parameter signal-to-noise ratio. Thus, to fulfil such a rapid expansion of internet capacity several techniques are being explored regularly to further enhance the performance of OFC transmission systems [3-11].

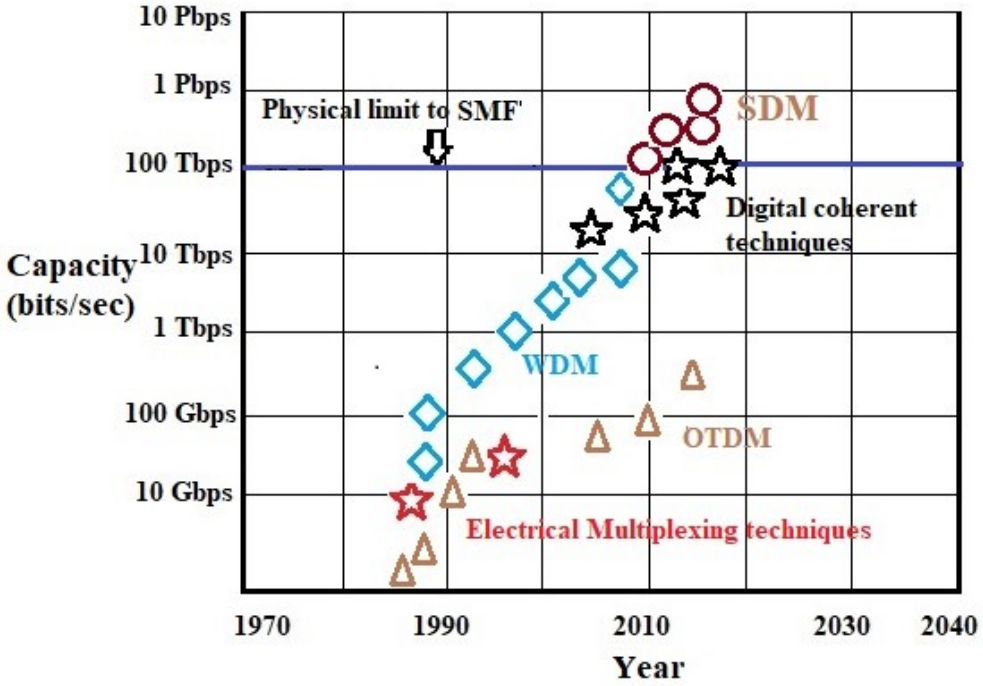

Fig. 1.1 Progress in optical communication systems to fulfil increasing capacity demand.

Over the past two decades, WDM has been extensively used in fiber optic communication system to extend the transmission bandwidth with a factor value as much as 100 or more. In the late 1990s, Erbium doped fiber amplifier and WDM technology having channel spacing at 100 GHz offered the transmission of nearly 40 channels (each at 2.5 Gbps) providing an capacity of 100 Gbps [12-13]. By utilizing the low loss transmission window beyond bands (C band and L band), the channel bandwidth could be further increased [14] but the expansion of bandwidth is limited to less than one order of magnitude and also, lack of an integrated amplification in system results in technical and economic issues. With the introduction of Forward Error Correction in FOC allowed transmission with the increase of 10 Gbps in bit rate per channel and further with DWDM with reduced channel spacing to 50GHz, overall capacity of approximately 1 Tbps is obtained [15]. The advancement in coherent detection results in remarkable capacity growth making use of high spectral efficiency modulation format [16]. Further, digital coherent optical fiber communication makes use

of polarization division multiplexing (PDM) that doubles the channel capacity [17]. As silica is having nonlinear refractive index so, it is not possible to continuously increase spectral efficiency by simply increasing the launched power. The logarithmical capacity scaling eventually cannot fulfil the demand of internet traffic growth from the technical point and from the point of view of power consumption per bit. Thus, to accomplish a cost-effective scaling in capacity of system, new paradigms in FOC are required. Earlier, this rapid growth has been supported by several novel multiplexing methods using amplitude, wavelength, phase and polarization of light as a means to encrypt data. The basic motivations behind each technique were to enhance the transmission fidelity, to boost the data rate and to improve the transmission distance. Space is a new paradigm that is employed for optical communication ahead of WDM [18-19].

SDM (Spatial Division Multiplexing) is thought to be best alternate for growing capacity of optical fiber communication technologies [20]. A massive source of enhancement has not been touched in systems: fibers are capable to support hundreds of spatial modes whereas present business systems (SM/MM) are not attempting to employ these fibers as parallel channels for individual data signals [21]. The transmissionof information propagating through modes or cores of fiber simultaneously is an efficient and reliable system of optical communication but its development pose challenges [22]. SDM including MDM (mode-division multiplexing) utilizing MMFs or FMFs (few-mode fibers) and multiplexing of core employing multicore fibers (MCFs), has caught up interest from last few years to boost internet data capacity of optical fiber communication [23-24].

1.2 Optical Multiplexing techniques

In optical fiber communication multiplexing is considered to be the significant means for the expansion of existing fiber networks. By utilizing different physical dimensions (time, phase, wavelength, frequency, space, polarization etc.) of light, data carrying capacity of an optical fiber can be increased. Several multiplexing techniques have been proposed over a few decades, some are already used to bring more improvements in progress of optical communication and research is exploring many more targeting high speed, high capacity long haul communication. Multiplexing techniques like Wavelength Division Multiplexing (WDM), Coarse Wavelength Division Multiplexing (CWDM), Dense Wavelength Division Multiplexing (DWDM), Optical Time Division Multiplexing (OTDM), Optical Code Division Multiplexing (OCDM) are already in use

but potential multiplexing techniques like Spatial Division Multiplexing (SDM), Mode Division Multiplexing (MDM) has remained untapped for many years inspite of manufacturing of fibers supporting multiple modes in single core and fibers having multiple cores.

1.2.1 Classification of multiplexing techniques

The concept of WDM system was proposed in 1970 and initiated in the late 1980s utilizing two broadly spaced channels belonging to two different bands (1310 nm and 1550 nm) [25-26]. In early 1990s, narrow-band WDM system with more than six optical channels was proposed in which channels were placed over the wavelength grid with channel spacing of 400 GHz. Afterwards in 1990s, DWDM transmission systems were developed having 20 to 50 channels with channel spacing of 100 GHz to 200 GHz. It had been observed that DWDM system provided transmission capability of 60 to 160 channels densely packed at 50 GHz [27-28].Then, with more innovations and improvements research started progressing in DWDM systems. With the advent of hybrid optical amplifiers DWDM supported more than one hundred signals providing data rate over ~ 1Tbps [13].

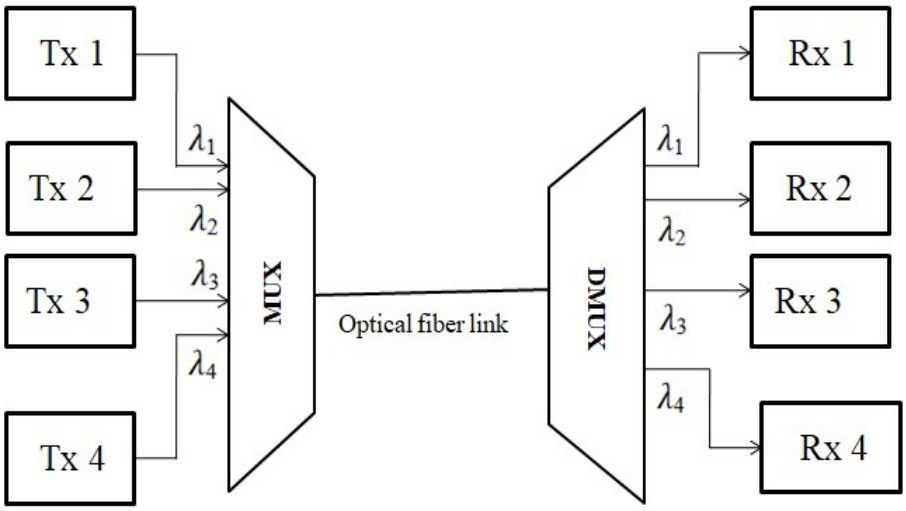

Fig.1.2 Architecture of Wavelength Division Multiplexing system.

WDM is a multiplexing technique that increases bandwidth by sending different optical carrier signals using different wavelengths onto a single optical fiber. It puts multiple signals together and sends them at same time along a fiber where transmission taking place at different wavelengths. Thus, increases the bandwidth and lowers the cost of network by reducing the number of fibers. It is often considered as analogous to

frequency division multiplexing, which typically uses radio carrier. CWDM and DWDM are wavelength patterns of WDM based on the same principle concept but differ in number of wavelengths, wavelength spacing, number of channels, and amplification of the multiplexed signals.

Fig. 1.2represents the conceptual diagram of WDM system in which different optical signals are multiplexed together at one terminal, transmitted over an optical fiber and demultiplexed into different channels at another terminal. It can be used for short or long distance transmission applications supporting data rate upto 100 Gbps. DWDM systems require regenerators which are complex, time consuming and costly because of different processing levels at multiplexing, de-multiplexing stage and during optical-electrical-optical (O-E-O) conversions. DWDM systems suffer from losses due to induced nonlinearities, crosstalk, costly amplification and noise induced (double Rayleigh backscattering, pump's relative intensity noise transfer) due to particular amplifiers, requirement of multi-pumps for gain flattening [13], [27].

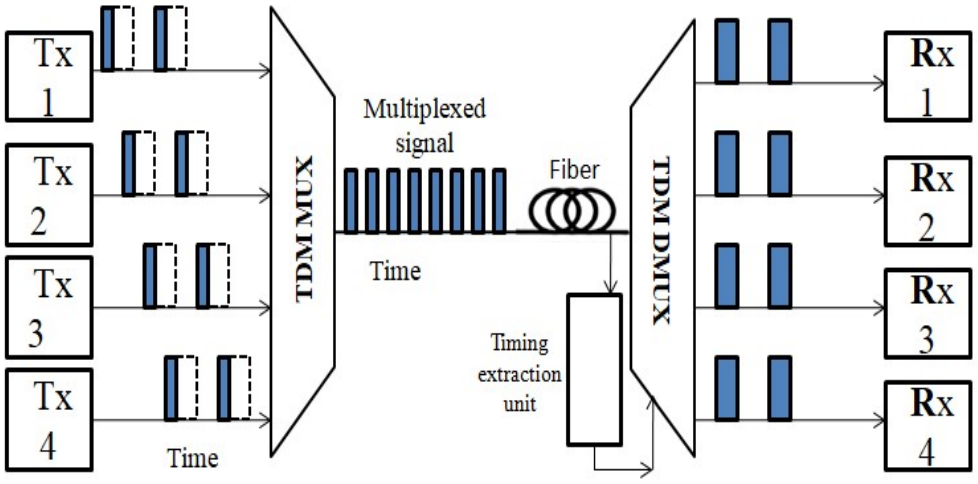

Fig. 1.3 Conceptual diagram of Optical Time Division Multiplexing system.

OTDM is a multiplexing technique that multiplexes multiple low bit rate data stream channels in time domain. This technique divides a transmission period into different time slots and data is loaded on each slot from different channels. To achieve a higher data rate, information from N channels is superimposed over N time slots and thus the multiplexed channel reaches a line rate of N times higher than single laser diodes narrow pulse width [29]. Its receiver consists of a timing extraction unit and the optoelectronic receiver, where the optical pulses for different channels are separated for subsequent detection shown by Fig. 1.3. In this technique, multiplexer and demultiplexer unit should

betimely synchronized and simultaneously provides switching to the next channel. Generally, the pulse width of optical signal is shortened so as to multiplex more number of channels within the fixed clock period but short pulse width outcomes large dispersion with increase in transmission distance.

OTDM can solve most problems faced by WDM systems like crosstalk caused by non-ideal filters, wavelength conversions, fibre nonlinearity, expensive filters and non-flatness of output spectrum due to cascading of optical amplifiers. OTDM system faces many challenges such as at the transmitting end, the width of pulse to be considerably shorter than the bit period of multiplexed information signal as well as the timing jitter to be much less than the width of pulse[29]. The signal in this system suffers from chromatic dispersion and polarization-mode dispersion (PMD) during transmission over optical fiber link. At the receiver end, high quality signal and demodulation techniques with low cost are required to recover the optical signals.

Earlier, modulation constellations of higher order used to obtain high data rates or higher symbol rates which leads to large signal bandwidth. The available channel bandwidth is limited because of increased loss and costly RF optical components such as: lasers, circuits, amplifiers etc. Further, transmitting large number of bits per second will significantly shrink E_b /N_o (ratio of Energy per bit to Spectral noise density) and high sampling rates implies higher sensitivity to ISI (inter-symbol interference). To overcome these problems, spatial division multiplexing was supposed as a way out to expand capacity and bandwidth efficiency. SDM is a multiplexing technique that uses space as an additional dimension which is orthogonal to time or frequency domain [30]. Multiplexing such as frequency/time/wavelength division can be applied within each space channel.

The N × N SDM architecture (Fig. 1.4) includes N transmitters that generates N signals which are mode multiplexed using spatial mode MUX. These N individual signals are superimposed over N spatial modes and then excited into a fiber that supports multiple spatial modes. A fiber that can support multiple modes like TMF, FMF, MMF, MCF, PCF, hybrid fiber can be utilized in this architecture [31]. The spatial modes that carry signals propagate through the SDM fiber and are then amplified by optical amplifier that supports these modes. After propagating through the SDM fiber, spatial mode DMUX is used to demultiplex the received modes. These received demultiplexed signals are

detected by N coherent receivers then, N signals are converted to electrical domain and finally processed and analyzed.

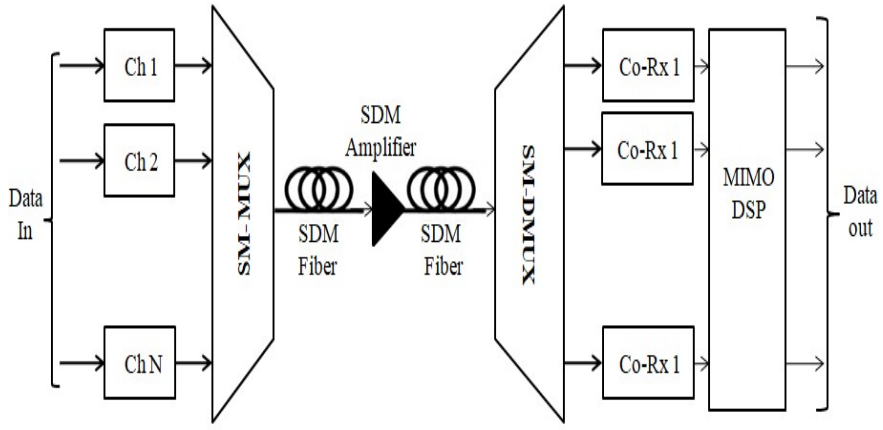

Fig. 1.4 Architecture of N x N Spatial Division Multiplexing system with N x N MIMO digital signal processing; Ch: Channel, SM-MUX: Spatial Mode Multiplexer, SM-DMUX: Spatial Mode Demultiplexer and Co-Rx: Coherent Receiver.

In SDM technique if transfer function of spatial mode MUX/DMUX having rank N equals number of spatial modes, then the capacity of channel can be increased by N folds than that of SMF system.

The advancement in FM (few-mode) transmission technique involve newer investigation in a broad variety of issues from device level to system like Few Mode Fiber design, FMF transmission, FMF amplification, FMF compatible component design etc. To reveal the viability of FM transmission devices by simulation or experimentally, considerable efforts have been made. Parallel signals coming from mode DEMUX are launched into the MDM receiver. Coherent receiver array can be utilized to recover each spatial channel since signals propagate independently on each other from different mode channels. Practically, multimode interference affect signals due to mode coupling taking place in fibers and mode components. So, Multi input multi output (MIMO) equalization must be implemented at the receiver section to recover the signals.

1.2.2 Comparison of multiplexing techniques

Table 1.1 represents the comparison of different optical multiplexing techniques based on the challenges faced during designing, data rate supported, applications and disadvantages.

Table 1.1 Comparison of multiplexing techniques

Multiplexing technique		**Advantages**	**Disadvantages**
WDM [12-13], [32] (data rate upto 100 Gbps)	CWDM	• Low cost • No need of signal amplification • Wide-range frequencies are used • Simple and easy to manufacture	• Supports 4 to 18 channels • Used for short distance applications • Low capacity
	DWDM [15], [27-28]	• High capacity • Support up to 160 channels • Narrow frequencies are uesd • Used for long distance applications	• Expensive • Signal amplification is required • Complex
OTDM [29] (data rate> 100Gbps)		• Ultrafast line rates (greater than 100 Gbps) • The channel can have variable data rate compatible with existing techniques. • The amplification and dispersion management are simple due to single wavelength transmission. • Solve problems faced in WDM	• Requirement of timing synchronization • Higher dispersion in fiber • Immature technology • Expensive
OCDM [33]		• Highly secured • No requirement of timing synchronization	• Higher dispersion in case of temporal codes • Bipolar optical coding is difficult • Adding and dropping of coded signals is complicated
PDM [17, 28] (Data rate~Tbps)		• Tolerance to polarization mode dispersion	• Increase in polarization crosstalk • Demultiplexing is complex • Polarization dependent losses

SDM [20-23] (High data rate ~ in Pbps)	• Capacity cannot exceed Shannon limit for SMF (Tbps) but by utilizing MMF capacity can exceed Shannon limit (Pbps) • High capacity as capacity increases with N times provided by SMF • Reduction in cost per bit • Only one amplifier and ROADM is required	• For MCF approach fabrication difficulty to limit large spatial density of cores and mode coupling prevails. • For MMF approach modal crosstalk and coupling exists but can be recovered by MIMO-DSP

In optical transmission system, 3 SDM techniques have been proposed. These schemes are multiplexing of core using MCF where a glass fiber supports multiple cores each communicating optical signals [34]; MDM using MMF or FMF where a fiber with one core of large cross section area supports different guiding modes and hybrid scheme using MCF along with (FMC) few mode core or (SMC) single mode core [35]. These schemes have fascinated interest in last three years to cope up the increasing capacity demands. SDM has been extensively used in combination with CDM/TDM/FDM (code/time/frequency) division multiplexing techniques. SDM technique can be achieved by utilizing either a MMF or MCF in optical communication [22]. For MMF or FMF based SDM transmission, MDM (mode-division multiplexing) is used. Table 1.2 represents the comparison of SDM techniques.

Table 1.2 Comparison of SDM techniques

SDM Techniques (Capacity: N times SMF)			
Parameters	**Bundled single mode fiber [20],[22]**	**Multicore fiber [30-31], [34], [40-41]**	**MDM over MMF link [22], [30], [35-39], [42]**
Fiber losses	Standard	Low as single mode fiber	Low as single mode fiber
Intra modal nonlinearity	Standard	High	Low
Inter-modal	No	Low	Low to medium

Nonlinearity			
Mode coupling	No	Medium	Low to high but can be optimized
Splicing	Easy	Complex	Easy
Amplifiers	N number of amplifiers can be used	N number of amplifiers can be used	1 amplifier
DSP complexity	Low	Medium	Medium to high MIMO is required
Cost	N times SMF	Low to medium	Low as one SMF
Challenges	• Several components are nedded to design it • Expensive	• To fabricate fibers that limit large spatial density of cores • To prevent spurious mode coupling due to fabrication or environmental conditions. • Complex structure	• To design components supporting multiple modes • No need to suppress linear mode coupling • Coupling generated due to mechanical stress and fiber imperfections can be recovered using MIMO-DSP .

1.3 Mode Division Multiplexing (MDM)

In MDM technique, using an optical fiber which permits several orthogonal spatial modes to be guided and transmitted simultaneously through a single core as shown in Fig. 1.5.Theoretically, it is possible to modulate N independent signals onto each spatial mode to obtain a channel capacity that is N times of single mode fiber. Thus, by adding spatial degree of freedom, fibre capacity of Few-mode fiber (FMF) or Multimode fiber (MMF) can be increased in the form of MIMO transmission [42].

MDM permits transmission of a number of channels upon different modes generated by different mechanisms like by few-mode fiber or multimode fiber [35], signal processing [36], spatial light modulator (SLM) [37], spatial modulation with lens [38], photonic crystal fiber [39] and dual mode fiber [40].The research in field of MDM was started in 1982 [41] but until 30 years researchers never took interest to this novel technique.

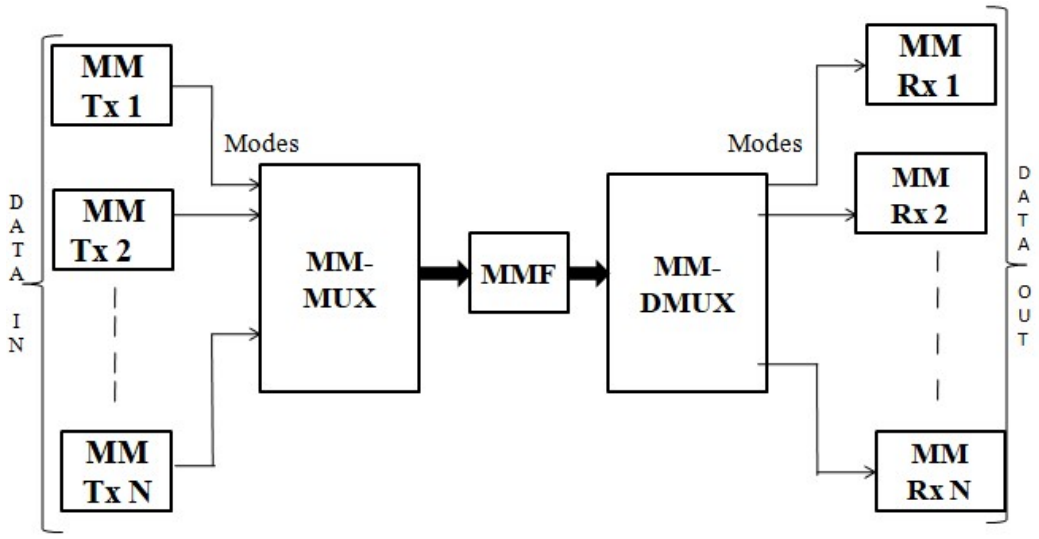

Fig. 1.5 Architecture of N x N Mode Division Multiplexing transmission system: MM Tx: Multimode Transmitter, MM-MUX: Multimode Multiplexer, MMF: multimode fiber, MM-DMUX: Multimode Demultiplexer and MM Rx: Multimode Receiver

The first experiment in this field was performed and it provided coverage of 10 km utilizing 3 spatial modes modulated at 14GBaud PDM-QPSK [42]. After that, numerous improvements came into picture.

1.3.1Fiber Modes

Modes are a set of guided electromagnetic waves that represent the propagation of light energy in fiber. Each guided mode is a solution of wave equation travelling along fiber forming pattern of electric and magnetic field distributions except for change in its total scaling and phase [43]. Light waves which are produced by electric charges vibrating in different directions results in electromagnetic waves to vibrate in different directions. A light wave vibrating in more than one plane (un-polarized) can be transformed to polarized light vibrating in single plane. The index gradient causes rays propagating at steeper angles (high order modes) to catch up with rays propagating at shallow angles in the fiber. Due to this feature of graded-index fiber, it provides less pulse dispersion than step-index fibers and therefore, superior bandwidth performance [44]. Each mode denotes a light beam travelling within the fiber core at different angles in case of multimode fibers. The propagating modes in a fiber is calculated by parameter normalized frequency V given as: $V = \frac{2\pi}{\lambda} a\sqrt{\eta_1^2 - \eta_2^2}$ where, a: core radius and λ: field wavength [45].

In case of multimode fibers each mode denotes light energy travelling within the core of fiber at different angles. Mostly for communication fibers where index difference between the core and cladding is moderately small, different modes can be grouped collectively into a single series of modes referred to as LP (Linearly Polarized) modes [45]. The two independent orthogonal plane waves in phase can be combined into a linearly polarized wave. The LP_{lm} modes can be represented as [45]:

$$E_t(r,\phi) = \Psi_{l,m}(r)\begin{Bmatrix}\cos l\phi \\ \sin l\phi\end{Bmatrix} \tag{1.1}$$

where, index $l \geq 0$corresponds to variation of light intensity in azimuthal plane with respect to ϕ and index $m \geq 1$ refers to the radial (r) dependence or number of zero crossings in the intensity pattern, $\Psi_{l,m}$ contains radial dependence and E_t depicts transverse field.

Table 1.3: LP_{lm} Modes

Mode index / number M= l+2m+1 [46]	**LP_{lm} Modes** l and m indices as light intensity patterns in azimuthal (ϕ) and radial direction
3	LP_{01}
4	$LP_{11a,b}$
5	LP_{02} $LP_{21a,b}$
6	$LP_{12a,b}$ $LP_{31a,b}$
7	LP_{03} $LP_{22a,b}$ $LP_{41a,b}$
8	$LP_{13a,b}$ $LP_{32a,b}$ $LP_{51a,b}$
9	LP_{04} $LP_{23a,b}$ $LP_{42a,b}$ $LP_{61a,b}$
10	$LP_{14a,b}$ $LP_{33a,b}$ $LP_{52a,b}$ $LP_{71a,b}$
11	LP_{05} $LP_{24a,b}$ $LP_{43a,b}$ $LP_{62a,b}$ $LP_{81a,b}$
12	$LP_{15a,b}$ $LP_{34a,b}$ $LP_{53a,b}$ $LP_{72a,b}$ $LP_{91a,b}$

All LP_{lm} modes with mode index, M = l+2m+1 must fulfill the equation as represented by Table 1.3. The value of refractive- index, ($\Delta \approx \eta_1 - \eta_2 / \eta_1$) is less than 1 as η_1 is very close to η_2 or $\eta_1 - \eta_2$ having very small value and this assumption of Δ is dictated as the weakly guiding approximation due to the fact that light energy would not be guided within any medium but uniformly distributed in whole medium [43]. When Δ becomes very small then a considerable amount of light energy lies in the cladding and as this

difference decreases further, more amount of light energy spreads into the cladding. Thus, light coupling or guiding ability of the fiber gets weaker and structure becomes weakly guiding in nature.

It is clear from equation (1.24), for LP_{lm} modes with $l \geq 1$: two spatial modes depicting sine: LP_{lma} or cosine: LP_{lmb} configuration and further each having 2 polarization states. Thus, in total of four degenerate (same propagation constant β) modes are formed. For LP_{0m}modes with $l = 0$: one spatial mode with only two polarization states forming two degenerate modes. The linearly polarized LP_{0m}modes are the two-fold degenerate hybrid HE_{1m}modes. The LP_{lm}modes are produced by addition of exact modes: HE_{2m}+ TE_{0m}or HE_{2m}+ TM_{0m} forming four-fold degenerate. Similarly, LP_{lm}modes for l >1are formed with the addition of hybrid modes: $HE_{l+1,m}$+ $EH_{l-1,m}$. LP_{01} mode is the dominant mode of propagation under the weakly guiding approximation and LP_{11} is the next mode that propagates in fiber [47]. In single mode fiber only fundamental mode LP_{01} is guided for small value of V but supports LP_{11} modes which contain its two degenerate even and odd modes ($LP_{11,e}$ and $LP_{11,o}$) if V exceeds 2.405 [43].

1.3.2 Fibers supporting MDM

A variety of optical fibers that can be employed in MDM are SMF (Single mode fiber), MMF (Multimode fiber), FMF (Few-mode fiber), MCF (Multicore fibers) and HCF (Hollow-core fiber) [22], [30], [34-42]. Existing communication fibers are SMFs and all other fibers including hybrid MCF-MMFs can support more than one transverse mode. MDM fibers can be categorized as coupled-mode fibers (CMF) and uncoupled-mode fibers (UMF) as shown in Fig. 1.6. UMF targets suppression of mode coupling to minimize crosstalk whereas CMF allow linear mode coupling giving rise to large crosstalk thus, require MIMO DSP at output recovered by coherent receivers. MCF is type of UMF with a core separation sufficiently large so as to reduce linear coupling between cores thus limits the spatial density of cores [48]. The main challenge in UMF is to fabricate fibers having a large spatial density of modes as well as preventing spurious mode coupling due to fabrication or environmental conditions.

On the other hand, for coupled mode MMFs, while designing there is no need to suppress linear mode coupling and coupling generated due to mechanical stress and fiber imperfections can be recovered using MIMO-DSP technology [42].

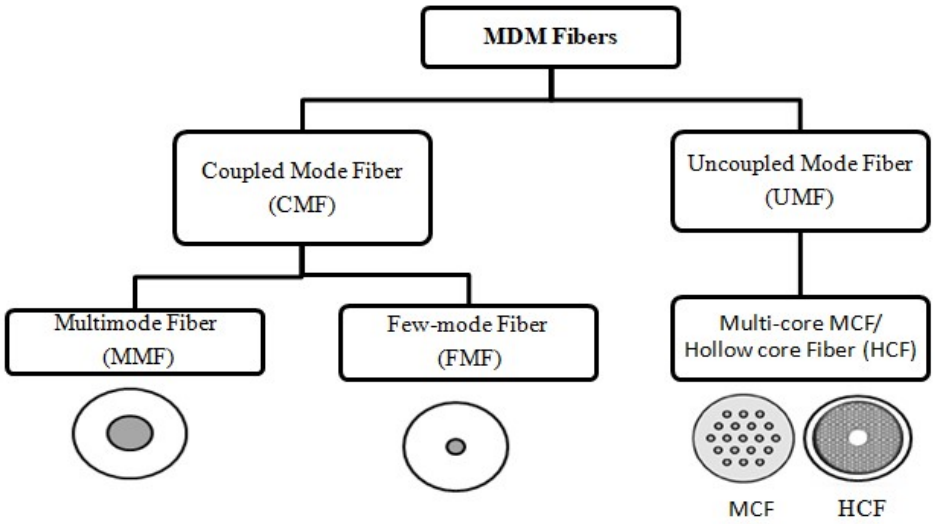

Fig. 1.6 Categorization of MDM fibers.

1.3.3 Design Strategies of MDM MIMO System

Over the past decades, a variety of MDM based communication networks have been developed for measurement of several parameters to cope up with the internet capacity demand. The upcoming MDM systems require advancement in fibers that support multiple spatial modes, optical amplifiers with less number of optical components, MM-MUX and MM-DEMUX MDM MUX/ DEMUX.

To enable MDM transmission system components required are mode multiplexer, mode demultiplexer, combiner, splitter and fiber supporting different modes. Components like mode MUX/ DEMUX play significant role as they convert signals from parallel SMF to MDM signals containing superposition of modes in FMF (few- mode fiber). Signals coming from SMF are converted to desired modes, combined and then coupled to few-mode fiber.

In Fig. 1.7, signals are coming from three different SMF (Single mode fibers), converted to different modes through PP (phase plates) and then these three different modes (M1, M2 and M3) are combined and coupled to FMF (Few mode fiber) through focusing lens [49]. MDM MUX comprises of two components: mode converters and combiners. Mode converter can be realized by using phase plates [49] but by utilizing this method insertions losses are high.

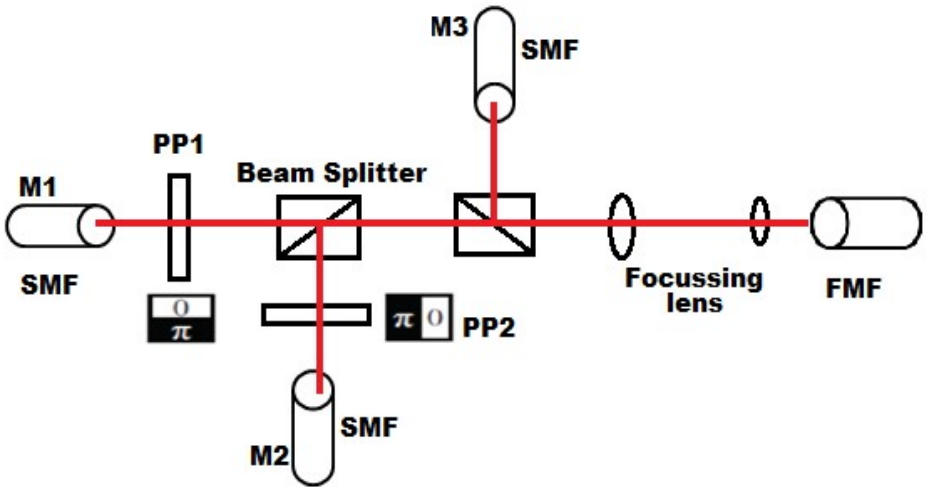

Fig. 1.7 Mode MUX/ DEMUX using phase plates; M: LP mode, SMF: Single mode fiber, PP: Phase Plate and FMF: Few mode fiber.

S. Randel et al. [50] used phase plates free space optics as multiplexer/ demultiplexer for MDM transmission experiments. They considered 3 modes LP_{01}, LP_{11a} and LP_{11b}along with 6 X 6 MIMO transmission [50] modulated to 20 Gbaud QPSK covering a distance of 1200km over FMF.

1.3.4 MIMO Signal Processing for MDM

The concept of multi-input multi-output (MIMO) is based on the installation of multiple antennas at transmitter and receiver end. Different MIMO algorithms have been developed as it provides increase coverage, higher data rate and achieves better BER as compared to SISO. The MIMO spatial diversity techniques were studied using free space optics link with diversity gain of 10^{-6}[51].Spatial Multiplexing employ MIMO system that offers higher data rate as multiple data symbols are transmitted simultaneously using multiple antennas. As waveguide modes are mutually orthogonal so, for data transmission they provide independent spatial dimensions. Though transmission of signals over long distances causes coupling in different modes, MIMO processing can be used to separate received signals.

Using MIMO MDM processing, it is estimated that number of modes (say N) in a Few mode fiber or MMF can support the capacity of a Single mode fiber (SMF) multiplied by a factor of N as shown in Fig. 1.8.

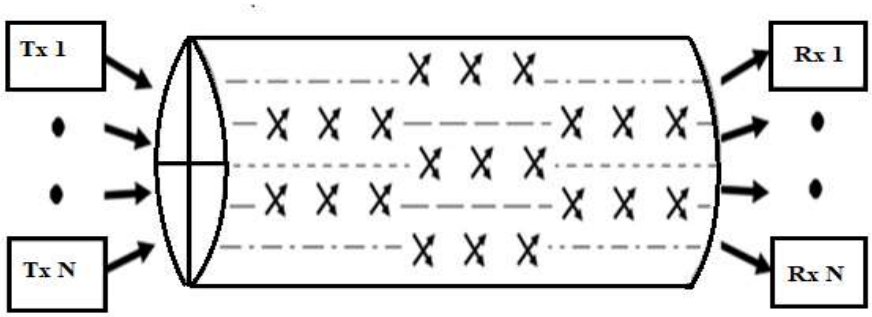

Fig. 1.8 MIMO based multimode transmission with N transmitters and receivers [45].

In these experiments, TMF (Two mode fiber) is used to achieve MDM with various combinations of modes e.g., two degenerate modes LP_{11} (LP_{11a}, LP_{11b}) [52], LP_{01} and LP_{11} modes and three modes (LP_{01}, LP_{11a}, LP_{11b}) [53]. There has been thrilling research progress on SDM in MCF (Multi core fiber) transmission and OAM (orbital angular momentum) multiplexing optical communication [54].

1.4 Optical Fiber Sensors

The global market for sensors is growing tremendously and the innovation rate is extremely high. From last two decades, sensor usage has been expanded in field of instrumentation, measurement and automation. These provide an interface to the real world and are used for production control and decision making. The scope of optical technique in the area of sensor has made an outstanding advancement with associated photonics, optoelectronics components and low loss optical fiber [55].

Optical fiber sensors offer the possibility of measurement in harsh environment where traditional electrical and electronic sensors possess difficulties. As quality improves and components prices have fallen, the ability of optical sensor to replace traditional sensor is enhanced. The advantages of fiber optical sensor include small size, higher sensitivity, light weight, low power, resistant to electromagnetic interference; all-solid-state construction, no moving parts and a sufficiently long lifetime have greatly overcome the disadvantage of high cost and end-user unfamiliarity [56].

A generalized optic sensing system consists of a light source, optical fiber, detector, transducer or sensing element. An applied perturbation modulates the properties of transmitted light and produces a change at the output detection end. Some of the benefits of fiber optic sensors are wide bandwidth, free from electromagnetic interference, compactness, economy and geometric versatility. The characteristics of an ideal sensor include low insertion loss, high resolving power, ease of fabrication, multiplexing

features and multi measured capabilities but generic fiber optic sensor is parameterized by high sensitivity if comparison to other sensors is done [57].

1.4.1 Optical Fiber Sensing Technology

Classification of Fiber optic sensors include: the location of sensing, the operating principal and application dependent [58]. Based on the sensor location, it is classified as intrinsic or extrinsic. Depending on the principal and demodulation technique, it is divided into phase, polarization, intensity and interferometer sensors. It can be grouped into physical, chemical and bio-chemical sensors based on application summarized by Table 1.4.

Table 1.4: Classification of Optical Fiber Sensors

S.No.	Sensor Property	Sensor Type
1.	Based on sensor location [58-59]	➢ IntrinsicSensor ➢ Extrinsic Sensor
2.	Based on operational principle and demodulation technique [59]	➢ Intensity Sensor [60] ➢ Phase Sensor [59] ➢ Polarization Sensor [59] ➢ Frequency Sensor [60] ➢ Interferometric Sensor • Sagnac Interferometric Sensor [61] • Mach-Zehnder Interferometric Sensor [62] • Michelson Interferometric Sensor[63] • Fabry-Perot etalon(FPI) [64] • Ring Resonator [65] • Dual mode Polarimetric Interferometric Sensor [66]
3.	Based on sensing technology [67-68]	➢ Serial or distributed Sensors • Optical time domain reflectometer • Raman optical time domain reflectometer • Brillouin optical time domain reflectometer ➢ Multiplexed Sensors ➢ Multipoint localized Sensors
4.	Application dependent [67]	➢ Physical Sensors ➢ Chemical Sensors ➢ Bio-chemical Sensors

- Extrinsic Sensor: This sensor includes optical fibers that "lead up to and out of a black box" that modulates light beam travelling through it in response to an ecological effect [59]. Light propagates through fiber from source to detector whereas modulation takes place outside the fiber and a separate sensing element is used.
- Intrinsic sensor: In an intrinsic sensor the effect of the measurand on the light takes place in the fiber itself as transducer [59]. The fiber itself converts an ecological effect into modulation of light travelling through it and acts as sensing element.

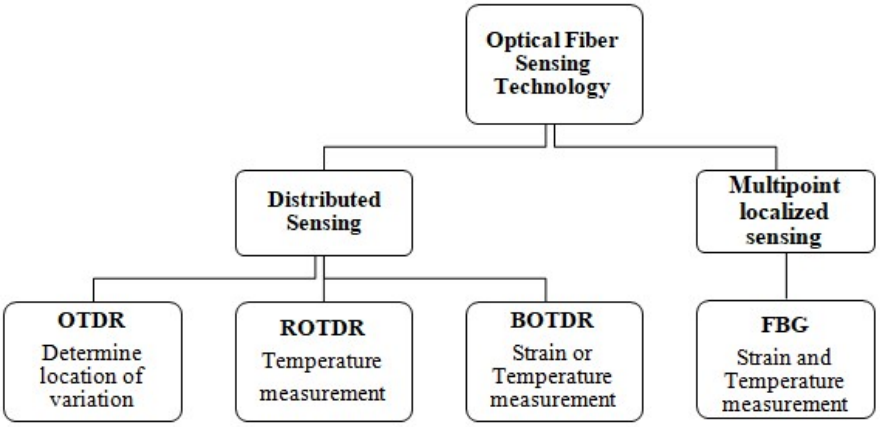

Fig. 1.9 Classification of Optical Fiber Sensing Technology

Optical fibre sensing technology may be grouped into Distributed or Serial sensing and Multipoint localized or spatial sensing or discrete sensing as shown in Fig. 1.9. Distributed sensing involves sensing along the fiber length and OTDR (optical time domain reflectometry) is required to find out the position of every variation in the measurand.

Localized or multipoint sensing identifies variation in measurand only in the vicinity of the sensor. For distributed measurement of temperature ROTDR (Raman optical time domain reflectometer) is utilized and for strain or temperature BOTDR (Brillouin optical time domain reflectometer) is utilized [68]. For separate measurement of temperature and strain a localized sensing technique i.e FBG (Fibre Bragg Grating) is utilized [69].

1.4.2 Optical sensing for monitoring civil structures

Monitoring health of civil structures such as highways, tunnels, dams, buildings, bridges, pipelines, power plants, storage containers etc. is valuable from the security, development and economic point [70]. The process of continuously tracking the

structural integrity and measuring the nature of damage in a civil structure is often referred to as structural health monitoring. The ageing factor of civil infrastructure is also an economic challenge for a country. It is approximated that 3% of total cost of a newly built civil structure will be invested every year for its maintenance purpose. Thus, major challenge exists in determining which structures require repair first and what procedure to be followed.

Corrosion, overweight loads, fatigue, cracks; geo factors like earthquakes, landslides put additional stress causes degradation and damage to civil infrastructure. It is possible to attain complete information about the health of a structure by using sensing techniques, visualization, instrumentation, communication, processing and modelling integrated together into a smart system. This information can be used for maintenance, repairing, replacement and for early detection of any degradation that might lead to a disastrous failure in the long-term. Structural health monitoring is the latest research hotspot having greater significance in civil engineering.

Traditionally, health monitoring of civil structures was based on visual inspection but fails to detect degradations that are very minute and not visible at the time of inspection. Moreover, one can visualize damage with respect to present state of structure or the state at the previous inspection but structural degradations due to manufacturing flaws that might be hidden cannot be detected [70]. Once the location of damage is detected then, different methods such as ultrasonic, radiography, acoustic, eddy currents, magnetic field or thermal techniques can be utilized for complete assessment of nature of defect. These procedures become very critical and costly when parts of civil structure might not be accessible. Thus, making the structure a comprehensive sensor based proficient of continuously collecting information on all parameters of structure monitoring its real behaviour. A variety of optical fiber sensors have been developed so far for measuring parameters (strain, temperature, pressure, corrosion, humidity, cracks, deflection, displacement etc.) of civil structure.

1.4.3 Pipeline monitoring using Optical sensing technology

Pipeline is an essential means to transport energy resources like oil, petrol, kerosene, natural gas, LPG through long distances [71]. In every country there is a network of energy, distribution and transmission pipelines like oil tankers, CO_2 cylinders, natural gas pipelines, gasoline, liquid petroleum, chemicals, water, sewer lines, LPG cylinders, oxygen cylinders, storm sewers, telephone lines, electric lines etc. In the present time

reliability of pipelines and possibility of failure are usually not noticed. Due to fluids or energy resources inside the pipeline and the harsh environmental conditions, these pipelines are prone to be corroded probably causing leakage or breakages. Leakage is the major hazard that occurs in pipelines due to failures like cracks, corrosion, drilling, bursting, manufacturing flaws, earthquakes put additional stress leading to major disasters (environmental pollution, loss of property and lives of people).

Pipeline monitoring is based on the variation in parameters of pipe like corrosion leakage acoustics strain, thickness reduction, temperature and pressure transient [71]. A variety of NDE (non-destructive evaluation) methods including ultrasonic, acoustic emission, radiography, eddy current and magnetic flux have been developed for detection of any kind of damage to pipe networks [68], [72-73]. Regular periodic inspections are done by pole climbing robots for detecting any welding defects and degradation of material [74]. Different inspection techniques like ultrasonic inspection robot, caterpillar-based pipeline robot were designed and developed for inspection of 80–100 mm pipelines in an indoor pipeline environment [75-76]. But these techniques were not able to provide real-time integrity monitoring of pipelines. These methods take into account different limitations like lack of portability, lack of ability for constant performance monitoring and susceptibility to electromagnetic interference. As, the oil and gas pipelines are buried underground to transport fuel to long distances thus, many conventional health monitoring technologies fail to perform monitoring of pipeline structures. These disadvantages can be overcome by optical sensorsthat put forward a comparatively newer technique to monitor pipeline networks.

The demand for optical fiber sensors is increasing day by day resulted into development of highly sensitive optimized sensor products that replaced traditional sensors in the market. Due to strain, corrosion and temperature fluctuations there are very minute deformations in the civil structure that might leads to crack formation with time. The fibre-optic sensors have several properties like small size, light weight, high-temperature performance, immunity to electromagnetic interference (EMI), large bandwidth, highly sensitive and dielectric nature [77].

Intensity based modulation sensors and interferometric modulation sensors fulfil majority of these features but are eventually limited due to one or more drawbacks. Interferometric modulation sensors provide higher sensitivity but require costly demodulation techniques (fringe counters) [57].On the other hand intensity modulation sensors offer absolute output but provides poor sensitivity. Surface Plasmon sensors are

highly sensitive to minute changes in refractive index but are difficult to fabricate and undergo polarization sensitivity [78]. The existing optical fiber sensors are either too complex or having limited sensitivities.

1.5 Optical in-fiber grating sensors

The optical in-fiber gratings are formed by inserting gratings inside the core of fiber. The gratings represent periodic modulation of the index of refraction and can be grouped as LPG (long period grating) and FBG (fiber Bragg grating). Both types of index gratings are identical in structure but grating period is different. The period of FBG (~10^{-4} meter) is smaller than the period of LPG (~10^{-6} meter). FBG couple energy contra directionally which means the guided energy of light from forward modes is transferred to propagating modes traveling in the opposite direction and referred as reflection gratings [62]. On the other hand, LPGs induce co-directional coupling in which guided energy of light from forward modes is transferred to forward cladding modes. The gratings represent periodic modulation of the index of refraction. Figure 1.10 shows how Bragg gratings can be utilized as a sensor. The light that is guided through coupler strikes the grating and gets scattered by each grating plane. The light reflected from each grating plane adds constructively in the backward direction [62]. The photodetector receives the reflected light with Bragg wavelength carrying information.

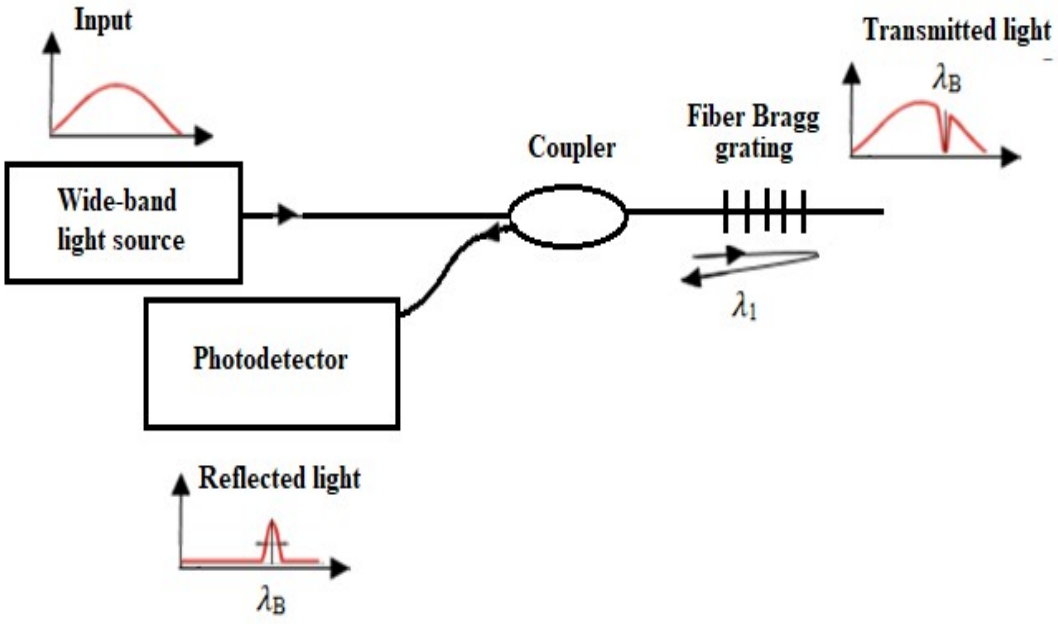

Fig.1.10 Fiber Bragg grating sensor system.

1.5.1 Mode coupled in-fiber grating sensor

The most significant progress in LPGs includes efficient coupling of guided mode with the cladding modes of a fiber. The presence of large number of cladding modes as well as there is no requirement of any method to separate these modes thus, LPGs or FBGs offer diverse applications in optical sensing [79-80].The coupled-mode theory can be used to analyze transmission characteristics of FBG or LPG written inside single mode fiber or multi-mode fiber [81-82]. The most important parameter is resonance wavelength which is a particular wavelength at which the coupling of guided mode with a particular cladding mode is highest. The central wavelength of both gratings is sensitive to different physical parameters such as strain, temperature, surroundings refractive index, distance between two gratings and fiber geometry. Any change in these parameters affects the central wavelength of the spectra. This feature of in-fiber gratings (LPG or FBG) has been explored to design sensors.

From application point of view in-fiber grating has two major advantages: first, there is no requirement of components (mode converter or polarizer) to separate the coupling modes and second, the light energy coupled to the fiber cladding is not shielded from the fiber and turn out to be susceptible to any variations in the surrounding medium. Due to its first advantage it is simply easy to deploy where many gratings are required and second feature opens the path for various sensor based applications. Thus, by manipulating cladding modes or coupling at resonant wavelength makes it possible to develop in-fiber grating based highly sensitive sensing devices. The cladding mode LPGs or FBGs has been considered, studied and developed from last fifteen years and many other forms had been investigated much prior. Many demonstrations and studies has been reported on strain, humidity, temperature and displacement sensing based on optical sensors but a few reports on cladding-mode in-fiber grating based sensors. It is predicted that the progress of optical in-grating fiber based sensing is always an open area of research and offers diverse applications [83].

1.5.2 Mode coupling inside in-fiber grating

In an optical fiber wave propagation is analyzed by Maxwell's equations and their solution provides decomposition of modes and if there are no perturbations these modes propagate without coupling. If a waveguide has amplitude or phase perturbations then coupling of propagating modes can takes place and coupled mode theory is utilized to analyze the grating waveguide structures. If boundary conditions are satisfied then light

energy can be transferred from one propagating mode to another mode. Index gratings inscribe inside fiber (in-fiber grating) is a passive waveguide structure having periodical variations in the refractive index causing mode coupling dependent on wavelength. In case of fiber Bragg gratings inscribed inside fiber the guided light energy couples or transfers from forward propagating core mode to modes travelling in the opposite direction. The phase matching condition can be written as below [84]:

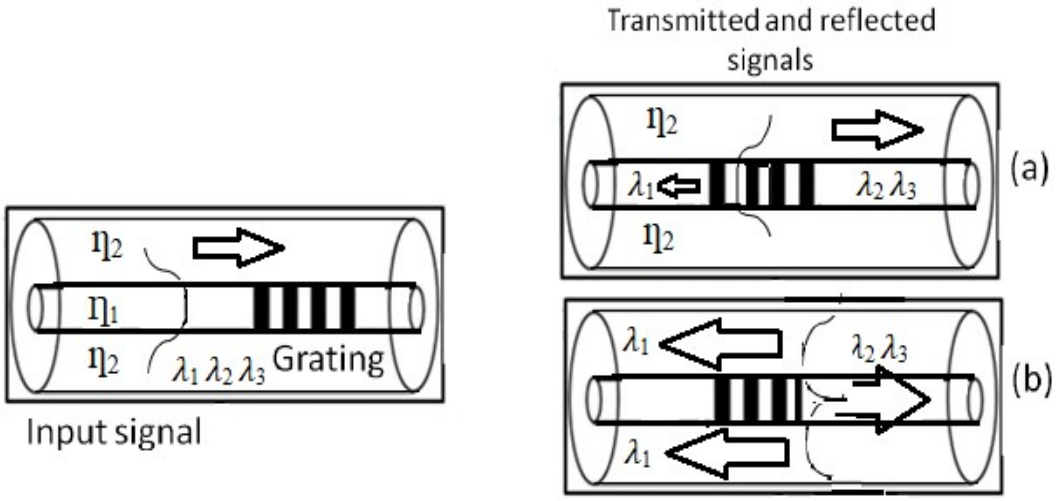

Fig. 1.11 Mode coupling in Bragg grating inscribed inside SMF for a) core to core mode and b) core to cladding mode [85].

$$\beta_f - (-\beta_b) - \frac{2\pi}{\Lambda} = 0 \Rightarrow \beta_f + \beta_b = \frac{2\pi}{\Lambda} \Rightarrow \frac{2\pi}{\lambda_0}(\eta_{efff} + \eta_{effb}) = \frac{2\pi}{\Lambda} \tag{1.2}$$

where, Λ is grating period, β_f represents the propagation constant for mode propagating in core of fiber in the positive z direction and $-\beta_b$ depicts the propagation constant for mode travelling in fiber core or cladding in the negative z direction as shown in Fig. 1.11(a, b).

From equation (1.2), resonant wavelength (λ) can be determined and written as [85]:

$$\lambda = (\eta_{efff} + \eta_{effb}) \times \Lambda \tag{1.3}$$

As in case of single mode fiber only one core mode travels in both directions thus, the value of propagation constants is equal and opposite in sign for core modes in both directions for core to core mode coupling or core to cladding mode coupling. The resonant wavelength also called Bragg wavelength, λ_B can be represented as [47]:

$$\lambda_B = 2 \times \eta_{eff} \times \Lambda \tag{1.4}$$

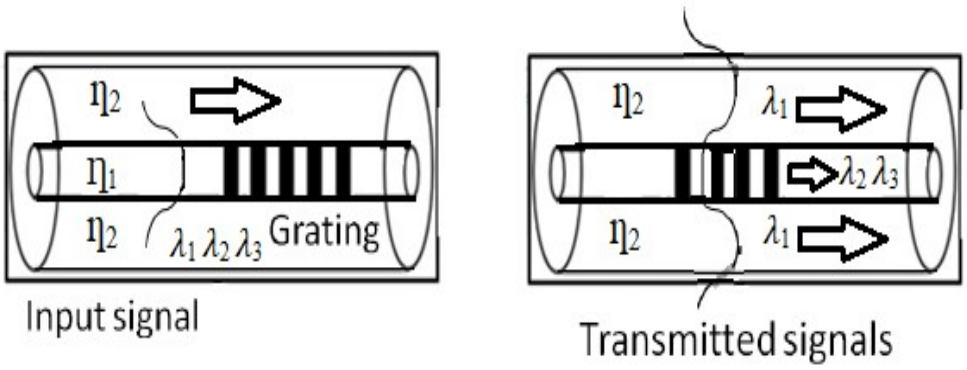

Fig. 1.12 Mode coupling in long period grating inscribed inside SMF for core mode to cladding mode [85].

On the other hand, LPGs induce coupling co-directionally in which energy of light from forward core modes is transferred to forward cladding modes in the positive z direction. As core mode in single mode fiber is not able to transfer energy to another mode in core so, energy transfers to cladding modes in positive z direction as shown in Fig. 1.12. In case of LPG written inside single mode fiber the resonant wavelength can be represented as [47, 85]:

$$\lambda = \left(\eta_{effco} + \eta_{effcl}\right) \times \Lambda \tag{1.5}$$

1.5.3 Concept of Bragg grating written inside MMF

Grating inside fiber represents periodic modulation of the index of refraction in core of an optical fiber. The light guided inside core is scattered by each grating plane. If phase matching condition given by equation (1.29) is satisfied, the light reflected from each grating plane adds constructively in the backward direction. This constructive reflected light forms a back-reflected peak with central wavelength (provided by the grating parameters). If condition is not satisfied then reflected light becomes out of phase and eventually cancel out [86].

When periodic index modulation with a spatial period of Λ are inscribed inside MMF, the phase matching or Bragg reflection condition for a specific spatial mode M1 is [87]:

$$\beta_{f1} + \beta_{b1} = \frac{2\pi}{\Lambda} \tag{1.6}$$

where, β_{f1} represents propagation constants of forward spatial mode M1 and β_{b1} is propagation constant of backward spatial mode M1. A MMF can support hundreds of

modes for the wavelengths around 1310 or 1550 nm. The propagation constant for N^{th} principal mode β_N in MMF can be defined by [87]:

$$\beta_N = \frac{2\pi\eta_1}{\lambda}\sqrt{1-\frac{4\Delta_{\max}(N+1)}{V_{norm}}}\ ,\ V_{norm} = \frac{2\pi.a.NA}{\lambda} \tag{1.7}$$

where, η_1: refractive index of core, $\Delta_{\max}$ is maximum relative index difference, V_{norm} is normalized frequency, a iscore radius, and NA presentsnumerical aperture. The phase matching condition can be fulfilled for reflection between degenerate modes and neighboring modes. The Bragg wavelength for reflection between same N^{th} principal mode can be determined by following equation [86]:

$$\lambda = \eta_1\Lambda\sqrt{1-\frac{4\Delta_{\max}(N+1)}{V_{norm}}} \tag{1.8}$$

For phase matching conditions between the N^{th} and the $(N-1)^{th}$ reflection modes, the Bragg wavelength can be calculated by taking the average of propagation constants for these neighboring modes, $\beta = \beta_N + \beta_{N-1}$. Thus, the reflection peak will fall between the N^{th} and the $(N-1)^{th}$ reflection modes.

When light enters through one end of an optical fiber it passes through the fiber with almost no reflection. As light enters the fiber with Bragg grating inscribed inside core of fiber, light reflects a narrowband portion of incoming light and rest transmitted through the optical fiber. The central wavelength of the incident signal, named Bragg wavelength λ_B is given by equation (1.4). Any change in either effective refractive index or grating period can cause central Bragg wavelength to shift to higher wavelength. Any change in strain and temperature thus affect the effective index of refraction and grating period [88]. Due to this change Bragg wavelength shifts to higher or lower wavelength which can be observed using Spectrum analyzer.

1.6 Conclusion

Internet traffic is increasing day by day and users are demanding for higher data capcity. In optical fiber communication multiplexing is considered to be the significant means for the expansion of existing fiber networks. Different multiplexing techniques have been discussed and compared on the basis of challenges faced during their design, data rate supported, applications and disadvantages. As compared to the multiplexing

techniques, the optical SDM transmission system is more reliable, flexible and can be used to fulfil demand for higher data capacity with cost effective solution. From the MIMO MDM system perspective, different design strategies are discussed. The concept of mode coupling between core and cladding modes and the effect of fluctuations in temperature and strain on fiber Bragg grating is theoretically discussed. Optical Fiber Bragg grating MMF sensors are studied that can be used for developing low cost sensing systems and provides great scope where leakage is the major issue.

CHAPTER 2
LITERATURE REVIEW AND OUTLINE

2.1 Introduction

The hasty increase in internet traffic is raising the demand for higher data capacity in existing communication networks. The demand for higher capacity has grown drastically that are motivated by various applications in the fields of video streaming, browsing, sharing files, video conferencing, smart homes etc. Therefore, to cope up with the internet capacity a variety of optical networks are being explored gradually [3-11]. In literature, several multiplexing techniques has been reported that utilize phase, amplitude and wavelength of light like WDM, DWDM (Dense WDM), 3-D OCDMA, 3-D coherent spatial-phase-time coding etc. that support SMF [89-90].

In late 1990 wavelength division multiplexing was proposed and several issues related to implementation of WDM systems have been reported in the literature. Wavelength stability of sources, channel spacing, wavelength multiplexers, demultiplexers, couplers are some of the issues which are discussed by different authors [12], [13], [91]. WDM technique allowed transmission of 40 channels with channel spacing 100 GHz at 2.5 Gbps providing an overall capacity of 100 Gbps. Then, WDM systems were designed with smaller channel spacing named optical FDM systems [92]. In OTDM technique, the pulses from various individual sources need proper time delay adjustment such that pulses can be multiplexed together as accurate timing information isrequired for demultiplexing [93]. Thus, the major issue related to implementation of OTDM system is requirement of tight clock jitter and synchronization of clock at very high frequencies (1 THz).

The authors in [32] presented the performance of a 40 Gbps WDM-PON (Wavelength Division Multiplexed Passive Optical Network) with 100 GHz channel spacing at 10 Gbps using different receiver filters. Monga et al. [92] demonstrated a 3-D spectral-phase-time OCDMA system having 6 users operating at 5 Gbps at minimal power requirement per user. This system supported (MPFR) message priority and faster routing mechanism to optimize routing performance so as to provide effective data transfer. Hasan et al. [95] demonstrated a 40 × 40 Gb/s DWDM network with 50 GHz of channel spacing to improve the performance of a real time wavelength division multiplexed network. Chung et al. [96] proposed a 16 × 10 Gbps long-haul communication system covering 1040 km over SMF link using the hybrid amplifiers. Singh et al [89] proposed

a flat-gain optical amplifier for 100 × 10-Gb/s DWDM system at 0.2 nm channel spacing. They concluded that the gain variation reduced from 2.01 to 1.15 dB efficiently for proposed EYDWA-SOA hybrid amplifier providing a capacity of ~1 Tbps. DWDM systems suffer from losses due to induced nonlinearities, noise (Rayleigh backscattering, pump's relative intensity noise transfer) and crosstalk. The major issue related to implementation of DWDM is costly amplification and requirement of multi-pumps for gain flattening [27], [89].The growth in coherent optical detection techniques results in remarkable capacity growth making use of high spectral efficiency modulation format [16]. Further, the digital coherent optical fiber techniques are discussed that makes use of polarization division multiplexing (PDM) that doubles the channel capacity [17].

But still research field is exploring spatial multiplexing with multi-moded domain to fulfill the demand of higher quality and forthcoming capacity as required by end-user applications [97].Optical Multi-input multi-output Mode Division Multiplexing (OMIMO-MDM) is an attractive multiplexing technology as it potentially offers flexible, reliable and robust communication to fulfill the increasing demand for higher internet capacity. MDM utilizing MMFs (multi-mode fibers) has recently been of immense interest from last 3 to 4 years to large extent for its capability to support multiple modes, boost capacity of optical communication systems and compensate for power losses [98]. On the basis of these issues the comprehensive literature survey and gaps in present study are described in following Sections.

2.2 Literature Survey

The research in field of MDM was started in 1982 [41] but until 30 years researchers never took interest to this novel technique. The first experiment in this field was performed and provided coverage of 10 km utilizing 3 spatial modes modulated at 14GBaud PDM-QPSK [42]. After that, numerous improvements came into picture. The distance of data transmission has been increased to 96 km with 3 modes [35] and successfully transmitted 5 spatial modes over 40 km [99].

Desurvire was the first who explored the theory of multimode EDFA [100]. Gong et al. [101] numerically modeled pumped multimode amplifiers and lasers for transmission of transverse modes in multi modes environment Ezra Ip [102] investigated equalization of gain in FM-EDFA amplifier along with FMF considering more than 2 groups of modes. He studied that doping profile optimization is essential in combining pump to equalize mode dependent gain of FMFs with more than 4 mode groups.

Amphawan et al. [103] investigated HG-MDM (Hermite-Gaussian Mode Division Multiplexing) system with MMF and achieved good BER for channel spacing with HG modes x-index (x=2, 3) over 800 m distance of MMF. Different numerical, simulation analysis and experiments have been made in the field of mode division multiplexing over MMF to increase internet capacity. Some of them are discussed below.

2.2.1 Mode Division Multiplexing issues

Ho et al. [45] provided a review on effects of linear propagation in a multimode fiber. They reviewed models and conditions of coupling. The parameters like Mode-dependent loss and Modal dispersion were studied that affects the complexity and channel capacity of MIMO MDM systems. They concluded that strong coupling regime minimizes complexity of MIMO with reduction in group delay spread due to MD and maximize channel capacity with reduction in loss due to MDL.

Schmidt et al. [104] investigated different modes and nonlinear interaction in strongly coupled multimode fibers. The results presented that the analysis of modes does not influence the nonlinear parameter. They numerically calculated the field distributions of LP and exact-vectored modes with finite difference mode solver. They compared and verified the analytical results with simulation results.

Rademacher et al. [105] presented a Gaussian noise model to estimate the nonlinearity in spatial division multiplexing system and related reduction in OSNR. They compared the analytical results with simulation based results for FMF (few-mode fiber) supporting three to six spatial modes and attained a good agreement between the two.

Antonelli et al. [106] reviewed key features of nonlinearity issues in space division multiplexed transmission during random mode coupling effect. They illustrated that modal dispersion reduces the effect of intra-channel interference between modes. The inference is that for practical values of modal dispersion the received signal exhibits dependence on particular MO realization thus, avoiding the use of back propagation techniques.

Ho et al. [107] studied theoretically the channel capacity of MDM systems in case of MDL (mode dependent loss). In strong mode coupling, mode dependent loss (MDL) can be statistically described as eigen value distribution of zero-trace Gaussian unitary ensemble in small MDL region. They approximated 23.4 dB as maximum mode dependent loss difference for fibers with two modes and 80 dB for fibers with many modes.

Mecozzi et al. [108] described that light propagation in degenerate group of randomly coupled modes over multimode fiber is explained by Manakov equation. They considered propagation of two degenerate modes ($LP_{11}(a)$ and $LP_{11}(b)$) of step index fiber; parameters of core as: radius= 7.5mm, refractive index= 1.4621, step refractive index= 9.7×10^{-3}; dispersion coefficient as $25ps^2/km$. In this the nonlinear coefficient was $2.6\times10^{-20}m^2W^{-1}$, k = 0.76 and fundamental mode's effective area of $126mm^2$. The analysis of this equation is important in space as well as wavelength multiplexed systems where nonlinearities exists.

Cristian et al. [109] studied nonlinear propagation in multimode fiber and their effect on performance of system. They extended Manakov equations to include Raman impact and studied the power scaling of nonlinear interference noise in SDM systems. They illustrated that MD improves the intra-channel nonlinear interference.

Mumtaz et al. [110] studied nonlinearities in SDM system using step-index and graded-index multimode fibers. They simulated the propagation of multiple 114 Gb/s bit streams in PDM-QPSK format over three spatial modes of a multimode fiber and verified the accuracy of Manakov equations by comparing numerical results with simulation. They concluded that the agreement between the two methods was excellent in all cases studied. Based on numerical results they concluded that fluctuations of birefringence improve system quality by reducing nonlinearities in fiber.

Prilepsky [111] analyzed the integrable nonlinear Schrodinger equation as transmission channel and extended the concept of eigen-value communications to non soliton coherent optical communications. They proposed Nonlinear Inverse Synthesis method for high-quality, processed and reliable long-haul transmission. This approach was based on encoding of data directly into nonlinear signal spectrum. They explained eigen value division multiplexing in optical fibers thus, provided efficient output with no nonlinear channel crosstalk. They demonstrated the robustness of nonlinear synthesis based transmission against nonlinearity and ASE noise using OFDM modulation format.

Mumtaz et al. [112] designed a model to investigate nonlinear penalties in MCFs having four cores in which each core transmits 80-Gb/s PDM-QPSK signal. They didnot considered rapidly varying birefringence. The outcomes show that a strong coupling can diminish the nonlinear impairments and improve the system performance.

Askarov et al. [113] studied fibers and EDFA amplifiers for 12 signal modes. Modal fields, GDs, areas and chromatic dispersion coefficients were numerically computed. They have done a comparison with parameters like relative index profiles, numerical

apertures and doping profiles for step-index (SI), graded-index (GI), step index depressed cladding (SIDC) and graded index depressed cladding (GIDC) fibers. Graded index depressed-cladding fibers offered a low GD spread in fibers with 0.15 NA, 583 ps/km rms and low MDG in EDFAs with 0.15 NA and 25 dB mode averaged gain.

Franz et al. [114] experimentally investigated principal mode groups for high bit rate transmission over OM4 GI-MMF. They identified 8 principal mode groups required for spatially separated channels operating at 1550 nm wavelength. It was proved that each mode group can be utilized for data transmission of 10-Gb/s over a 5-km long GI-MMF.

Freund[115] discussed multimode fiber transmission theoretically along with summary of scheme characteristics. They considered recent drifts in development of components and system designs to provide an outline on high-speed transmission in MMFs. They reviewed capacity extension techniques, reach and speed of transmission systems. Transmitter, fiber link and receiver components were developed for 40 Gbps transmission serially covering distance greater than 400 m.

Kahn et al. [116] reported first demonstration on MIMO using Adaptive Equalization method to improve inter symbol interference. They achieved improvement in bandwidth-distance product in MMF using different techniques like selective modal excitation, M-ary coding, electronic equalization and SCM (subcarrier multiplexing). With each technique there was significant increase in bandwidth-distance product but still MMF capacity not exploited to its full potential.

Kahn et al. [36] concluded that the strong mode coupling decreases the modal group delay spread reduce the intricacy of MIMO processing. They proved that the statistical distribution of modal group delay or gain depends on modes and fluctuation in accumulated delay. It can be obtained from eigen value distributions of arbitrary matrices. They suggested different approaches for MDM MIMO processing that tender minimized power expenditure in short reach optical detection systems.

Song et al. [117] demonstrated Acoustooptic Mode Convertor (AOMC) for MDM system at telecommunication wavelength. AOMC used for higher order modes in a fiber which guides LP_{01}, LP_{11}, LP_{21} and LP_{02} modes. They further characterized the AOMC by analyzing the coupling spectra and far-field intensity distributions. They achieved coupling efficiency higher than 90% with extinction ratio better than 10dB for all higher order modes.

Arik et al. [118] compensated modal crosstalk and modal dispersion in long haul MDM system by employing adaptive MIMO equalization. To minimize computational

complexity MIMO- Frequency domain equalization was used in comparison to Polarization Dispersion Mode or Time domain equalization systems in single mode fiber. They studied two adaptive algorithms for MIMO Frequency domain equalization: LSE (least mean squares) and RLS (recursive least squares). Adaptation to an unknown fiber supporting 6-30 modes was achieved in 3-5 microseconds using RLS or 15-25 microseconds using LMS.

Ho et al. [119] studied the delay spread of multimode fiber in strong mode coupling regime using three techniques: Fredholm determinant, Andreief identity and Tracy–Widom distribution. In the strong mode coupling scenario, group delay of MMF has identical statistics as a zero-trace guassian unitary ensemble. It was reported that obtained results are almost identical for Fredholm determinant and Andreief identity but results come out to be adequately accurate for Tracy–Widom distribution up to 12 modes.

Ho et al. [120] modeled multimode fiber as cascade of several individual sections illustrated statistically by random matrices. In strong mode coupling, length of the multimode fiber is considered to be much larger than the correlation length where local principal modes are made constant. They considered group delay to be proportional to the number of individual sections or overall fiber length. The marginal probability density function of group delay was derived analytically up to 7 modes. The PDF of group delay approaches a semicircle distribution for more than 7 modes. For fibers with modes (D= 16, 64 and 512), numerical simulations have been done as compared to semicircle distribution.

Shemirani [121] extended field-coupling propagation model to describe higher order modal dispersion in GI-MMF. This model follows the concept of first-order principal modes having GD that is dependent on mode coupling strength. They modeled multimode fiber as a cascade of independent sections having random curvature and angular orientation. They showed that higher order modal dispersion leads to many effects like depolarization, broadening of pulse, output pattern blurring and nonlinear response of I/O intensity waveforms. They validated the results of first and second order analyses using simulation and experimentally confirmed the nonlinear response of I/O intensity patterns.

Panicker et al. [122] put forward the idea of adaptive algorithms to reduce ISI (inter symbol interference) in multimode fiber using a spatial light modulator. They proposed suboptimal algorithms having faster speed of convergence and lesser hardware

complexity so as to improve resilience to noise. Simulation outcome shows the performance of system due to existence of noise and CPSCA to be the best algorithm in terms of convergence speed.

Coupled multi core fibers are advantageous for spatially multiplexed long haul transmission [123]. They studied modal characteristics like group delay spread, chromatic dispersion, intermodal beat lengths and intramodal and intermodal effective areas. They characterized multi-core fibers with closely spaced cores and showed the limited accuracy of perturbation based analyses.

2.2.2 OMIMO-MDM Architectures

Koebele et al. [99] used phase plates free space optics as multiplexer/demultiplexer for MDM transmission experiments. They considered 5 modes LP_{01}, LP_{11a}, $LP_{11b,}$ LP_{21a} and LP_{21b} receiver modulated to 28 Gbaud QPSK along with 4 X 4 MIMO covering a distance of 40km over FMF with low mode coupling.

Sim et al. [124] proposed that the bandwidth of multimode fiber increases significantly by employing center-launching technique (mode-field matched). The technique of center-launching was achieved by fusion-splicing of SMF-pigtailed transmitter to MMF with controlled core diffusion method. By this technique, launched power of 94% was coupled into LP_{01} mode of MMF. They demonstrated transmission of NRZ signals (10-Gb/s and 40-Gb/s) excluding dispersion compensation and errors. They also demonstrated bit rate-distance product (1.95 Tb/s.km) of WDM transmission over 12.2 km of MMF span.

Amin et al. [40] reported a dual-mode and polarization transmission method with grating based LP_{01}- LP_{11} mode converter for detection of mode selection based on two-mode fiber (TMF). TMF used had step-index profile which was 3.62 V, cutoff wavelength of LP_{11} mode was 2323nm and loss was 0.26 dB/km. Transmission of107 Gb/s using CO-OFDM through 4.5km TMF was achieved to increase fiber capacity and spectral efficiency of MDM system.

Chen et al. [125] investigated a 30-Gb/s and 3 X 3 mode group division multiplexed (MGDM) system using multimode fiber link with graded index profile. Mode-Selective Spatial Filtering (MSSF) was utilized to reduce the crosstalk amongst mode groups so as to improve the complexity of signal recovery. They demonstrated experimentally that MSSF with 50/ 125 μm GI-MMF pigtail with 0.2 numerical aperture could limit mode

group crosstalk into neighbouring modes. This setup minimizes the complication of DSP (digital signal processing) technique thus, improves system performance.

Adrian et al.[126] investigated the effect of principle modes for MDM transmission with the increase in number of eigen-modes in a MMF. For high data rate transmission the eigen-modes in fiber is used as supplementary degree of freedom. They observed an exponential decay in principle modes after reaching a local maximum.

Chen et al. [127] demonstrated a 30-Gbit/s 3 X 3 MIMO-MGDM system with MSSF using SMF over 20m graded index MMF. To analyze the performance of the system bit error rate versus data rates curves were compared for three sub channels.

Amphawan et al. [128] designed OFDM based transmission system for transmission of 2 independent spatial channels using MDM technique based on Radio-over-Free-Space-Optics (Ro- FSO). Optical modes LG_{00} and LG_{10} were multiplexed for transmitting two 40 GHz QAM-OFDM radio signals through free space modulated at 20Gbps for long haul communication. At the receiver, LG_{00} mode surpasses LG_{10} for retrieval of signal in terms of the received power and signal constellation in spite of the distance. They achieved transmission over a distance of 90km under clear weather condition whereas 65km when scintillation is considered.

Ryf et al. [129] experimentally presented results for hybrid multiplexing (mode and wavelength) transmission over 50-μm core diameter GI-MMF. They utilized spatial mode filters, mode multiplexers (mode-selective photonic-lantern) and MIMO DSP. For 3 spatial modes they achieved overall capacity of 18 Tbit/s with 9 bit/s/Hz of spectral efficiency over a distance of 305 km. For 6 spatial modes spectral efficiency of 7 bit/s/Hz and transmission distance of 17 km with 23 Tb/s of aggregate WDM line rate were achieved.

Tripathi et al. [130] investigated mode division multiplexing with MMF link up to nine modes with bit rates of 2.5 to 10Gbps and 1 to 100km of transmission lengths of MMF to cope up with the growing need of data transport. Simulation results hold successful up to 9 modes in MDM transmission technique whereas received OSNR is unsteady at longer transmission length and higher bit rate. It was concluded that performance degraded due to transmission of large number of multiplexed modes. MDM serves as supplementary aid to costly pre-existing transmission networks.

Ryf et al. [131] used waveguides as multiplexer/demultiplexer for MDM transmission experiments. They considered 5 modes LP_{01}, LP_{11a}, $LP_{11b,}$ LP_{21a} and LP_{21b} and receiver

modulated to 20 Gbaud 16 QAM X 32 WDM along with 12 X 12 MIMO covering a distance of 177km over FMF.

Boffi et al. [54] proposed MDM optical communication system depending on the choice of OAM modes for the purpose of increasing capacity of system. They investigated the option of utilizing optical 1vortices with various OAM values and topological charge for MDM in optical fibers. The demultiplexing is achieved by Interferometric scheme along with Dove prisms in WDM and PDM systems.

2.2.3 Pipeline Monitoring using Optical sensor

Rajeev et al. [68] summarized optical fiber technologies like localized FBGs (Fibre Bragg Gratings) and distributed optical fiber sensing techniques like Brillouin Optical Time Domain Reflectometry (BOTDR) and Raman distributed temperature sensor (RDTS). They gave an overview of applications for these technologies in geotechnical engineering and water pipeline monitoring. They considered issues regarding pipeline characteristics, failure points and environmental, physical factors and thus a conceptual approach was developed.

Inaudi et al. [132] reviewed their nine years success in fiber optic sensors installation in various civil structures such as tunnels, dams, bridges, pipes, anchors, nuclear power plants, historical monuments etc. They installed 1300 sensors up to date in 70 different civil structural monitoring applications. They proved that for fiber optic sensors survivability rate of 95-100% can be achieved during installation and also after many years.

Zhou et al. [133] designed a distributed type of strain sensor based on Brillouin scattering nonlinearity. They used this sensor to compute strain (longitudinal and hoop) of steel pipe having wall thinning defects alongwith locations of structural defects.

Kister et al. [134] introduced an optical sensor based on FBG for strength monitoring of civil structure (West Mill Bridge, Oxfordshire, UK). Alhandawi et al. [135] studied and modeled a distributed type of sensor with fiber cables (having metal coated polymer cladding) to identify corrosion of pipeline.

Lee et al. [136] introduced FBG sensors to examine the pipeline damage by measuring guided wave responses. Moreover, the existing optical sensor based monitoring techniques have not presented parallel monitoring of corrosion and leakage in water pipeline. It can be accomplished that the strain sensor focuses on the pipeline leakage and corrosion monitoring.

Sunil et al. [137] developed a method that used ultrasonic sensors with surface image assessments to automatically detect defects in pipelines. They added that a research is ongoing at Penn State to find out if Non-Contact Ultrasound (NCU) be used to enumerate the defects in pipelines. They reviewed different multi-sensor systems for detecting defects in concrete, steel and plastic pipelines. They superimposed an ultrasonic image into its optical counterpart and created a context to achieve interpretation and analysis of data.

Liang [138] introduced OFDR technique to observe defects like corrosion and leakage in pipeline. They conducted simulation tests for monitoring performance of pipeline. To test the corrosion they formed sensor arrays and created a hoop strain nephogram to check level and location of corrosion and concluded that pipeline leakage defects can be detected by the distributed optical fiber sensor (DOFS).

L. Wong et al. [139] experimentally monitor the growth of crack along pipe using distributed strain sensor. They considered a pipe made of cast iron having dimensions (diameter of 660 mm and wall thickness of 18 mm) and made an artificial patch on pipe that represent corroded portion. The pipe was subject to a cyclic pressure loading and they utilized swept wavelength interrogator distributed fibre to measure strain and to detect cracks on pipe.

John et al. [140] fabricated fiber optic pressure sensing arrays based on fiber bragg grating to demonstrate monitoring of subsurface pressures under water waves in a wave tank. They used two sensing arrays: horizontal and vertical spaced at 1-cm intervals to achieve high resolution less than 0.1 cm H_2O. This method provided pressure sensing upto 10.5 m long wave tank and can be extended to pressure monitoring in applications like surf-zones, groundwater aquifers and rivers.

Abhinav et al. [141] proposed an optical sensor based model for pipeline monitoring. They established an theoretical relation and simulated it successfully using four wavelengths. A monitoring unit with optical heterodyning concept was used to achieve four wavelengths at photodiode's output that represents four different fiber bragg gratings. They sensed pressure variations in pipelines and verified the theoretical design architecture with simulation results.

Table 2.1 represents the literature summary of progress in Optical Multi input multi output (MIMO) Mode Division Multiplexed Transmission, reported between 2011 & 2019.

Table 2.2: Progress in OMIMO Mode Division Multiplexed Transmission, reported between 2011 & 2019

Fiber Type	YEAR	REF.	Core / No of Modes	Distance in km	Span Length (km)	Data Rate (Gbps)	No. of WDM channels per core per mode	Net Spectral Efficiency (b/s/Hz)	Net total capacity (Tb/s)	Capacity x Distance Product (Pb/s x km)
FMF	2011	42	1/3	10	10	56	1	--	0.15	0.002
FMF	2011	49	1/3	33	33	112	6	6.19	1.86	0.06
FMF	2011	142	1/3	50	50	112	88	6.19	27.23	1.36
TMF	2011	52	1/2	4.5	--	--	--	5.4	0.0133	--
TMF	2011	143	1/2	10	--	10	--	--	0.0025	--
MCF	2011	144	7/1	16.8	16.8	172	90	11.25	109.14	1.83
MCF	2011	145	7/1	76.8	76.8	107	80	14	56	4.3
MCF	2011	146	7/1	76.8	76.8	107	160	14	112	8.6
MCF	2011	147	3/1	1200	60	80	1	--	0.22	0.27
MCF	2011	148	7/1	76.8	76.8	1120	1	--	7.84	0.6
FMF	2012	149	1/6	130	65	--	8	7.68	3.07	0.40
SMF-MCF	2012	150	12/1 + 2/3	3	3	1050	385/354	109	1050	3.15
MCF	2013	151	19/1	10.1	10.1	172	100	30.5	305	3.08
MCF	2012	152	7/1	845	76.8	603	8	42.2	33.77	28.53
MCF	2013	153	7/1	6160	55	128	40	14.44	28.88	177.87
FMF	2013	154	1/3	500	50	76	146	7.3	26.63	13.32
MCF	2012	155	12/1	52	52	456	222	91.4	1012.32	52.64
MCF	2013	156	12/1	1500	50	90	748	36.8	344	516
MMF	2014	128	1/9	100	1	10	--	--	0.0112	1.12
OM4	2014	157	1/6	17	8.3	120	32	7	23	--
FM-MCF	2014	158	12/3	40	40	105	20	247.9	55.08	2.2
MMF	2015	103	1/25	0.8	--	25	25	--	0.028	0.022
MMF	2015	159	1/3	0.1	--	40	4	--	0.1	0.01
OM3	2015	129	1/3	310	43.5	--	60	9	18	5.49
MMF	2016	160	1/25	0.4	--	25	25	--	--	--
MMF	2017	161	1/36	5.6	0.05	--	--	--	--	--
MCF	2019	162	7/1	53.7	2	10	--	--	--	0.0004
MCF	2019	163	32/1	1850	--	100	--	--	--	0.023

2.3 Gaps in present study

This section lists the common limitations encountered while dealing with mode division multiplexed systems. This would make the reader realize the importance of these drawbacks and elucidate the reasons for making an attempt to get solution to these problems.

1. Emerging MDM systems require improvements in traditional fibers, optical amplifiers with less optical components, MDM compatible MUX/ DEMUX to better exploit the spatial domain.
2. Less development in this area poses significant challenges as there is concurrent transmission of spatial signals through multiple modes or cores of fiber.
3. In present technology MCF approach is being explored but its fabrication imposes major challenge by limiting the spatial density of cores.
4. In future, MDM systems will provide growth in capacity-per-fiber, reduction in cost-per-bit and improvements in energy efficiency.

2.4 Objectives

Keeping in view the above mentioned aspects, the objectives of research were formulated which are listed as follows:

1. To model and analyze the nonlinear propagation effects in multimode fiber.
2. To investigate Optical Multi Input Multi Output signal processing utilizing coupling of linearly polarized modes to minimize crosstalk.
3. To propose modified architectures of Mode Division Multiplexed system including different amplification schemes, fibers supporting multiple modes to increase the capacity of system.
4. To investigate MMF based sensor for monitoring spatially distributed water pipeline structures.

2.5 Organization of Thesis

The thesis has been organized into seven chapters. The content of each chapter is briefly described as below.

Chapter1: introduces the basic introduction along with motivation of research. After introduction, the literature review of MIMO mode division multiplexing, problem formulation and objectives are presented in **Chapter 2**. Further, the organization of the thesis is presented.

Chapter 3: This chapter deals with the first objective which is to model and analyze the nonlinear propagation effects in multimode fiber. In this chapter, a model is proposed that describes nonlinear propagation effects like Nonlinear Kerr effect and SPM (Self Phase Modulation) during propagation of N spatial modes in MMF.

Chapter 4: This chapter deals with the second objective which is to investigate Optical Multi Input Multi Output signal processing utilizing coupling of linearly polarized modes to minimize crosstalk. This chapter includes the analysis of different LP modes over MMF link to investigate MIMO Mode Division Multiplexing. The transmission performance is enhanced by

Chapter 5: This chapter deals with the third objective which is to propose modified architectures of Mode Division Multiplexed system including different amplification schemes, fibers supporting multiple modes to increase the capacity of system. In this chapter, first architecture of MDM is proposed that includes design of multimode EDFA and comparison of different MM-EDFA amplification configurations (pre-, boost- and inline MM-EDFA) to boost system performance. Then, second architecture is proposed in which wavelength and mode division multiplexing techniques are combined to increase the capacity of system.

Chapter 6: This chapter deals with the fourth objective which is to investigate MMF based sensor for monitoring spatially distributed water pipeline structures. In this chapter gratings are inscribed inside MMF to design MMF based sensor for monitoring strain and temperature of water pipeline. Then experiment was performed to validate the strain applied on two types of water pipeline structures: open and closed.

Finally, **Chapter 7:** summarizes the thesis and present recommendations on the basis of results obtained in the Chapters three to seven.

CHAPTER 3

NON LINEAR PROPAGATION IN MULTIMODE FIBERS

3.1 Introduction

In this chapter, the first research objective is discussed which is to model and analyze nonlinear propagation effects in multimode fiber link. The nonlinear parameters in MMF like Nonlinear Kerr effect, inter-modal and intramodal Four Wave Mixing are taken into account to investigate MIMO MDM over MMF link. The effect of inter-modal and intramodal FWM for different pump LP modes (LP_{01}, LP_{02} and LP_{11} and LP_{12}) has been analyzed with the help of optical spectrum analyser. To reduce the effect of FWM, chromatic dispersion has been increased throughout the link. This objective is presented in different Sections as follows: Section 3.2 presents the propagation of signal in optical fiber, Section 3.3.1 and Section 3.3.2 discusses nonlinear propagation inside MMF including TM-NLSE (Two Mode-Nonlinear Schrodinger Equation) extended to form MM-NLSE (Multimode Nonlinear Schrodinger Equation); in Section 3.3.3 simulation setup is demonstrated that illustrates the effect of nonlinear parameters like Intermodal Four-Wave Mixing (IMFWM) and Intramodal FWM in MMF and further, in Section 3.4, outcomes are discussed.

3.2 Signal propagation in optical fiber

Let us consider optical fiber to be an ideal cylindrical structure inside a coordinate system. Light propagates inside a fiber in +z or –z-direction and a transverse plane orthogonal to z-direction can be described by Cartesian coordinates (x, y) or polar coordinates (φ, ρ). Pulses of light in dielectric media can be represented as electromagnetic wave having separate electric and magnetic field governed by Maxwell's equations [25] as:

$$\nabla . D = \rho \qquad \text{(Gauss law)} \qquad 3.1(a)$$

$$\nabla \times E = -\frac{\partial B}{\partial t} \qquad \text{(Faraday's law of induction)} \qquad 3.1(b)$$

$$\nabla . B = 0 \qquad \text{(Gauss law of magnetism)} \qquad 3.1(c)$$

$$\nabla \times H = J + \frac{\partial D}{\partial t} \qquad \text{(Ampere circuital law)} \qquad 3.1(d)$$

where, ∇ is nabla operator, '.'and '$\times$' depicts the scalar and vector product, t represents time, E and H are electric and magnetic field respectively, D and B denotes

corresponding electric and magnetic flux density respectively, J is current density and ρ is charge density. The propagation of electric and magnetic fields inside fiber gives rise to flux densities (D and B) and related as given below [47]:

$$\begin{aligned} D &= \varepsilon_0 E + P_e \\ B &= \mu_0 H + P_m \end{aligned} \tag{3.2}$$

where, ε_0 and μ_0 are vacuum permittivity and permeability respectively and P_e and P_m are corresponding induced electric and magnetic polarizations. Optical fibers denote nonmagnetic medium (P_m =0) and no free charges (J=0, ρ =0). Taking curl of Faraday's law of induction (3.1b) and using above equations terms B, H and D can be eliminated in terms of E and P_e, equation becomes [25]:

$$\nabla \times \nabla \times E = -\frac{1}{c^2}\frac{\partial^2 E}{\partial t^2} - \mu_0 \frac{\partial^2 P_e}{\partial t^2} \tag{3.3}$$

Also, the general expression for (3.3) can be written as: $\nabla \times \nabla \times E = \nabla(\nabla.E) - \nabla^2 E$, put ρ =0 in Gauss's law, $\nabla.D = 0 \Rightarrow \nabla.E = 0$ and equation (3.3) can be written as [47]:

$$\nabla^2 E = \frac{1}{c^2}\frac{\partial^2 E}{\partial t^2} + \mu_0 \frac{\partial^2 P_e}{\partial t^2} \tag{3.4}$$

$$\nabla^2 \hat{E} = -\frac{\omega^2}{c^2}\hat{E} - \omega^2 \mu_0 \hat{P}_e \tag{3.5}$$

The equation (3.4) is wave equation that describes the light propagation in optical fibers using Maxwell equations and equation (3.5) corresponds to wave equation in frequency domain. The polarization P can be divided into linear and nonlinear polarization in time and frequency domain given by equation (3.6) and (3.7) respectively [43]:

$$P_e(r,t) = P_{eL}(r,t) + P_{eNL}(r,t) \tag{3.6}$$

$$\hat{P}_e(r,\omega) = \hat{P}_{eL}(r,\omega) + \hat{P}_{eNL}(r,\omega) \tag{3.7}$$

Now, electric polarization P can be defined in terms of electric field E to describe the interaction between light propagating inside fiber and propagation medium fiber. In general, $\chi^{(j)}$ represents j-th order susceptibility with tensor of rank j+1. Here, in equation (3.8a) and (1.8b) first order susceptibility depicts linear propagation effects and in equation (3.9a) and (1.9b) third order susceptibility corresponds to nonlinear propagation effects [43-44].

$$P_{eL}(r,t) = \varepsilon_0 \int_{-\infty}^{\infty} \chi^{(1)}(t-t').E(r,t')dt' \tag{3.8a}$$

$$\hat{P}_{eL}(r,\omega) = \varepsilon_0 . \hat{\chi}^{(1)}(\omega) \hat{E}(r,\omega) \tag{3.8b}$$

$$P_{eNL}(r,t) = \varepsilon_0 \iiint_{-\infty}^{\infty} \chi^{(3)}(t-t_1, t-t_2, t-t_3) \vdots E(r,t_1)E(r,t_2)E(r,t_3)dt_1 dt_2 dt \tag{3.9a}$$

If wave equation in frequency domain equation (3.5) is to be applied then P_{eNL} is first to be transformed into frequency domain. Let us assume the impulse response of nonlinear polarization to be instantaneous and thus, integral vanish in equation (3.9a) and simplified to [43]:

$$P_{eNL}(r,t) = \varepsilon_0 \chi^{(3)} \vdots E(r,t)E(r,t)E(r,t) \tag{3.9b}$$

$$P_{eNL}(r,t) \approx \varepsilon_0 \varepsilon_{NL} E(r,t) \tag{3.9c}$$

$$\varepsilon_{NL} = \frac{3}{4} \chi^{(3)} |E(r,t)|^2 \tag{3.9d}$$

To further solve the propagation equation it is assumed ε_{NL} to be quasi constant in time t. As envelope of wave *A(z, t)* varies very slowly as compared to the carrier wave and fiber represents slightly nonlinear medium and $P_{eNL} << P_{eL.}$ Thus, the fourier transform of P_{eNL} is done and equation becomes [44]:

$$\hat{P}_{eNL}(r,\omega) \approx \varepsilon_0 \varepsilon_{NL} \hat{E}(r,\omega) \tag{3.9e}$$

Put the value of linear and nonlinear polarization in frequency domain ($\hat{P}_{eL}(r,\omega)$ and $\hat{P}_{eNL}(r,\omega)$) from equations (3.8b) and (3.9e) respectively into wave equation (3.5) [44]:

$$\nabla^2 \hat{E} = -\frac{\omega^2}{c^2} \hat{E} - \omega^2 \mu_0 (\varepsilon_0 . \hat{\chi}^{(1)}(\omega) \hat{E} + \varepsilon_0 \varepsilon_{NL} \hat{E}) \tag{3.10}$$

$$\nabla^2 \hat{E} + \omega^2 \mu_0 \varepsilon_0 (1 + \hat{\chi}^{(1)}(\omega) + \varepsilon_{NL}) \hat{E} = 0 \tag{3.11}$$

$$\nabla^2 \hat{E} + \varepsilon(\omega) k_0^2 \hat{E} = 0 \tag{3.12}$$

The wave equation (3.10) results in Helmholtz equation given by (3.12) where, wave number, k_0 is given by [25], [44]:

$$k_0 = \frac{\omega}{c} = \frac{2\pi}{\lambda} \text{ and } \varepsilon(\omega) = 1 + \hat{\chi}^{(1)}(\omega) + \frac{3}{4} \chi^{(3)} |E|^2 \tag{3.13}$$

In general first and third order susceptibility can be complex and thus, can be written as [43]:

$$\varepsilon(\omega)=\left(n(\omega)+n_2|E|^2+\frac{i\tilde{\alpha}(\omega)}{2k_0}\right) \tag{3.14}$$

where, frequency dependent first term and intensity dependent second term in combination represents refractive index and in third term $\tilde{\alpha}(\omega)$ denotes the absorption coefficient. To model the propagation of electric field in z-direction in xy-plane, eigenvalue $\tilde{\beta}$ is considered. It can be splitted into two terms: linear and nonlinear part. The first term which is frequency dependent represents linear part and second term with nonlinear part as defined in equation (3.15) [43-44]:

$$\tilde{\beta}(\omega)=\beta(\omega)+\Delta\beta \tag{3.15}$$

$$\text{where, } \Delta\beta=\frac{k_0\iint \Delta n\,|F(x,y)|^2\,dxdy}{\iint |F(x,y)|^2\,dxdy} \tag{3.16}$$

To get the solution of Helmholtz's differential equation we convert it into frequency domain and consider $\tilde{A}$ is a slowly varying function of z, we get [43-44]:

$$2i\beta_0\frac{\partial\hat{A}}{\partial z}+\left(\tilde{\beta}^2-\beta_0^2\right)\hat{A}=0 \tag{3.17}$$

Here, to further solve this equation given approximation can be utilized, $\tilde{\beta}^2-\beta_0^2\approx 2\beta_0\left(\tilde{\beta}-\beta_0\right)$ in equation (3.17) which leads to equation (3.18) [43-44]:

$$\frac{\partial\hat{A}}{\partial z}=i\left(\beta(\omega)+\Delta\beta-\beta_0\right)\hat{A} \tag{3.18}$$

Now, substitute value of $\tilde{\beta}(\omega)$ from (3.15) to equation (3.18) results in equation (3.19) as [43]:

$$\frac{\partial\hat{A}}{\partial z}=i(\beta(\omega)+\Delta\beta-\beta_0)\hat{A} \tag{3.19}$$

$$\text{where, } \beta(\omega)=\beta_0+(\omega-\omega_0)\beta_1+\frac{1}{2}(\omega-\omega_0)^2\beta_2+\frac{1}{6}(\omega-\omega_0)^3\beta_3+\ldots\ldots \tag{3.20}$$

Here, put value of $\beta(\omega)$ in equation (3.19) upto fourth term as higher terms are neglected and after applying fourier transform equation (3.19) becomes [44]:

$$\frac{\partial A}{\partial z} = -\beta_1 \frac{\partial A}{\partial t} - i\frac{\beta_2}{2}\frac{\partial^2 A}{\partial t^2} + \frac{\beta_3}{6}\frac{\partial^3 A}{\partial t^3} + i\Delta\beta A \tag{3.21}$$

$$\Delta\beta = \gamma \mid A\mid^2 + i\frac{\alpha}{2}, \gamma = \frac{n_2\omega_0}{cA_{eff}} \text{ where, } A_{eff} = \frac{(\iint \mid F(x,y)\mid^2 dxdy)^2}{\iint \mid F(x,y)\mid^4 dxdy} \tag{3.22}$$

where, γ dictates nonlinear coefficient, A_{eff} is effective area of fundamental mode at central frequency and $F(x,y)$ denotes mode function. Now, substitute all terms of equation (3.22) to (3.21) yields NLSE (Nonlinear Schrodinger equation) that governs the propagation of optical pulses [43-44]:

$$\frac{\partial A}{\partial z} + \frac{\alpha}{2}A + \beta_1\frac{\partial A}{\partial t} + i\frac{\beta_2}{2}\frac{\partial^2 A}{\partial t^2} - \frac{\beta_3}{6}\frac{\partial^3 A}{\partial t^3} = i\gamma\left|A\right|^2 A \tag{3.23}$$

The factor A corresponds to slowly varying amplitude of the pulse envelope, second term represents fiber loss α is absorption coefficient, β_1 is inverse of group velocity, β_2 represents chromatic dispersion, β_3 denotes slope of dispersion and γ represents nonlinearity that exists in pulses propagating in fiber.

3.3 Nonlinear propagation inside MMF:

MDM utilizing MMFs (multi-mode fibers) has recently been of immense interest from last 3 to 4 years to large extent for its capability to support multiple modes, boost transmission capacity of optical fiber communication systems and reduce power losses [164]. The effect of nonlinear propagation inside MMF depends on the amplitude of the electric field as material of fiber is SiO_2 which show very small nonlinearity. There are two major factors that lead to nonlinear effects in an optical fiber: high power densities and long transmission distance. Thus, in today's scenario long haul transmission systems undergo signal distortions due to nonlinear effects. Thus, it has become essential to analyze these effects in order to mitigate them. Nonlinear effects like Kerr effect, inter-modal and intramodal Four Wave Mixing in MMF have been demonstrated in the previous years of optical fiber communication [110], [165].

Recently, hypothetical analysis for different modes has been done [166]. Friis et al. [167] demonstrated four-wave mixing between spatial modes of two-mode fiber (TMF) with 1 km length at telecommunication wavelengths. They considered two pumps that excite modes (LP01 and LP11) with the probe signal that excites LP01 mode. They considered the effect of four wave mixing and observed that Bragg scattering and phase conjugation idlers were generated in the LP11 mode. R.-J. Essiambre [168]

experimentally demonstrated intermodal four wave mixing with Terahertz wave spacings over few mode fiber (FMF) with 4.7 km length.

3.3.1 Nonlinear Kerr effect in TM-NLSE

The dominant nonlinearity in multimode fiber is caused by Kerr-effect and due to this nonlinearity coupling is induced in multimode fiber. As coupling is induced by nonlinearity so, let's start NLSE equation (3.23) with coupled set of NLSE to clearly define the picture of nonlinear effects. Here, we consider two spatial mode propagation where each spatial mode having two polarization states or modes. Thus, in this model total number of modes is twice the number of spatial modes. The coupled NLSE model for *j* modes (*j*= 1 to 2N: *p, l, m* and *n*) is given by[168-169]:

$$\frac{\partial \vec{A}}{\partial z}+\frac{\alpha_j}{2}\vec{A}+\beta_{1j}\frac{\partial \vec{A}}{\partial t}+i\frac{\beta_{2j}}{2}\frac{\partial^2 \vec{A}}{\partial t^2}-\frac{\beta_{3j}}{6}\frac{\partial^3 \vec{A}}{\partial t^3}=i\gamma\sum_{plmn}C_{plmn}A_p^{*}A_lA_m\hat{A}_n \tag{3.24}$$

where, *p, l, m* and *n* are four polarization modes where *j*=1 to 2N; α_j is absorption coefficient of j modes, β_{1j} is inverse of group velocity for *j* modes, β_{2j} represents chromatic dispersion produced, β_{3j} denotes slope of dispersion. The third, fourth and fifth term on left hand side accounts for linear propagation. The term on right hand side represents coupling induced by the Kerr nonlinearity of the fiber. The nonlinear coefficient, γ for two modes is having same value as for single mode fiber given in equation (3.22) [170].

The overlap integral of supported modes (in this case 4 modes: *p, l, m* and *n*) is given by dimensionless constant C_{plmn} that depends on spatial mode profile of these modes. The orientation of field vector must be uniform such that probability density of complex field may depend only on its modulus. Thus, multi-mode field propagation can be approximated by averaging the nonlinear terms with respect to this distribution. The averaged non linearity terms right side of equation (3.24) reduces to [109]:

$$\sum_{plmn}C_{plmn}A_p^{*}A_lA_m\hat{A}_n=\kappa\,|\vec{A}|^2\,\vec{A} \tag{3.25}$$

where, κ : dimensionless parameter which is dependent only on nonlinear coupling coefficients C_{plmn} given by equation (3.26) [109], [170]:

$$\kappa=\sum_{plmn}C_{plmn}Q_{plmn} \tag{3.26}$$

In this orientation of field $\vec{A}$ can be considered as uniformly distributed and thus, statistical averaging can be done [166]. Here, Q_{plmn} is statistical averaging of $[A_p^{*} A_l A_m \hat{A}_n]/|\vec{A}|^4$. Putting values of equation (3.25) and (3.26) to equation (3.24) we get[169-170]:

$$\frac{\partial \vec{A}}{\partial z}+\frac{\alpha_j}{2}\vec{A}+\beta_{1j}\frac{\partial \vec{A}}{\partial t}+i\frac{\beta_{2j}}{2}\frac{\partial^2 \vec{A}}{\partial t^2}-\frac{\beta_{3j}}{6}\frac{\partial^3 \vec{A}}{\partial t^3}=i\gamma\kappa|A|^2 A \qquad (3.27)$$

The equation (3.27) corresponds to TM-NLSE (Two mode Nonlinear Schrodinger Equation).

3.3.2 Nonlinear Kerr effect in MM-NLSE

In this model it is assumed that *N* different modes are propagating through MMF where these modes to be sorted into groups. Here '*N*' spatial modes are divided into '*w*' groups where $G_1, G_2 \ldots\ldots G_w$ represent first group, second group up to *w* groups. In each group the modes are assumed to be strongly linearly coupled and perfect coupling can be achieved for length much shorter than length for nonlinear interactions such that nonlinear effects can be averaged over all modes belonging to the corresponding group. The TM-NLSE can be extended to MM-NLSE to analyze nonlinear propagation effects.

$$\begin{aligned}
&\frac{\partial \vec{A}_1}{\partial z}+\frac{\alpha_1}{2}\vec{A}_1+\beta_{11}\frac{\partial \vec{A}_1}{\partial t}+i\frac{\beta_{21}}{2}\frac{\partial^2 \vec{A}_1}{\partial t^2}-\frac{\beta_{31}}{6}\frac{\partial^3 \vec{A}_1}{\partial t^3}=i\gamma(\kappa_{11}|\vec{A}_1|^2+\kappa_{12}|\vec{A}_2|^2+\ldots..+\kappa_{1w}|\vec{A}_w|^2)\vec{A}_1\\
&\frac{\partial \vec{A}_2}{\partial z}+\frac{\alpha_2}{2}\vec{A}_2+\beta_{12}\frac{\partial \vec{A}_2}{\partial t}+i\frac{\beta_{22}}{2}\frac{\partial^2 \vec{A}_2}{\partial t^2}-\frac{\beta_{32}}{6}\frac{\partial^3 \vec{A}_2}{\partial t^3}=i\gamma(\kappa_{21}|\vec{A}_1|^2+\kappa_{22}|\vec{A}_2|^2+\ldots..+\kappa_{2w}|\vec{A}_w|^2)\vec{A}_2\\
&\frac{\partial \vec{A}_3}{\partial z}+\frac{\alpha_3}{2}\vec{A}_3+\beta_{13}\frac{\partial \vec{A}_3}{\partial t}+i\frac{\beta_{23}}{2}\frac{\partial^2 \vec{A}_3}{\partial t^2}-\frac{\beta_{33}}{6}\frac{\partial^3 \vec{A}_3}{\partial t^3}=i\gamma(\kappa_{31}|\vec{A}_1|^2+\kappa_{32}|\vec{A}_2|^2+\ldots..+\kappa_{3w}|\vec{A}_w|^2)\vec{A}_3 \qquad (3.28)\\
&\ldots\ldots\ldots\\
&\ldots\ldots\ldots\\
&\ldots\ldots\ldots\\
&\frac{\partial \vec{A}_w}{\partial z}+\frac{\alpha_w}{2}\vec{A}_w+\beta_{1w}\frac{\partial \vec{A}_w}{\partial t}+i\frac{\beta_{2w}}{2}\frac{\partial^2 \vec{A}_w}{\partial t^2}-\frac{\beta_{3w}}{6}\frac{\partial^3 \vec{A}_w}{\partial t^3}=i\gamma(\kappa_{w1}|\vec{A}_1|^2+\kappa_{w2}|\vec{A}_2|^2+\ldots..+\kappa_{ww}|\vec{A}_w|^2)\vec{A}_w
\end{aligned}$$

The above set of equations (3.28) represents Manakov MM-NLSE. The first equation corresponds to nonlinear propagation of modes of first group G_1, second equation presents to nonlinear propagation of modes of second group G_2,….., and so on upto w^{th} group G_w. Adding all these equations of equation set (3.28) and taking summation where *k* can be defined from first group to w^{th} group, we get:

$$\sum_{k=1}^{w}\left(\frac{\partial\vec{A}_k}{\partial z}+\frac{\alpha_k}{2}\vec{A}_k+\beta_{1k}\frac{\partial\vec{A}_k}{\partial t}+i\frac{\beta_{2k}}{2}\frac{\partial^2\vec{A}_k}{\partial t^2}-\frac{\beta_{3k}}{6}\frac{\partial^3\vec{A}_k}{\partial t^3}\right)=i\gamma\sum_{k=1}^{w}\left(\left(\kappa_{k1}\left|\vec{A}_1\right|^2+\kappa_{k2}\left|\vec{A}_2\right|^2+.....+\kappa_{kk}\left|\vec{A}_w\right|^2\right)\vec{A}_k\right)$$

As constant terms are taken outside summation and terms varying with k are summed up and elaborating above equation it finally leads to equation (3.29) representing the model of nonlinear propagation of multiple w groups (where each group having *N* modes) with Kerr effect in MMF.

$$\sum_{k=1}^{w}\frac{\partial\vec{A}_k}{\partial z}+\frac{1}{2}\sum_{k=1}^{w}\alpha_k\vec{A}_k+\sum_{k=1}^{w}\beta_{1k}\frac{\partial\vec{A}_k}{\partial t}+\frac{i}{2}\sum_{k=1}^{w}\beta_{2k}\frac{\partial^2\vec{A}_k}{\partial t^2}-\frac{1}{6}\sum_{k=1}^{w}\beta_{3k}\frac{\partial^3\vec{A}_k}{\partial t^3}=$$
$$i\gamma\left(\left|\vec{A}_1\right|^2\sum_{k=1}^{w}\kappa_{k1}\vec{A}_k+\left|\vec{A}_2\right|^2\sum_{k=1}^{w}\kappa_{k2}\vec{A}_k+.....+\left|\vec{A}_w\right|^2\sum_{k=1}^{w}\kappa_{kw}\vec{A}_k\right) \quad (3.29)$$

The equation (3.29) represents multimode version of nonlinear propagation of w groups (containing *N* spatial modes in each group) with Kerr effect. The vectors $\vec{A}_1,\vec{A}_2.....\vec{A}_w$ dictates the envelope of corresponding modes belonging to each group say $G_1,G_2.....G_w$: Each group contains *N* spatial modes where each mode is having two polarization states: *x* and *y*. Thus, vector $\vec{A}_1$ can be represented as a column vector with 2*N* entries.

$$\vec{A}_1=\begin{bmatrix}A_{1,1}^{x}\\A_{1,1}^{y}\\A_{1,2}^{x}\\.....\\A_{1,N}^{x}\\A_{1,N}^{y}\end{bmatrix}$$

$$|\vec{A}_1|^2=\left|A_{1,1}^{x}\right|^2+\left|A_{1,1}^{y}\right|^2+.....+\left|A_{1,N}^{x}\right|^2+\left|A_{1,N}^{y}\right|^2$$

$$|\vec{A}_w|^2=\left|A_{w,1}^{x}\right|^2+\left|A_{w,1}^{y}\right|^2+.....+\left|A_{w,N}^{x}\right|^2+\left|A_{w,N}^{y}\right|^2$$

where, $A_{1,1}^{x}$: Envelope of *x* polarized first mode within first group

$A_{1,1}^{y}$: Envelope of *y* polarized first mode within first group

$A_{1,2}^{x}$: Envelope of *x* polarized second mode within first group

$A_{1,N}^{x}$: Envelope of *x* polarized N^{th}mode within first group

$A_{1,N}^{y}$: Envelope of y polarized N^{th}mode within first group

$A_{w,N}^{x}$: Envelope of x polarized N^{th}mode within w^{th} group

The nonlinear propagation effects include self-phase modulation (SPM) and cross-phase modulation (XPM) in MMF. The nonlinear factors account for nonlinear term correction because of averaging over strongly coupled modes within different mode groups [168].

3.3.3 Simulation model

The simulation setup illustrates the nonlinear effect like Intermodal Four-Wave Mixing (IMFWM) in MMF as presented in Fig. 3.1. Each multimode transmitter (MM Tx) includes spatial laser source tuned at different wavelengths (λ_1=1530 nm, λ_2=1542 nm, λ_3=1554 nm and λ_4=1566 nm).

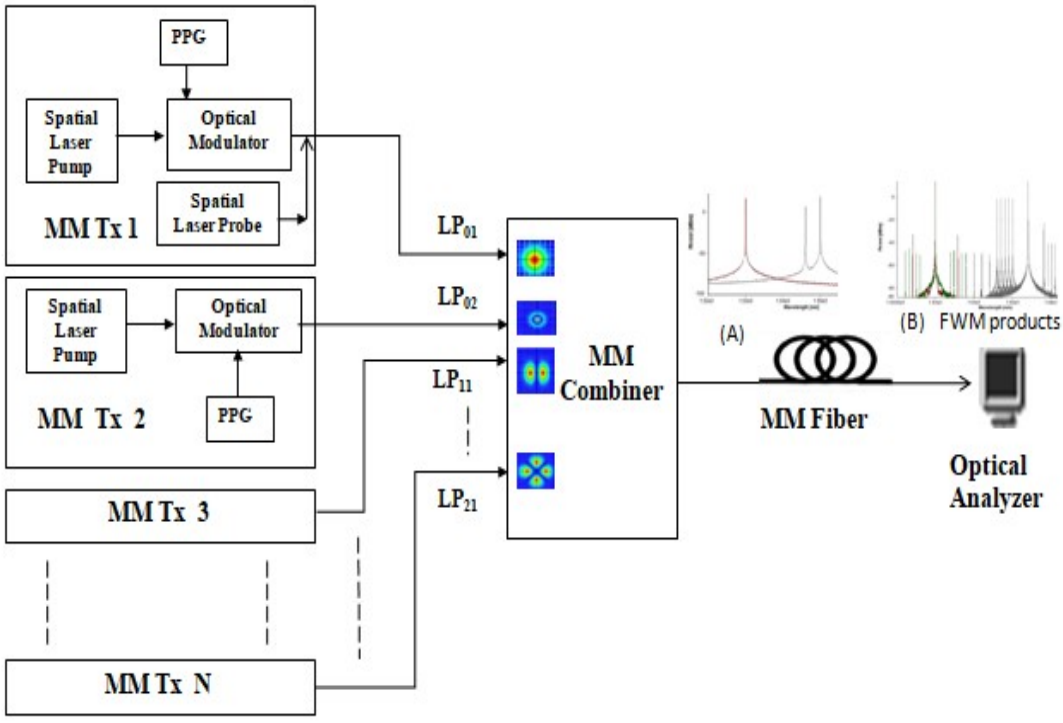

Fig. 3.1 Schematic of Intermodal Non Linear propagation effects in MM Fiber.

The information source is in NRZ format with 10 Gb/s bit rate. The electrical driver creates the suitable data format, converts the binary input signal into electrical one and optical phase modulator modulates the laser pump beam. MM Transmitters superimpose N individual data signals over N different LP_{lm} (linearly polarized) modes.

These different LP_{lm} modes having information are fed to MM (Multi-mode) combiner for multiplexing of all LP_{lm} modes. Further, multiplexed modes propagate through MM Fiber where nonlinear factors affect the propagation of modes. Here, in this setup nonlinear propagation effects like IMFWM (Inter mode four wave mixing) and Kerr nonlinearity are taken into account.

Here, to validate this model with simulation we considered transmission of fourLP modes in MDM over MMF link. It is assumed that these LP modes denoted by *p*, *l*, *m* and *n* propagates within two mode groups (G_u and G_v) over MMF.Here, two mode groups G_u and G_v are assumed to simply analyze the nonlinear factor. The nonlinear factors κ_{uv} are considered that define averaging over the strongly coupled modes within the mode groups G_u and G_v. The factors κ_{uu} are considered to get the averaging within the same mode group G_u. Let us suppose if G_u contains only one spatial mode with two polarizations then κ_{uu} factor can have value of 8/9 according to single mode Manakov equation [108].The nonlinear factors κ_{uv} can be calculated using equation (3.30) [169]:

$$\kappa_{uv} = \sum_{m,n \in M_{u,v}} \sum_{p \in M_u} \sum_{l \in M_v} C_{plmn} \frac{\delta_{lm}\delta_{pn} + \delta_{l\mathrm{n}}\delta_{pm}}{|M_u|(|M_v| + \delta_{uv})} \quad (3.30)$$

where, Kronecker delta function δ_{ij}can be defined as follows [169]:

$$\delta_{ij} = \begin{Bmatrix} 1, i = j \\ 0, i \neq j \end{Bmatrix}$$

The termsM_u and M_v denotes sets of mode indices for modes belonging to the mode groups labeled by *u* and *v*, respectively. The indices *m*, *n* can consider all values in $M_{u,v}$i.e. union of M_u and M_v. The modulus of M_u and M_v represents the number of modes in G_u and $G_{v.}$

The coupling coefficients C_{plmn} can be defined by taking overlap integrals of the modal distributions [170], $\vec{F}_i = \vec{F}_i(f, x, y)$.

$$C_{plmn} = A_0 \frac{2D^{(1)}_{plmn} + D^{(2)}_{plmn}}{3} \quad (3.31)$$

where, coefficients $D^{(1)}_{plmn}$ and $D^{(2)}_{plmn}$ are overlap integrals and subscript 1 and 2 refers to *x* and *y* polarization states of considered. These integrals can be defined by equation (3.31) as [171-173]:

$$D^{(1)}_{plmn} = \frac{\int (\vec{F}_p{}^*.\vec{F}_n)(\vec{F}_l{}^*.\vec{F}_m)dxdy}{N_p N_l N_m N_n}, D^{(2)}_{plmn} = \frac{\int (\vec{F}_p{}^*.\vec{F}_l)(\vec{F}_n{}^*.\vec{F}_m)dxdy}{N_p N_l N_m N_n} \quad (3.32)$$

$\vec{F}_p, \vec{F}_n, \vec{F}_l$ and $\vec{F}_m$ represents real-valued modal fields of modes *p*, *l*, *m* and *n* respectively, '*' dictates complex conjugate of field and $N_p = \int \left|\vec{F}_p\right|^2 n_{ref} dxdy$, where n_{ref} corresponds to refractive index. Now, values of C_{plmn} from equation (3.31) can be substituted to equation (3.7) to calculate nonlinear Kerr factors as shown in Table 3.1. Nonlinear Kerr effect can be calculated for nonlinear propagation of 4 LP modes (*p*, *l*, *m* and *n*) within two mode groups (G_u and G_v) from equation (3.30). Table 3.2 depicts the parameters for the simulation setup.

Table 3.1: Values of Overlap coefficient and nonlinear factors

Mode 1 *p*	Mode 2 *L*	Mode 3 *m*	Mode 4 *N*	Overlap coefficient (C_{plmn})	ModeGroup1 G_u	ModeGroup2 G_v	Nonlinear Factor κ_{uv}
0	0	0	0	1	0	1	0.330835414932
0	0	1	1	$3.33e^{-1}$	1	0	0.330835414932
0	1	1	0	$6.66e^{-1}$	0	0	0.888888888889
1	0	0	1	$6.66e^{-1}$	1	1	0.597493734336

Table 3.2: Model Parameters representing intermodal nonlinear propagation effects in MMF

Component	**Parameters**	**Value**
Spatial Laser	Central frequency	193.2 THz
	Line width	1×10^5 Hz
MMF	No. of core	1
	Modes	LP_{01}, LP_{02}, LP_{11} and LP_{12}
	Length	83 km
	Nonlinear Index	$2.9 \times 10^{-20} m^2/W$
	Attenuation	0.234 dB/km
	Intermodal group delay	5.2×10^{-15}
	Dispersion	$18.6 \times 10^{-6} s/m^2$ to 23.5×10^{-6} s/m^2
	Differential Group Delay	-0.4×10^{-12} s/m^2 to -0.1×10^{-12} s/m^2

Finally, Optical analyzer was used to observe the effect of non-linearity on different modes propagating through the MM Fiber.

3.3.4 Result and Discussion

Figure 3.2 represents the light intensity patterns at input and output of MM Fiber when nonlinear propagation effects are not taken into account. The intensity patterns of 4 LP modes (LP_{01}, LP_{02} and LP_{11} and LP_{12}) as generated at MM transmitter section are shown in the left side of curve.

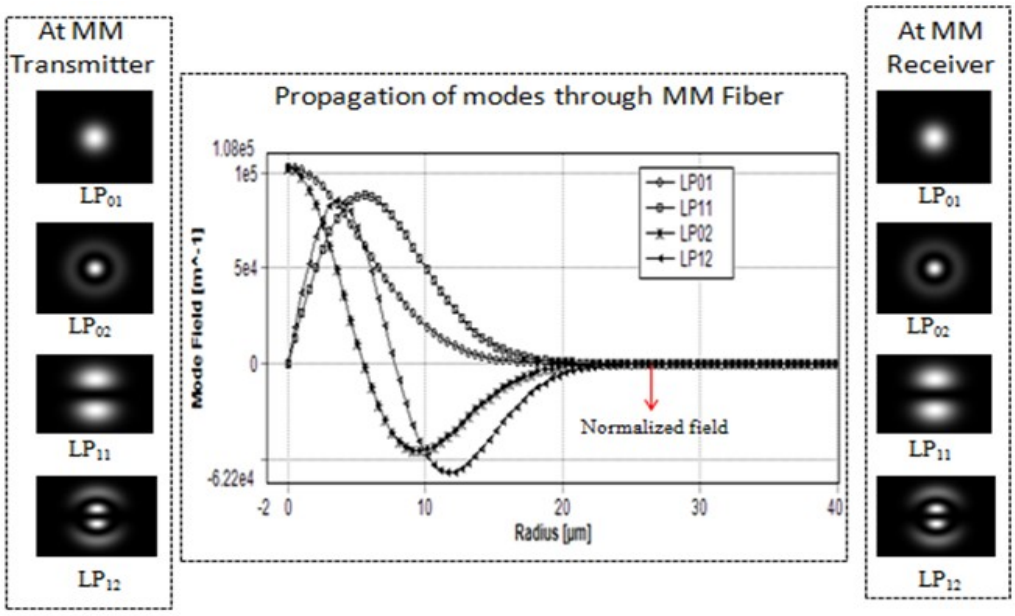

Fig. 3.2 Intensity distribution of LP_{lm} modes at input and output of MM Fiber.

The field of these modes was normalized by mode combiner and then the normalized mode fields with respect to radius as propagating through MM fiber is represented by curve. After propagation through MM fiber the intensity distribution of modes as observed by Spatial Analyzer is shown by right side of curve.

The powers launched into the GI-MMF for the simulation setup: 18 dBm for the LP01 pump P1, 17 dBm for the LP11 pump P2, 8 dBm for the LP11 probe PB, 12 dBm for the LP02 pump P3 and 10dBm for the LP12 pump P4. Fig. 3.3 depicts the observed spectrum at input of multimode fiber when wavelengths of pumps P1, P2, P3 and P4 are set to 1530 nm, 1542 nm, 1554 nm and 1566 nm and LP11 probe is set to 1538 nm respectively. The information signal superimposed over multiple modes encounter nonlinear propagation effects after propagating through MMF.

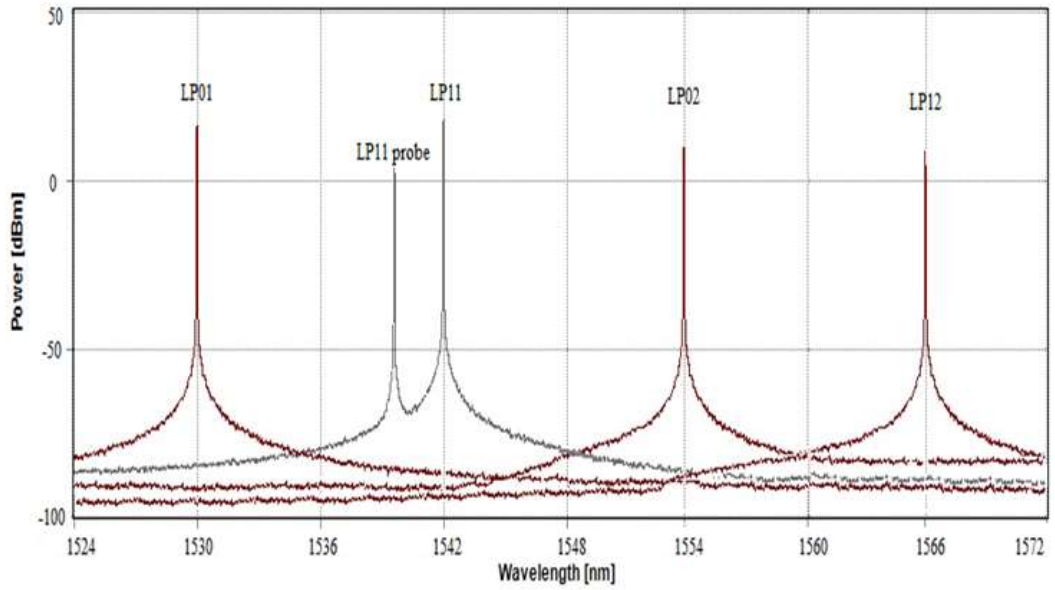

Fig. 3.3 Observed spectrum at input of MMF when pump modes: LP01, LP11, LP02 and LP12 are set to 1530 nm, 1542 nm, 1554 nm and 1566 nm respectively.

Fig. 3.4 depicts the optical spectrum representing four wave mixing products generated between the considered modes at the output of MMF. It can be seen that inter-modal FWM takes place between all the considered pump modes: LP_{01}, LP_{11}, LP_{02} and LP_{12} whereas intramodal FWM takes place between pump and probe of LP_{11} mode.

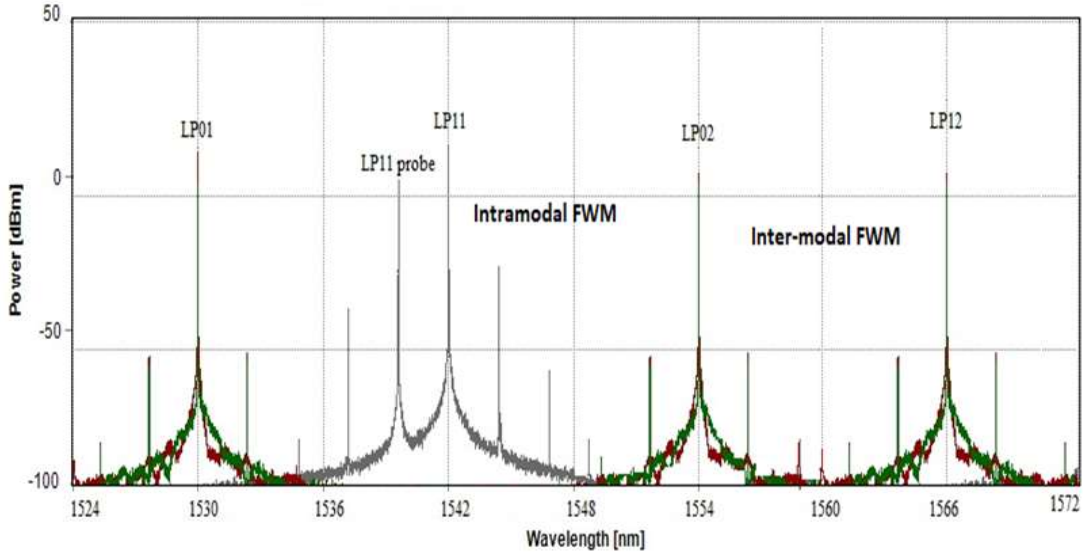

Fig. 3.4 Observed spectrum with inter-modal and intramodal four wave mixing effect in MMF.

It is observed from Fig. 3.4 that there are four different pump modes at different frequencies that co-propagate along the MMF, get mixed and generated new sidebands. Here, for four co-propagating modes launched into the MMF, generated a total of 24 mixing products. Now, LP_{11} probe and pump are moved to different wavelengths to analyze the effect of inter and intra modal FWM in MMF. In Fig. 3.5 (a), the LP_{11}probe is varied with a sweep of 1538 nm to 1541 nm and LP_{11} pump P2is moved from 1542 nm to 1544 nm keeping pumps P1, P3 and P4 fixed. Let us consider the case in which there are only two waves: LP_{11}probe and LP_{11}pump.

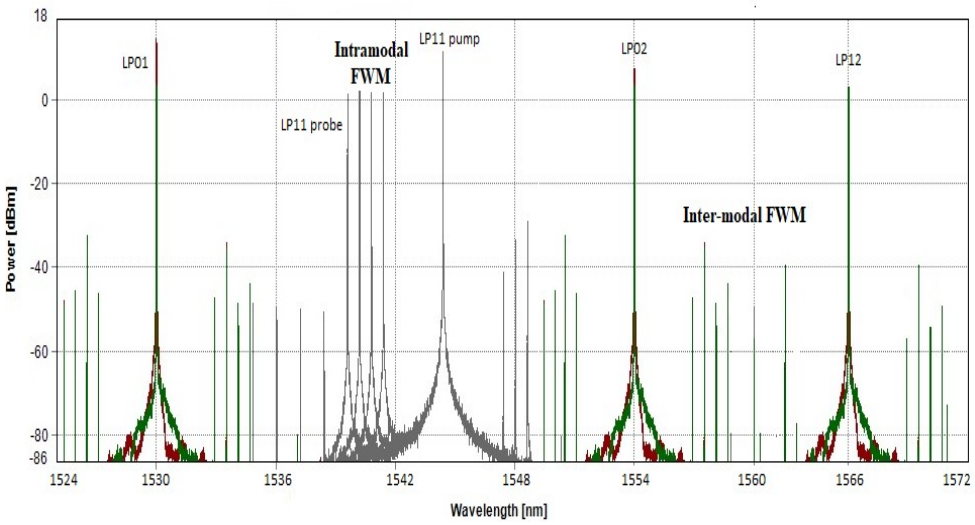

(a)

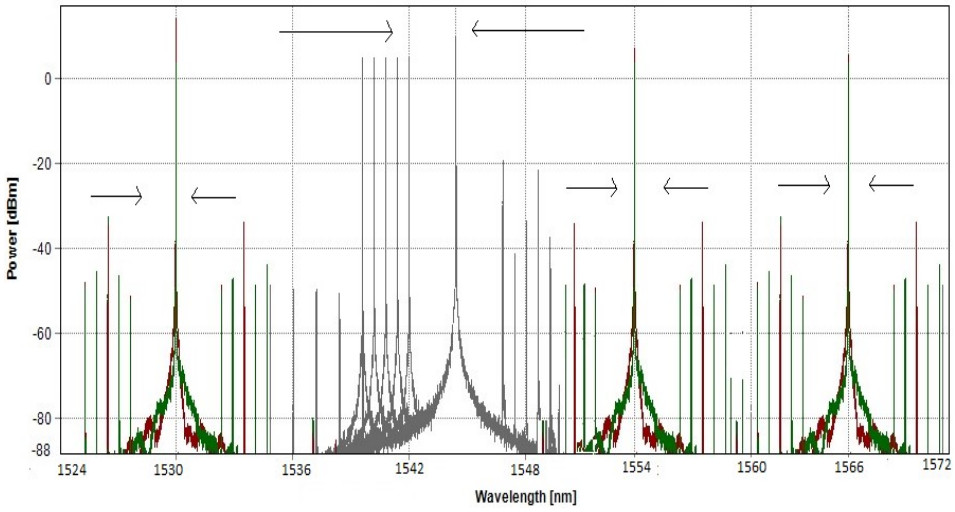

(b)

Fig. 3.5(a) IMFWM products when LP_{11} probe and pump modes are moved to different wavelengths in MMF and (b) Further, generated FWM products grow in number with further variation in wavelength of probe.

It can be examined from Fig. 3.5 (a) that when wavelengths of LP_{11} probe and pump are at 1538 nm and 1542 nm then generated sidebands are at 1534 nm and 1546 nm whereas when both LP_{11} probe and pump are moved to wavelengths of 1541 nm and 1544 nm then new generated sidebands also moved to 1534 nm and 1546 nm respectively.Further, these generated sidebands along with the considered modes travel inside the MMF resulting in the increase in number of sidebands as shown in Fig. 3.5(b). It can be concluded that high launch power and low dispersion generated sidebands both in case of inter-modal and intramodal FWM. These FWM products grow in number with variation in wavelength of probe as well as these products grows towards the central pump frequency of that particular mode. Thus, nonlinear interaction between modes resulted into interference that degraded the performance of multichannel mode division multiplexed system.

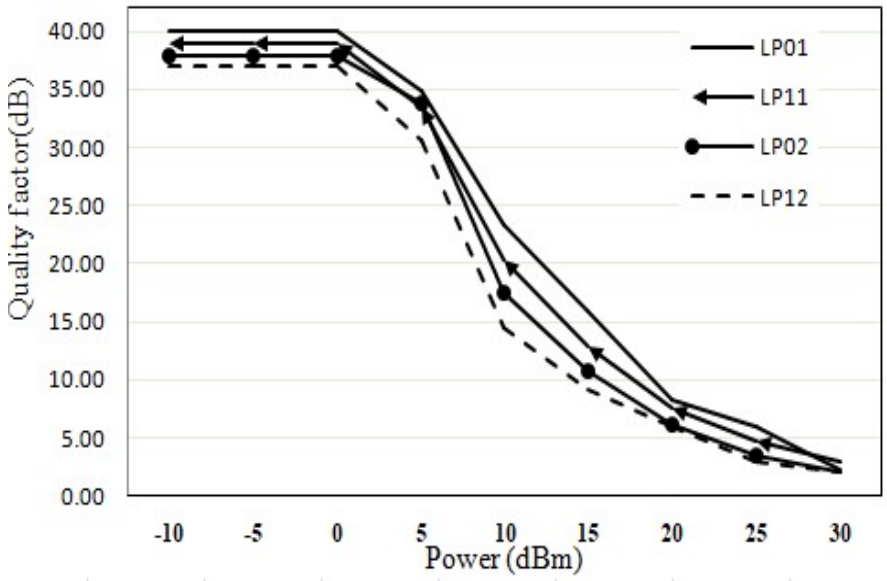

Fig. 3.6 Quality of 4 LP modes in Optical MDM MMF link with variation in power.

Figure 3.6 illustrates that as input power of optical mode division multiplexed system over MMF link is increased, nonlinear effects starts originating and the quality of system starts degrading. Here, at optimal power of 0dBm the quality of LP modes is near 39 dB and above 21.8 dB nonlinear interaction between modes resulted into interference that degraded the performance of mode division multiplexed system.

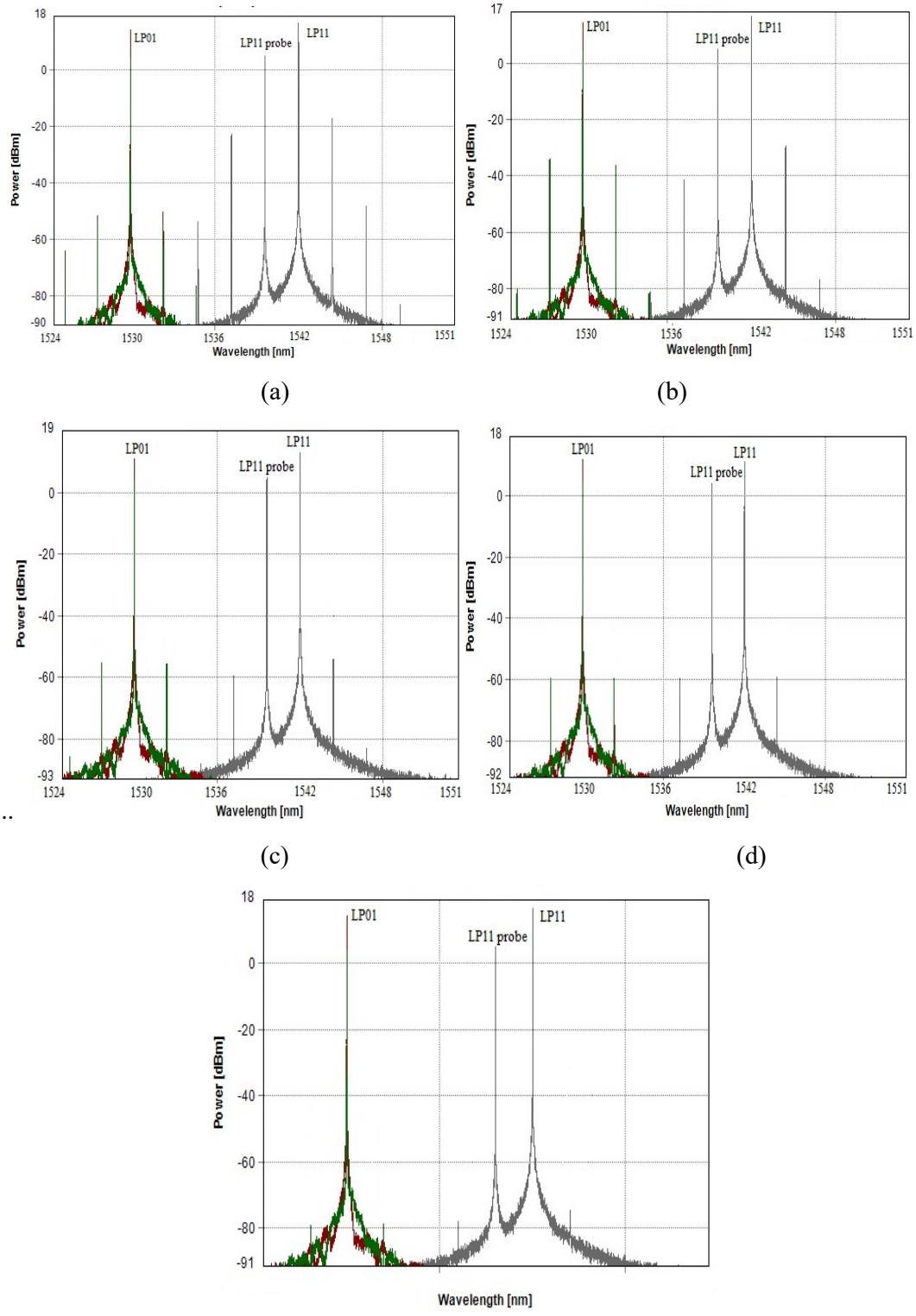

Fig. 3.7 Observed spectrum when chromatic dispersion of LP_{11} pump mode is at (a) 18.5 s/m^2, (b) 19.5 s/m^2, (c) 20.5 s/m^2, (d) 21.5 s/m^2 and (e) 22.5 s/m^2.

In Fig. 3.7, chromatic dispersion has been increased throughout the link to reduce the effect of intermodal four wave mixing. Here, in this value of chromatic dispersion of pump mode LP_{11} is increased from 18.5 s/m^2 to 22.5 s/m^2. Fig. 3.7 depicts optical spectrum representing the effect of intermodal FWM when chromatic dispersion of LP11 pump mode is at (a) 18.5 s/m^2, (b) 19.5 s/m^2, (c) 20.5 s/m^2, (d) 21.5 s/m^2 and (e) 22.5 s/m^2.

It can be concluded that with the increase in chromatic dispersion the effect of inter-modal FWM over MMF link gets reduced. The efficiency of FWM is dependent on matching phase relation between interacting waves. As dispersion varies with wavelength and original modes and generated wave modes have different group velocities. So, the phase matching between these interacting modes gets destroyed and the efficiency (at which power transferred to newly generated waves) lowers down. Therefore, higher the value of chromatic dispersion, higher is group velocity mismatch between interacting waves and lower is the four wave mixing effect.

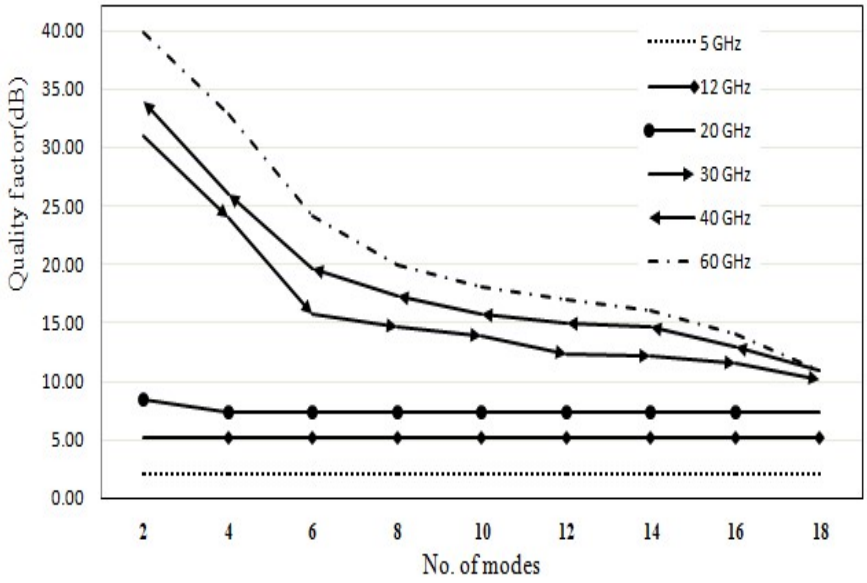

Fig. 3.8 Performance of MDM system with increase in number of modes at different channel spacing.

Fig. 3.8 depicts the performance quality of MDM system with increasing number of LP modes at different values of channel spacing covering 83 km transmission distance. The increase in number of modes, increases interference, decreases Q-factor thus, increases Inter-modal FWM. It can be examined that when channel spacing is small (5 GHz, 12

GHz and 20 GHz) then quality is very poor and with increase in channel spacing up to 60 GHz, interference decreases, Q-factor increases and Inter-modal FWM decreases. These results prove better performance over [173] in which authors demonstrated FWM between 2 spatial modes (LP_{01} and LP_{11}) over 5 km few-mode fiber.

3.4 Conclusion

This chapter represents the effect of nonlinear propagation in mode division multiplexed multimode fiber link. The effect of inter-modal four wave mixing (IMFWM) and intramodal FWM for waves with different spatial modes (LP_{01}, LP_{02} and LP_{11} and LP_{12}) over MMF having THz wave spacing has been analyzed. Further, the multi-mode nonlinear propagation of different mode groups (containing N spatial modes in each group) due to Kerr effect has been discussed mathematically. It can be concluded that high launch power (> 15dBm) and low dispersion (18 s/m^2) generated sidebands both in case of inter-modal and intramodal FWM but with increase in value of chromatic dispersion of pump mode LP_{11} from 18.5 s/m^2 to 22.5 $s/m^2$and channel spacing up to 60 GHz, interference decreases, Q-factor increases up to 40 dB and Inter-modal FWM decreases in optical mode division multiplexed MMF link.

CHAPTER 4
INVESTIGATION OF OPTICAL MIMO MDM USING LINEARLY POLARIZED MODES

4.1 Introduction

In order to achieve this objective, firstly LP_{lm} modes are investigated over multimode fiber link to enhance MIMO Mode Division Multiplexing. Four different groups of linearly polarized modes are taken into account to observe the receiver performance of OMIMO-MDM system. The transmission distance for four different groups of LP_{lm} modes with mode index M (Even, Odd, Random Even+Odd and Symmetric with mode gap unity) has been varied to observe the performance for different configurations of OMIMO MDM over MMF link. The performance of the system is restricted due to mode group coupling and only a maximum distance of 90 km is achieved with acceptable BER ($<10^{-9}$). So, the output signal is optimized using signal LMS (least mean square) adaptive MIMO filter algorithm in order to reduce mode coupling and intermodal crosstalk. This objective is presented in different Sections as follows: Section 4.2 deals with mode calculation algorithm and how LP_{lm} modes affect the performance of MIMO MDM; in Section 4.3 mode coupling is discussed and effect of different mode groups on MM receivers is presented and further, performance optimization is described in Section 4.4. In Section 4.5, outcomes are discussed.

4.2 Investigation of LP modes over MMF link to enhance MIMO Mode Division Multiplexing

4.2.1 Mode Calculation Algorithm

Each guided mode is a solution of wave equation travelling along fiber forming pattern of electric and magnetic field distributions except for change in its total scaling and phase [43]. In case of multimode fibers each mode denotes light energy travelling within the core of fiber at different angles. Mostly for communication fibers where index difference between the core and cladding is moderately small, different modes can be grouped collectively into a single series of modes referred to as LP (Linearly Polarized) modes [45]. All LP_{lm} modes with mode index, $M = l+2m+1$ (as discussed in Section must fulfill the equation with same phase constant β and group delay τ_g.

The mode calculation algorithm is used to calculate modes in MDM system. For GI-MMF modes can be computed by utilizing Helmholtz radial equation with different

index profile in particular defined computational window Δ_{tot}. Thus, the equation defining transversal field is following [174]:

$$\hat{D}E = \left[\frac{1}{r}\frac{\partial}{\partial r}\left(r\frac{\partial E}{\partial r}\right) - \frac{l^2}{r^2}E + \varepsilon(r)k_0^2 E\right] = n_{eff}^2 k_0^2 E \tag{4.1}$$

where, D: differential operator, E depicts mode field distribution, l represents variation of light intensity in azimuthal plane, n_{eff} is effective propagation index and $k_0$represents wave vector of incident light.

In this algorithm a scalar approach is followed where terms related to polarization mode coupling are neglected. An adaptive solution grid is utilized where the total number of grid points or radial points can be defined by G_{tot}. It is considered here that the spacing between the grid points is not constant. The grid is chosen such that: Δ_1 grid is made dense for the areas where major part of mode power is focused and Δ_2 grid is made rough within areas having lower refractive index. Thus, the ratio of Δ_2 grid to Δ_1 grid can be defined as grid discrete factor (G_f). If it is unity then a grid with constant mesh is utilized. The index of discretized point (G_I) provides the index profile for which the spacing of grid is varied is given as [175]:

$$G_I = \frac{\frac{1}{2}(1-G_p) + (G_{tot}-1)}{G_p + G_f - 1} \tag{4.2}$$

where, $G_p = G_{tot} / \Delta_M$presents the proportion of fiber core within the whole computational window. Here, term Δ_M is dependent on the method of attaining the refractive index profile. As graded index profile is used in block diagram thus, Δ_M is considered to be $2a$, where a: diameter of core. The computational window is to be made large enough for mode power to attenuate significantly at the boundaries. The grid discretization intervals can be calculated by putting value of G_I from equation (4.2) in (4.3) as [175]:

$$\Delta_1 = \frac{\Delta_M}{G_I + 1/2}, \Delta_2 = \Delta_1 . X \tag{4.3}$$

The coordinate r_i can be defined by equation (4.4) as below [175]:

$$r_i = \begin{cases} (i+1/2)\Delta_1, i \le G_I \\ (G_I + 1/2)\Delta_1 + (i - G_I)\Delta_2, G_I < i \le G_{tot} - 1 \end{cases} \tag{4.4}$$

By solving all these equations a computational grid is set with profile then finally mode intensity profiles of LP modes can be computed in polar coordinates as [174]:

$$i^{(u,k)}(r,\phi) = i^{(u,k)}(r)\begin{Bmatrix}(\cos l\phi)^2\\(\sin l\phi)^2\end{Bmatrix} \quad (4.5)$$

where, $i^{(u,k)}(r)$ represents the radial dependence of mode intensity and terms of cosine and sin depicts two spatial configurations of mode u.In optical fibers with $\Delta<<1$ (low index contrast between core and cladding), linearly polarized modes are dictated as weakly guided. It is clear from equation (1.1) as discussed in Chapter1, for LP_{lm}modes with $l \geq 1$: two spatial modes depicting sine: $LP_{lm\text{a}}$ or cosine: $LP_{lm\text{b}}$ configuration and further each having 2 polarization states. Thus, in total of four degenerate (same propagation constant β) modes are formed. For LP_{0m}modes with $l = 0$: one spatial mode with only two polarization states forming two degenerate modes. The linearly polarized $LP_{0\text{m}}$ modes are the two-fold degenerate hybrid HE_{1m}modes. The $LP_{1\text{m}}$ modes are produced by addition of exact modes: HE_{2m}+ TE_{0m}or HE_{2m}+ TM_{0m} forming four-fold degenerate as shown in Table 4.1. Similarly, $LP_{l\text{m}}$ modes for l >1are formed with the addition of hybrid modes: $HE_{l+1,\text{m}}$+ $EH_{l-1,\text{m}}$ [25].

Table 4.1: Formation of LP_{lm} Modes

Hybrid or Exact modes	**LP_{lm} modes**	**Spatial intensity distribution**	**3D profile**
HE_{11}	LP_{01}	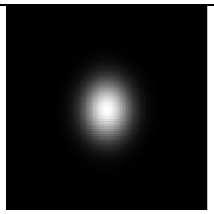	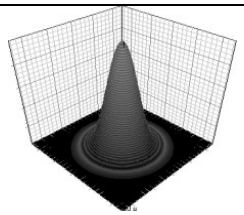
HE_{21} + TE_{01} + TM_{01}	LP_{11a}	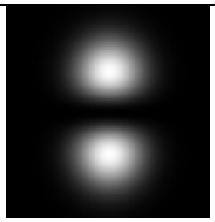	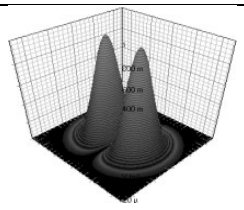
	LP_{11b}	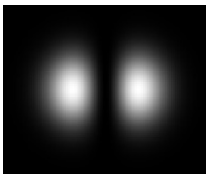	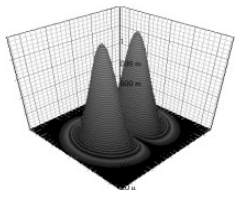

HE_{12}	LP_{02}	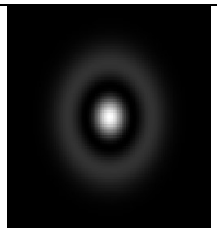	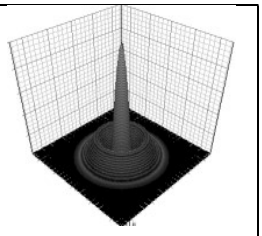
$HE_{31}+EH_{11}$	LP_{21a}	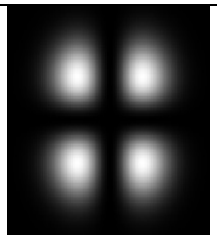	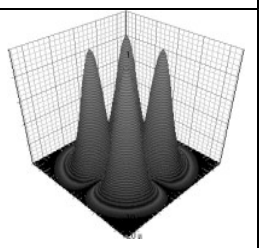
	LP_{21b}	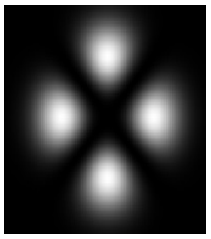	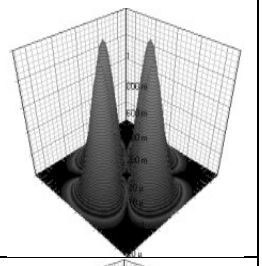
$HE_{41}+EH_{21}$	LP_{31}	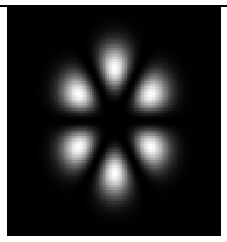	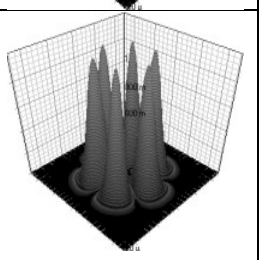
$HE_{22}+TE_{02}+TM_{02}$	LP_{12}	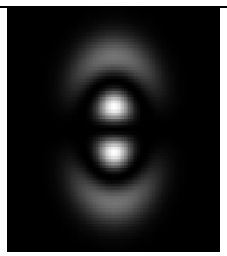	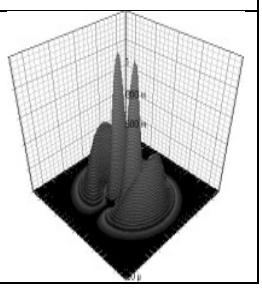

4.2.2 System Setup

The simulation setup of proposed optical MIMO (Multi input multi ouput) Mode division multiplexed system is done is OptiSystem version 7 presented in Fig.4.1. Each MM Tx(multimode transmitter) includes spatial laser source tuned at 1550 nm and MZ modulator for each information source. The information source is in NRZ format with 10 Gb/s bit rate. The electrical driver creates the suitable data format, converts the binaryinputsignal into electrical one and MZ modulator modulates the laser light. The independent data signals superimposed over N number of LP_{lm} (linearly polarized)

modes from N transmitters are fed to mode converter for mode conversion and then to mode combiner for multiplexing of all LP_{lm} modes. Inline Multimode EDFA is designed as MM amplifier using phasor plates to amplify multiple spatial modes having multi-mode information signals at 1550 nm through graded index MMF with parabolic index.

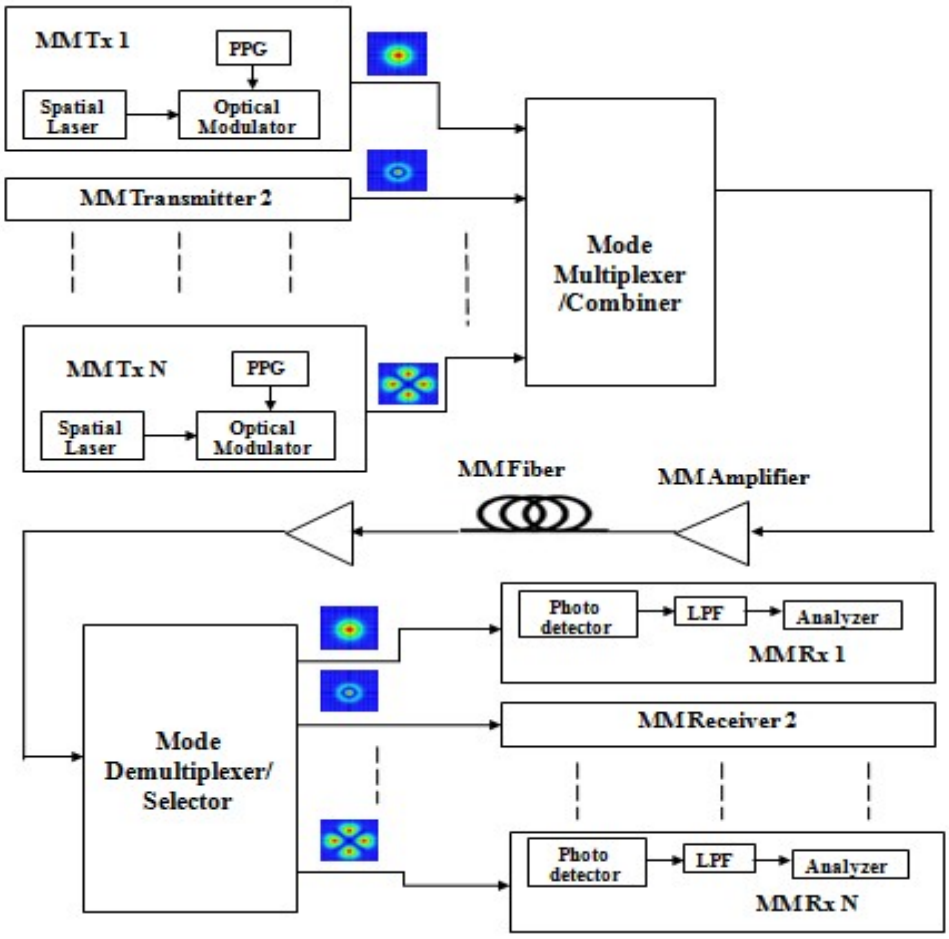

Fig. 4.1 Schematic of MIMO MDM transmission system

The index gradient causes rays propagating at steeper angles (high order modes) to catch up with rays propagating at shallow angles in the fiber. Due to this feature of graded-index fiber, it provides less pulse dispersion than step-index fibers and therefore, superior bandwidth performance. In inline-MM EDFA configuration transmitted modes in the system are symmetrically amplified to reduce transmission losses.

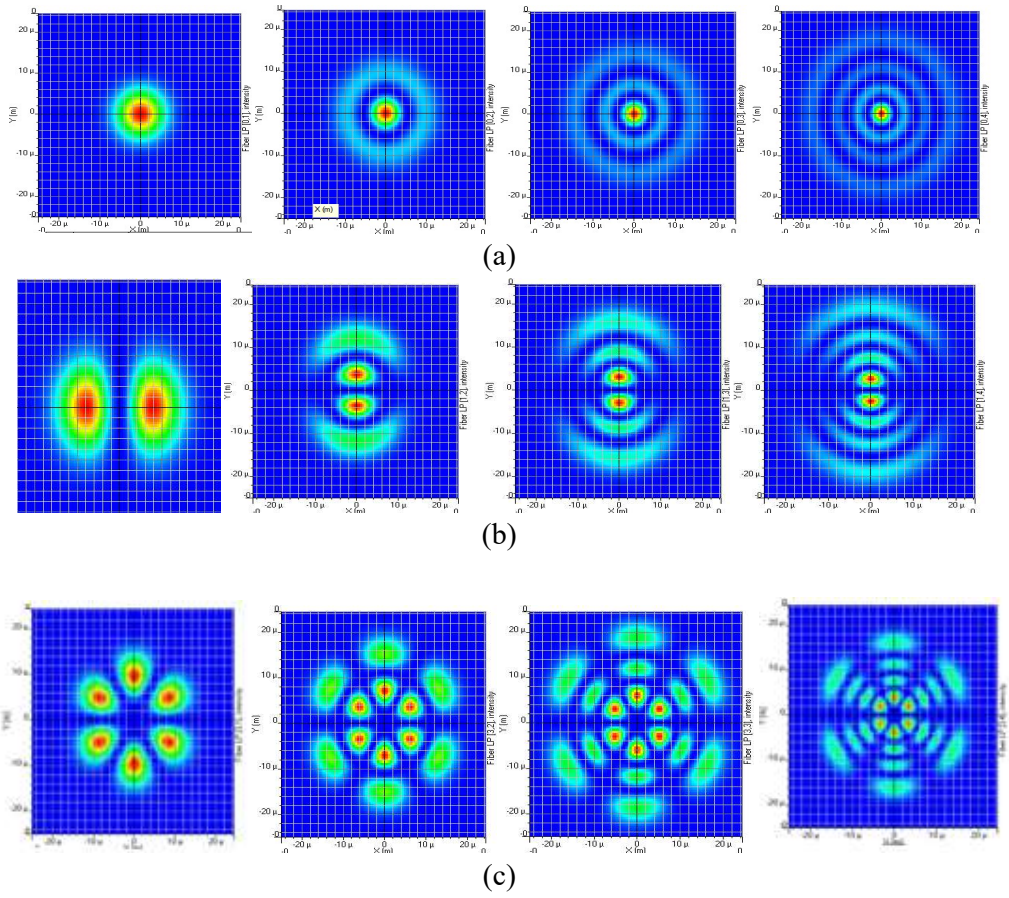

Fig. 4.2 Spatial intensity field patterns of LP modes for different values of *l* and *m* indices as observed by spatial analyzer (a) for *l*=0, *m* varies from 1 to 4, (b) for *l*=1, *m* varies from 1 to 4 and (c) for *l*=3, *m* varies from 1 to 4.

Table 4.2: Simulation parameters of MIMO MDM system

Sr. no.	Name of parameter	Value
1	Wavelength	1550 nm
2	Power	0 dBm
3	Linewidth	10 MHz
4	Attenuation	2.61 dB/km
5	Noise Figure	4 dB
6	Dispersion	-100 ps/nm/km
7	Responsivity	1 A/W
8	Dark current	10 nA

Here, 9 different linearly polarized modes are first multiplexed, transmitted through MMF link and then received. In receiver section, signals having different LP modes are selected by spatial mode selectors. The independent signals from *N* MM (multi-mode) receivers are recovered by MIMO processing technique. The various simulation parameters of MIMO MDM transmission system are described in Table 4.2. Each MM receiver contain PIN photo detector with responsivity of 1 A/W is used to convert the received light signal into electrical signal followed by a LPF; optical analyzer for monitoring the BER, eye diagram and Quality-factor of transmission link and SA (spatial analyzer) to observe intensity profiles of LP_{lm} modes in the entire schematic (Fig. 4.2).

4.2.3 Result and Discussions

The transmission distance from 10 to 90 km for various LP modes has been increased to investigate the performance quality of (4×4, 6×6 and 9×9) MIMO MDM configurations. Fig.4.3 illustrates the graphical representation of Q^2 factor as a function of transmission length.

It is observed from Fig.4.3(a) that 4×4 MIMO MDM system containing LP_{01}, LP_{02} and LP_{11} modes provide Q^2 factor above 8.6 dB covering long distance of 90 km but LP_{12} mode covering 80 km. For 6×6 MIMO system; modes LP_{01}, LP_{02}, LP_{11} and LP_{12} travel over 90km MMF link, LP_{03} over 82 km whereas LP_{04} over 75km with quality of signal more than minimum acceptable level.

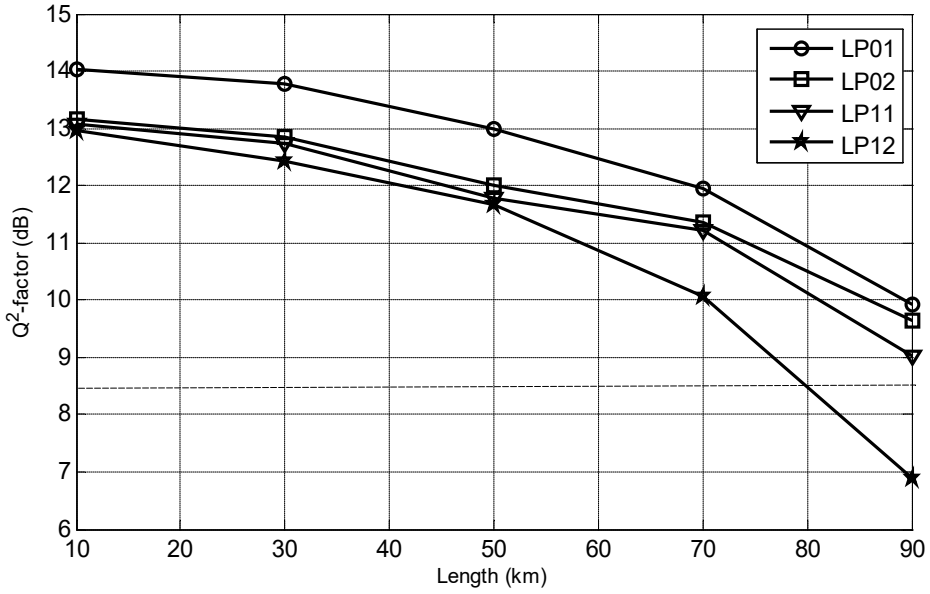

(a)

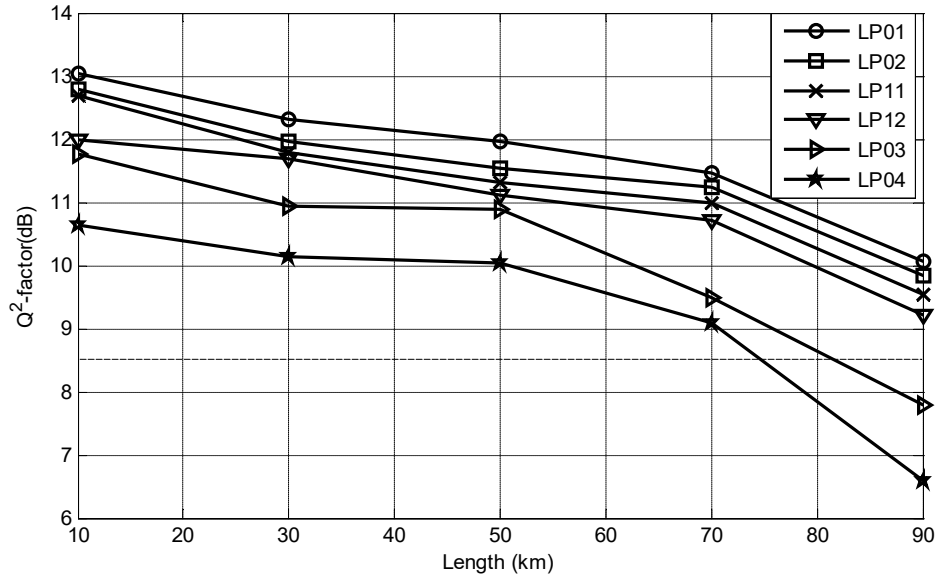

(b)

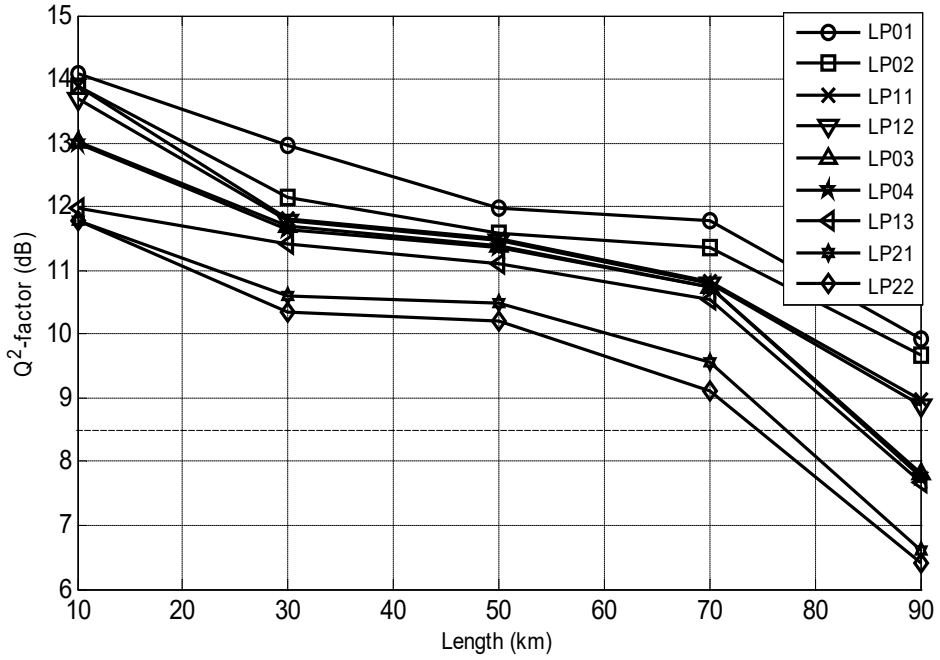

(c)

Fig. 4.3 Quality of LP modes as a function of transmission distance for (a) 4×4 (b) 6×6and (c) 9×9 MIMO MDM systems.

It is shown in Fig. 4.3(c) that modes (LP_{01}, LP_{02}, LP_{11} LP_{03}, LP_{12}; LP_{04}, LP_{13} and LP_{11}, LP_{22}) propagate with good quality of signal (> 8 dB) covering transmission distance of 90, 85 and 75 km over MMF link. It is seen that, system provided best results even for 9 different LP modes over MMF link travelling a long distance of 75 km with Q^2 factor

above 8 dB. These results indicate that LP_{01}, LP_{02} and LP_{11} modes provide quality more than the power margin i.e. 10 dB over 90km for all considered MDM configurations, this shows an improvement over [35].

Fig.4.4 shows the graphical representation of BER as a function of transmission length for different LP modes propagating in 4×4, 6×6 and 9×9 MIMO MDM systems. It is necessary to observe the transmission quality of MIMO MDM system with respect to bit error rate to determine the longest possible distance.

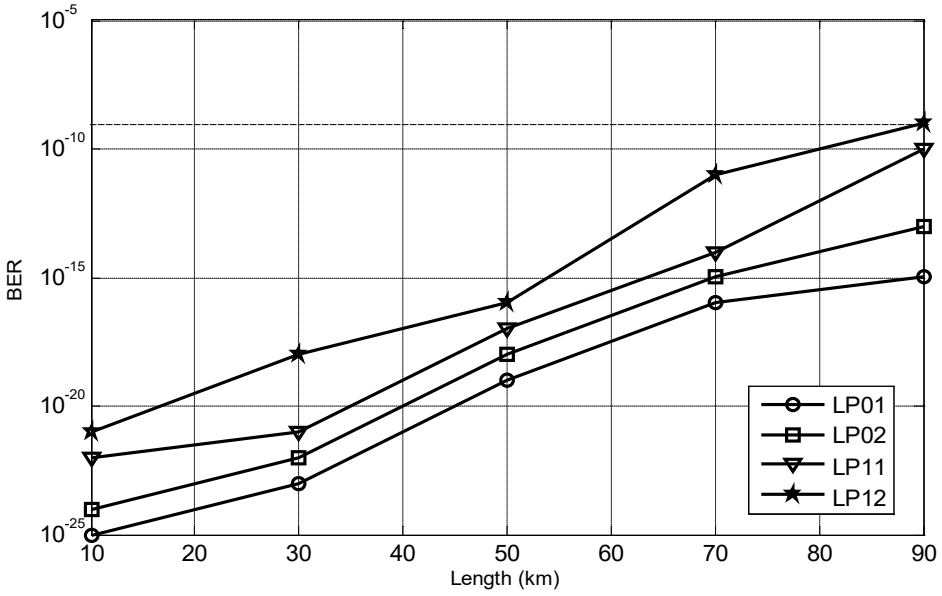

(a)

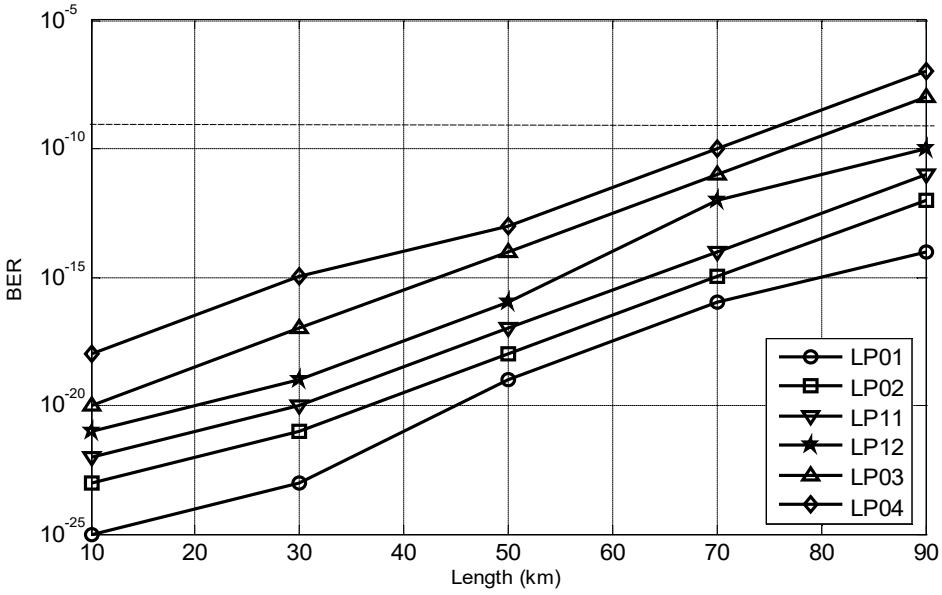

(b)

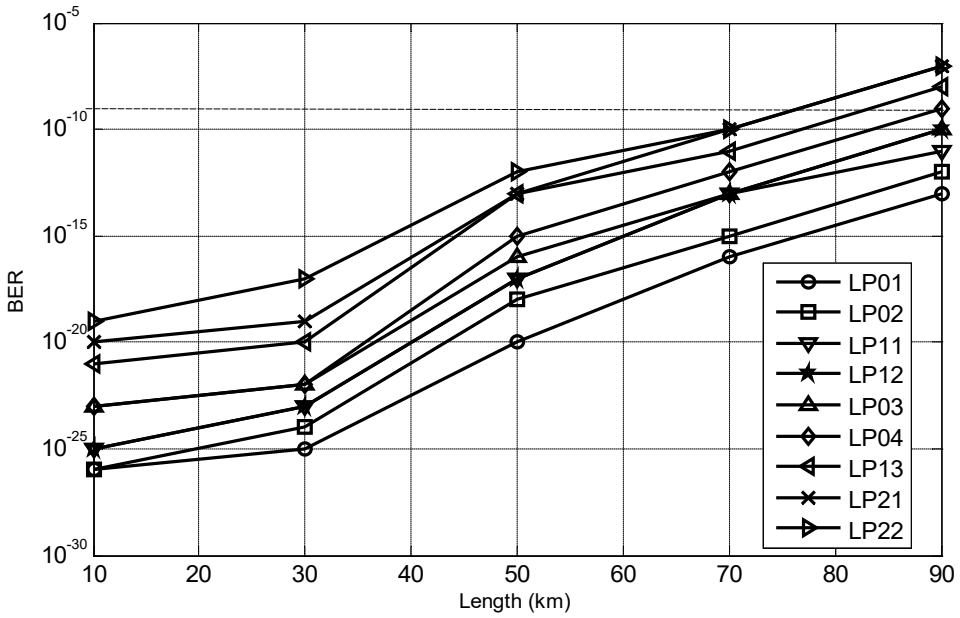

(c)

Fig. 4.4: BER across LP modes as a function of distance for (a) 4×4 (b) 6×6 and (c) 9×9 MIMO MDM systems.

The bit error rate is measured for different MIMO formats over different modes with different transmission distances as shown in Fig.4.4. It is observed that a maximum of 90 km transmission distance is covered by modes (LP_{01}, LP_{02}, LP_{11} and LP_{12}) with acceptable bit error rate of 2.6×10^{-9} for 4×4, 6×6 and 9×9 MIMO MDM system. On the other hand, LP modes (LP_{03}, LP_{13} and LP_{04}, LP_{21}, LP_{22}) performs with poor quality above distance (i.e. 82km and 75km)respectively as presented in Fig.4.4(b, c).

4.3 Investigation of OMIMO-mode group division multiplexing with mode coupling over MMF

4.3.1 Concept of Mode coupling

Mode coupling can be defined as the transfer of energy from one mode to another. During the propagation of modes through MMF, perturbations like imperfections and mechanical stress leads to relatively weak mode coupling. In the absence of perturbations, no mode coupling takes place inside fiber. According to theoretical analysis, mode coupling can be related to effective index differences between the considered spatial modes [176]. If mode coupling to be minimized, the expression $\left|\eta_{eff,M1} - \eta_{eff,M2}\right|$ has to be maximized [177]. Some experiments had already been performed to measure mode coupling in transmission system after transmission over

fiber spans of different length [176,178]. For having long transmission MDM system it is required to interconnect fibers without affecting system performance.

If incident light beam is coupled from single mode fiber to multimode fiber then coupling of energy takes place between different spatial modes of input fiber and output fiber. In order to calculate the energy which is transferred between different modes of input and output fiber, we have to calculate mode field of input mode (E^{in}) and mode field of j^{th} output mode (E_j^{out}) from all possible guided output modes. This can be mathematically related as [43], [178]:

$$E_j^{out}(t) = \eta_j E^{in}(t) \tag{4.6}$$

where, η_j can be defined as coupling coefficient from k^{th} mode of the input field (rotated or inclined) to j^{th} mode of the output field. These coefficients can account for the offset and rotation of input beam with respect to MMF as output fiber. The power coupling coefficients can be calculated as[43]:

$$\eta_{k\to j} = \frac{\left|\iint r E_j E^* dr d\phi\right|^2}{\left(\iint r \left|E_j\right|^2 dr d\phi\right)\iint r \left|E\right|^2 dr d\phi)} \tag{4.7}$$

These power coupling coefficients represents an overlap integral of the non-normalized electric mode field of j^{th} mode E_j and the non-normalized incident mode field E.

4.3.2 System Setup

To investigate the effect of mode index grouping combinations on performance of different MIMO-MGDM configurations, the simulation layout is shown in Fig.4.5. Each MM transmitter includes laser source and MZ modulator for each information source and the information source is in NRZ format with 10 Gb/s bit rate. Signals over N (= 3, 4, 5, 6, 7, 8 and 9) different LP_{lm} (linearly polarized) modes from N corresponding transmitters are fed to mode converter for mode conversion and then to spatial mode combiner (indicated as SC) for multiplexing of all the LP_{lm} modes. The values of coupling coefficients for different LP modes are shown in Table 4.3.

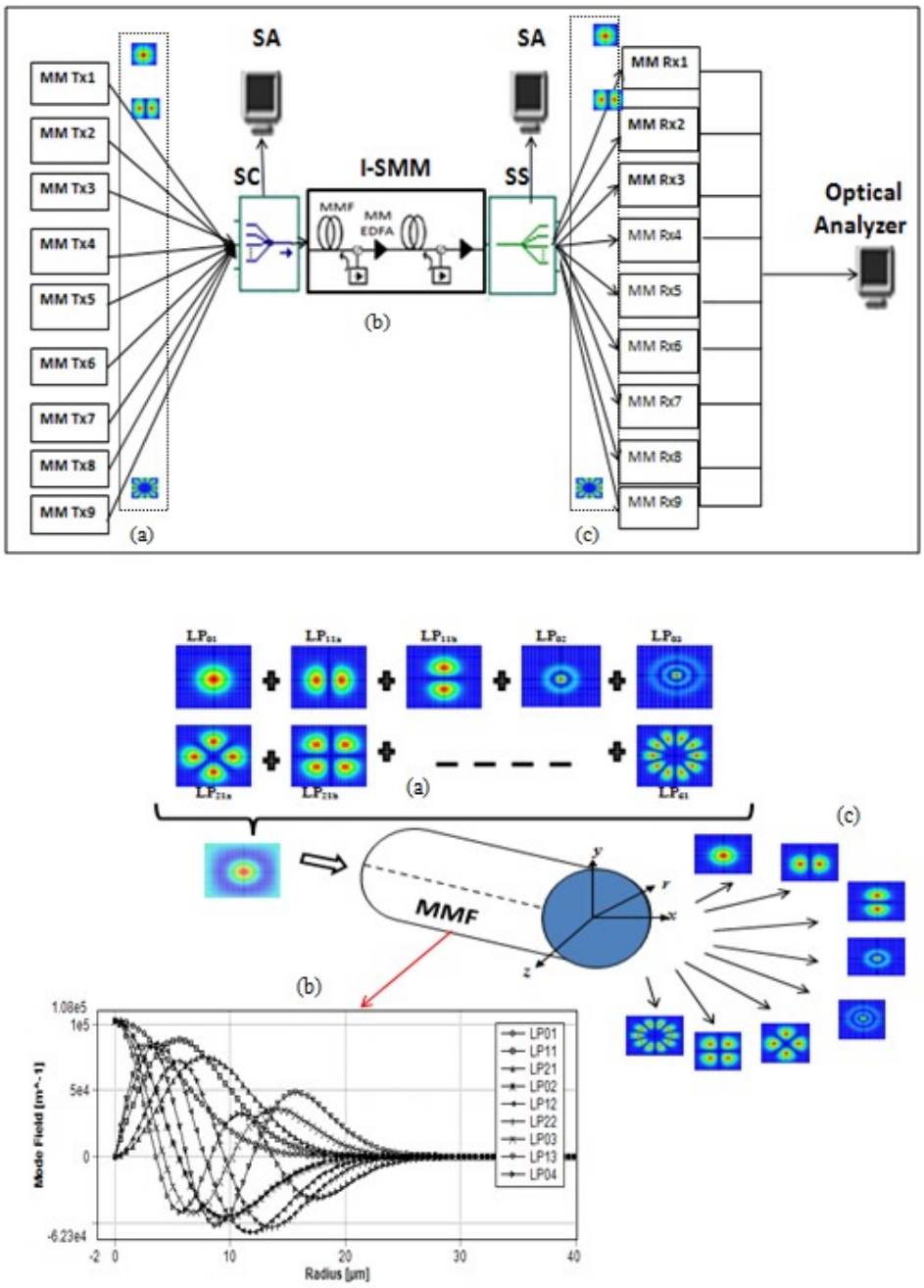

Fig.4.5. System setup of 9 channel OMIMO-MGDM communication system; SC: spatial combiner, SS: spatial selector + splitter, SA: spatial analyzer, I-SMM: inline-MM EDFA amplifier configuration, MMF: multimode fiber, MM EDFA: multimode EDFA amplifier (a) Intensity profile of LP modes at MM Transmitter, (b) Normalized mode field distribution of modes propagating through MM fiber and (c) Intensity profile of LP modes at MM Receiver.

Table 4.3: Coupling coefficient values

Fiber Modes	Coupling Coefficient	Coupling phase
LP_{01}	1.25E-09	3.141592654
LP_{11}	1.21E-41	0
LP_{02}	1.83E-07	3.141531741
LP_{21}	1.87E-07	3.141592654
LP_{12}	6.19E-40	6.61E-07
LP_{31}	1.90E-39	0
LP_{03}	6.31E-06	0.000351918
LP_{22}	8.63E-06	-1.04E-05
LP_{41}	2.33E-06	0
LP_{13}	9.62E-39	-9.94E-08
LP_{32}	5.68E-38	1.32E-08
LP_{51}	6.63E-38	0
LP_{04}	9.20E-05	3.141084173
LP_{23}	0.0001415	7.10E-05
LP_{42}	6.11E-05	1.893939104
LP_{61}	1.16E-05	0

Inline-spatial multimode (I-SMM) EDFA is designed to amplify multiple spatial modes having multi-mode information signals at 1550 nm through graded index MMF with parabolic index. Four different groups of mode combinations are considered step by step in the setup (Table 4.4)to observe effect of mode coupling on performance of MIMO MGDM system:-

Table 4.4: Grouping of Modes

Groups	Mode index M	LP_{lm} Modes
Group G-I	M is even 4, 6, 8, 10, 12	$LP_{11}, LP_{12}, LP_{13}, LP_{14}, LP_{15}$ $LP_{31}, LP_{32}, LP_{33}, LP_{34}$ $LP_{51}, LP_{52}, LP_{53}$ LP_{71}, LP_{72} LP_{91}
Group G-II	M is odd 3, 5, 7, 9, 11	$LP_{01}, LP_{02}, LP_{03}, LP_{04}, LP_{05}$ $LP_{21}, LP_{22}, LP_{23}, LP_{24}$ $LP_{41}, LP_{42}, LP_{43}$ LP_{61}, LP_{62} LP_{81}
Group G-III	Random mix Even + Odd	$LP_{01}, LP_{02}, LP_{11}, LP_{04}, LP_{13}$ $LP_{01}, LP_{21}, LP_{02}, LP_{03}, LP_{13}$ $LP_{01}, LP_{02}, LP_{12}, LP_{32}, LP_{13}, LP_{21}$
Group G-IV	Symmetric mix Gap of M=1	$LP_{01}, LP_{11}, LP_{02}, LP_{12}, LP_{03}$ $LP_{01}, LP_{11}, LP_{21}, LP_{31}, LP_{41}, LP_{51}$ $LP_{11}, LP_{02}, LP_{31}, LP_{03}, LP_{51}, LP_{61}$

Group G-I includes combination of modes having even mode index with (a) same azimuthal index (l) like LP_{11}, LP_{12}, LP_{13}, LP_{14}, LP_{15}; LP_{31}, LP_{32}, LP_{33}, LP_{34}; LP_{51}, LP_{52}, LP_{53}; and (b) same radial index (m) like LP_{11}, LP_{31}, LP_{51}, LP_{71}, LP_{91}; LP_{12}, LP_{32}, LP_{52}, LP_{72}; LP_{13}, LP_{33}, LP_{53}, LP_{73} as shown in Table 4.5. Group G-II includes combination of modes having odd mode index with (a) same azimuthal index (l) like LP_{01}, LP_{02}, LP_{03}, LP_{04}, LP_{05}; LP_{21}, LP_{22}, LP_{23}, LP_{24}; LP_{41}, LP_{42}, LP_{43}; and (b) same radial index (m) like LP_{01}, LP_{21}, LP_{41}, LP_{61}, LP_{81}; LP_{02}, LP_{22}, LP_{42}, LP_{62}; LP_{03}, LP_{23}, LP_{43}, LP_{63}. Group G-III contains mixed groups of modes with odd and even mode index chosen randomly like LP_{01}, LP_{02}, LP_{11}, LP_{04}, LP_{13}; LP_{01}, LP_{21}, LP_{02}, LP_{03}, LP_{13}; LP_{01}, LP_{02}, LP_{12}, LP_{32}, LP_{13}, LP_{21}. In Group G-IV a gap of one mode index between two adjacent mode index is considered and further modes include combinations of mixed modes with odd and even mode index in sequence like LP_{01}, LP_{11}, LP_{02}, LP_{12}, LP_{03}; LP_{01}, LP_{11}, LP_{21}, LP_{31}, LP_{41}, LP_{51}; LP_{11}, LP_{02}, LP_{31}, LP_{03}, LP_{51}, LP_{61}. In receiver section, signals having different modes are demultiplexed by spatial mode selectors (indicated as SS). Different independent signals over N modes are recovered by N MM (multi-mode) receivers. Each MM receiver contain PIN photo detector which is used to convert the optical signal into electrical followed by a LPF; optical analyzer for monitoring the BER, eye diagram

and Quality-factor of transmission link and SA (spatial analyzer) to observe intensity profiles of LP_{lm} modes in the entire schematic.

4.3.3 Result and Discussions

Different groups of linearly polarized modes are taken into account to observe the transmission performance of OMIMO-MGDM system. The transmission distance for four different combinations of LP modes with mode index M (Even, Odd, Random Even+Odd and Symmetric with mode gap unity) has been varied to observe the transmission performance for different configurations of OMIMO MGDM over MMF link.

Different possible mode groups are considered to observe the performance quality of MIMO-MGDM system for longest possible transmission. The transmission length has been varied to investigate the quality of signal as received by different MM receivers in MIMO MGDM system considering four different mode groups. Fig. 4.6 illustrates the effect of G-I modes on transmission quality of 5 × 5 MIMO-MDM system. In Fig. 4.6(a), G-I LP_{lm} modes (LP_{11}, LP_{12}, LP_{13}, LP_{14} and LP_{15}) with same azimuthal index (say l=1) are considered. It is observed that signal received by MM receivers (Rx 1, Rx 2, Rx 3 and Rx 4, Rx 5) provides good quality above 8.8 dB with long transmission distance of (90km and 88km) respectively.

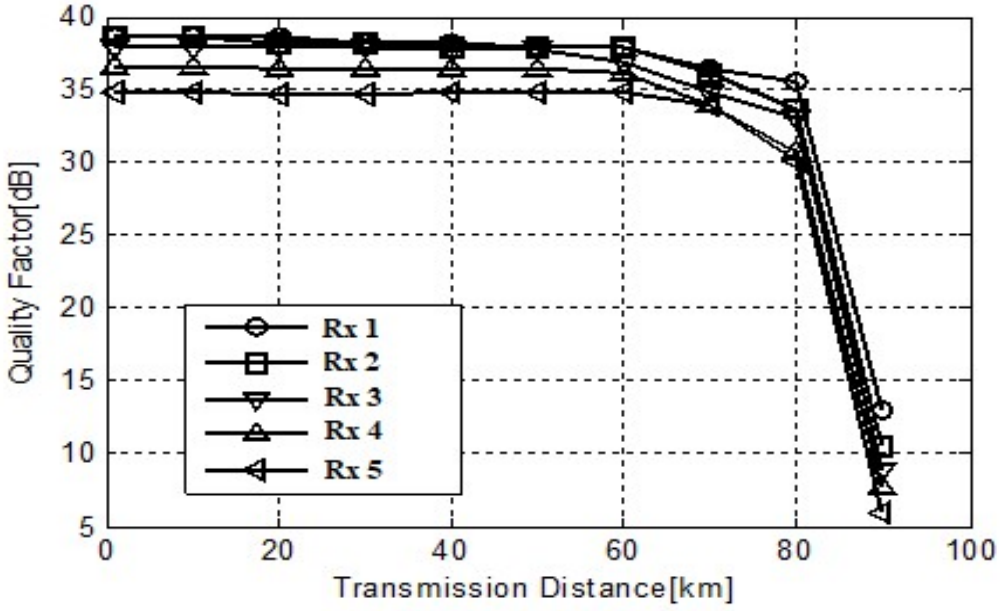

(a)

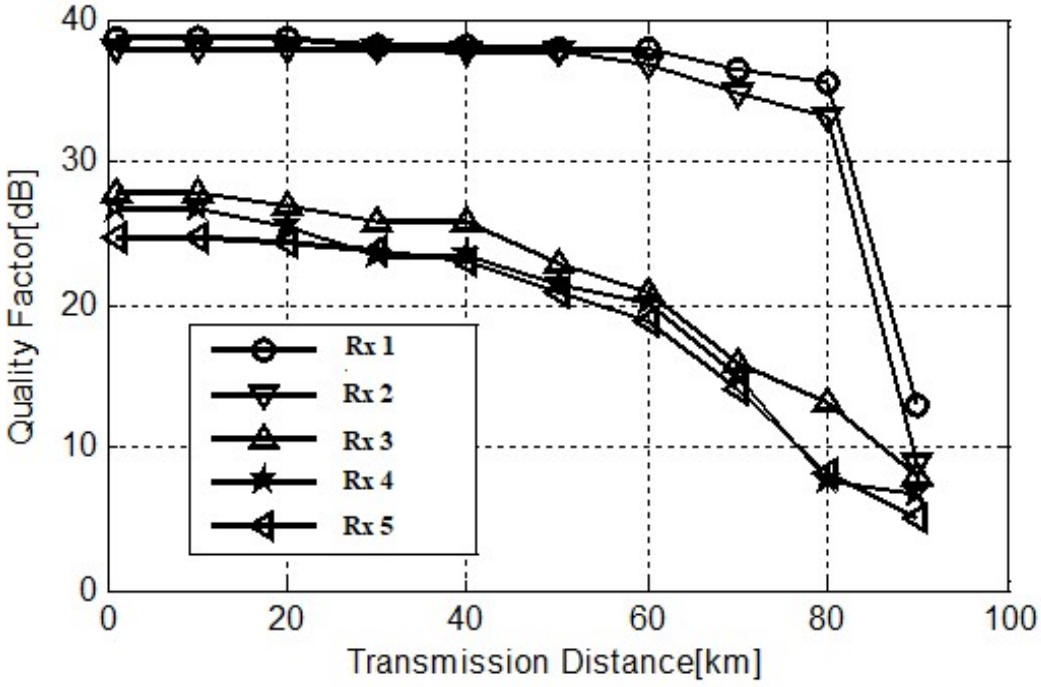

(b)

Fig. 4.6 Transmission quality of 5 × 5 MIMO-MGDM system using group G-I with same (a) azimuthal index *l* and (b) radial index m.

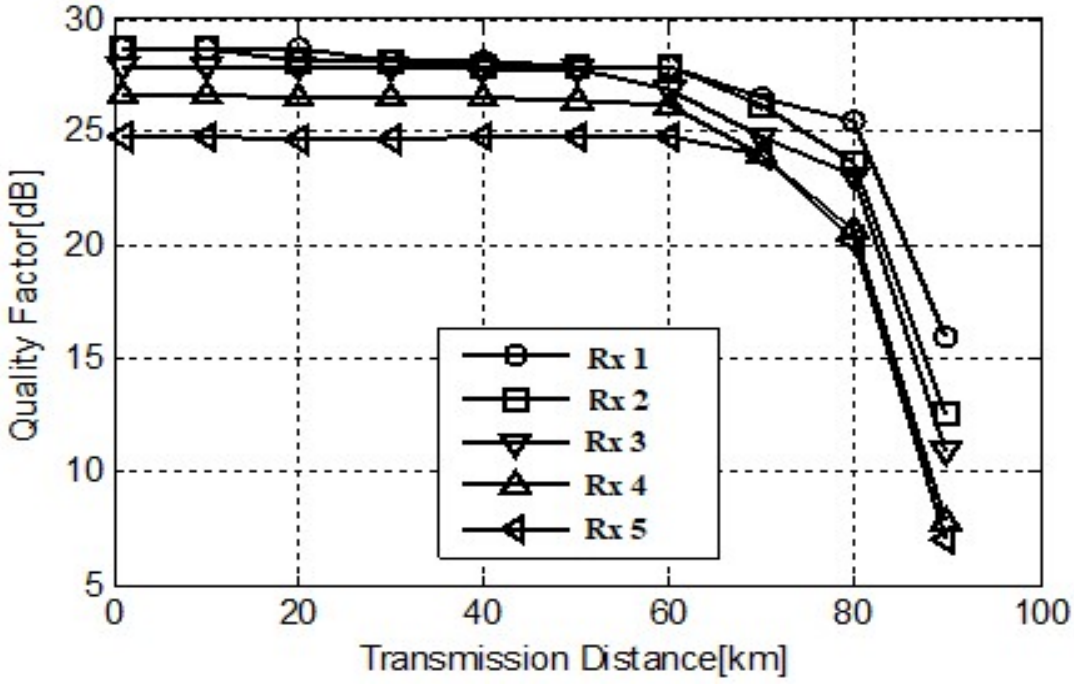

(a)

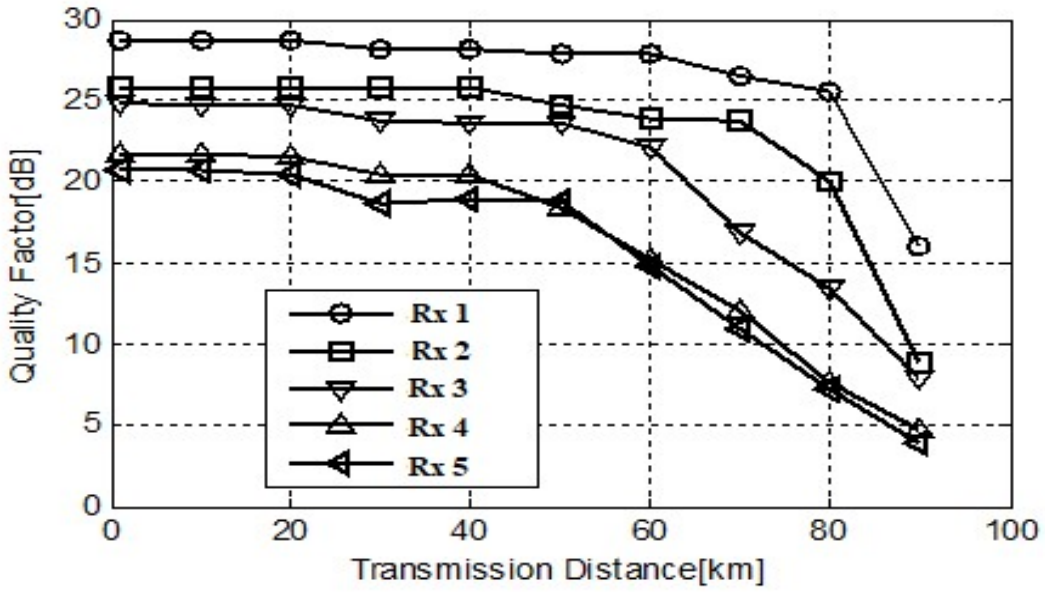

(b)

Fig. 4.7 Transmission quality of 5 × 5 MIMO-MDM system using Group G-II with same (a) azimuthal index *l* and (b) radial index *m*.

For same radial index (say m=1) G-I LP_{lm}modes: LP_{11}, LP_{31}, LP_{51}, $LP_{71}$and LP_{91} are considered in Fig. 4.6(b). For G-I with same *m*, the quality of signal received by MM receivers (Rx 1, Rx 2) is same as in case of same *l* but received by MM receivers (Rx 3, Rx 4 and Rx 5) is poor after 82km of transmission.

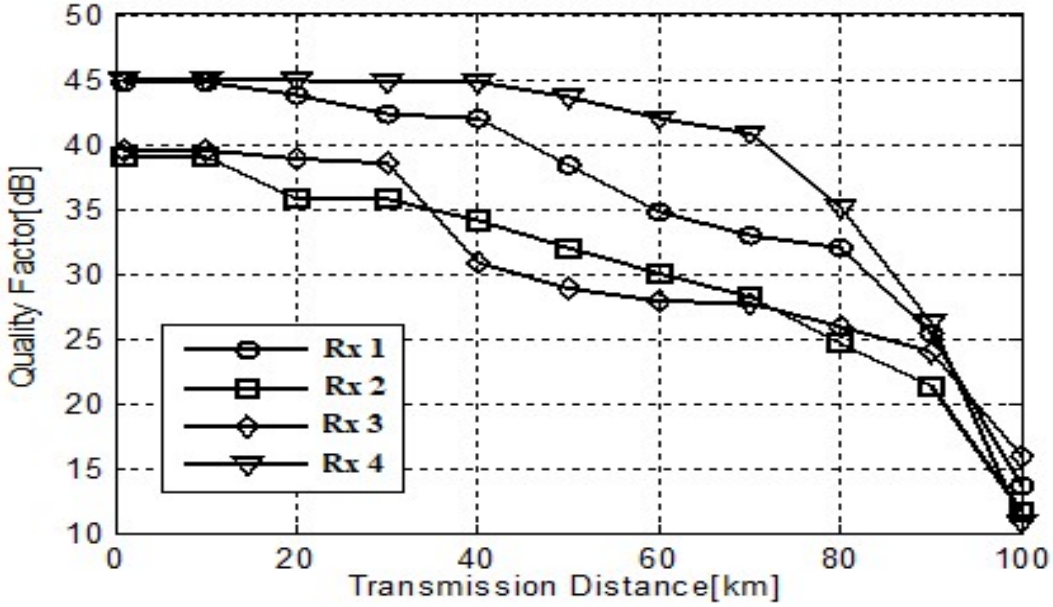

(a)

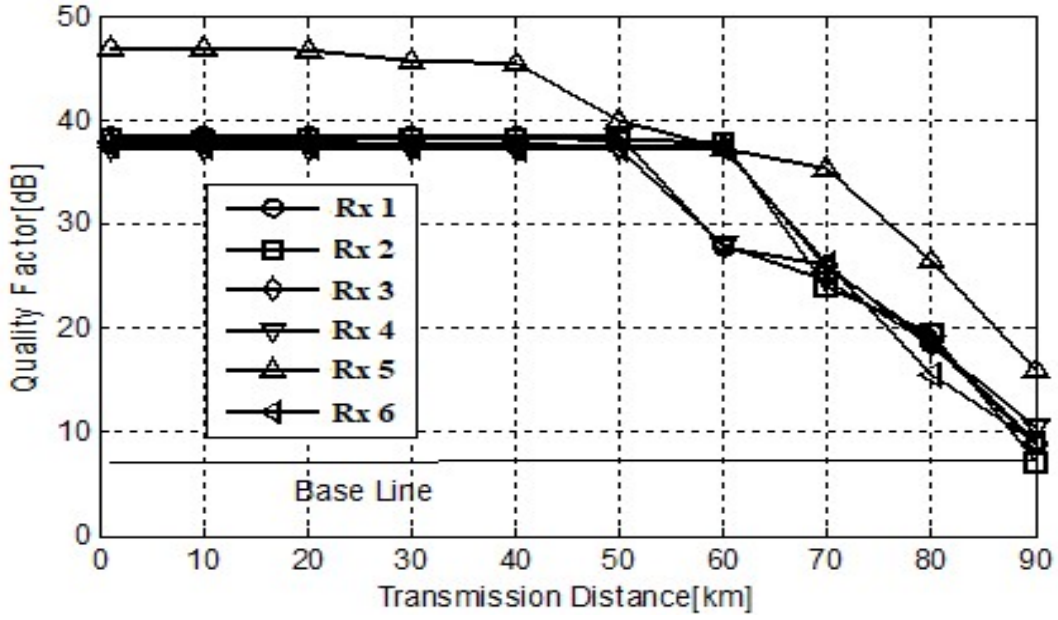

(b)

Fig. 4.8 Effect of Group G-III on transmission quality of (a) 4 × 4 and (b) 6× 6 MIMO-MDM system configurations.

The effect of odd mode index groupingof LP modes (G-II) on transmission performance of 5 × 5 MIMO-MDM system is shown in Fig. 4.7. It is examined in this case that quality of signal decreases up to acceptable level (> 8dB) with rise in the length (82km) of MMF transmission link for different MIMO-MDM (3 × 3, 4 × 4, 5 × 5, 6 × 6, 7 × 7, 8 × 8 and 9 × 9) configurations.

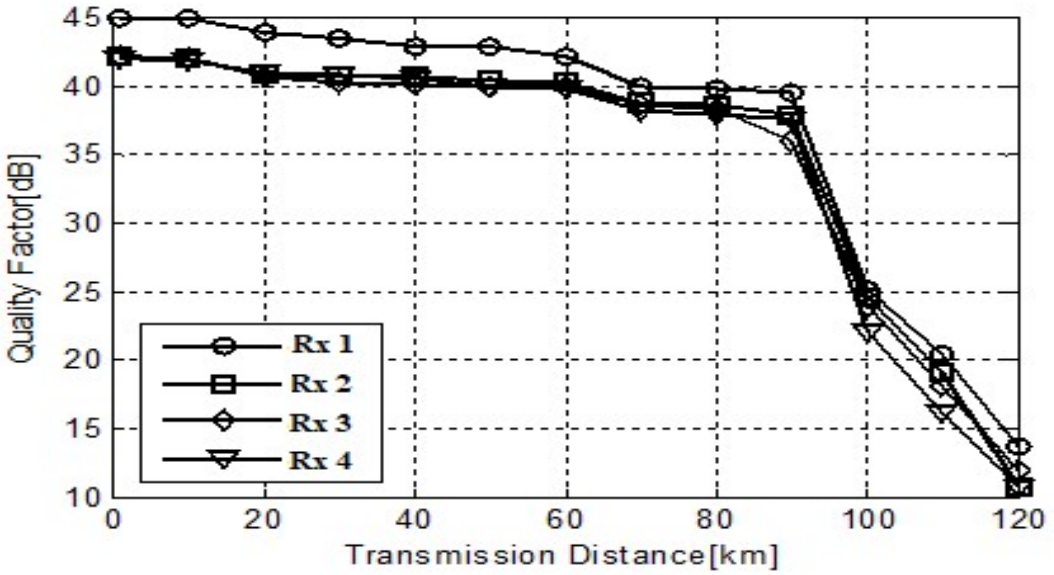

(a)

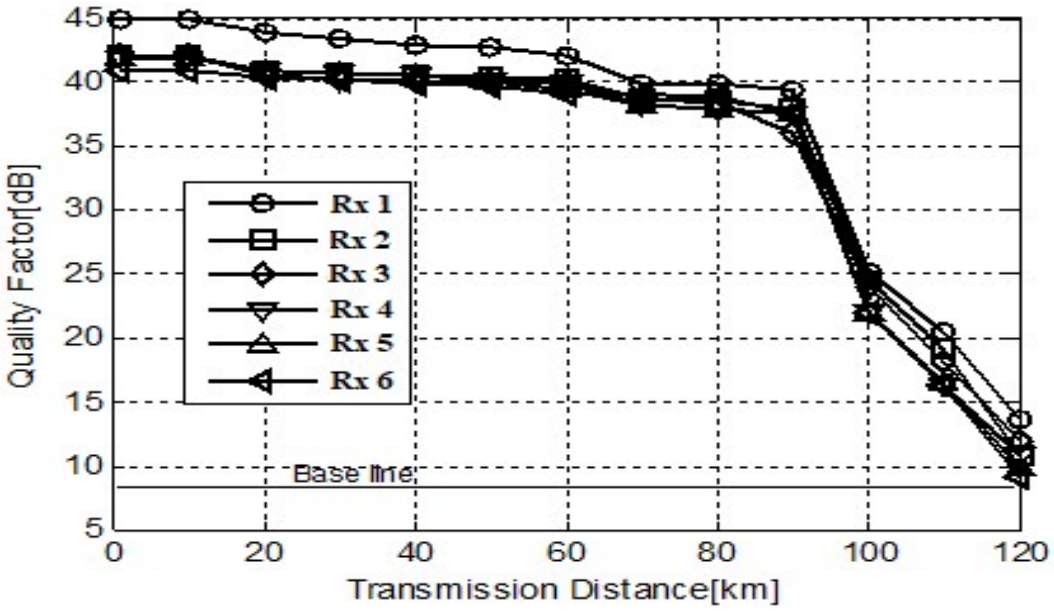

(b)

Fig. 4.9 Effect of Group G-IV on transmission quality of (a) 4 × 4 and (b) 6 × 6 MIMO-MDM system configurations.

Fig.4.8 presents the effect of modes with mixed random odd and even mode index on quality of MIMO-MDM system. Here, different combinations of random O+E mode groups (G-III) are considered in setup to check the performance of 3 × 3, 4 × 4, 5 × 5, 6 × 6, 7 × 7, 8 × 8 and 9 × 9 MIMO-MDM configurations. It is observed from Fig. 4.8(a) that all MM receivers received signal with good quality up to 100km for 3 × 3 and 4 × 4 MIMO-MDM configurations but all receivers except Rx 1 in MIMO-MDM configurations (5 × 5, 6 × 6, 7 × 7, 8 × 8 and 9 × 9) providesgood performance only upto 80 km of transmission linkdue to modal interference as shown in Figs. 4.8(b).

Fig. 4.9 represents G-IV that includes mixed odd and even modes in sequence with gap of one mode group to avoid modal interference of higher modes. It is seen from Fig. 4.9(a) that by considering G-IV modes (LP_{01}, LP_{11}, LP_{21} and LP_{31}) all receivers provide high-qualityabove threshold (> 10dB) with transmission distance up to 120 km for 3 × 3 and 4 × 4 MIMO-MDM configurations.The same trends are examined for 5 × 5, 6 × 6 and 7 × 7 MIMO-MDM systems and results are shown in Fig. 4.9(b) for 6 × 6 MIMO configuration.

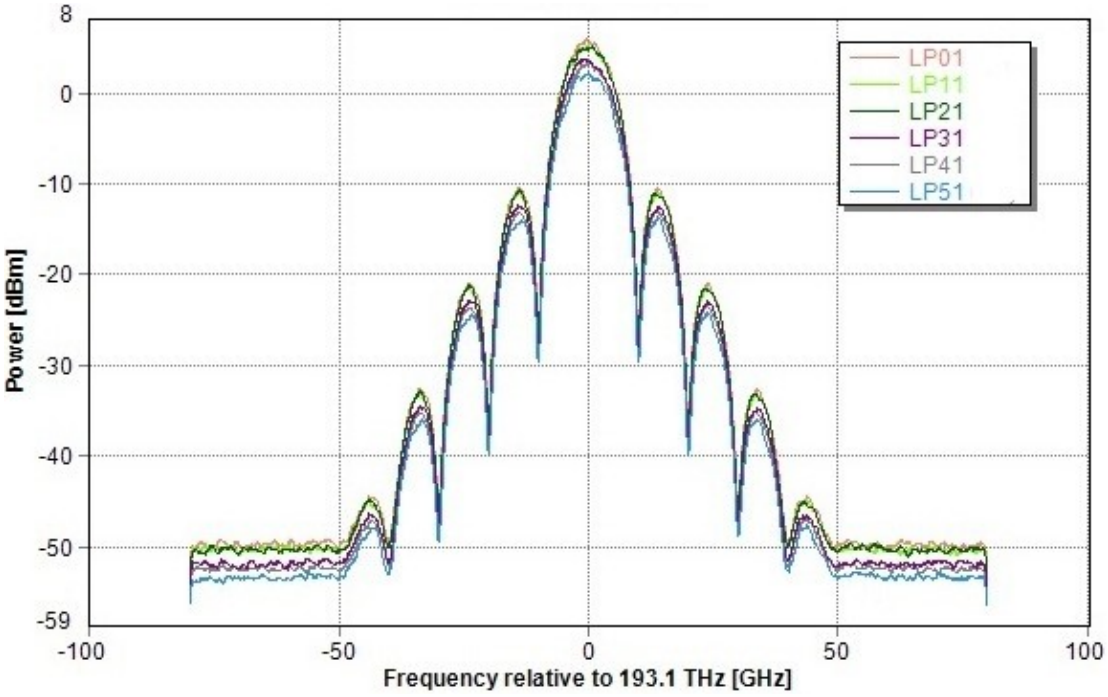

Fig. 4.10Received power of 6 considered modes (G-IV) in 6 × 6 MIMO-MDM system configuration.

It is observed from Figs. 4.6, 4.7, 4.8 and 4.9, maximum distance for acceptable Q-factor using mode index grouping combinations (G-I, G-II, G-III and G-IV) is approximately 85 km, 83 km, 90 km and 120 km respectively. On comparing all considered mode groups (G-I, G-II, G-III and G-IV) for all the MIMO-MDM configurations (3 × 3, 4 × 4, 5 × 5, 6 × 6, 7 × 7, 8 × 8 and 9 × 9) it is concluded that the latter (G-IV) is superior to the former.

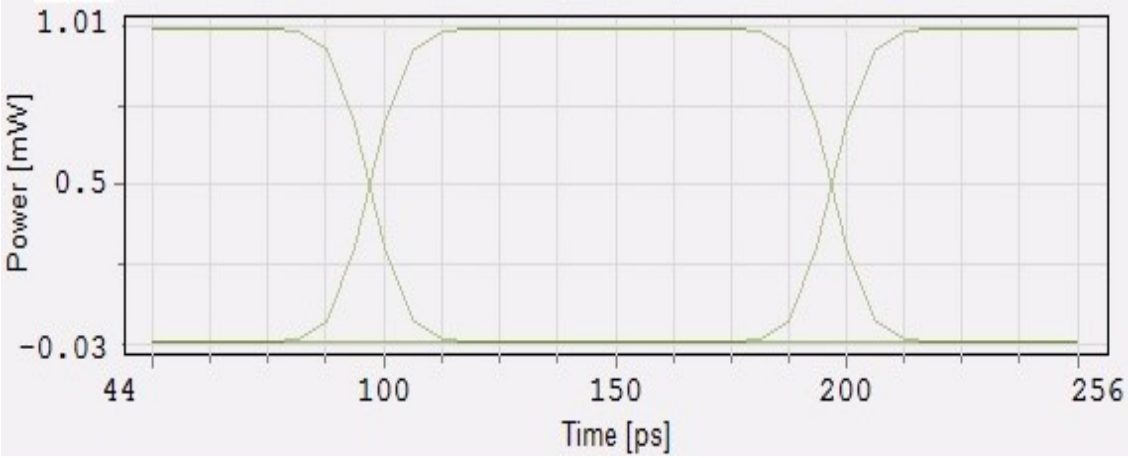

(a)

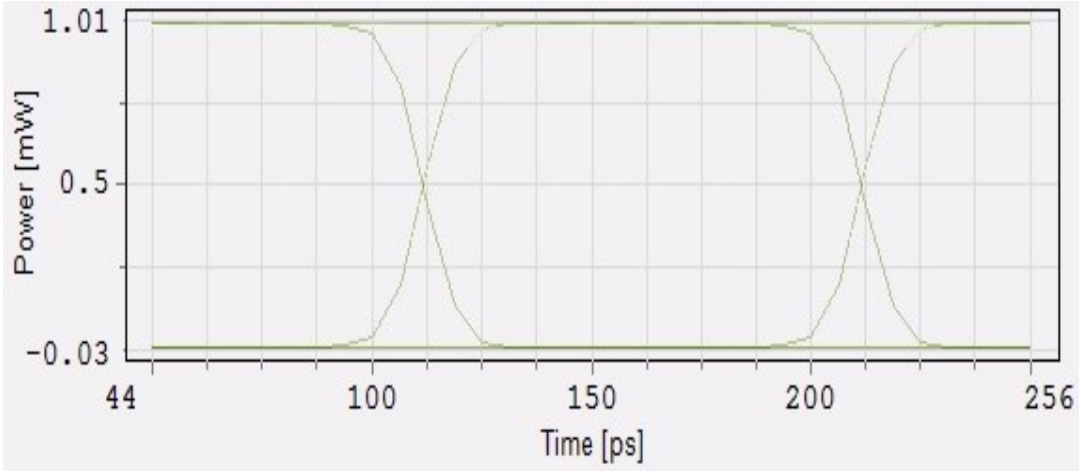

(b)

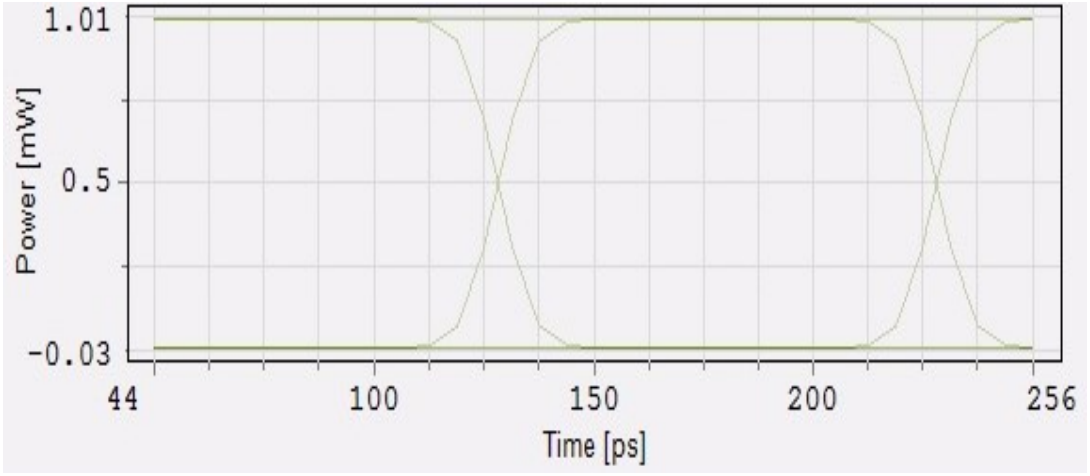

(c)

Fig. 4.11. Eye diagrams of received modes (a) LP01, (b) LP11 and (c) LP21in 9 × 9 OMIMO-MGDM system over MDM link without mode coupling.

Fig. 4.10 provides information about the power of modes (LP_{01}, LP_{11}, LP_{21}, LP_{31}, LP_{41} and LP_{51} considered in case IV) as received by 6 MM receivers after propagating through the core of MMF. The graph represents a substantial decrease in intensities with lower order modes to higher order modes within a particular range of frequency relative to 193.1 THz.

Figs. 4.11 (a-c) represents Eye diagrams of received modes (LP01, LP11 and LP21) in 9 × 9 OMIMO-MGDM system over MDM link without mode coupling.It is seen from Fig. 4.12 that the quality of the received signal is impacted by mode coupling and modal crosstalk in MDM link at receiver, thus signal processing would be required in this case for error- free reliable transmission.

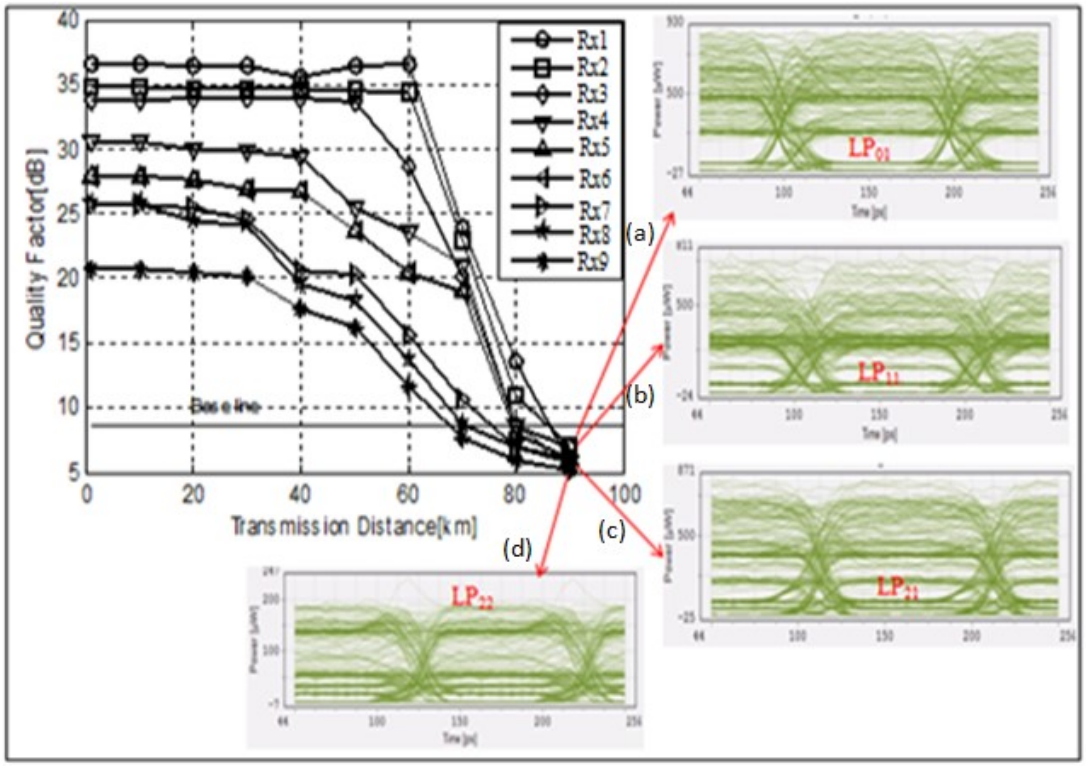
Quality Factor[dB]
Transmission Distance[km]
Baseline
Rx1
Rx2
Rx3
Rx4
Rx5
Rx6
Rx7
Rx8
Rx9
(a)
(b)
(c)
(d)
LP01
LP11
LP21
LP22

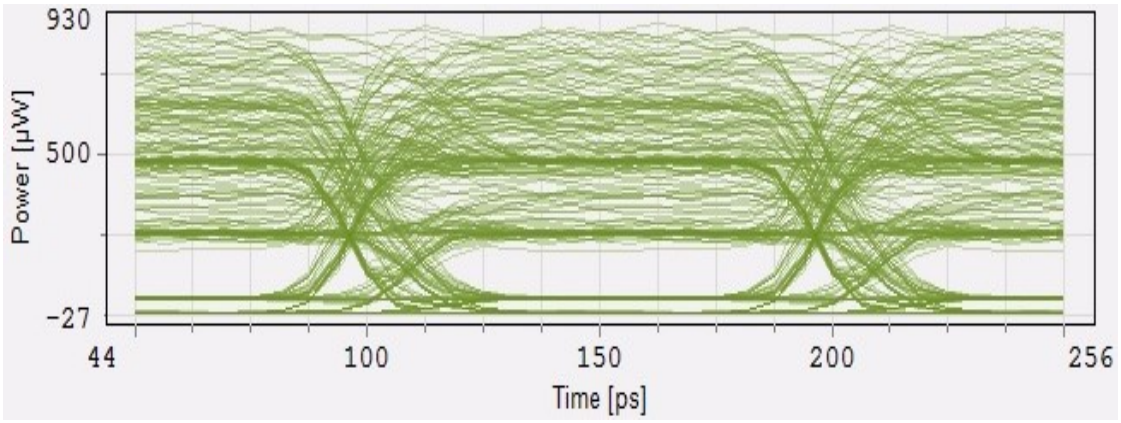
930
500
-27
Power [μW]
44
100
150
200
256
Time [ps]

(a)

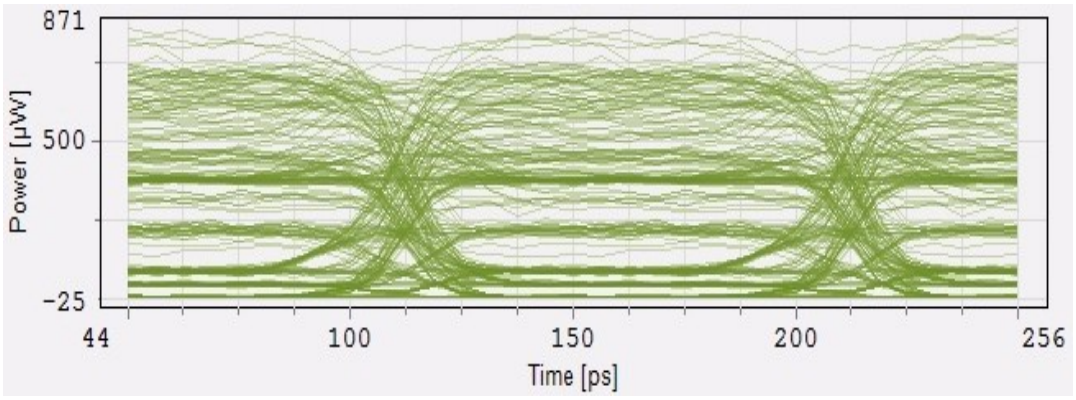
871
500
-25
Power [μW]
44
100
150
200
256
Time [ps]

(b)

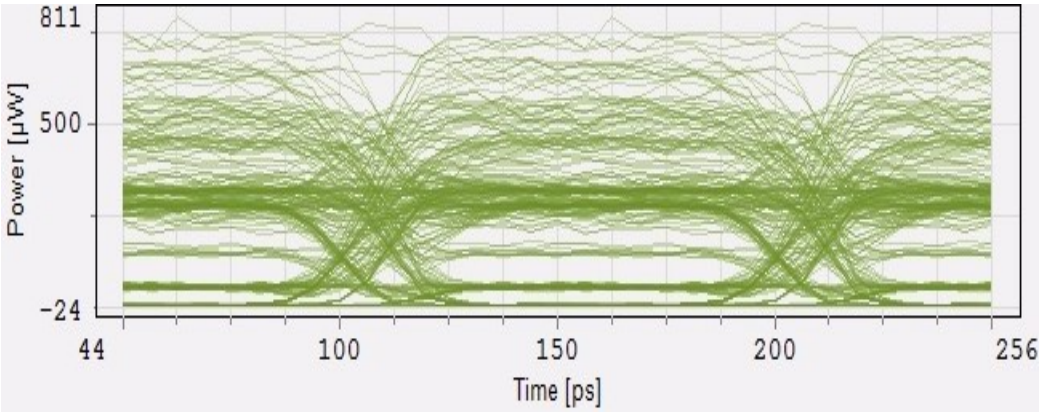

(c)

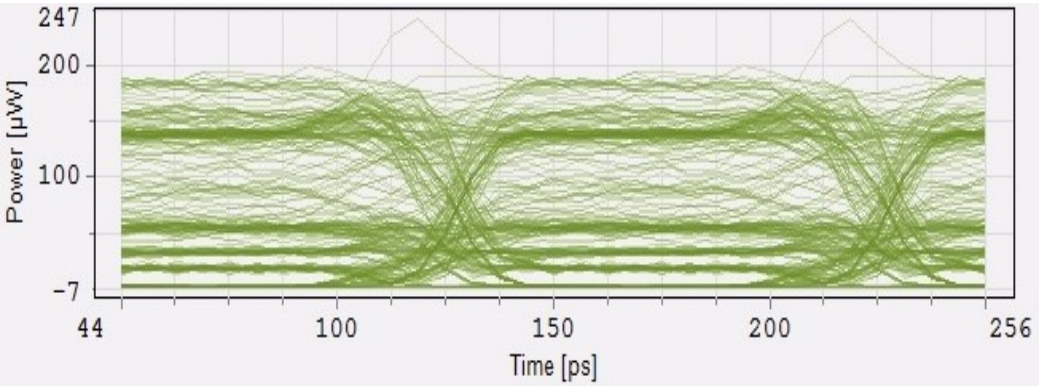

(d)

Fig. 4.12. Performance quality of received signal in 9 × 9 OMIMO-MGDM system over 90 km MDM link with mode coupling; Eye diagrams of modes (a) LP_{01}, (b) LP_{11}, (c) LP_{21} and (d) LP_{22} representing crosstalk due to mode coupling.

Insets consist of the received eye diagrams for all modes received in MDM link with same scale. The quality of signals received by all 9 MM receivers (Rx 1, Rx 2, Rx 3, Rx 4, Rx 5, Rx 6, Rx 7, Rx 8 and Rx 9) is very poor above 82 km of transmission as shown in Fig. 4.12.Eye diagrams as received in 9 × 9 OMIMO-MGDM system over MDM link fordifferent modestravelling inside MMF are shown in Figs. 4.12(a-d).

4.4 Optimization of MIMO MDM utilizing signal processing to minimize intermodal crosstalk

The performance of the system is restricted due to intermodal crosstalk and only a maximum distance of 90 km is achieved with acceptable BER ($<10^{-9}$). The transmission performance is then enhanced by demultiplexing the modes using DSP filter to lower the

intermodal crosstalk. During propagation of the signal mode coupling takes place as the modes travels at different velocities in MMF. So, the output signal must be processed using DSP MIMO filter in order to reduce coupling. The time dispersion and mode coupling caused by channels can be compensated by Equalization technique which is performed in the frequency domain [116], [118]. The optimization of taps (filter coefficient) is done by utilizing LMS (least mean square) adaptive MIMO filter algorithm to minimize the mean-squared error at the output signal in order to avoid mode group coupling in MDM based system.

The input-output relation of mode division multiplexed system having M (M1 to M25)spatial modes can be represented as [179]:

$$y(t) = H(t) * x(t) \tag{4.8}$$

where$x(t)$ denotes transmitted signal, $H(t)$ is channel or coupling matrix having M×M matrix (here in proposed: 25×25)of tap delay line filters and $y(t)$ is received signal respectively. To recover signals from different mode channels and to completely compensate the signal distortion at the receiver, an adaptive equalizer implements matrix $C(t)$ that should be the inverse of channel matrix $H(t)$ such that:

$$x(t) = C(t) * y(t) \tag{4.9}$$

At the coherent receiver signals from different mode channels are demodulated and then digitalized. The digital sequence $x_1(n), x_2(n)\ldots\ldots\ldots\ldots x_M(n)$ is fed to equalizer block for adaptive compensation. The equalization of k^{th} sample on i^{th} mode is calculated as [116]:

$$y_i(k) = \sum_{j=1}^{M} \sum_{i=0}^{Ntaps} h_{ij}(i) X_j(k-i) \tag{4.10}$$

where, *Ntaps* is the number of filter taps and *i;j* are values of mode index ranging from 1 to *M*. In frequency Equalization LMS, filter coefficient values are taken in frequency domain and computed using following equation [180]:

$$\overline{\overline{C^{(j)}}} = \overline{\overline{C^{(j-1)}}} + \mu \begin{bmatrix} \overline{E_{1,j}(k)} \otimes \overline{Y^*_{1,j}(k)} & \overline{E_{1,j}(k)} \otimes \overline{Y^*_{2,j}(k)} \\ \overline{E_{2,j}(k)} \otimes \overline{Y^*_{1,j}(k)} & \overline{E_{2,j}(k)} \otimes \overline{Y^*_{2,j}(k)} \end{bmatrix} \tag{4.11}$$

where, $\overline{\overline{C^{(j)}}}$ represents inverse channel equalizer filters, μ is convergence step size, $\overline{E_{i,j}(k)}$ depicts j^{th} error block for i^{th} mode, $\overline{Y^*_{i,j}(k)}$ is conjugate of the received signal block in frequency domain for i^{th} mode and symbol $\otimes$ denotes element to element multiplication.

The error signal (obtained by subtracting received signal from desired signal, $e_i(k) = d_i(k) - y_i(k)$) and the received signal are taken in time-domain. For adaptive Equalization method, to adjust the equalizer coefficients error block is calculated in time domain first and then FFT is taken [181]. After the computation of equalization, comparison of each output sample is done with the desired output and the resultant error is then fed back to Gradient estimation block. The gradient estimation processes the error signal and then updates the value of equalizer filter tap coefficients to minimize the coupling error in the system.

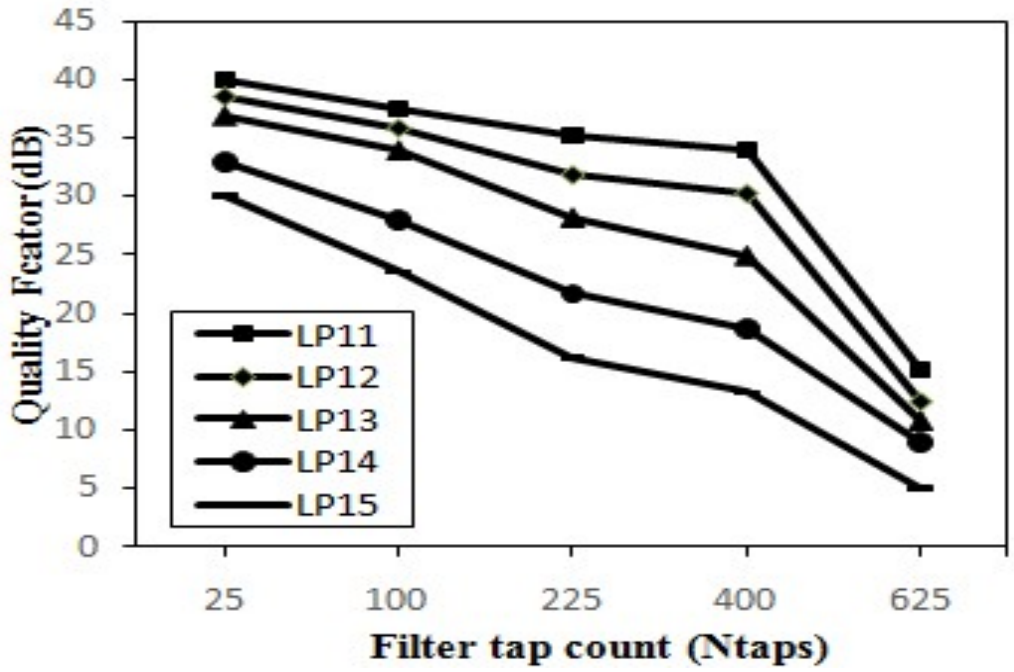

Fig. 4.13 Optimizedperformance of LP modes with M ×M MIMO filter taps after equalization.

The quality performance of different LP modes (LP_{11}, LP_{12}, LP_{13}, LP_{14} and LP_{15}) in LP-WDM-MDM systems has been investigated by varying the MIMO filter tap coefficient as shown in Fig. 4.13. After equalization, performance of modes in system is optimized by taps thus minimizing the mean square error. It can be seen from Fig. 4 that with the increase in $M \times M$ MIMO filter tap size (where $N_{taps}=M^2$) LP modes (LP_{11}, LP_{12}, LP_{13} and LP_{14}) provide good quality above 10dB except higher order mode LP_{15} performs poorely with $N_{taps}>= 625$.

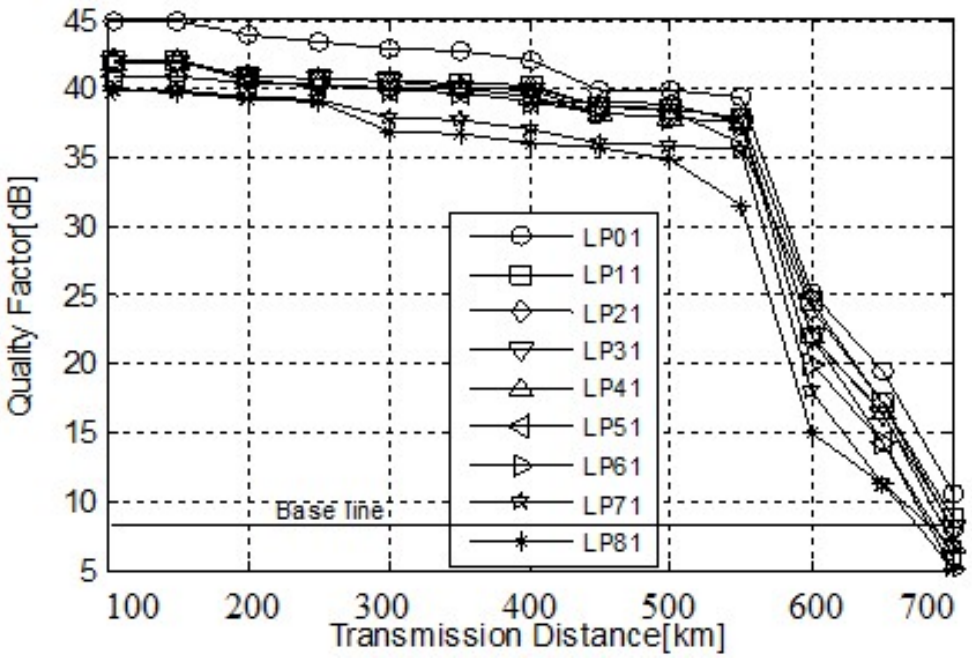

Fig.4.14. Performance quality of received signal in 9 × 9 OMIMO-MGDM system over 700 km MDM link with Adaptive MIMO LMS equalization.

Fig. 4.14depicts that high-quality signals (quality factor above 8 dB) are received by all MM receivers covering distance of 700 kmfor received modes (LP_{01}, LP_{11}, LP_{21}, LP_{31},LP_{41}, LP_{51}, LP_{61} and LP_{71}) with Adaptive MIMO LMS equalization.

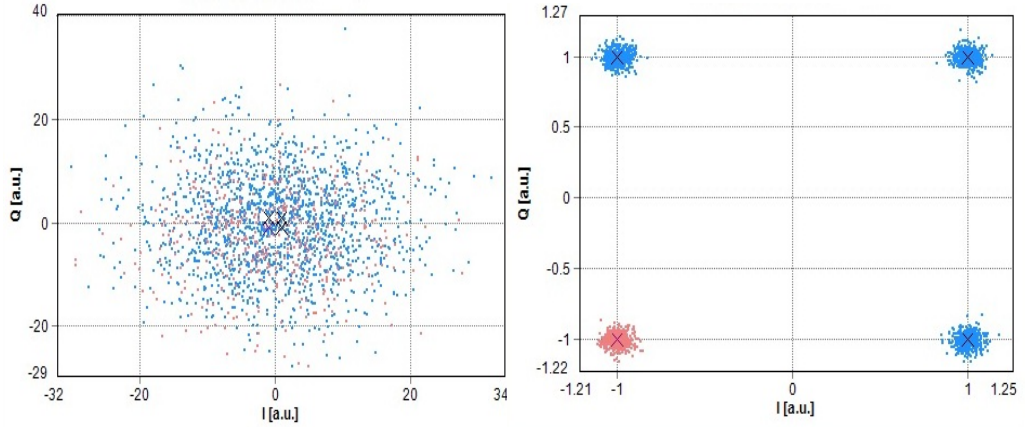

(a) (b)

Fig.4.15. Constellation diagram of received signal over (a) 90 km MDM link with modal coupling and (b) 700 km MDM link with Adaptive MIMO LMS equalization.

Fig. 4.15 represents the received constellations for 9x9 MIMO MDM link with 9 modes where each mode is QPSK-modulated and transmitted power was set to 0 dBm and

maximum differential delay between modes was kept to be 0.2ps/m. It can be observed from Fig. 4.15(a) that without MIMO equalization there is scattering of received symbols due to intermodal crosstalk whereas Fig. 4.15(b) shows a notable reduction in modal crosstalk due to the application of Adaptive MIMO equalization.

4.5 Conclusion

This Chapter demonstrates MIMO based MDM system for transmission of 9 signals over 9 different LP modes at 1550 nm wavelength with low input power travelling long distance of 90 km over MMF link. In this paper it is found that LP_{01}, LP_{02}, LP_{11} and LP_{12} modes provide better results for 4×4, 6×6 and 9×9 MIMO configurations. It can be observed that even for 9×9 MIMO MDM system maximum Q^2 factor of 14 dB with minimum BER of 10^{-9} was achieved. Further, it deals with the effect of different LP mode index grouping combinations (Even, Odd, Random Even+Odd and Symmetric Even+Odd with mode gap) on transmission performance of 3 × 3, 4 × 4, 5 × 5, 6 × 6, 7 × 7, 8 × 8 and 9 × 9 OMIMO-Mode division multiplexed systems. The maximum distance covered with Quality-factor (>8.3dB) using mode index grouping combinations (Even, Odd, random Even+Odd and symmetric Even+Odd with mode gap) is approximately 82km, 79km, 80km and 114km respectively for even 9 × 9 OMIMO-MDM system. It is concluded that higher Q-factor and received power with longest transmission is achieved with symmetric Even+Odd with mode gap but moderate with rest cases for all considered OMIMO-MDM configurations. This analysis can be used for MGDM (mode group division multiplexing)to increase the capacity of high speed transmission over MMF link.

CHAPTER 5
MODE DIVISION MULTIPLEXED SYSTEM TO ENHANCE CAPACITY

5.1 Introduction

This chapter deals with the third objective of this thesis work, which is to design modified architecture of MDM including design of inline MM-EDFA(Multimode Erbium Doped Fiber Amplifier) amplifier, hybrid mode and wavelength division multiplexing technique to increase the capacity of system. Further, the performance quality of the system is analyzed with respect to transmission distance.The transmission length from 1 to 100 km for 3 different (pre-, booster- and inline-) Multimode Erbium doped fiber amplifier configurations has been varied to examine the performance of 4 different (3 × 3, 4 × 4, 5 × 5 and 6 ×6) MIMO Mode division multiplexed configurations.This objective is achieved and presented in different Sections as follows: in Section 5.2, different configurations of MM EDFA are presented; Section 5.3 deals with the proposed design of hybrid mode and wavelength multiplexing to enhance system capacity. In Section 5.4, conclusion is discussed.

5.2 Comparison of pre-, boost- and inline-MM EDFA configurations

5.2.1 Theory

Multimode fiber links between MM transmitter and MM receiver are designed with pre-, booster- and inline-MM Erbium doped fiber amplifier configurations. During the designing of configurations an assumption is made that multi-mode information signal (information signals superimposed over multiple modes) at 1550 nm are generated by mode multiplexers and multi-mode pump signal at 980 nm is passed through phasor plates. The fields of multi-mode information signal and multimode pump signal are combined, passed through a dichoric mirror and launched to EDFA amplifier. The function of Multimode Erbium doped fiber amplifier can be represented by rate equations (5.1, 5.2) and propagation equation (5.3) containing multiple spatial modes for information and pump signal. The power of information signal and pump signal are calculated numerically with the help of these equations. The power of an information signal mode is dependent on the extent of spatial overlap between density of Er ions and intensity profile of signal which further depends on intensity profile of pump and spatial doping profile of Er ions[182].

$$N_t(r,\varphi) = N_1(r,\varphi,z) + N_2(r,\varphi,z) \tag{5.1}$$

$$\frac{dN_2(r,\varphi,z)}{dx} = \sum_n \frac{P_n(z)I_n(r,\varphi)\sigma_{an}}{h\upsilon_n} N_1(r,\varphi,z) - \sum_n \frac{P_n(z)I_n(r,\varphi)\sigma_{en}}{h\upsilon_n} N_2(r,\varphi,z) - \frac{N_2(r,\varphi,z)}{\tau_s} \tag{5.2}$$

$$\frac{dP_n(z)}{dz} = \mu_n \sigma_{en}[P_n(z) + 2h\upsilon_n \Delta\upsilon_n] \int_0^{2\pi} \int_0^a I_n(r,\varphi) N_2(r,\varphi,z) r dr d\varphi$$

$$-\mu_n \sigma_{an} P_n(z) \int_0^{2\pi} \int_0^a I_n(r,\varphi) N_1(r,\varphi,z) r dr d\varphi - \mu_n \alpha P_n(z) \tag{5.3}$$

where, $N_t(r,\varphi)$ is total doping density;$N_1(r,\varphi,z)$: density of Erbium ions in the ground state and$N_2(r,\varphi,z)$: Erbium ions density in the excited state;n dictates the index assigned to beam or optical ray travelling with different modes;$P_n(z)$ represents the power of$n$th optical ray;$I_n(r,\varphi)$ is normalized mode intensity profile of optical ray;$\upsilon_n$presents optical frequency of the nth ray; μ_n : value unity represents the forward direction of nth optical ray andτ_s depicts spontaneous lifetime of the excited state and α denotes the EDF intrinsic loss coefficient.

5.2.2 Design of MDM system with different amplification schemes:

The schematic of proposed MIMO MDM system is shown in Fig. 5.1 and the simulation setup is done by VPI Photonics/ VPI transmission Maker™ Version 9.7 simulator. Each Multimode Transmitter block consists of spatial laser which is tuned at wavelength of 1550 nm acting as optical source with light beam of 0 dBm power. The data source is in NRZ format with 10 Gb/s bit rate, electrical driver drives the required format of data, converts the input data binary signal into electrical signal and MZ modulator is used then to modulate the laser beam. Information signals from *N* different transmitters are superimposed over *N* different linearly polarized modes and then fed to mode combiner (denoted by C) for multiplexing of all the modes carrying information.

Here, 6 LP modes are multiplexed using optical mode combiner, transmitted with MM transmitters over MMF link and received using MM recievers. A MM-EDFA is designed to amplify different spatial modes and supports these modes to travel through Parabolic index MMF in three different configurations to investigate system performance. After propagating through MMF spatial modes are demultiplexed by optical mode selectors (indicated as S) and different signals over modes travels to *N*

different MM receivers. Each multimode receiver consists of PIN photo detector that translates the optical signal into electrical followed by a low pass filter and analyzer for examining the parameters like Q-factor, eye diagram and BER for transmission link. Table 5.1 represents the parameters used in the setup of MDM system.

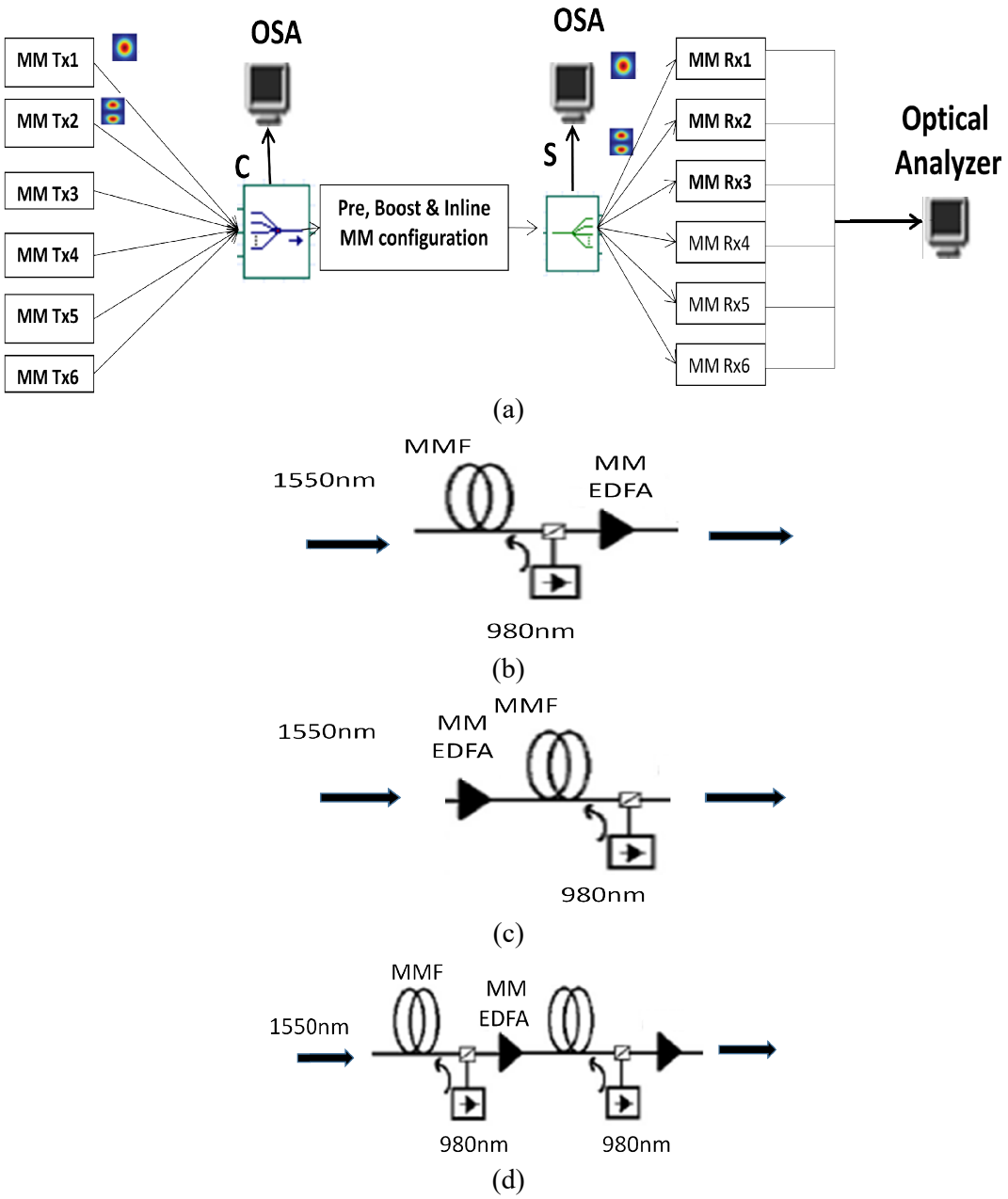

Fig 5.1 (a)System setup for 6 channels MDM optical communication system; C: combiner, S: selector + splitter, OSA: optical spectrum analyzer, (b) pre-, (c) booster- and (d) inline- MM configuration techniques; MMF: multimode fiber, MM EDFA: multimode EDFA amplifier.

Table 5.1: Parameters of 6 channel MDM over MMF link

Name of parameter	Value
Power	0 dBm
Linewidth	10 MHz
Attenuation	2.61 dB/km
Signal wavelength	1550 nm
EDFA Pump type	Counter-propagate
EDFA Pump wavelength	980 nm
EDFA Noise Figure	4 dB
EDFA Gain	Flat
Dispersion	-100 ps/nm/km
Responsivity	1 A/W
Dark current	10 nA
Length	100 km

In the pre-MM configuration method, transmissionof multimode signal is pre-amplified by MM EDFA before travelling to receiver section, as shown in Fig. 5.1(b). Fig. 5.1(c) depicts booster-configuration in which the signal is amplified after transmitter to boost the transmitted power and in inline-configuration optical communication system is symmetrically amplified to compensate for transmission loss as shown in Fig. 5.1(d).

5.2.3. Result and discussion

The performance of optical communication system is generally measured by common parameters like BER (bit error rate) and Q-factor. BER is measure of probability of erroneous bits with respect to total bits received during transmission and Q-factor is the measure of quality of transmitted signals in form of SNR. SNR is better for higher value of Q-factor and with lower the percentage of erroneous bits. The Q-factor and bit error rate can be approximated by equations (5.4) and (5.5) [183].

$$\text{Bit error rate} = \frac{1}{2}\,\text{erfc}\left(\frac{Q}{\sqrt{2}}\right) \approx \frac{\exp\left(-\frac{Q^2}{2}\right)}{Q\sqrt{2\pi}} \tag{5.4}$$

$$\text{Quality factor, } Q = \frac{\mu_1 - \mu_0}{\sigma_1 - \sigma_0} \tag{5.5}$$

where; (μ_1, μ_0) and (σ_1, σ_0) are the mean and standard deviation of signal received at sampling instant when bit 1 and 0 is transmitted respectively.

The transmission length from 1 to 100 km for 3 different (pre-, booster- and inline-) MM EDFA amplifier configurations has been varied to investigate the performance of 4 different (3 × 3, 4 × 4, 5 × 5 and 6 × 6) MIMO MDM configurations. Fig. 5.2 illustrates the variation of Quality factor with transmission length. It is observed that signal quality decreases up to acceptable level with increase in the length of MMF transmission link for four different configurations. The graph between quality of the signal and variation in transmission length for 3 × 3 MIMO MDM system using pre-, boost- and inline configurations is shown in Fig. 5.2(a, b, c).

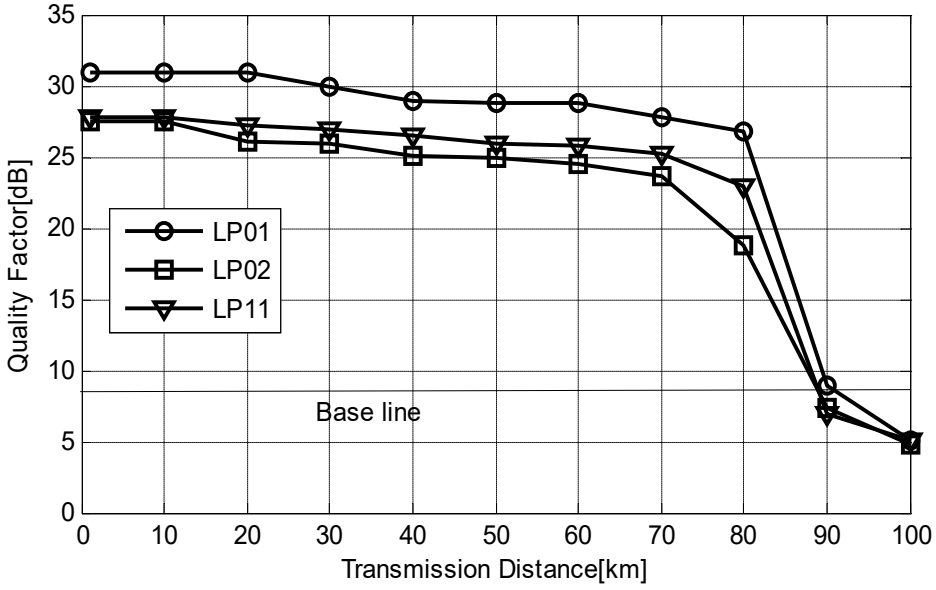

(a)

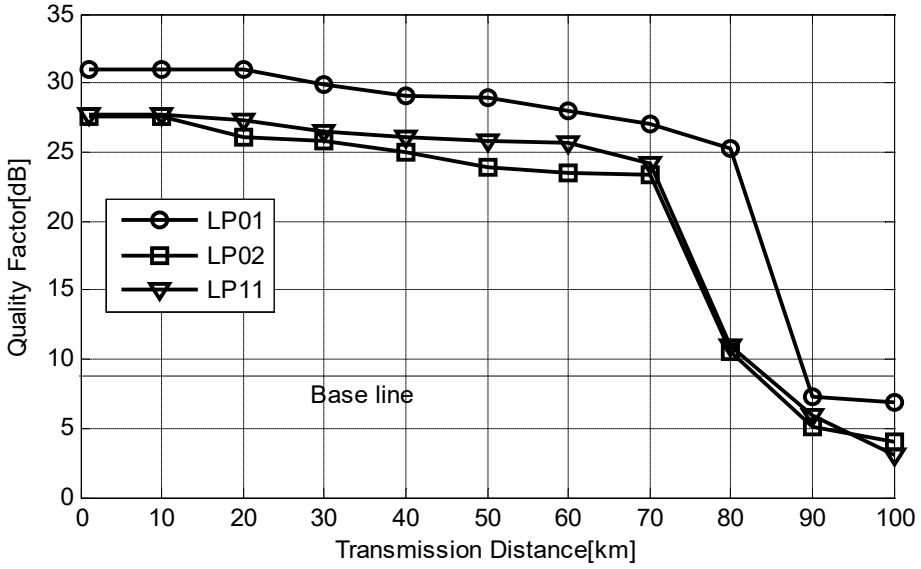

(b)

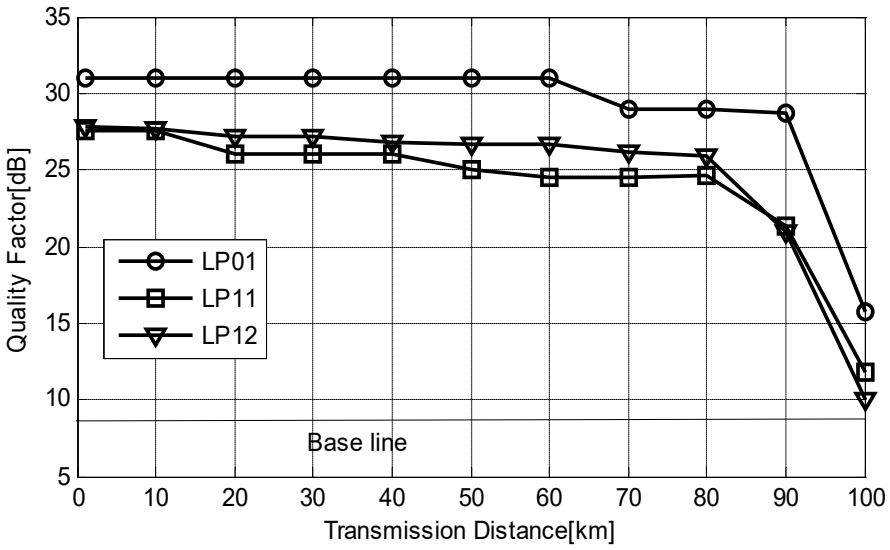

(c)

Fig. 5.2 Quality of 3 × 3 MIMO MDM system as a function of distance using (a) pre-, (b) boost- and (c) inline-MM EDFA configuration.

For 3 × 3 MIMO MDM system, the quality factor of pre- and boost-configuration method is above 8 dB for increase in length of fiber up to 89 km and 83 km respectively as shown in Fig. 5.2(a, b). But in case of inline-configuration method LP modes are transmitted with good quality (> 10dB) covering a distance of 100 km to boost the performance of 3 × 3 MIMO MDM system as represented in Fig. 5.2(c). It is observed that for inline-configuration, the Quality factor is indicating best performance and LP_{01} mode provides better quality than the modes LP_{02} and LP_{11} for all the three configurations.

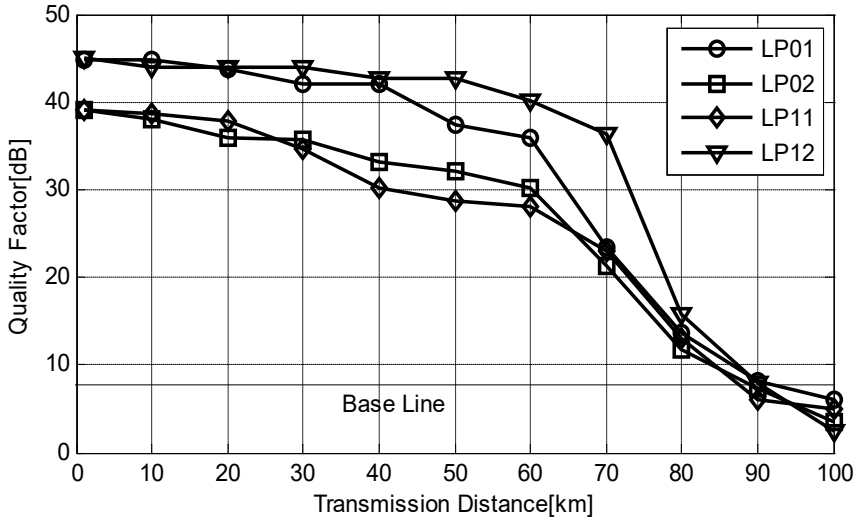

(a)

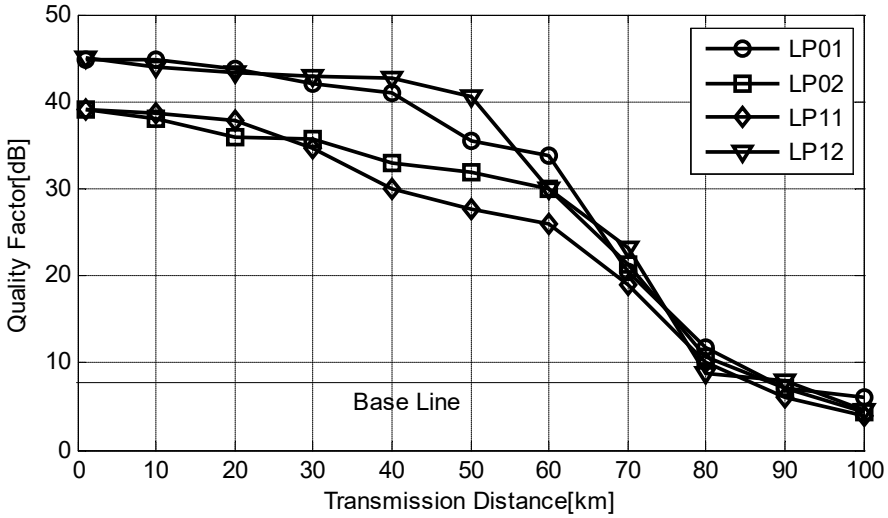

(b)

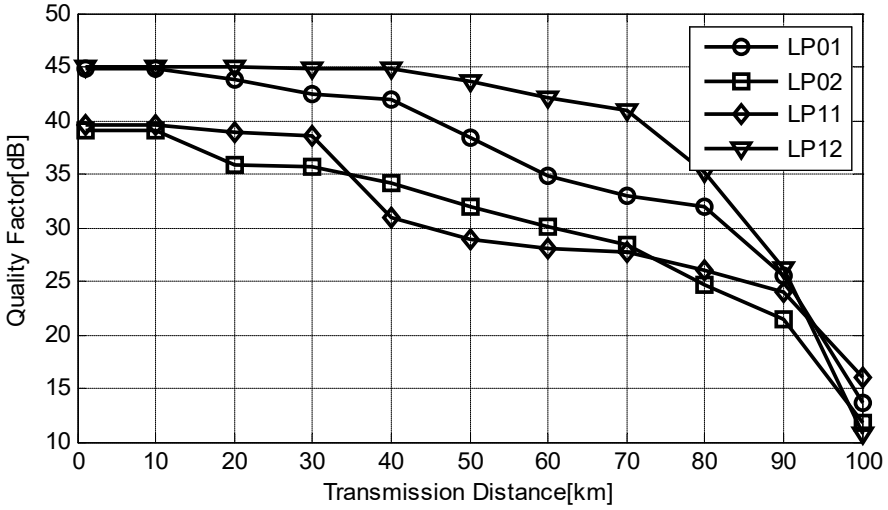

(c)

Fig. 5.3 Quality of 4 × 4 MIMO MDM system as a function of distance for (a) pre-MM and (b) boost-MM and (c) inline-MM configuration.

It is obligatory to examine the performance of MIMO MDM system using three configuration methods with respect to Quality factor to determine the longest possible transmission distance. Fig. 5.3 shows the graphical view of variation in Quality-factor with transmission length using three MM amplifier configurations for 4 × 4 MIMO MDM system.

It is observed that pre- and boost-MM configurations show poor performance after covering transmission distance (i.e. 88 km and 84 km) respectively as shown in Fig. 5.3(a, b). On the other hand, Fig. 5.3(c) depicts that maximum transmission distance

(100 km) is allowed by inline- configuration with LP_{01}, LP_{02}, LP_{11} and LP_{12} modes providing maximum quality of 45 dB for 4 × 4 MDM system.

The same trends are observed in Fig. 5.4 for quality factor measurement. Fig. 5.4(a,b) represents that LP_{03} mode is having higher Q-factor for both pre- and boost-MM configuration. In case of pre and boost-configuration; LP_{01}, LP_{02}, LP_{11} and LP_{12} modes performs consistently up to 50km, then their quality decreases from (50 to 78 km and 50 to 70 km) but above acceptable level and after (78km and 70km) of distance all modes provide poor performance respectively.

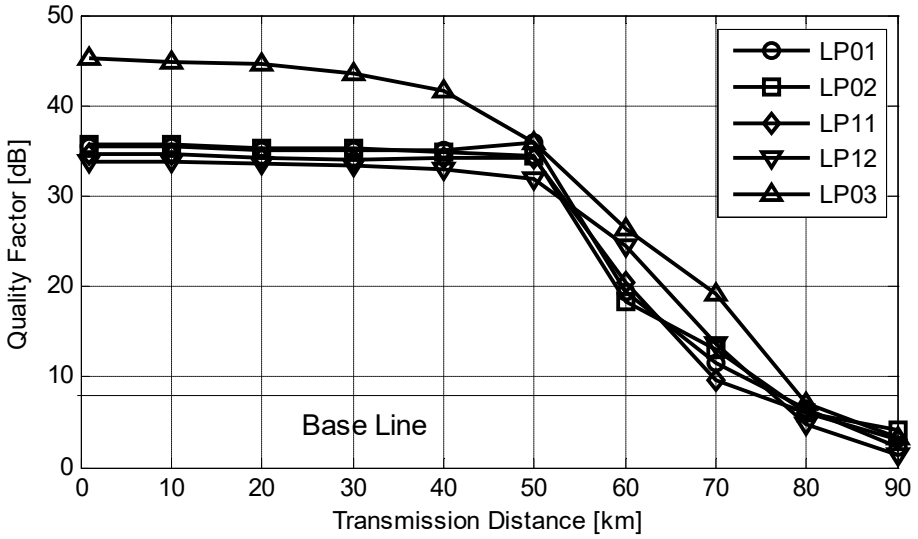

(a)

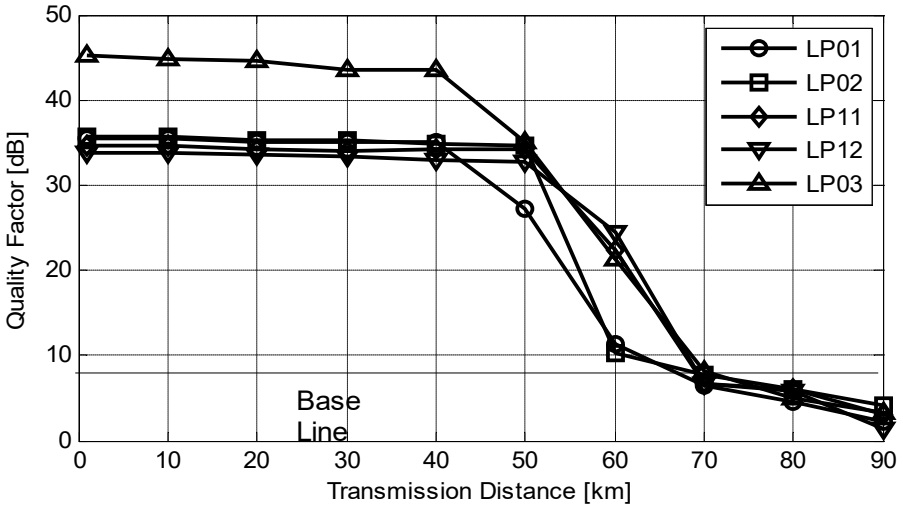

(b)

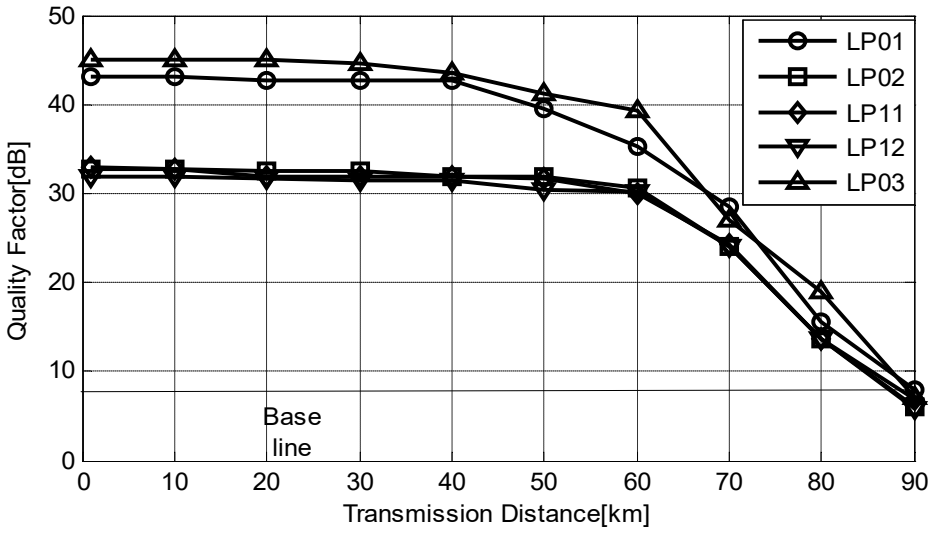

(c)

Fig. 5.4 Quality of 5 × 5 MIMO MDM system as a function of distance for (a) pre-MM and (b) boost-MM and (c) inline-MM configuration.

It is seen from Fig. 5.4(c) that in inline-configuration mode LP_{03} is having higher quality than LP_{01} mode but LP_{01} mode performs better than all other modes. It is concluded that using inline-configuration higher quality factor is achieved and with boost-configuration moderate quality is attained for the same cases.

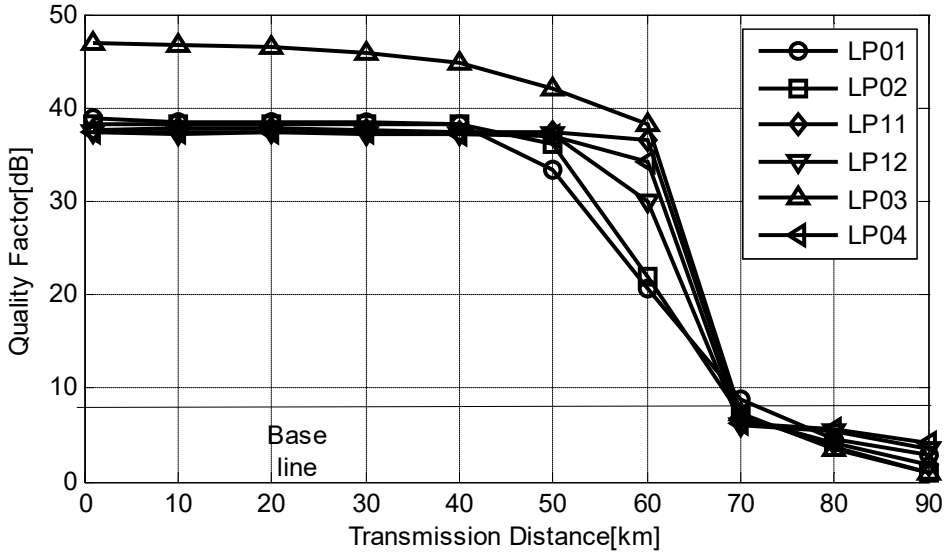

(a)

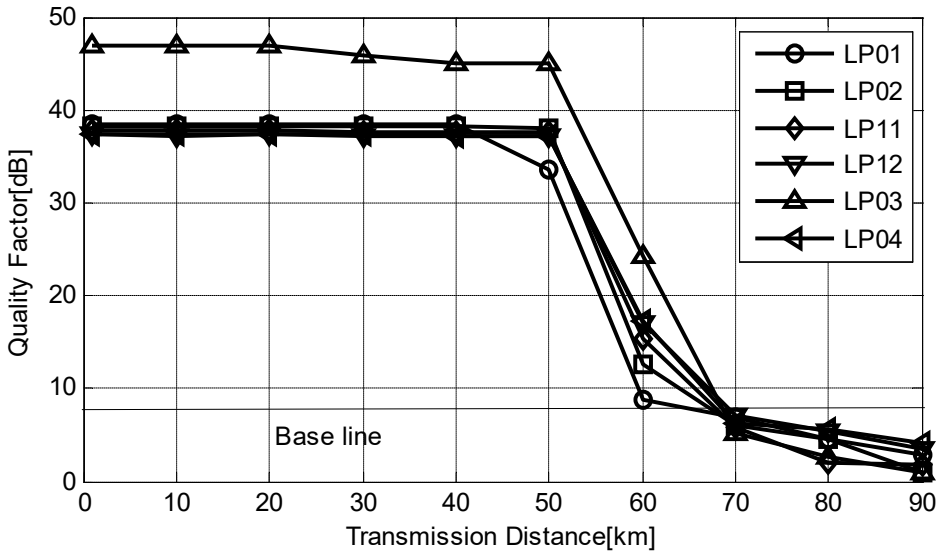

(b)

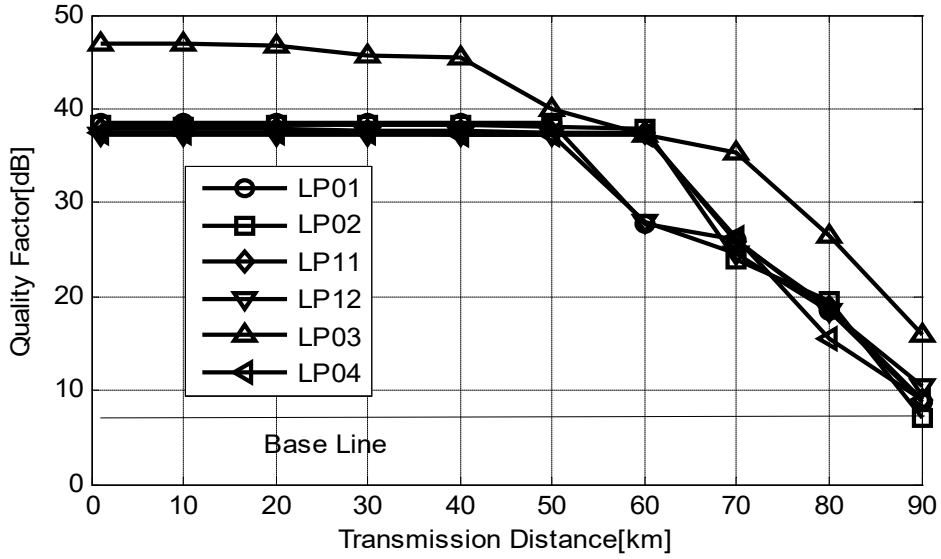

(c)

Fig. 5.5 Quality of 6 × 6 MIMO MDM system as a function of distance for (a) pre-MM and (b) boost-MM and (c) inline-MM configuration.

Again for pre-configuration method, the quality of signal is good even for 75 and 70 km of transmission distance in 5 × 5 and 6 × 6 MIMO MDM system, respectively. It can be seen that from Fig. 5.4(b) and Fig. 5.5(b), for acceptable Q-factor of 8 dB, the maximum distance for boost-configuration is up to 68 km while it is around 86 km for inline-MM EDFA configuration, these results illustrate enhanced performance even for 6 channel MDM system. On comparing pre- and inline-compensation methods for all the system

configurations (3 × 3, 4 × 4, 5 ×5 and 6 × 6) it is found that the later is superior to the former.

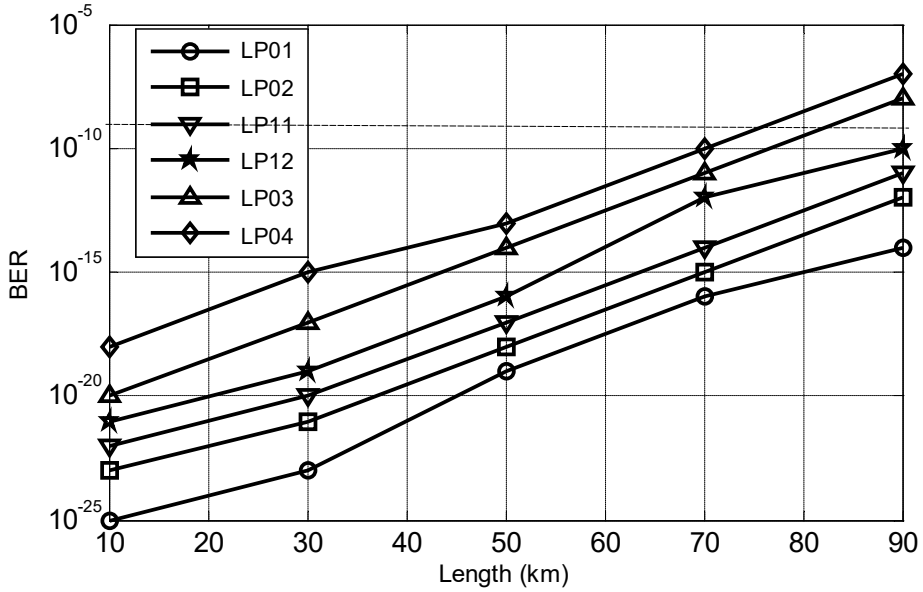

Fig. 5.6 BER of 6 × 6MIMO MDM systems as a function of MMF length.

Fig. 5.6 depicts the bit error rate of all the 6 channels after transmission at optimal low power of 0 dBm. It is noticed that maximum transmission distance (i.e. 90 km) is allowed by modes LP_{01}, LP_{02}, LP_{11} and LP_{12} which provide acceptable BER of 2.6×10^{-9} for 6 × 6 MIMO MDM system. These results prove better performance over [184] in which authors achieve BER for modes of all channels below the threshold of 3.8×10^{-3} over 50km of few mode fiber.

5.3. Investigation of LP hybrid mode and wavelength division multiplexing to enhance system capacity

5.3.1. Concept of LP-mode division multiplexing

The basic concept behind MDM is utilization of an optical fiber that permits propagation of different spatial modes through core. In LP-MDM technique, several independent data signals are modulated over *N* different spatial modes over multimode fiber to increase the capacity by *N* folds.

MDM permits several orthogonal spatial modes to be guided and transmitted simultaneously through a single or multiple cores of an optical fiber. Thus, total capacity is the product of capacity per fiber multiplied by number of modes. Thus, by adding

spatial degree of freedom, fibre capacity of MMF (multimode fiber) can be increased in the form of MIMO (multi-input multi-output) transmission.

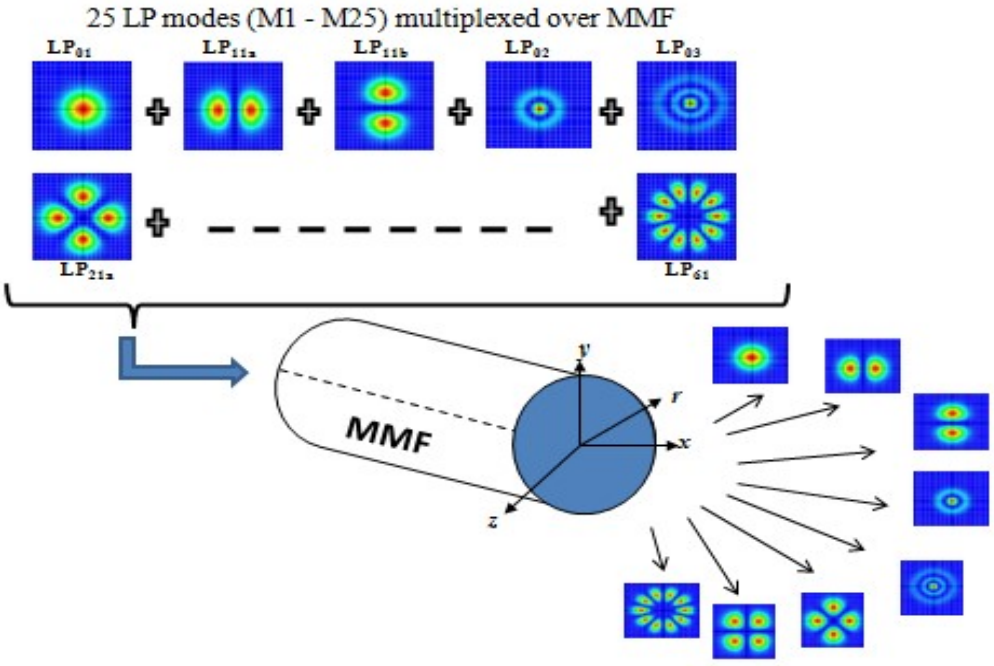

Fig. 5.7 Concept of LP mode division multiplexing scheme

MDM permits transmission of a number of channels upon different modes generated by different mechanisms like by few-mode fiber or multimode fiber [36-37], signal processing [35], [180-181], photonic crystal fiber [185] etc.

5.3.2. Design of LP-MDM-WDM system over MMF link

The schematic of proposed hybrid 10 Tb/s LP-WDM-MDM system is provided by Fig.5.8. The software 'VPI transmission Maker/ VPI component Maker 9.7' was utilized to simulate the results. The transmitter section of proposed system consists of five MM Tx (multi-mode transmitter) arrays tuned at wavelengths from 1550 nm to 1550.2 nm with channel spacing of 0.05 nm. Each MM Tx array includes laser source and MZ modulator for each information source (D1 to D25). The information source is in NRZ format with 10 Gb/s bit rate for each wavelength per LP mode producing system data rate of 10 Tb/s. The electrical driver creates the suitable data format for transmission, converts the input binary logical signal into electrical one and MZ modulator modulates the laser beam. Signals from 5 different transmitter arrays over 25 channels are fed to

mode converters for mode conversion and then to 5 mode combiners (indicated as MC) for grouping of modes each with 5 LP modes.

Table 5.2:LP-MDM-WDM system parameters

Name of parameter	**Value**
Signal wavelengths	1550 to 1550.2 nm
Channel spacing	0.05 nm
No. of modes	25
Data rate	10 Tb/s
Linewidth	10 MHz
Attenuation	1.81 dB/km
EDFA Pump type	Counter-propagate
EDFA pump wavelength	980 nm
EDFA gain	Flat
EDFA noise figure	4 dB
MMF refractive index peak	1.80
Dispersion	-99 ps/nm/km
Dark current	10 nA
Length	15 km

Here, 5 mode groups at 5 different wavelengths as individual data signals with *x*-index and *y*-index separations are multiplexed using WDM multiplexer. Inline-multimode (I-MM) EDFA is designed to amplify multiple modes and support modes (wavelength and mode division multiplexed) through MMF having parabolic index.

The mode calculation algorithm (discussed in detail in Section 4.2.1) is used to calculate modes in LP-WDM-MDM system. For GI-MMF modes can be computed by utilizing Helmholtz radial equation with different index profile in particular defined computational window Δtot. Different parameters of source MM transmitter array, MMF fiber and MDM system are described in Table 5.2. In receiver section, signals having different modes at different wavelengths are demultiplexed first by WDM demultiplexer and then by 5 optical mode selectors (indicated as MS).Different independent signals over 25 modes are recovered by 5 MM (multi-mode) receivers. Each MM receiver contain PIN photo detector which is used to convert the optical signal

into electrical followed by a LPF and optical analyzer for monitoring the BER, eye diagram and Quality-factor of transmission link.

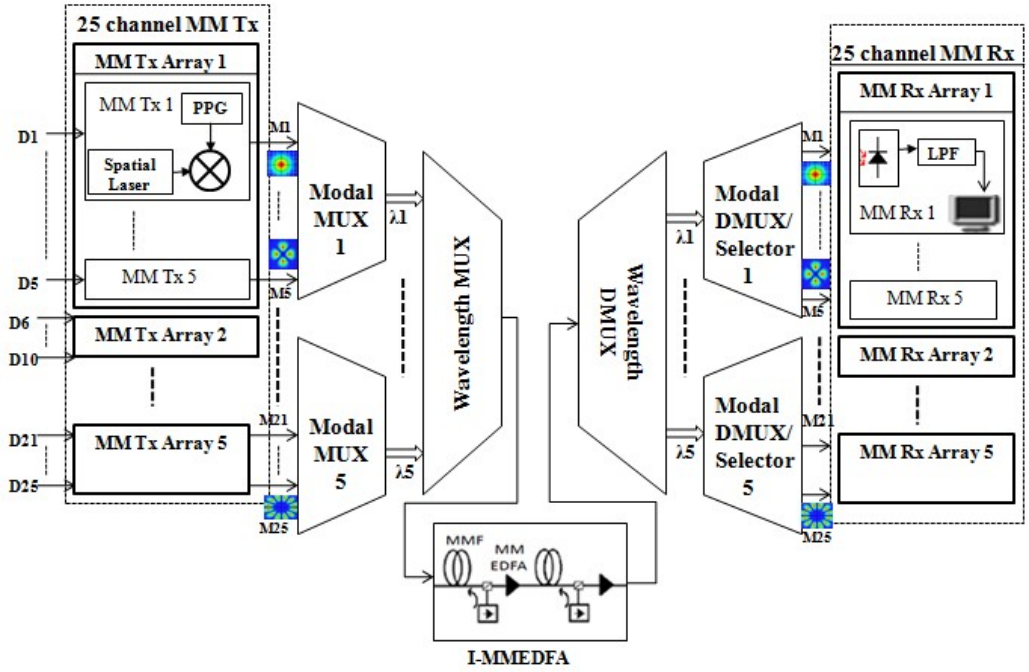

Fig. 5.8 System setup for 25 channel LP-WDM-MDM optical communication system; MM: multimode, Tx: transmitter, Rx: receiver, I-M MEDFA: inline-multimode EDFA amplifier configuration, LPF: low pass filter, M: modes (M1-M25) and D: data (D1-D25).

5.3.3 Result and Discussion

The key point of the simulation of LP-WDM-MDM system is to determine the intensity profile of modes while propagating through MMF. The LP modes travelling inside core under weakly guided condition are determined by solving Helmholtz equation (4.1) as discussed in Section 4.2.1 with varying index profile.

Fig. 5.9 represents the normalized mode field of different linearly polarized modes (Mode 1 to Mode 5: LP_{11}, LP_{12}, LP_{13}, LP_{14}, LP_{15}) propagating through MMF at 1550 nm as calculated by considering adaptive solution grid approach. These 5 modes were generated at MM Tx Array 1 and then normalized by mode combiner (MC1) as shown in Fig. 5.9. Similarly, 25 modes (Mode 1 to Mode 25) were generated at 5 different MM transmitters (MM Tx Array1 to 5) and then normalized by 5 different mode combiners (MC1 to MC5) presented by Fig. 5.10.

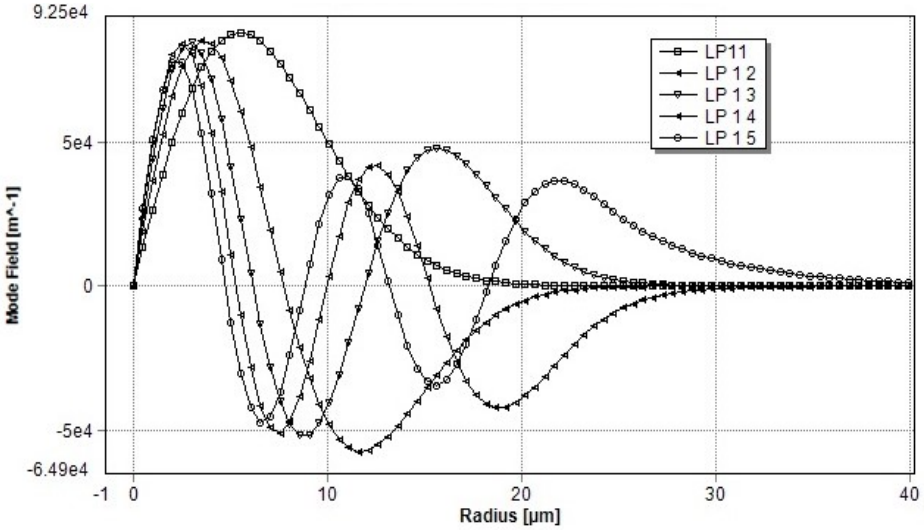

Fig. 5.9 The mode field intensity distribution of 5 different LP modes as function of the radius in the MMF.

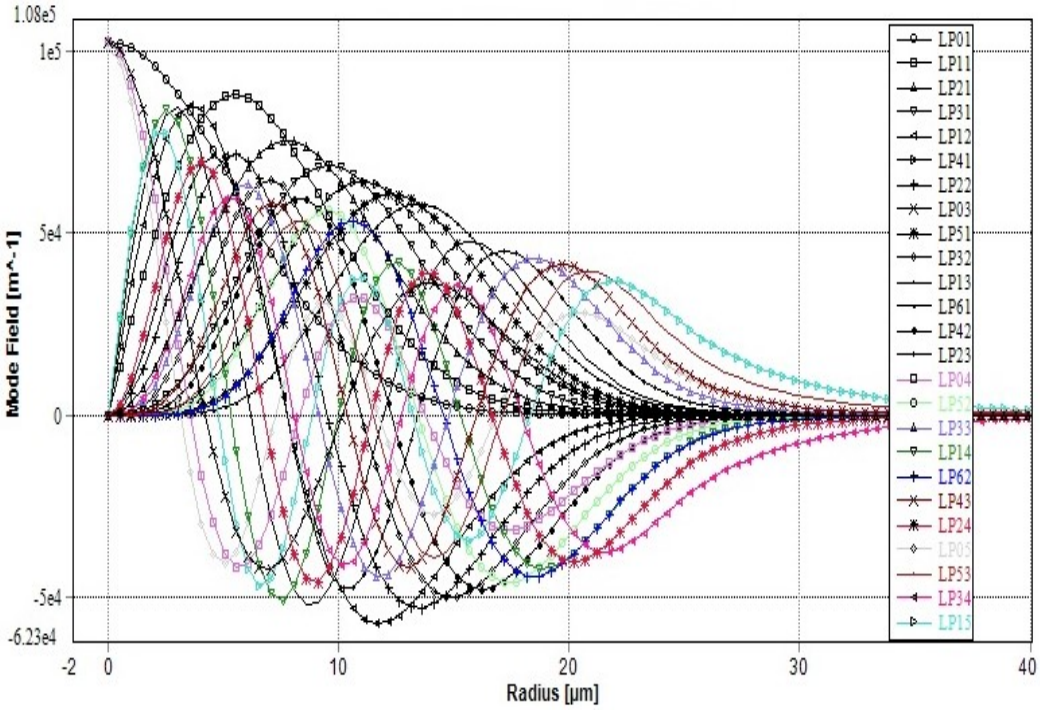

Fig. 5.10 The mode field intensity distribution of 25 LP modes in 10 Tb/s LP-WDM-MDM system.

The length of MMF has been varied from 1 km to 50 km to investigate the outcome of channel index spacing on performance of hybrid LP-WDM-MDM system. Thus, channel spacing with varied *x* and *y*-index of LP modes is observed in terms of bit error rate to evaluate the performance of MDM WDM system.

Fig. 5.11 illustrates the variation of bit error rate with MMF length for different channel indices of LP modes for each mode group. Three cases are considered to observe the result of channel index spacing of LP modes on performance of system:- case1: when x-index spacing is narrow (i.e x=0,1 for y-index= 1 to 5) represented by upper left graph; case 2: when x-index spacing is moderate (x=2 for y-index= 1 to 5) and case 3: when x-index spacing is too large (x=3, 4 for y-index= 1 to 5) represented by upper right graph.

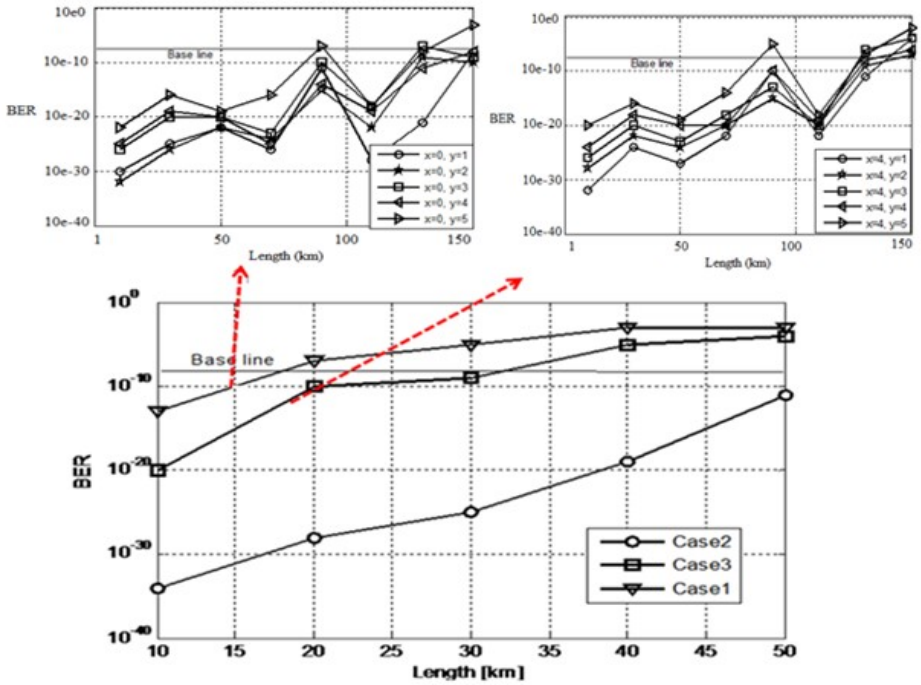

Fig. 5.11 BER of 25 channel LP- WDM-MDM system as a function of distance for index separations case1: x=0 and 1, y= 1 to 5; case2: x=2, y= 1 to 5; case3: x=4, y= 1 to 5.

From upper left graph for case1, it is observed that from length 1km to 50km, power coupling between LP modes increases and then decreases but modal delay difference is moderate resulting in low interference. From 50km to 90km, power coupling still prevails but modal delay difference becomes large giving rise to interference but after 130km interference goes on increasing.

Same trends are seen in upper right graph (Case3) when x-index separation is too large, modal delay is large and higher interference. When x-index separation of modes is moderate (x=2 in Case2) then good BER is attained for all y-index configurations, therefore low propagation delay and improved interference. It is concluded that maximum transmission distance (i.e. 700 km over MMF) is achieved with low

interference and acceptable BER (<10^{-9}) for moderate x-index channel spacing (Case 2: x=2, y=1 to 5) between LP modes. These results prove better performance over [95] in which authors achieve good BER for channel spacing (x=2, 3) of HG modes over distance of 800 m MMF.

The performance of system has also been investigated with the variation in power of input signal at each terminal unit. The quality of system is observed for different input powers (0 dBm, 10 dBm and 20 dBm) at each terminal unit with different number of users as shown in Fig. 5.12(a). With the increase in input power, performance quality of system improves.

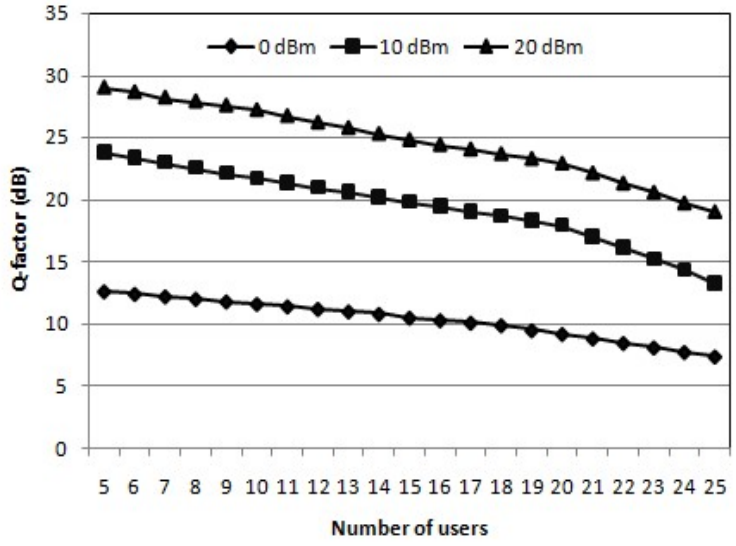

(a)

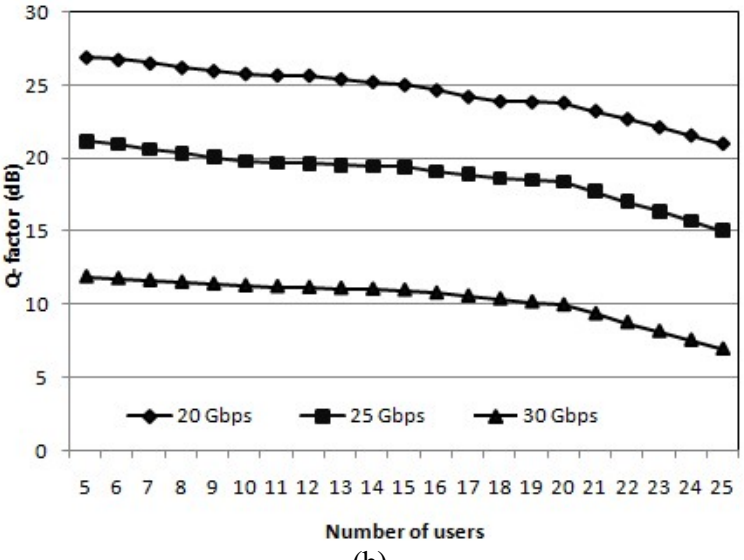

(b)

Fig.5.12 Quality performance of MIMO WDM-MDM system with number of users (a) with the variation in input power and (b) at different data rates.

Fig. 5.12(b) depicts the effect of number of channels on the performance of MIMO WDM-MDM system in terms of quality factor for different data rates (20 Gbps, 25 Gbps and 30 Gbps). Generally, with the increase in number of channels and data rate, quality of system starts degrading due to interference. But by controlling channel spacing in the system interference can be reduced. Thus, it is clearly examined that as the number of users increases from 5 to 25 in system along with increase in data rate, quality of signal starts distorting but not below acceptable level.

It is necessary to observe the performance of LP-WDM-MDM system after applying DSP MIMO filter at receiver end with respect to Q-factor to determine the higher possible capacity and transmission. Fig. 5.14 shows the enhanced performance of LP-WDM-MDM system (with MIMO filter tap optimization) supporting different number of users (25, 100, 225, 400 and 625) for longest possible transmission. It is noticed that for an acceptable quality factor (> 8.01 dB) system supports upto 225 users with maximum transmission distance of 700 km whereas it supports 400 users allowing 685 km and supports 625 users covering maximum transmission of 640 km respectively.

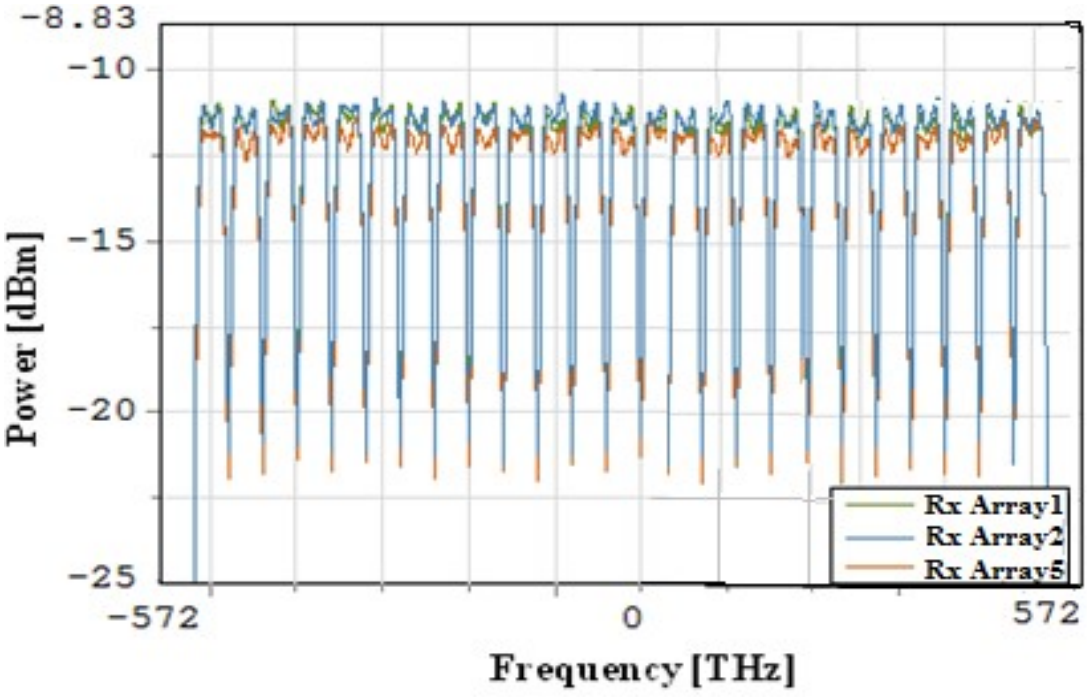

Fig.5.13 Optical spectrum of received WDM-MDM signal in LP-WDM-MDM system.

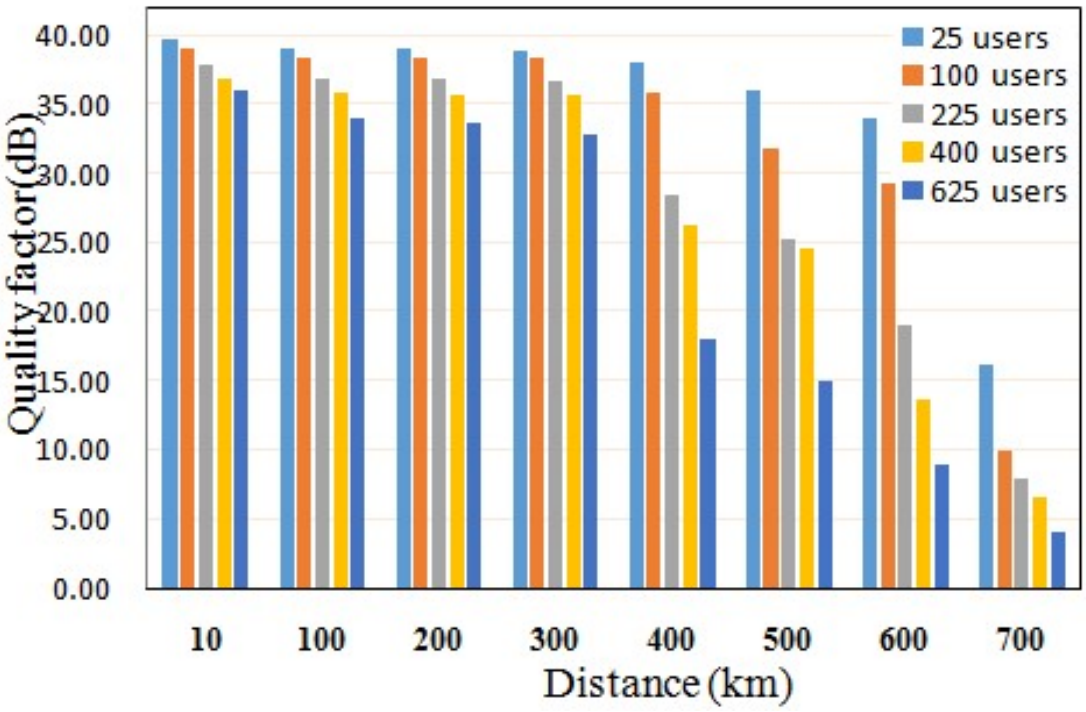

Fig. 5.14 Enhanced performance of 10 Tb/s LP-WDM-MDM system using MIMO Adaptive LMS equalization.

It is concluded that using MIMO filter DSP approach, LP-WDM-MDM system achieved Q-factor (> 8.01dB) supporting 625 users with higher data capacity of 10 Tb/s covering 640 km of transmission distance.

5.4 Conclusion

Simulation results of pre-, boost- and inline-configuration methods for 3 × 3, 4 ×4, 5 × 5 and 6 × 6 MIMO 10 Gbps non-return to zero Mode division multiplexed systems using MMF are presented. Further, the influence of transmission distance on the quality and reliability of system has been discussed for these methods. It is found that inline-configuration method provide better results for all considered MIMO MDM configurations. For acceptable quality factor more than 8 dB and BER < 10^{-9}, maximum distance covered (for 3 × 3 and 4 × 4 cases) using pre- and boost- configuration is approximately up to 85 km whereas it is up to 100 km for the inline-configuration method. Further, it is concluded that 10 Tb/s LP-WDM-MDM system utilizing adaptive MIMO equalization algorithm supports 625 users covering 700 km with acceptable BER (<10^{-8}) and Quality-factor (>9.8 dB) over MMF link. Featuring distinctive simplicity with reduced interference and low power consumption, the proposed design can be used

in optical network interconnects at data centres to fulfill the higher internet capacity at reduced channel spacing of 0.05 nm.

CHAPTER 6
OPTICAL SENSOR FOR MONITORING PERFORMANCE OF PIPELINES

6.1 Introduction

Every country depends on network of pipelines (energy, transmission and distribution pipelines like oil, natural gas, gasoline, liquid petroleum, chemicals, water, sewer lines, storm sewers, telephone lines, electric lines etc.) to efficiently and safely moves energy resources from energy storage to fuel their countries economic engine. Leakage is the major hazard that occurs in pipelines due to failures (cracks, corrosion, drilling, bursting, manufacturing flaws etc.) and geohazards (landslides, earthquakes put additional stress) leading to major disasters (environmental pollution, loss of property and lives of people).

A variety of technologies including ultrasonic, acoustic emission, microwave wireless sensors, radiography, multimode sensing, eddy current and magnetic flux have been developed over the past few decades but these lack portability, constant monitoring and susceptibility to electromagnetic interference [72], [73]. Hence, there is a need to supplement or replace these methods with an efficient and reliable non-destructive in-situ periodic monitoring technique for pipeline structures. Corrosion of pipeline assets is the major cause for incredible leakage and contamination threats. Alhandawi et al. [135] studied and modeled a distributed sensor with metal coated polymer cladding fiber cables to detect internal corrosion of pipeline. Lee et al. [136] proposed FBG sensors to monitor the pipeline damage measuring guided wave responses.

Moreover, the existing optical sensor based monitoring techniques have not presented parallel monitoring of corrosion, strain and temperature fluctuations in different pipelines [70-71], [81].It can be accomplished that the proposed strain sensor focuses on the pipeline leakage and corrosion monitoring. This Chapter addresses the issues discussed above by experimentally monitoring the variation in pipeline parameters (like leakage acoustics strain and thickness reduction due to corrosion)utilizing surface mounted Fibre Bragg Grating (FBG) Optic Sensors. This objective is presented in different Sections as follows: Section 6.2 explains simulation investigation of MMF based sensor for pipeline monitoring; Section 6.3 deals with experimental set up for leak detection and in Section 6.4, conclusion is discussed.

6.2 Investigation of MMF based sensor for monitoring performance of pipeline

6.2.1 Mode theory for in-grating fiber

The mode field interaction between core and cladding mode inside in-grating fiber can be studied by treating the coupling between the fiber core mode and multiple cladding modes concurrently at a specific wavelength with the help of CMT(Coupled mode theory) [84]. The individual resonances are adequately narrow in most of the cases and can be spectrally separated such that coupling between core and cladding mode exactly describes the transmission spectra. Simply, two mode coupling theory can be utilized in such cases.

The approximate solution to Maxwell's equations for layered media is provided by Coupled-mode theory. In case of an optical fiber in the absence of perturbations, the field propagating in the fiber can be assumed as a linear combination of modes written as [186]:

$$E(x,y,z,t)=\sum_{N}A_N\psi_N(x,y)e^{-i(\omega t-\beta_N z)} \quad (6.1)$$

where, A_N denotes constant amplitudes, $\psi_N(x,y)$: represents the transverse field profile of the N^{th} mode having propagation constant β_N when a field of frequency ω is excited into the fiber. Let us consider the total field due to only 2 co-propagating modes with maximum interaction due to perturbation, Equation (6.1) becomes [187]:

$$E(x,y,z,t)=A_1(z)\psi_1(x,y)e^{-i(\omega t-\beta_1 z)}+A_2(z)\psi_2(x,y)e^{-i(\omega t-\beta_2 z)} \quad (6.2)$$

where, β_1 and β_2 are the propagation constants of the modes calculated in the absence of perturbation in the fiber, $A_1(z)$ and $A_2(z)$ are their corresponding amplitudes, $\psi_1$and ψ_2 represent the normalized field profiles. Putting equation (6.2) in wave equation assuming weak perturbation, variation in amplitude of mode is slow and considering orthogonality relation between 2 modes [84]:

$$\frac{\partial A_1}{\partial z}=-i\kappa_{11}A_1-i\kappa_{12}A_2e^{-i(\beta_1-\beta_2-K)z} \quad (6.3a)$$

$$\frac{\partial A_2}{\partial z}=-i\kappa_{22}A_1-i\kappa_{21}A_1e^{-i(\beta_1-\beta_2-K)z} \quad (6.3b)$$

where, $K=2\pi/\Lambda$ indicates the grating vector; κ_{11}, κ_{22} symbolize dc coupling coefficient; κ_{12}, κ21 corresponds to cross coupling and substitute $\kappa = \sqrt{\kappa_{12}\kappa_{21}}$ resulting into coupled mode equations as [187]:

$$\frac{\partial A_1}{\partial z} = -i\kappa A_2 e^{i(\beta_1-\beta_2-K)z} \text{ and } \frac{\partial A_2}{\partial z} = -i\kappa A_1 e^{-i(\beta_1-\beta_2-K)z} \tag{6.4}$$

By making a variable transformation coupled mode equation reduces to [188]:

$$\frac{dR}{dz} = -i\kappa S - i\delta R \text{ and } \frac{dS}{dz} = -i\kappa R + i\delta S \tag{6.5}$$

Here,$\delta = (\beta_1-\beta_2-K)/2$ corresponds to the detuning factor. The coupling between two modes is maximum when frequency satisfying zero detuning condition, δ=0 can be written as $\beta_1 - \beta_2 = \frac{2\pi}{\Lambda}$ representing phase matching condition between 2 modes.

In case of uniform gratings the length and period of grating is uniform throughout the grating length in which set of coupled mode equations can be solved analytically and general solution can be written as [188]:

$$R(z=L,\delta) = \cos(\gamma L) - i\frac{\delta}{\gamma}\sin(\gamma L) \tag{6.6a}$$

$$S(z=L,\delta) = -i\frac{\kappa}{\gamma}\sin(\gamma L) \text{where, } \gamma = \sqrt{\kappa^2+\delta^2} \tag{6.6b}$$

The transmitted power related to two modes at the end of grating is specified by $|R(z=L,\delta)|^2 = |S(z=L,\delta)|^2$ and the transmitted power of core mode can be written as [84], [188]:

$$|R(z,\delta)|^2 = 1 - \frac{\kappa^2}{\gamma^2}(\sin(\gamma L))^2 \tag{6.7}$$

For a wavelength related to zero detuning (δ = 0, $\gamma = \kappa$) the power transmitted in the core is simply $((\gamma z))^2$ but for a considered grating the output power at core fluctuates as a function of cosine with increasing grating length. The coupling efficiency can be determined as power lost in the cladding mode from the core mode given as [84, 188]:

$$\eta = 1 - |R(z,\delta)|^2 = \frac{\kappa^2}{\gamma^2}(\sin(\gamma z))^2 \tag{6.8}$$

6.2.2 Theoretical analysis of strain and temperature monitoring

When light enters at one end of an optical fiber it passes through the fiber with almost

no reflection. Bragg gratings are periodic structures of indentation written in the core of fiber causes small light to reflect [88]. As light enters fiber Bragg grating it reflects a narrowband portion of incoming light and rest passes through the optical fiber. The central wavelength of the incident signal, named Bragg wavelength λ_B, is given by equation (1.25) [88]. Any change in either effective refractive index or grating period can cause central Bragg wavelength to shift to higher wavelength. The reflection wavelengths of gratings inside MMF can also be modulated by temperature and strain similar to gratings in single mode fiber. The shift in the grating center wavelength due to strain (ε) and temperature (T) changes is given by [189]:

$$\Delta\lambda_B = 2(\Lambda\frac{\partial\eta_{eff}}{\partial l} + \eta_{eff}\frac{\partial\Lambda}{\partial l})\Delta l + 2(\Lambda\frac{\partial\eta_{eff}}{\partial T} + \eta_{eff}\frac{\partial\Lambda}{\partial T})\Delta T \tag{6.9}$$

In Equation (6.4), first term represents the effect of strain on MMF. Whenever there is strain (ε) on fiber, stretching of the fiber grating takes place (change in grating length Δl) which further leads to change of grating period (Λ). Due to this, photoelastic effect occurs which causes change in effective refractive index. Thus, Bragg wavelength shifts due to this strain effect is given by following equation [189]:

$$\Delta\lambda_B = K_\varepsilon\varepsilon \tag{6.10}$$

where, $\Delta\lambda_B$ is bragg wavelength shift due to strain, ε is strain and K_ε represents strain sensitivity coefficient which can be calculated as [190]

$$\mathrm{K}_\varepsilon = (1\text{-}P_e)\,\lambda_B \tag{6.11}$$

where, P_e is the effective photo-elastic coefficient of fiber. Putting the value of K_ε in equation (6.10) as:

$$\Delta\lambda_B = (1-P_e)\lambda_B\varepsilon \tag{6.12}$$

where, P_e is given as [191]:

$$P_e = \frac{n^2}{2}(P_{12} - \nu(P_{11}P_{12}) \tag{6.13}$$

For the silica single-mode fiber, P_e= 0.22, n is refractive index, P_{ij} depicts photo-elastic coefficient (P_{11}, P_{12}) and υ is Poisson's ratio. This characteristic of Bragg grating can be utilized by optical strain sensor to sense small movements or strains such as cracks created on the surface of pipeline structure.

In Equation (6.9), the second term presents the effect of temperature on MMF. As thermal expansion cause changes in the grating period and the index of refraction so, there is a shift in the Bragg grating centre wavelength. The Bragg wavelength shifts due to effect of temperature is given by following equation [190]:

$$\Delta\lambda_B = K_T \Delta T \tag{6.14}$$

where, $K_T = (\alpha + \zeta)\lambda_B$ represents temperature sensitivity coefficient, α : thermal expansion coefficient and $\zeta = \frac{\left(\frac{dn}{dt}\right)}{n}$ represents thermo-optic coefficient [189-190].

6.2.3 Design of Bragg grating inscribed inside MMF based sensor for temperature and strain monitoring

Fig. 6.1 shows the simulated design of optical strain and temperature sensor based on FBG utilizing VPI Photonics/ VPI transmission Maker™ Version 9.7 simulator. In the first stage circular three layer model of multimode fiber is taken with core and cladding parameters: radii (25, 62.5 μm) and refractive indices (η_1:1.457,η_2:1.444) respectively. Further, infinitely extending surrounding material or sensing area around the MMF with another refractive index η_0 is considered. Here, air is considered as surrounding medium around fiber so, η_0=1.Coupled-mode theory is utilized in which coupling of the core mode with true cladding modes is taken into account whereas coupling to radiation modes if any is discarded. Thus, η_0 should be smaller than η_2 (cladding refractive index) for accurate modeling of grating spectrum.

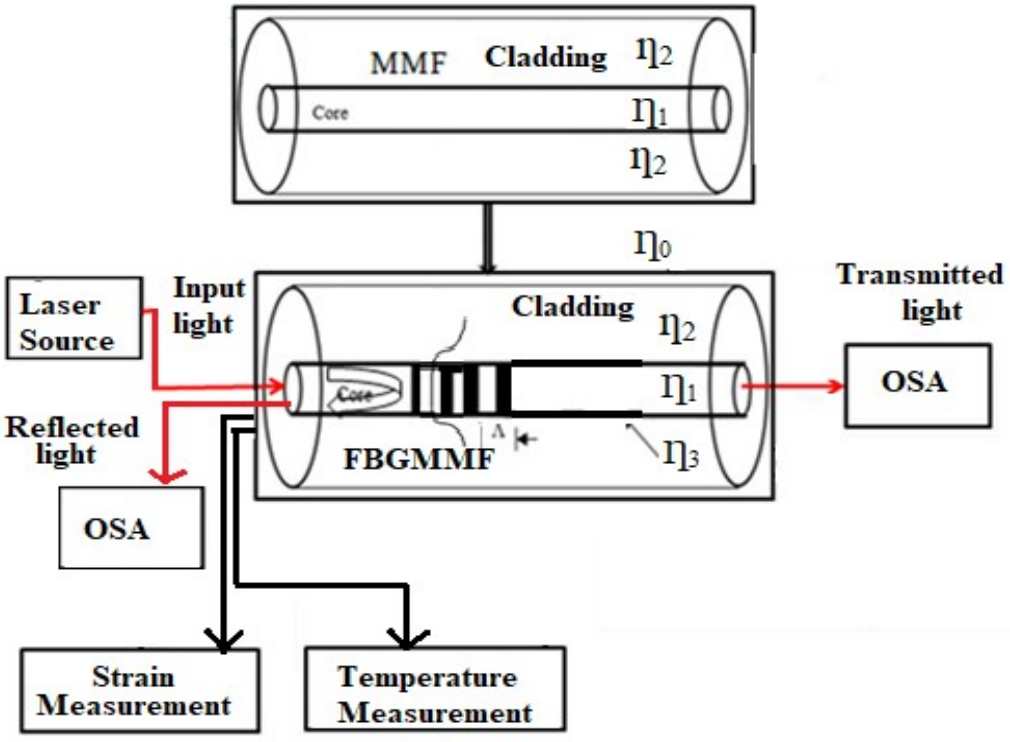

Fig. 6.1 Simulated design of optical strain and temperature sensor based on BG-MMF (Bragg gratting-Multimode fiber).

In second stage fiber Bragg grating is written inside the core layer of MMF with a similar grating-induced refractive index change across the whole core area. The considered FBG is of uniform shape with grating period (Λ) of 0.55 μm. For this Bragg grating based MMF design, photo-elastic coefficients: P_{11}= 0.122, P_{12}= 0.272, Poisson's ratio: υ = 0.16, thermo-optic coefficient for core and cladding (ζ_{core}= 7.6x10^{-6}, ζ_{clad}= 7.8 x10^{-6}) and thermal expansion coefficient = 0.58x10^{-6}. Now, light is passed through the proposed FBG MMF, light pulse at Bragg wavelength is reflected back from gratings and remaining light is transmitted to a spectrum analyzer for measuring different physical parameters like strain, curvature, temperature and surrounding refractive index. In third stage temperature is varied from 20^{o}C to 50^{o}C with zero strain to observe the changes in design parameters and shift in Bragg wavelength.

In fourth stage strain is applied at constant temperature of 20^{o}C to observe the shift in Bragg wavelength. Further,in fifth stage, to enhance the temperature sensitivity of sensor cladding thermo-optic coefficient(ζ_{clad}) is varied from 7.8 x10^{-6} to 9.12x10^{-6}alongwith coupling to chosen higher mode $LP_{21}$to characterize the temperature sensor.

6.2.4 Result and Discussions

Fig. 6.2 represents resonance grating periods for weak Bragg gratings (having very small average refractive index change inside the grating) written into the core of the fiber. Here, resonant coupling of 9 cladding modes with the fundamental core mode at frequency *f*. The resonant grating period of N^{th} mode can be defined as [192]:

$$\Lambda_N = \frac{\lambda}{\eta_0 \pm \eta_N} = \frac{c/f}{\eta_0 \pm \eta_N} \tag{6.15}$$

where, η_N and η_0 denotes effective indices of *N* modes and core's zeroth mode, in denominator '±' sign indicates type of grating inscribed inside fiber: '+' for FBG and '–' for LPG.

The Bragg grating with a period of 0.535 μm written inside the core of the fiber causes resonant coupling with the contra propagating fundamental core mode at the frequency 193.0408 THz and with contra propagating cladding modes at the frequencies exceeding 193.1940 THz.

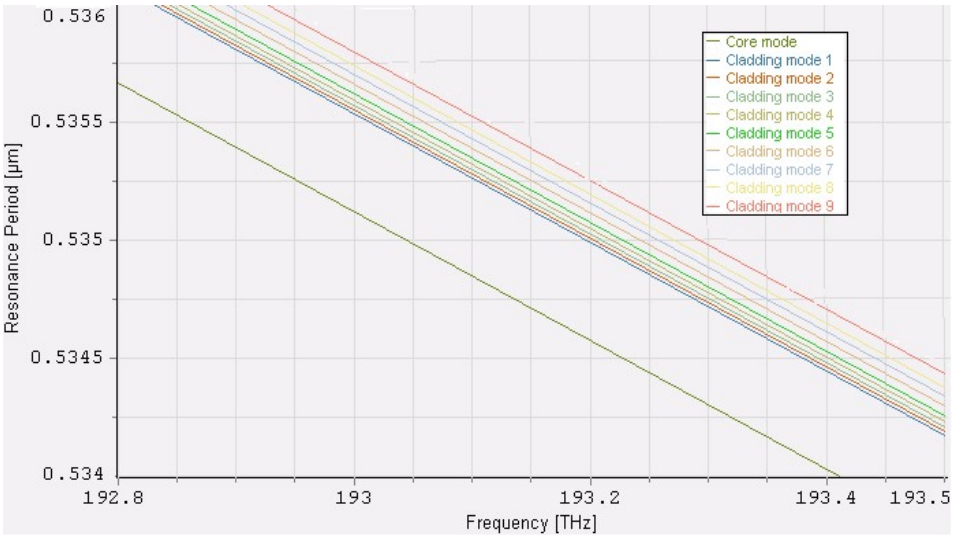

Fig. 6.2 The resonance grating period of fiber modes as a function of frequency.

It is concluded that as Bragg gratings become stronger, the resonance grating periods at given frequencies start to shift. This shift can be taken into account by adding the average grating-induced index change to the fiber core refractive index.Thus, effective indices have to be calculated with respect to frequency.

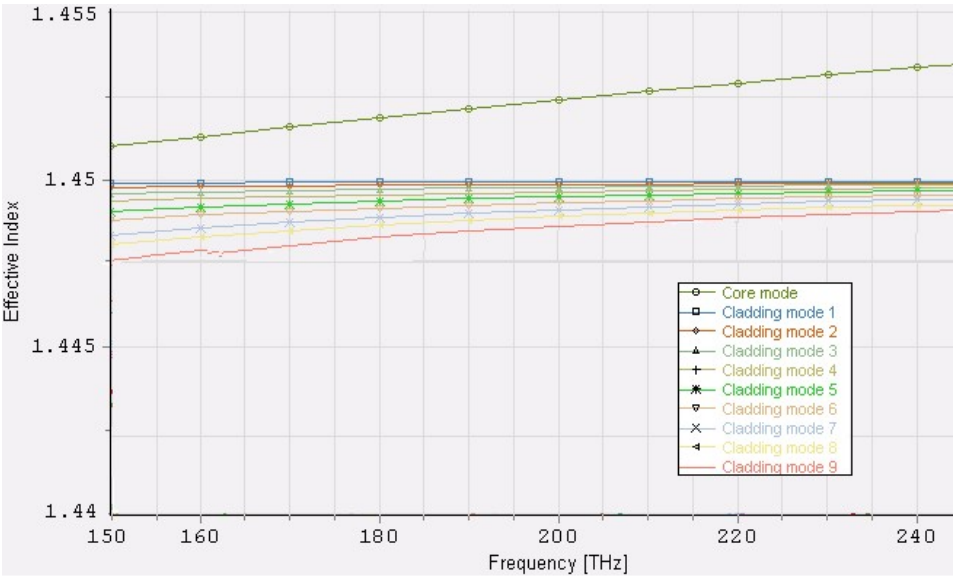

Fig. 6.3 Values of effective indices of the fiber core and cladding modes as a function of frequency.

Fig. 6.3 represents the plot of effective indices of the fiber core and cladding modes as a function of frequency. The modes are grouped according to their effective indices, starting with the fundamental core mode characterized by the largest effective index

located in between the core and cladding refractive indices. The Cladding mode 1 characterized by the next highest effective index but smaller than cladding refractive index. It is observed that 9 cladding modes are shown that have nonzero coupling with the fundamental core mode.

Overlap integral represents the strength of resonant coupling. The strength of resonant couplings between modes depends on the product of refractive index modulation inside the grating and the overlap integral of the fiber mode under consideration with the fundamental core mode. The frequency dependence of overlap integrals can be determined by [84]:

$$\kappa_v = f.\pi\varepsilon_0\eta_1 \int_0^{2\pi} d\phi \int_0^{r_1} \vec{E}_v(r,\phi).\vec{E}^*_{core}(r,\phi)dr \tag{6.16}$$

where, f represents particular frequency, ε_0: vacuum permittivity, η_1: refractive index of fiber core, r_1: radius of fiber core, $\vec{E}_v(r,\phi)$presents vectorial electric field component of considered modes and $\vec{E}^*_{core}(r,\phi)$ vector electric field of the fundamental core mode.

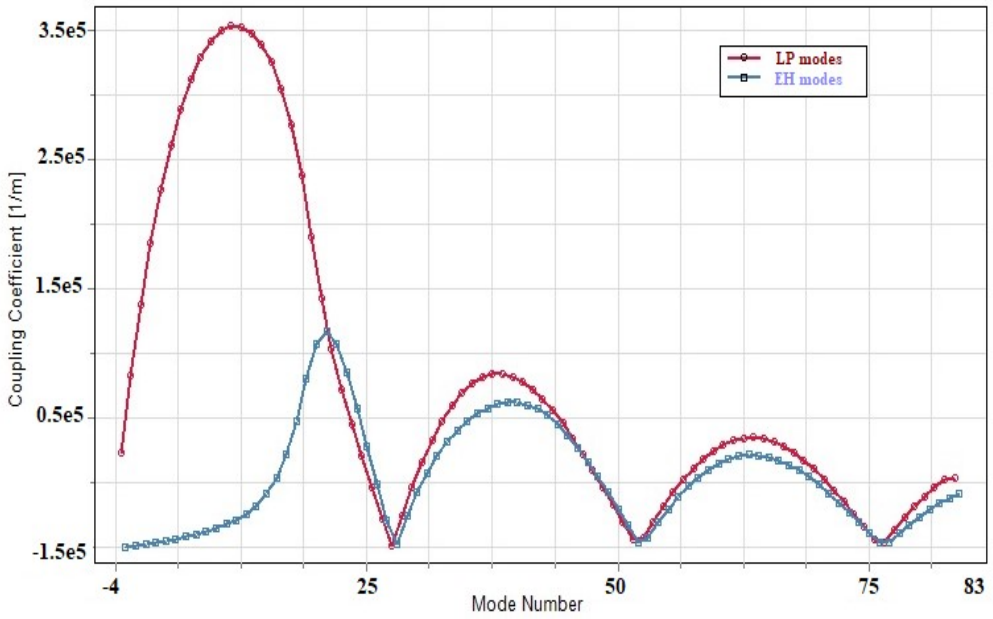

Fig.6.4 Overlap integral of fundamental mode with chosen cladding modes to achieve mode with highest coupling.

The multimode fiber supports multiple modes and couples power from core modes to cladding modes. If FBG is inscribed inside core of MMF then, fundamental core mode starts coupling power towards cladding modes with periodic perturbation of refractive index. The effective indices of cladding modes strongly depend on refractive index (η_0)

of the surrounding medium around the cladding. If there is any change in surrounding $\eta_0$then, effective index of cladding modes results in large variation. As coupling wavelength to a particular cladding mode depends on effective index of cladding modes through phase matching. So, ambient change in η_0 will affect the resonant wavelength. The coupling of the fundamental core mode with the same counter propagating mode results in strongest coupling that causes resonance in gratings.

Fig. 6.4 represents the plot of overlap integrals as a function of mode number for different modes travelling inside fiber. Here, in this case MMF fiber has 81 cladding modes at wavelength of 1545 nm. It can be observed that the highest coupling of fundamental core mode with cladding modes is achieved for LP mode with mode number 12. With the increase in order of both LP and EH cladding modes, the difference between the overlap integrals of both cladding modes is less pronounced.

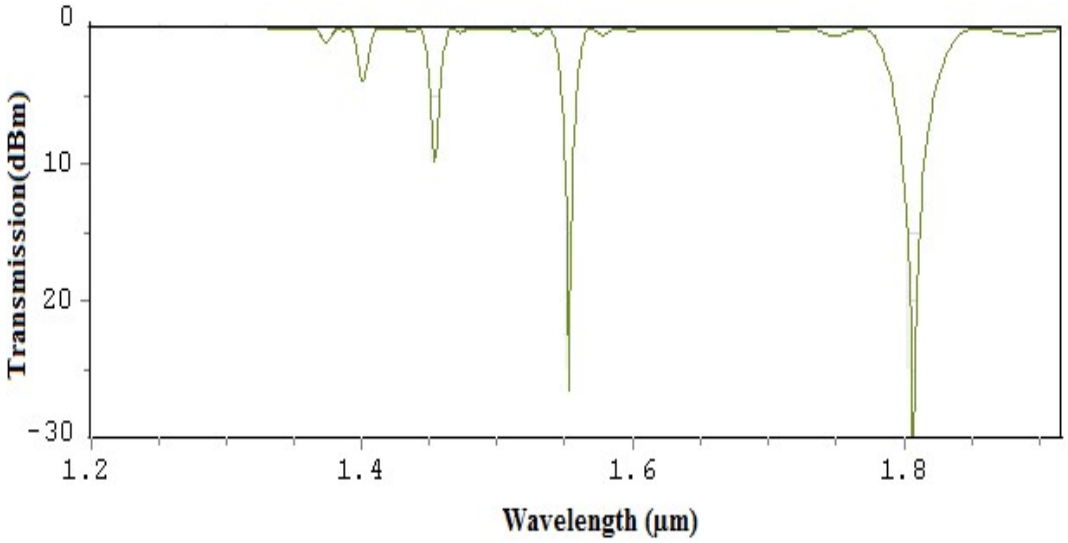

Fig.6.5 The simulated transmission spectrum of Bragg grating induced in core of MMF.

The number of Bragg wavelengths are dependent on number of modes being excited in an optical fiber as discussed in Section 1.6.2. Here, in case of MMF excitation of more than 15 Bragg wavelengths can be observed because of larger diameter of core carrying more number of modes. The simulated transmission spectrum for grating written in core of MMF with core and cladding radii (25, 62.5 μm) and refractive indices (1.457, 1.443) respectively surrounded by air and grating period of 0.55 μm is shown in the Fig. 6.5.

The effect of strain and temperature on grating inside MMF has been theoretically analyzed and investigated using simulator. The effect of strain on Bragg wavelength keeping temperature constant is shown in Fig. 6.6.

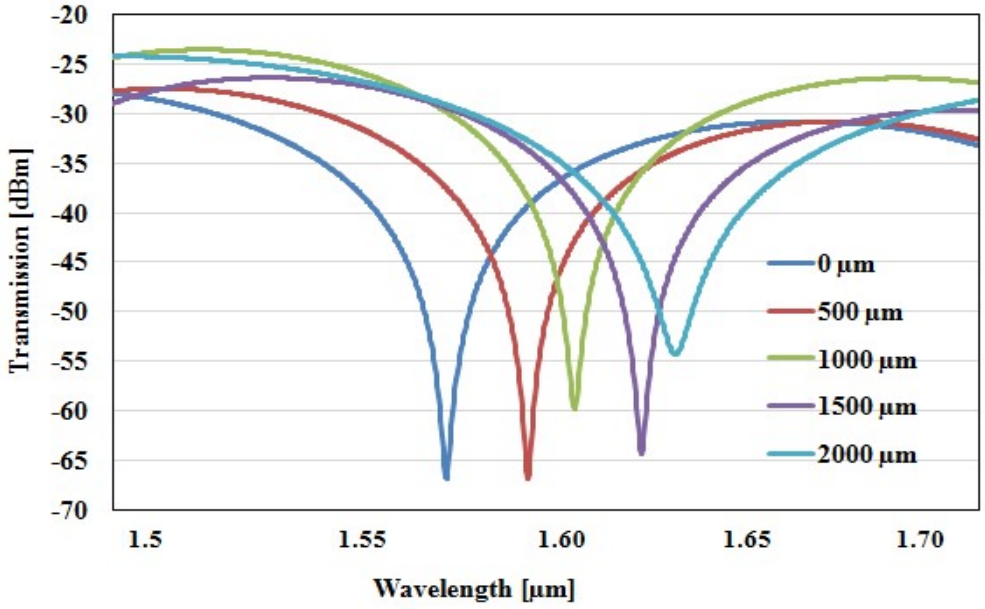

Fig.6.6 The shift in Bragg wavelength with variation in applied strain keeping temperature constant at 20°C.

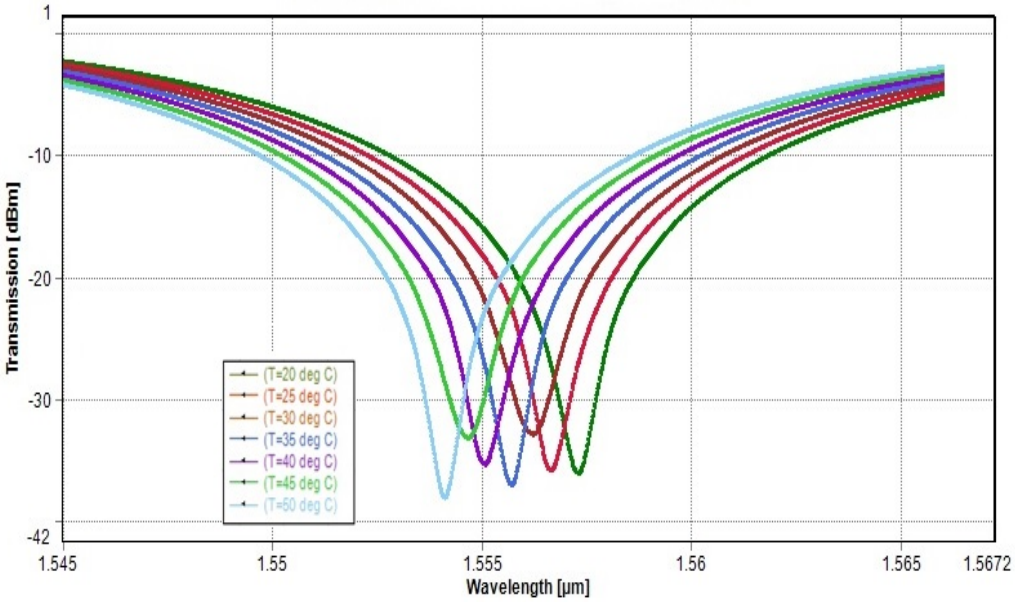

Fig.6.7 The shift in Bragg wavelength with variation in temperature with zero strain applied on it.

It can be observed that when zero strain is applied then, Bragg wavelength (λ_B= 1.57 µm) is the central wavelength but as strain is increased then Bragg wavelength started shifting towards higher wavelength. Fig. 6.7 represents the simulated results of shift in Bragg wavelength with temperature variation from 20°C to 50°C with zero applied strain.

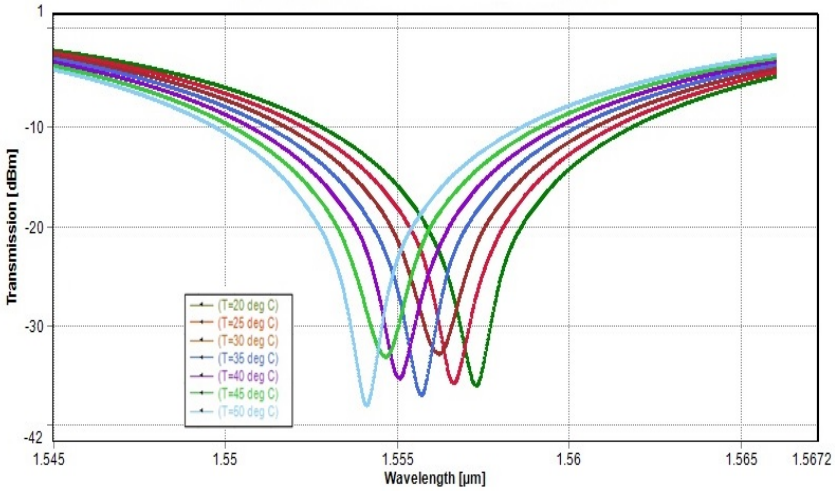
Transmission [dBm]
1
-10
-20
-30
-42
1.545
1.55
1.555
1.56
1.565
1.5672
Wavelength [µm]
(T=20 deg C)
(T=25 deg C)
(T=30 deg C)
(T=35 deg C)
(T=40 deg C)
(T=45 deg C)
(T=60 deg C)

(a)

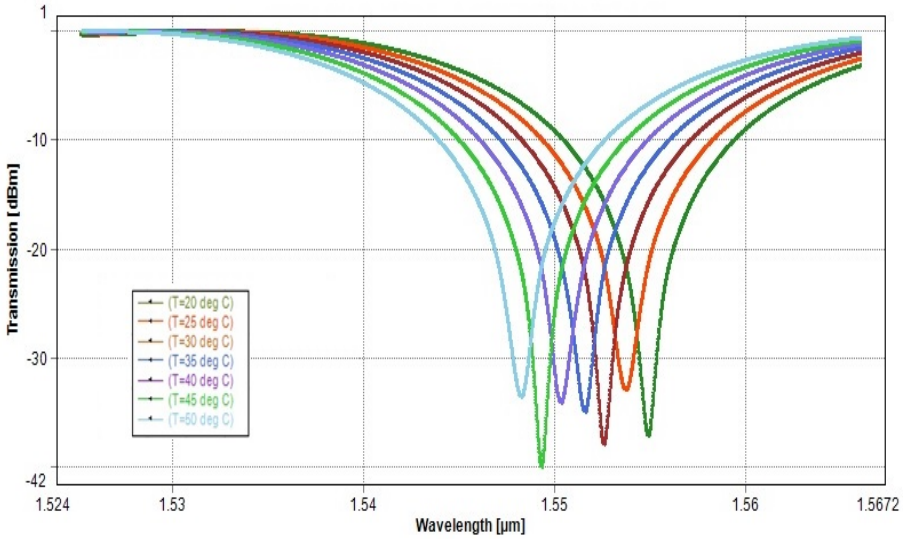
Transmission [dBm]
1
-10
-20
-30
-42
1.524
1.53
1.54
1.55
1.56
1.5672
Wavelength [µm]
(T=20 deg C)
(T=25 deg C)
(T=30 deg C)
(T=35 deg C)
(T=40 deg C)
(T=45 deg C)
(T=60 deg C)

(b)

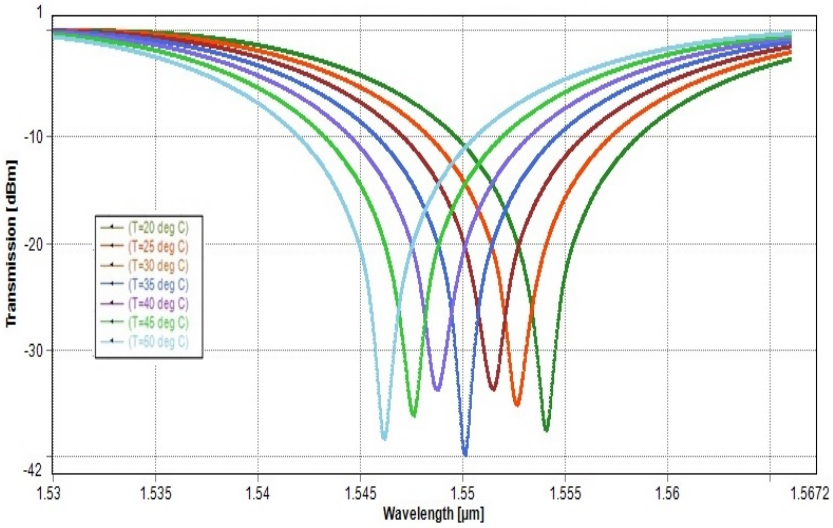
Transmission [dBm]
1
-10
-20
-30
-42
1.53
1.535
1.54
1.545
1.55
1.555
1.56
1.5672
Wavelength [µm]
(T=20 deg C)
(T=25 deg C)
(T=30 deg C)
(T=35 deg C)
(T=40 deg C)
(T=45 deg C)
(T=60 deg C)

(c)

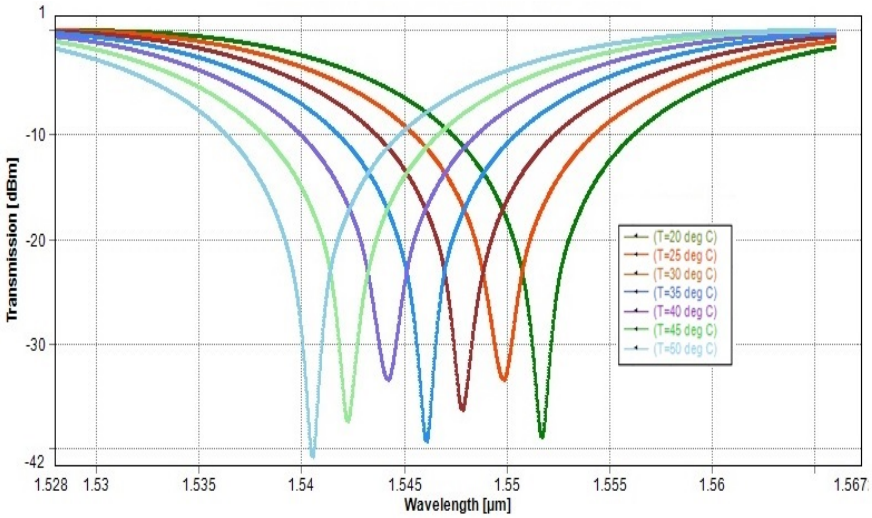

(d)

Fig. 6.8 Observed spectrum for variation in thermo-optic coefficient (a) 7.9 x 10^{-6}, (b) 8.2 x 10^{-6}, (c) 8.5 x 10^{-6} and (d) 8.8 x 10^{-6} to characterize temperature sensor.

As sensitivity of temperature sensor depends on cladding thermo-optic coefficient (ζ_{clad}). Further, cladding thermo-optic coefficient has been varied from 7.9 x 10^{-6} to 9.1 x 10^{-6} along with variation in temperature from 20^{o}C to 50^{o}C to observe the sensitivity in terms of wavelength shift as shown in Fig.6.8. Table 6.1 summarize the sensitivity of Bragg grating MMF based temperature sensor with variation in thermo-optic coefficient.Fig. 6.9 depicts the simulated spectrum of temperature sensor based on MMF-BG with enhanced sensitivity.

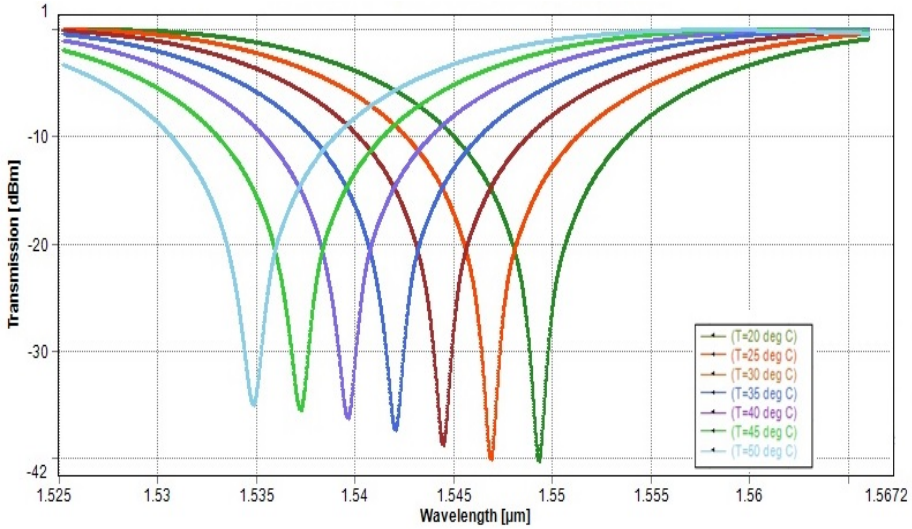

Fig.6.9 The simulated spectra of temperature sensor based on MMF-BG with enhanced sensitivity.

Table 6.1 Wavelength shift of temperature sensor

S.No.	Thermo-optic coefficient	Wavelength (μm) at temperature 20°C	Wavelength (μm) at temperature50°C	Wavelength shift
1.	7.9×10^{-6}	1.557	1.554	3 nm
2.	8.2×10^{-6}	1.555	1.548	7 nm
3.	8.5×10^{-6}	1.554	1.546	8 nm
4.	8.8×10^{-6}	1.552	1.541	11 nm
5.	9.1×10^{-6}	1.549	1.535	14 nm

6.3 Experiment on Fiber Bragg Grating Optical Sensor for leak detection in underground energy storage pipelines

6.3.1 Experimental Setup I:

The experimental setup for detecting leak point in different pipeline structures (open and close) by applying load is shown in Fig. 6.10 and 6.11 respectively. This setup includes Interrogator as transreceiver unit with wavelength range (minimum: 1510 nm and maximum: 1590 nm), Optical bragg grating strain sensor, 1metre long stainless-steel pipeline and computational device.

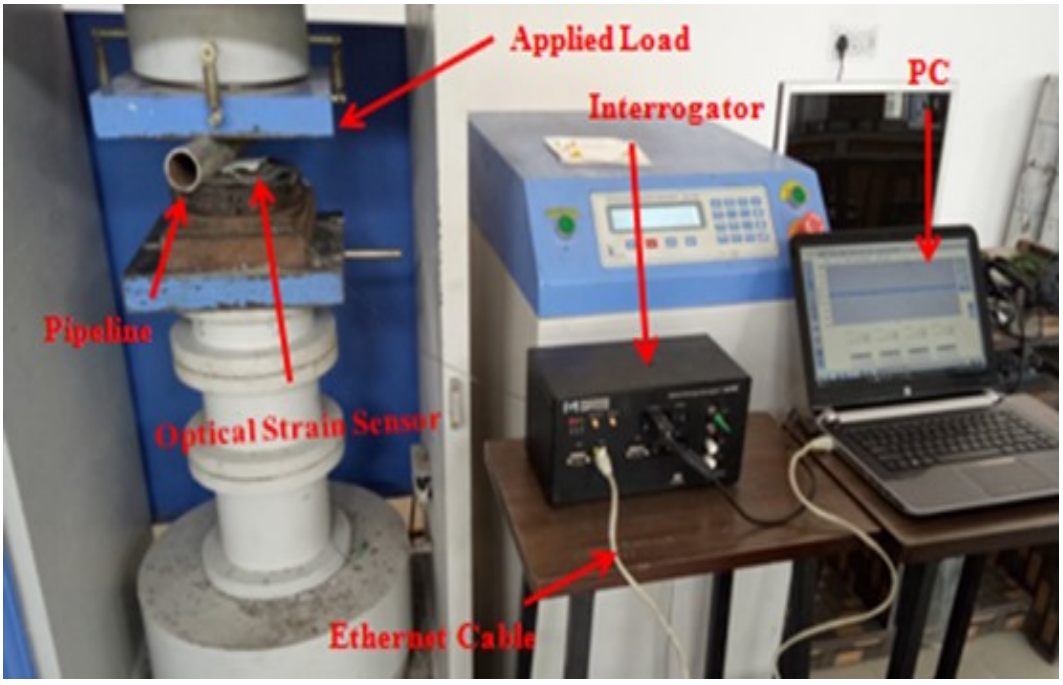

(a)

(b)

Fig. 6.10(a) Experimental Setup for detecting crack point in open pipeline structure (Case I) and (b) Side view of optical strain sensor mounted on pipeline.

The Interrogator is connected to optical strain sensor (Bragg grating sensor) mounted on the surface of water pipeline which is further linked to the interrogator to analyze the output spectrums. Then, the interrogator is further connected to computational device (PC) via Ethernet cable to analyze the outcomes through MOI ENLIGHT sensing software. Thus, complete picture of sensing data is visualized on PC. The transreceiver send laser light through channel to strain sensor. External stress or load is applied on the pipeline by the civil Compression Testing Machine. This machine applies the scheduled compression with maximum capacity of 5000 kN. Here, same experiment is performed on different pipeline structures. Case I: Monitoring crack in open pipeline structures (electrical, telephone lines etc.); Case II: Monitoring crack in energy stored closed pipeline structures (oil, natural gas, O_2, CO_2 cylinders, gasoline, liquid petroleum, chemicals, water, sewer lines etc.).

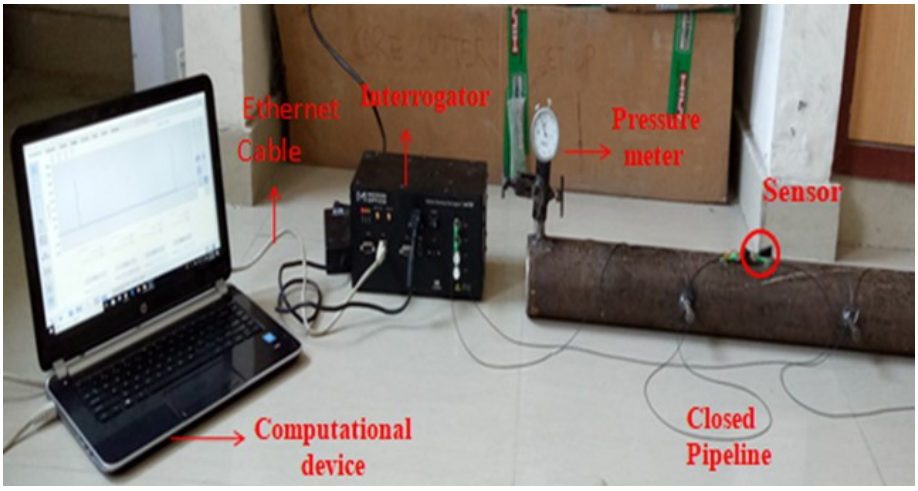

Fig. 6.11 Experimental pipeline setup when closed energy storage pipeline structure (Case II) is subject to load for detecting crack**.**

As stress is applied on pipeline elongation of pipeline takes place which can be related to reduction in wall thickness of pipeline. This elongation of pipeline is strain which can be described by equation (6.12) as below:

$$\varepsilon_p = \frac{P \times d}{E \times 2 \times t} \tag{6.12}$$

where, ε_p represents strain on pipeline, P is applied load, t is wall thickness, E dictates Young's modulus of stainless steel and d represents diameter of pipeline. For corrosion monitoring of pipeline, strain of pipeline is inversely proportional to wall thickness. According to equation (6.12) reduction in wall thickness can be due to corrosion that can be determined from strain.

Table 6.2: Experiment I Parameters

Components	**Parameter**	**Value**
Optical strain sensor	Grating shape	Uniform
	Gage factor	0.796
	Gage constants	constant1= 6.156 μm/m constant 2= 0.70 μm/m
	Poisson's ratio	0.22
	Strain	Uniform
Interrogator	Wavelength	1510 to 1590 nm
	Number of channels	4 (Ch1 to Ch 4); Ch1 used
	Capacity of connecting number of sensors	16 sensors per channel
	Scan frequency	1000Hz
Pipeline	Material	Stainless steel
	Length	1 m
	Diameter	22 mm
	Wall thickness	4 mm

As load is applied on the pipeline it is sensed by the optical strain sensor and the shift in wavelength can be observed on the screen of computational device. This experiment has been done in Civil Structure Laboratory II, Department of Civil Engineering, Thapar Institute of Engineering and Technology, Patiala, Punjab, India. Different parameters of optical strain sensor, pipeline and interrogator are listed in Table 6.2.

6.3.2 Result and Discussions:

Fig. 6.12 shows wavelength versus time graph, where Y-axis indicates the range of wavelengths over which the Bragg wavelength shifts can be observed with respect to an applied load with time. In our experiment, we used FBG strain sensor where the Bragg grating wavelength (λ_B= 1520.295 nm) is the centre wavelength of the input light that will be back-reflected from the Bragg grating.

The tensile load was applied from 1kN to 65kN in steps of 5kN where each load applied for duration of 5 minutes and then slowly load was decreased to 0kN. This experiment was repeated many times to reduce the measurement noise. It can be observed from Fig. 6.12 that when load is not applied on pipeline then Bragg grating wavelength (λ_B= 1520.295 nm) is the center wavelength.

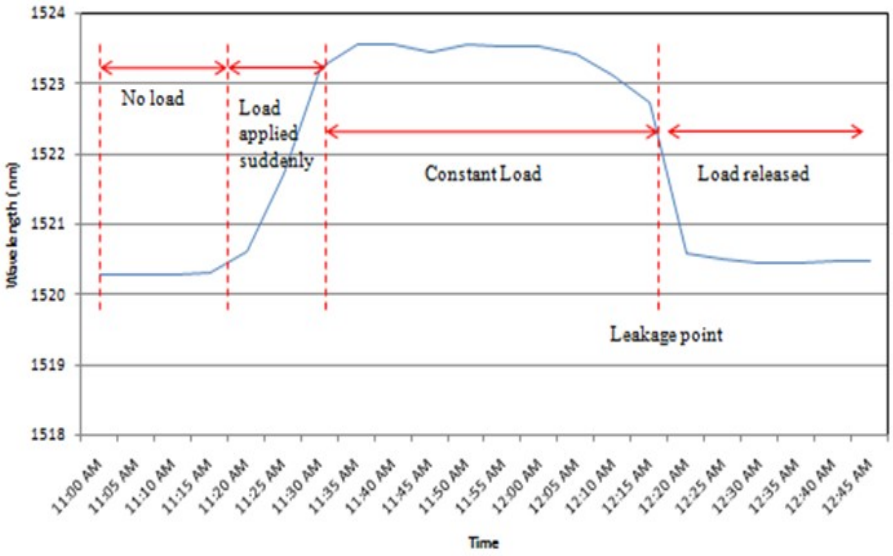

Fig. 6.12 Wavelength as a function of time with respect to applied load.

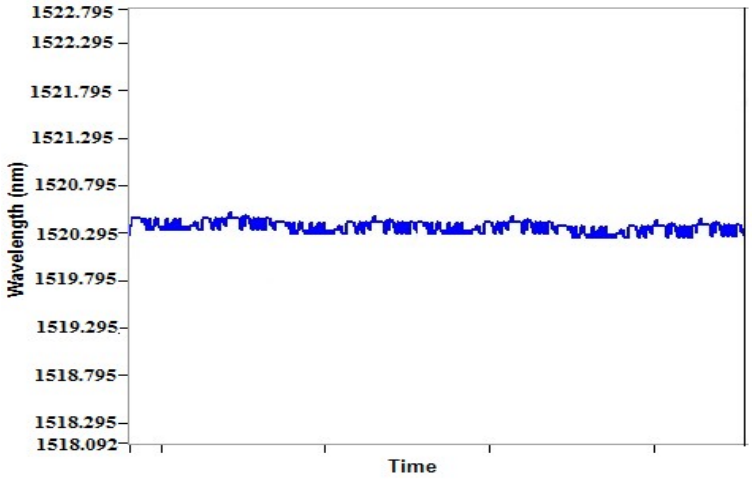

(a)

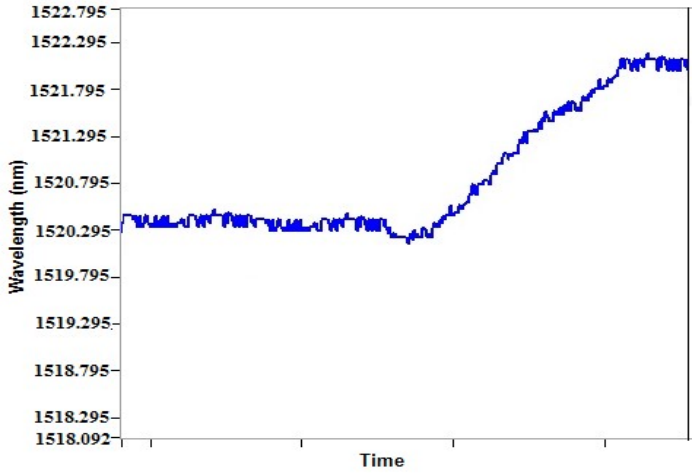

(b)

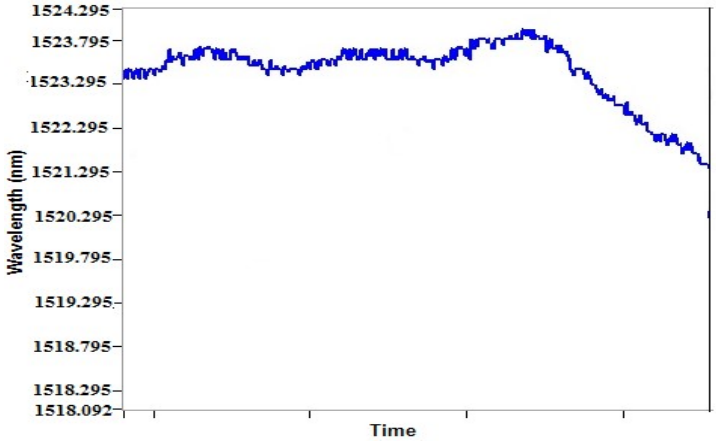

(c)

Fig. 6.13 Time domain spectral graph of Bragg wavelength at different applied load (a) 0kN, (b) 35kN and (c) 65kN.

As load applied on pipeline, the wavelength of the reflected light started shifting towards higher wavelength due to the property of the FBG. This reflected light carries strain information. When uniform load was applied then pipeline gets deformed and a saturation point came where crack occurs in pipeline and can be called as leakage point. The acquired sinusoidal traces obtained due to applied dynamic load over optical Bragg grating strain sensor are reported in the graphs of Figs. 6.13(a-c). These changes in wavelength peaks with respect to time were observed during the experiment in time-domain spectral analyzer of MOI ENLIGHT software. When initially load was not applied by machine then there is no change in wavelength and central wavelength remains same (λ_B= 1520.295 nm) as represented by Fig. 6.13(a).

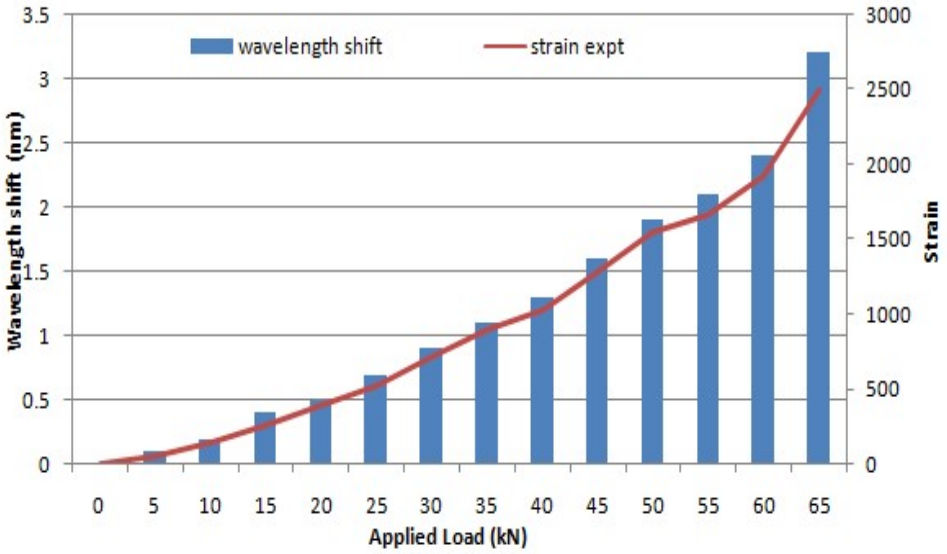

Fig. 6.14 Performance monitoring of fiber Bragg grating strain sensor to monitor open pipeline structure in terms of wavelength shift and strain as a function of applied load.

Normalized time-domain trace (Fig. 6.13(b)) reported the sudden increase in wavelength trace with increase in applied load in steps from 1 kN to 50 kN. It can be observed from Fig. 6.13(c) that at 65kN wavelength shifts to 1523.495 nm and after some time peak becomes near to its initial stage (λ_B= 1520.295 nm) which means load is released.

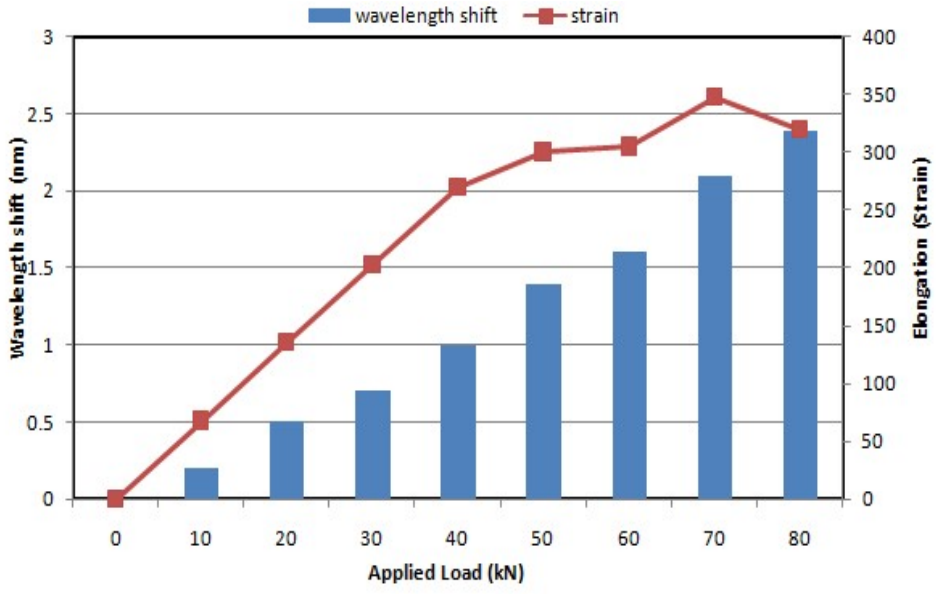

Fig. 6.15 Performance of fiber Bragg grating strain sensor to monitor storage closed pipeline in terms of wavelength shift and strain with respect to applied load.

The experimental analysis of applied force verses strain for monitoring performance of energy storage open and closed pipeline structure is shown in Figs. 6.14 and 6.15. The

wavelength shift can be computed by taking difference of center wavelength and shifted wavelength.It is concluded that open pipeline structure and closed storage pipeline structure design achieved a shift in wavelength of 3.2 nm and 2.39 nm with applied load of 65 kN leads to strain of 2495με and 320 με respectively where readings were acquired every 5 minutes to decrease measurement noise.So, the proposed sensor detects the strain with large sensitivity at early stage.

6.3.3 Experimental Setup II:

The experimental setup for monitoring crack in energy storage pipelineusing 2 optical Bragg gratting strain sensors is shown in Figs. 6.16(a-c). This setup includes Interrogator as transreceiver unit with wavelength range (minimum: 1510 nm and maximum: 1590 nm), Optical Bragg grating strain sensors S1 and S2, 1metre long stainless-steel pipeline and computational device.

The Interrogator is connected to optical strain sensors (Bragg grating sensors S1; S2) mounted on the surface of pipeline structure which is further linked to the interrogator to analyze the output spectrums.Then, the interrogator is further connected to computational device (PC) via Ethernet cable to analyze the outcomes through MOI ENLIGHT sensing software. Thus, complete picture of sensing data is visualized on PC.

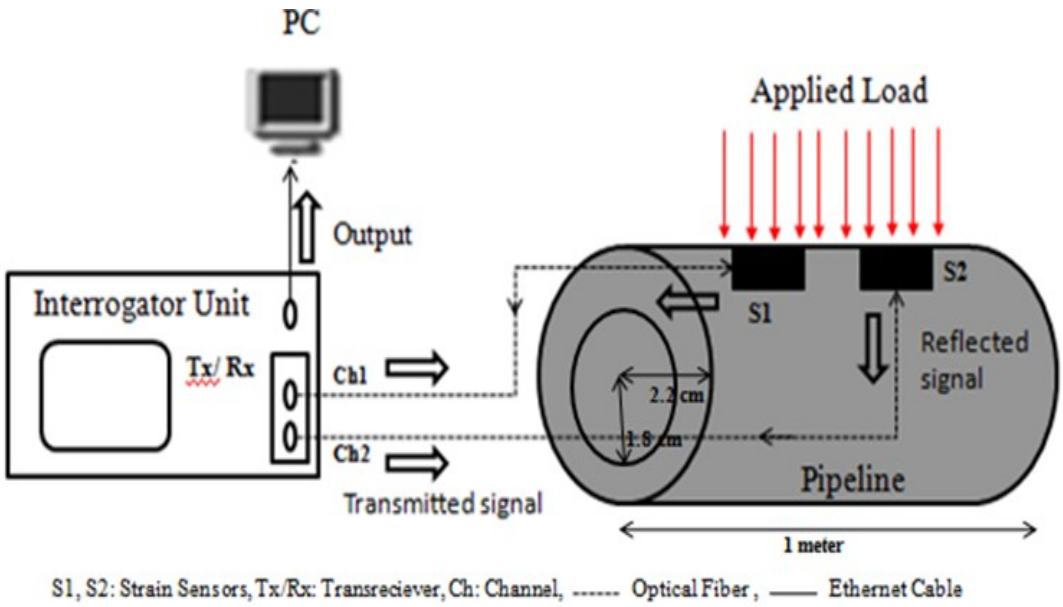

(a)

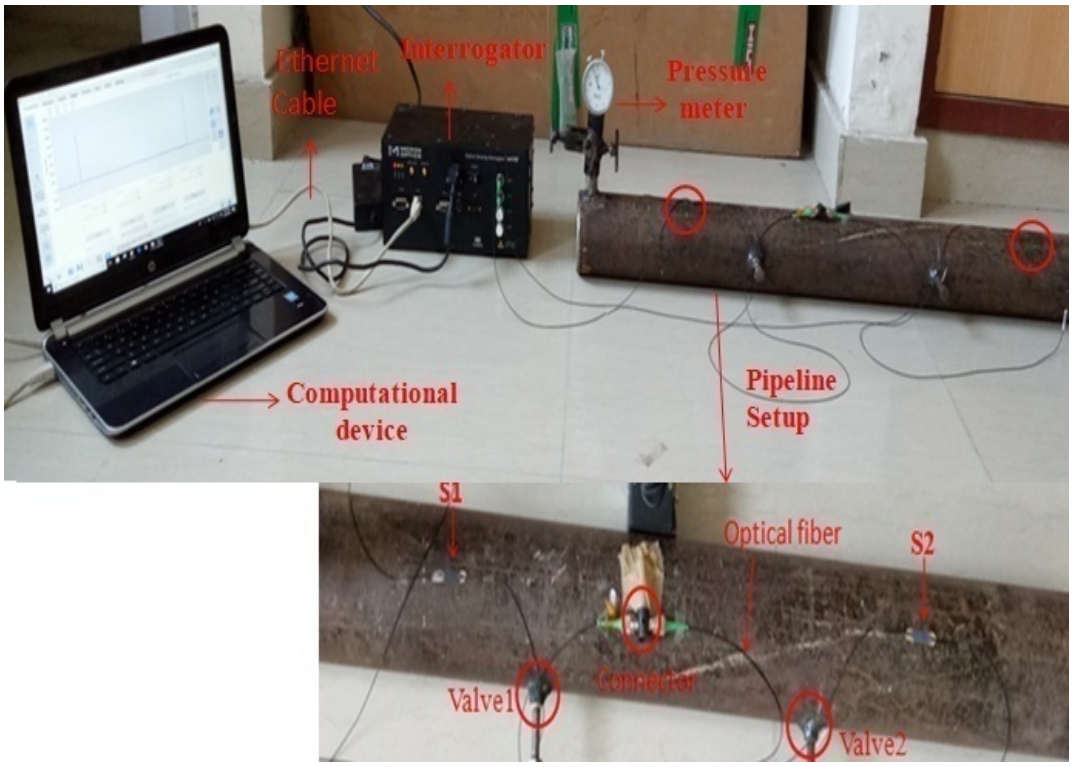

(b)

(c)

Fig. 6.16 (a) Schematic of experimental setup, (b)Setup for testing pipeline model and side view of optical strain sensors mounted on pipeline and (c) Experimental setup for detecting storage pipeline for detecting crack point in energy storage pipeline.

As load is applied on the pipeline it is sensed by the strain sensors attached to the pipeline and the shift in wavelength can be examined using computational device. This experiment was set up for detecting crack in pipeline in Civil Structure Laboratory II, Civil Engineering Department, TIET, Patiala, Punjab, India. Different parameters of FBG strain sensor, pipeline and interrogator are listed in Table 6.3.

Table 6.3: Experiment II Parameters

Components	**Parameter**	**Value**
Optical strain sensors	Grating shape	Uniform
	Gage factor	0.796
	Bragg wavelength of sensors (S1; S2)	1520.295nm; 1575.894 nm
	Poisson's ratio	0.22
	Strain	Uniform
Interrogator	Wavelength	1510 to 1590 nm
	Number of channels	4 (Ch1 to Ch 4); Ch1 and Ch2 used
	Capacity of connecting number of sensors	16 sensors per channel
	Scan frequency	1000Hz
Pipeline	Material	Stainless steel
	Length	1 m
	Outer diameter(d_o)	44 mm
	Inner diameter(d_i)	36 mm

Fig. 6.17 shows wavelength versus time curve, where Y-axis represents the wavelengths for which the shifts can be noticed with application of load whereas X-axis represents time taken by experiment. In our experiment, we used FBG strain sensors (S1, S2) with λ_B(1520.295 nm, 1575.894 nm) indicating input central wavelength that will be reflected back from the grating respectively.

The tensile load was applied from 1 kN to 80 kN in steps of 5 kN where each load applied for duration of 5 minutes and then gradually load was reduced to 0 kN. It can be observed from Fig. 6.17 that when load is not applied on pipeline then Bragg grating wavelength (λ_B= 1520.295 nm) is the center wavelength for sensor S1.

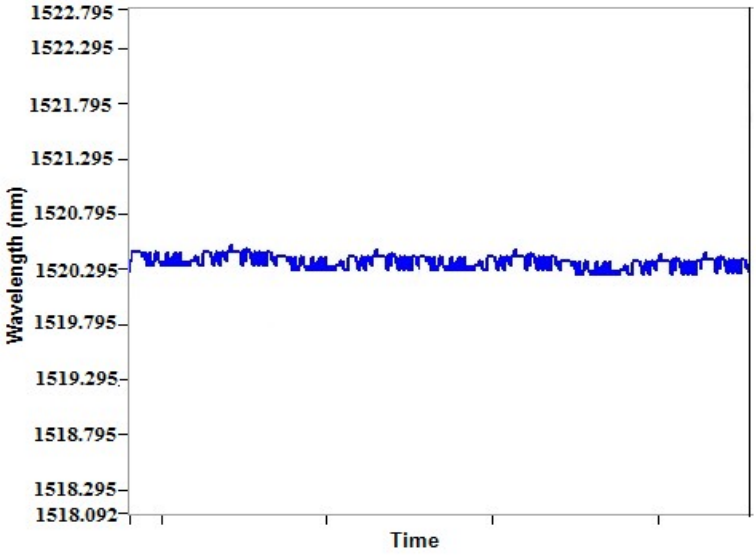

(a)

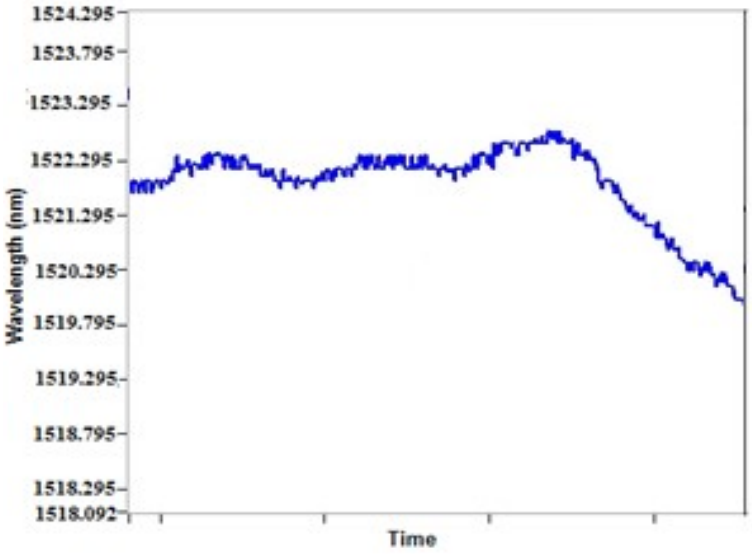

(b)

Fig. 6.17 Time domain spectral graph of Bragg wavelength at different applied load (a) 0 kN, (b) 80 kN when one sensor is connected.

As load applied on pipeline, the wavelength of the reflected light started shifting towards higher wavelength due to the property of the FBG. This reflected light carries strain information. When uniform load was applied then pipeline gets deformed and a saturation point came where crack occurs in pipeline and can be called as leakage point.The acquired sinusoidal traces obtained due to applied dynamic load over optical Bragg grating strain sensor are reported in the graphs of Figs. 6.17(a,b).

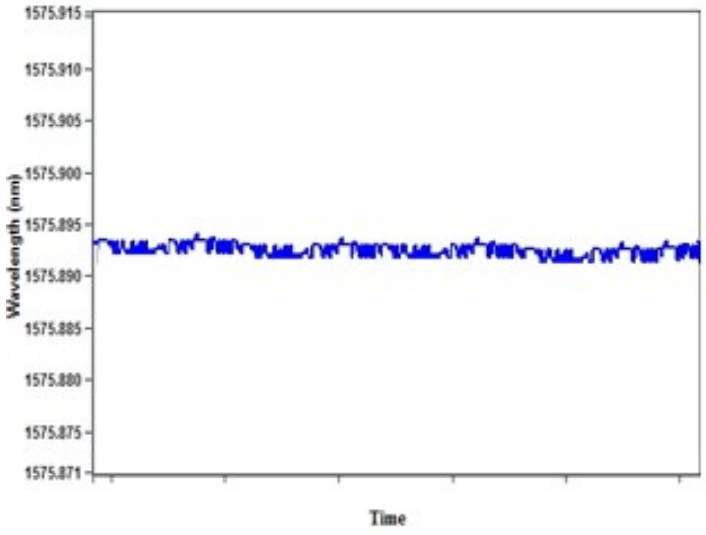

(a)

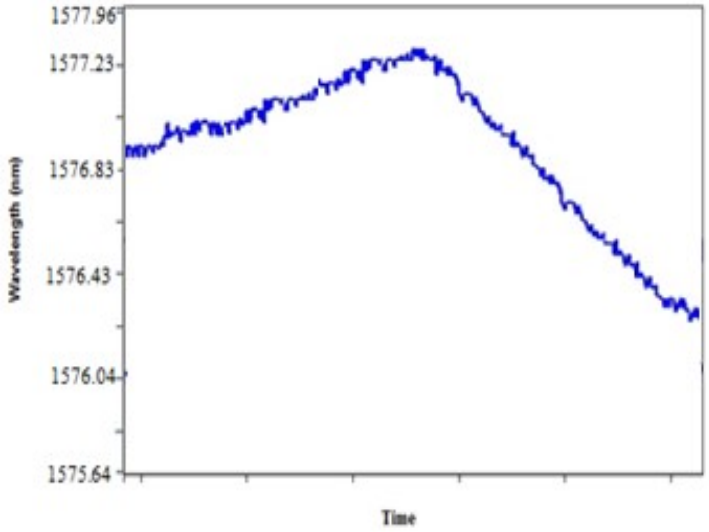

(b)

Fig. 6.18 Time domain spectral graph of Bragg wavelength at different applied load (a) 0 kN and (b) slowly increases to 80 kN and released for sensorS2 when both S1 and S2 are connected.

These crests and troughs in wavelength signal with time (μs) were observed by spectral analyzer on PC during the experiment. When initially load was not applied by machine then there is no change in wavelength and central wavelength remains same (λ_B= 1520.295 nm) as represented by Fig. 6.17(a). Normalized time-domain trace (Fig. 6.17(b)) reported the sudden increase in wavelength trace with increase in applied load in steps from 1 kN to 80 kN.

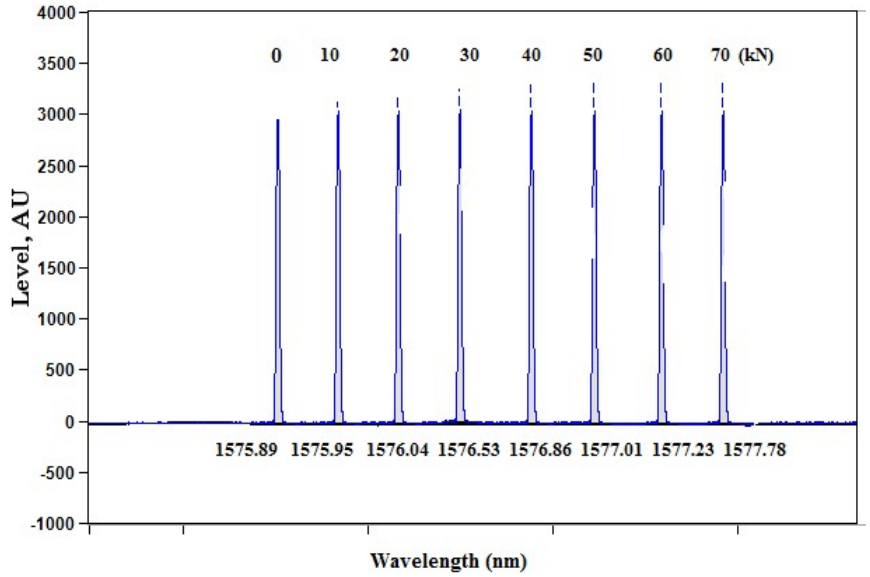

(a)

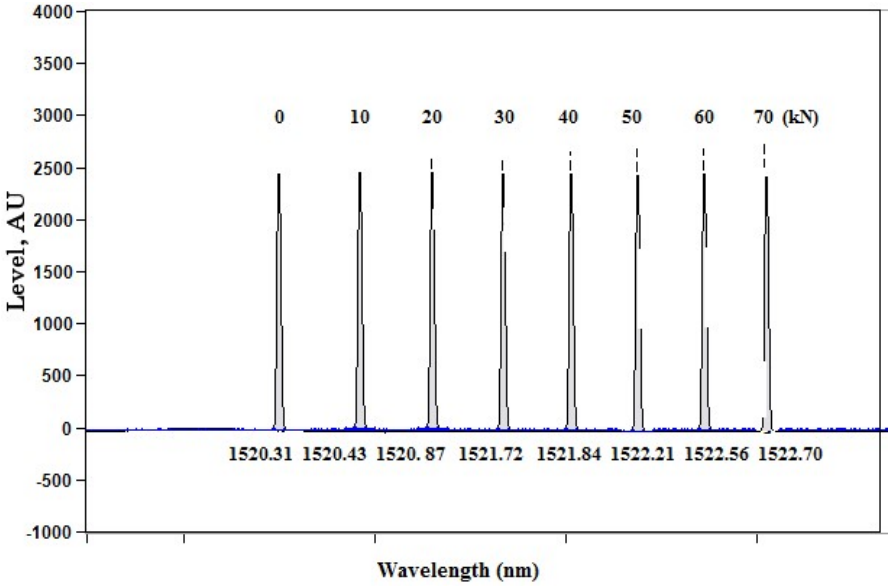

(b)

Fig. 6.19 Optical spectrum observed experimentally at different applied force for sensor (a) S1 and (b) S2.

It can be observed from Fig. 6.17(b) and 6.18(b) that at 80kN wavelength shifts to (1522.685 nm for S1; 1577.79 nm for S2) and after some time peak becomes near to its initial stage (λ_B= 1520.295 nm; 1575.89 nm) which means load is released. Fig. 6.19 represents the optical spectrum as observed experimentally for different applied force on pipeline.

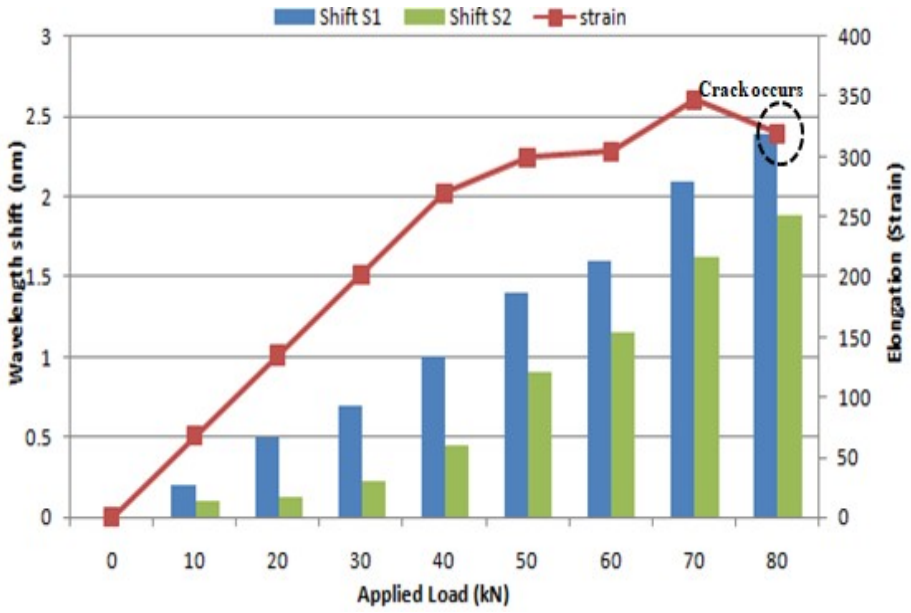

Fig. 6.20 Performance of both sensors mounted on pipeline in terms of wavelength shift and strain with respect to applied load.

The experimental analysis of stress (applied load) verses strain for monitoring performance of energy storage pipeline for both sensors is shown in Fig. 6.20. The wavelength shift can be computed by taking difference of center wavelength and shifted wavelength. It is concluded that strain monitoring of pipeline design achieved a shift in wavelength of 2.39 nm and 1.9 nm with applied load of 80 kN leads to strain of 332 με respectively where readings were acquired every 5 minutes to decrease measurement noise. The authors [121] sensed pressure variations in pipelines and verified the theoretical design architecture with simulation results. This proposed sensor provides improved performance over [121] with enhanced sensitivity.

6.4 Conclusion

In this Chapter, fiber optic Bragg grating multimode fiber based sensor is proposed for leakage detection in energy storage pipelines. The simulation results report that the proposed sensor design achieved a wavelength shifts of (0.07 μm towards higher wavelength and 0.003 μm towards lower wavelength) for strain and temperature sensor with applied strain of 2000 με and at temperature of 50^{o}C respectively. Further, temperature sensitivity of proposed sensor is enhanced by varying claddings thermo-optic coefficient (ζ_{clad}) from 7.8 x10^{-6} to 9.12x10^{-6} along with coupling to chosen higher mode LP_{21} obtaining highest sensitivity of 14 nm/^{o}C.The experimental strain outcomes

are observed both for open (telephone and transmission pipelines) and closed pipeline structures (gasoline, liquid petroleum, chemicals, water, sewer lines, storm sewers) and it is examined that the proposed sensor achieved a wavelength shift (3.2 nm and 2.39 nm) for open and closed pipeline structure respectively. It is further experimentally reported that the Bragg grating strain sensors (S1 and S2) provides sensitivity in terms of wavelength shift (2.4 nm and 1.89 nm). It is concluded that the experimental outcomes hold good for different network of pipelines. For Liquefied petroleum gas leakage applications, the cost effective and efficient proposed design is expected to attain an ideal response with additional optimization.

CHAPTER 7
CONCLUSIONS, RECOMMENDATIONS AND FUTURE SCOPE

7.1 Conclusion

This thesis presents the investigation of optical multi input multi output mode division multiplexed transmission systems. The main motive of this thesis is to provide a comprehensive analysis of the features, properties, design strategies and factors affecting the performance of OMIMO MDM system over multimode fiber. The hasty increasing demand for internet traffic with smart multimedia need newly developed techniques in optical communication systems. Optical Mode division multiplexing (OMDM) , a new paradigm is best way out to the forthcoming capacity crunch of optical communication technologies worldwide. The multiplexing of spatial domain with fibers capable of supporting multiple modes is an efficient way as capacity scales with number of modes. Less development in this area poses different challenges as there is simultaneous transmission of signals through multiple modes of fiber.

The work presented in this thesis covers two main areas: performance enhancement of OMIMO MDM transmission system and investigation of Bragg grating inscribed inside MMF based sensor for monitoring underground energy storage pipelines. The effect of nonlinear propagation in mode division multiplexed multimode fiber link is discussed. In order to model the nonlinear propagation effects in multimode domain SM-NLSE (Single Mode-Nonlinear Schrodinger Equation) and TM-NLSE (Two Mode-Nonlinear Schrodinger Equation) are theoretically extended to analyze MM-NLSE (Multimode Nonlinear Schrodinger Equation).The effect of inter-modal four wave mixing (IMFWM) and intramodal FWM for waves with different spatial modes (LP_{01}, LP_{02} and LP_{11} and LP_{12}) over MMF having THz wave spacing has been analyzed. Further, the multi-mode nonlinear propagation of different mode groups (containing N spatial modes in each group) due to Kerr effect has been discussed mathematically. It can be concluded that high launch power and low dispersion generated sidebands both in case of inter-modal and intramodal FWM. Thus, it is found that to achieve phase matching chromatic dispersion has been increased in each spatial mode throughout MMF link.

This thesis analyzed different linearly polarized (LP_{lm}) modes over MMF link to boost MIMO Mode Division Multiplexing. It demonstrated multi input multi output based MDM system for transmission of 9 information signals over 9 different LP modes at 1550 nm wavelength with low input power travelling long distance of 90 km over MMF

link. It is examined that even for 9×9 MIMO MDM system maximum Q^2 factor of 14 dB with minimum BER of 10^{-9} was achieved.The concept of mode coupling in multimode fiber is explained. This thesis deals with the effect of different LP mode index grouping combinations on transmission performance of 3 × 3, 4 × 4, 5 × 5, 6 × 6, 7 × 7, 8 × 8 and 9 × 9 OMIMO-Mode division multiplexed systems. The maximum distance covered with Quality-factor (>8.3dB) using mode index grouping combinations (Even, Odd, random Even+Odd and symmetric Even+Odd with mode gap) is approximately 82km, 79km, 80km and 114km respectively for even 9 × 9 OMIMO-MDM system. Further, system performance is optimized by LMS (least mean square) adaptive MIMO filter algorithm to avoid mode group coupling and transmission is thus enhanced covering 700 km in MDM based system. It is concluded that higher Q-factor and received power with longest transmission is achieved with Symmetric Even+Odd with mode gap group but moderate with rest cases for all considered OMIMO-MDM configurations. This analysis can be used for MGDM (mode group division multiplexing)to increase the capacity of high speed transmission over MMF link.

The MM-EDFA amplifier is designed in three configurations (pre-, boost- and inline-) to investigate the performance of MDM system. It is seen that for acceptable quality factor more than 8 dB and bit error rate $\leq 10^{-9}$, maximum transmission distance (for 3 X 3 and 4 X 4 MIMO) for pre and boost configuration is approximately up to 85 km whereas it is up to 100 km for the inline-MM EDFA configuration method. It is concluded that inline-MM EDFA configuration outcomes better results for all considered MIMO MDM configurations. The hybrid wavelength and mode division multiplexed system is designed for transmission of 25 independent channels over multimode fiber link that offered high capacity with minimum use of bandwidth for upcoming optical communication at reduced channel spacing.The mode calculation algorithm is discussed first time to calculate modes in 10 Tb/s LP-WDM-MDM transmission system. It is concluded that moderate channel index spacing (x-index=2 and varying y-index) provide best results for 25 channel 10Tb/s hybrid LP-MDM-WDM system at input power of 20 dBm covering transmission distance of 15 km with acceptable BER ($<10^{-8}$) and Quality-factor (>9.8 dB) over MMF link. Featuring unique simplicity with low power consumption, the proposed design is ideal to cope up with the higher data capacity and short reach applications.

An efficient and cost effective optical Bragg grating multimode fiber based sensor is proposed for leakage detection in underground energy storage pipelines. The effect of

temperature and strain on fiber Bragg grating is theoretically analyzed. The simulation results reported that the proposed sensor design achieved a wavelength shift of (0.07 μm towards higher wavelength and 0.003 μm towards lower wavelength) for strain and temperature sensor with applied strain of 2000 με and at temperature of 50^{o}C respectively. By varying claddings thermo-optic coefficient (ζ_{clad}) from 7.8 x10^{-6} to 9.12x10^{-6}temperature sensitivity of sensor is enhanced to 14 nm/^{o}C.

The leakage detection is also done by performing experiments on different pipeline structures to evaluate the performance of Optical Bragg grating strain sensor. The experiment reported that the optical Bragg grating strain sensor achieved a wavelength shift of 3.2 nm with applied load of 65 kN resulting into strain of 2495με. Here, readings were acquired every 5 minutes to decrease measurement noise. The strain is applied on both closed energy storage pipeline structuresand open pipeline structures and it is examined that the experimental outcomes hold good for different network of pipelines. Further, two Optical FBG strain sensors (S1 and S2) are connected using one optical fiber to perform sensing at different points on pipeline structure. It is experimentally demonstrated that both sensors (S1 and S2) provides better sensitivity in terms of wavelength shift (2.4 nm and 1.89 nm). This proposed sensor is different from available strainsensors in terms of its simple design, sensitivity, low cost and capability to survivein harsh environment thus, having great scope in chemical industries, power plants, energy storage reservoirs where leakage is the major issue.

7.2 Recommendations

- Rapid increase in internet traffic with smart phone users and trendy multimedia are raising the need for higher data capacity; pushing-up the demand for capacity in pre-existing communication networks. Thus, MIMO MDM technique is recommended to cope with the hasty expansion of internet data capacity in optical communication. It is recommended in long haul optical transmission system where higher data rate in Tbps and high speed is required.
- Featuring distinctive simplicity with reduced interference and low power consumption, the proposed LP-MDM-WDM transmission design can be used in optical network interconnects at data centres to fulfil the higher internet capacity at reduced channel spacing of 0.05 nm.

- The proposed FBG multimode based sensor is recommended in commercial transportation like chemical storage containers, tankers, marine cargo ships, special vessels for military where leakage is a major issue.
- For monitoring critical stress points of equipments used in racing cars, racing yachts and skiing sport events taking place at the Olympics. Thus, equipment health monitoring can be done using Optical Fiber Bragg grating strain sensor.
- For pipeline leakage monitoring in oil refineries, hot boiler furnaces in industries, energy storage (LPG, oxygen, CO2 cylinders) the proposed design is expected to attain an ideal response with additional optimization.

7.3 Scope for future work

- The research on Optical mode division multiplexing system is still an open area that requires deeper insight into the optimization of components to cope up with the increasing demand of internet data rate and capacity in exabytes persecond (storing 1 trillion movies each of 1Gbps).
- In future, not only number of modes can be increased but parallelly insertion losses to be reduced. Thus, scalability for large number of modes is a major concern that can be worked upon in future.It will provide growth in capacity-per-fiber, reduction in cost-per-bit and improvements in energy efficiency.
- As strain and temperature variations are precisely and accurately detected and transmitted at the speed of light thus, FBG sensor based surgery probes or endoscopic probes can be developed to reduce level of interference while performing tests and procedures on patients. This sensor can be recommended in medical and biomedical applications.
- Many Optical FBG-MMF sensor can be multiplexed in one array for multi-point and multi parameter sensing so, it is gaining momentum in aerospace development centers, airplane and spaceship industries.
- With further optimization the proposed FBGs can be used for monitoring monuments, tunnels, dams, mines, slopes of mountains, airport runways, highways, and the tracks for various types of railways.
- By including pressure and vibration sensing along with temperature and strain our FBG sensor can be deployed in different applications.

References

[1] R. S. Kaler, T. S. Kamal, A. K. Sharma, S. K. Arya, and R. A. Agarwala, "Large signal analysis of FM-AM conversion in dispersive optical fibers for PCM systems including second order dispersion," *Fiber and Integrated Optics*, vol. 21, no. 3, pp. 193-203, 2002.

[2] R. Essiambre and R. Tkach, "Capacity Trends and Limits of Optical Communication Networks," in *Proceedings of IEEE Conference*, vol. 100, no. 5, 2012, pp. 1035–55.

[3] J. Malhotra, A. K. Sharma, and R. S. Kaler, "On the performance analysis of wireless receiver using generalized-gamma fading model," *Annals of Telecommunications-Annales Des Telecommunications*, vol.64, no. 1-2, pp. 147-153, 2009.

[4] A. Wason, and R. S. Kaler, "Rerouting technique with dynamic traffic in WDM optical networks," *Optical Fiber Technology*, vol. 16, no. 1, pp. 50-54, 2010.

[5] A. Wason, and R. S. Kaler, "Wavelength assignment algorithms for WDM optical networks," *Optik*, vol. 122, no. 10, pp. 877-880, 2011.

[6] S. Kaur, and R. S. Kaler, "Ultrahigh speed reconfigurable logic operations based on single semiconductor optical amplifier," *Journal of the Optical Society of Korea*, vol. 16, no. 1, pp. 13-16, 2012.

[7] K. S. Bhatia, T. S. Kamal, and R. S. Kaler, "An adaptive compensation scheme-based coded direct detection optical–orthogonal frequency division multiplex (OFDM) system, *Computers & Electrical Engineering*, vol. 38, no. 6, pp. 1573-1578, 2012.

[8] K. S. Bhatia, R. S. Kaler, T. S. Kamal, and R. Randhawa, "Simulative analysis of integrated DWDM and MIMO-OFDM system with OADM," *Optik-International Journal for Light and Electron Optics*, vol. 124, no. 2, pp. 117-121, 2013.

[9] S. Singh, and R. S. Kaler, "Investigation of hybrid optical amplifiers with different modulation formats for DWDM optical communication system," *Optik-International Journal for Light and Electron Optics*, vol. 124, no. 15, pp. 2131-2134, 2013.

[10] R. S. Kaler, A. K.Sharma, and T. S. Kamal, "Comparison of pre-, post-and symmetrical-dispersion compensation schemes for 10 Gb/s NRZ links using standard and dispersion compensated fibers,"*Optics Communications*, vol. 209,

no. 1-3, pp.107-123, 2002.

[11] S. Singh, and R. S. Kaler, "Placement of optimized semiconductor optical amplifier in fiber optical communication systems,"*Optik-International Journal for Light and Electron Optics,* vol. 119, no. 6, pp. 296-302, 2008.

[12] S. Singh, and R. S. Kaler, "Review on recent developments in hybrid optical amplifier for dense wavelength division multiplexed system," *Optical Engineering*, vol. 54, no. 10, p. 100901, 2015.

[13] A. Yina, L. Li, and X. Zhanga, "Analysis of modulation format in 40 Gbit/s optical communication system," *Optik-International Journal for Light and Electron Optics,* vol. 121, no. 3, pp. 1550-1557, 2010.

[14] J. P. Turkiewicz, A. M. J. Koonen, G. D. Khoe, and H. De Waardt, "Do we need 1310 nm transmission in modern networks?," in *Optical Communication (ECOC), European Conference and Exhibition*, 2006, pp. 1-2.

[15] S. Singh, and R. S. Kaler, "Investigation of hybrid optical amplifiers for dense wavelength division multiplexed system with reduced spacings at higher bit rates," *Fiber Integrated Optics*, vol.31, no. 3, pp. 208–220, 2012.

[16] G. Li, "Recent advances in coherent optical communication," *Advance Optical Photonics,* vol. 1, pp. 279-307, 2009.

[17] Y. Han, and G. Li, "Coherent optical communication using polarization multiple-input-multiple-output," *Optics Express,* vol. 13, no. 19, pp. 7527-7534, 2005.

[18] R. Ryf, S. Randel, R. J. Essiambre, and P. J. Winzer, "Space-Division Multiplexed Transmission over Few-Mode and Coupled-Core Fiber Based on Coherent MIMO Digital Signal Processing," in *Proceedings of SPIE Next-Generation Optical Communication: Components, Sub-Systems, and Systems*, vol. 8284, 2012, Paper 828402.

[19] R. G. H. van Uden, R. A. Correa , E. A. Lopez, F. M. Huijskens , C. Xia, G. Li, A. Schulzgen, H. de Waardt, A. M. J. Koonen, and C. M. Okonkwo, "Ultra-high-density spatial division multiplexing with a few-mode multicore fibre," *Nature Photonics*, vol. 8, no. 11, p. 865, 2014.

[20] A. R. Chraplyvy, "The coming capacity crunch," presented at *35th European Conference on Optical Communication ECOC '09*, Vienna, Austria, 20-24 Sept. 2009.

[21] R.W. Tkach, "Scaling optical communications for the next decade and beyond," *Bell Labs Technical Journal*, vol. 14, no. 4, pp. 3-9, 2010.

[22] A. Mecozzi, C. Antonelli and M. Shtaif, "Nonlinearities in space-division multiplexed transmission," in *Proceedings IEEE Optical Fiber Communications Conference and Exhibition*, 2015, pp.1-29.

[23] D. Richardson, J. Fini, and L. Nelson, "Space-division multiplexing in optical fibres," *Nature Photonics*, vol. 7, no. 5, pp. 354–362, 2013.

[24] P. J. Winzer, "Optical networking beyond WDM," *IEEE Photonics Journal*, vol. 4, no. 2, pp. 647–651, 2012.

[25] D. K. Mynbaev, and L. L. Scheiner, *Fiber-Optic Communications Technology.* Upper Saddle River, NJ: Prentice Hall*,* 2001.

[26] K. N. Sivarajan, The Optical Transport Network Revolution, Chennai: Networking Workshop, vol.2, 2010.

[27] J. D. Downie, J. Hurley, S. Ten , C. Towery, M. Sharma, Y. Mauro, C. Malouin, B. Zhang, J. Bennike, T. Schmidt and R. Saunders, "DWDM 43 Gbit/s DPSK transmission over 1200 km with no inline dispersion compensation," *Electronics Letters*, vol. 46, no. 1, pp. 60-62, 2010.

[28] J. Yu, "1.2 Tbit/s orthogonal PDM-RZ-QPSK DWDM signal transmission over 1040 km SMF-28," *Electronics Letters,* vol. 46, no. 11, pp. 775-777, 2010.

[29] T. Ohara, H. Takara, I. Shake, K. Mori, K. Sato, S. Kawanishi, S. Mino, T. Yamada, M. Ishii, I. Ogawa, T. Kitoh, K. Magari, M. Okamoto, R. V. Roussev, J. R. Kurz, K. R. Parameswaran, and M. M. Fejer, "160-Gb/s OTDM Transmission Using Integrated All-Optical MUX-DEMUX With All-Channel Modulation and Demultiplexing," *Photonics Technology Letters*, vol.16, no. 2, pp. 650-652, 2004.

[30] R. Essiambre, R. Ryf, N. K. Fontaine, and S. Randel, "Breakthroughs in Photonics 2012: Space-Division Multiplexing in Multimode and Multicore fibers for High-Capacity Optical Communication," *IEEE Photonics J*ournal, vol. 5, no. 2, pp. 0701307-0701307, 2013.

[31] Y. Kokubun and M. Koshiba, "Novel multi-core fibers for mode division multiplexing: proposal and design principle," *IEICE Electronics Express*, vol. 6, no. 8, pp. 522-528, 2009.

[32] K. P. Kaur, R. Randhawa, and R. S. Kaler, "Performance analysis of WDM-PON architecture using different receiver filters," *Optik*, vol. 125, no. 17, pp. 4742-4744, 2014.

[33] H.Monga, andR. S. Kaler, "Performance analysis and improvement of spectrally

amplitude encoded/decoded OCDMA system,"*Optik*, vol. 122, no. 22, pp. 2006-2010, 2011.

[34] R. Ryf, R. Essiambre, A. Gnauck, S. Randel, M. A. Mestre, C. Schmidt, P. Winzer, R. Delbue, P. Pupalaikis, A. Sureka, T. Hayashi, T. Taru, and T. Sasaki, "Space-division multiplexed transmission over 4200 km 3-core microstructured fiber," in *National Fiber Optic Engineers Conference OSA,* 2012, Paper PDP5C-2.

[35] R. Ryf, S. Randel, A. H. Gnauck, C. Bolle, A. Sierra and S. Mumtaz, "Mode-Division Multiplexing Over 96 km of Few-Mode Fiber Using Coherent 6x6 MIMO Processing," *Journal of Lightwave Technology*, vol. 30, no. 4, pp. 521-531, 2012.

[36] J. M. Kahn and K. P. Ho, "Mode Coupling Effects in Mode-Division-Multiplexed Systems," *IEEE Transactions,* vol. 11, no. 1, pp. 440-446, 2012.

[37] R. Y. Gu, E. Ip, M. Li, Y. Huang and J. M. Khan, "Experimental Demonstration of a Spatial Light Modulator-based Few-Mode Fiber Switch for Space-Division Multiplexing," in *Proceedings of OSA Annual Meeting*, Orlando, 2013, Paper FW6B-4.

[38] A. Amphawan, "Binary spatial amplitude modulation of continuous transverse modal electric field using a single lens for mode selectivity in multimode fiber," *Journal of Modern Optic*, vol. 59, no. 5, pp. 460–469, 2012.

[39] A. Amphawan, B. Nedniyom, and N. A. Samman, "Selective excitation of LP01 mode in multimode fiber using solid-core photonic crystal fiber," *Journal of Modern Optics*, vol. 60, no. 20, pp. 1675-1683, 2013.

[40] A. Al Amin, A. Li, X. Chen, and W. Shieh, "Spatial Mode Division Multiplexing for Overcoming Capacity Barrier of Optical Fibers," in *IEEE16th Opto-Electronics and Communications Conference*, Kaohsiung, Taiwan, 2011, pp. 415-416.

[41] S. Berdague and P. Facq, "Mode division multiplexing in optical fibers," *Applied Optics*, vol. 21, no. 11, pp. 1950-1955, 1982.

[42] R. Ryf, S. Randel, A. H. Gnauck, C. A. Bolle, R.-J. Essiambre, P. J. Winzer, D. W. Peckham, A. McCurdy, and R. Lingle, "Space-division multiplexing over 10 km of three- mode fiber using coherent 6 x 6 MIMO processing," in *Proceeding of OSA Optical Fiber Communication Conference*,2011, Paper PDPB10.

[43] G. P. Agrawal, *Nonlinear Fiber Optics,* 5th ed. Optics and Photonics, Academic

Press, 2013.

[44] R. W. Boyd, *Nonlinear Optics*, San Diego, CA: Academic Press, 1992.

[45] Keang-P. Ho and J. M. Kahn, "Linear Propogation Effects in MDM systems," *Journal of Lightwave Technology*, vol. 32, no. 4, pp. 614-628, 2014.

[46] D. Gloge, "Weakly guiding fibers," *Applied Optics*, vol. 10, no. 10, pp. 2252–2258, 1971.

[47] G. Keiser, Coherent Optical Fiber Communications, New York: Mc Graw-Hill, 1991.

[48] T. Hayashi, T. Taru, O. Shimakawa, T. Sasaki and, E. Sasaoka, "Characterization of crosstalk in ultra-low crosstalk multi-core fiber," *Journal of Lightwave Technology*, vol. 30, no. 4, pp. 583–589, 2012.

[49] S. Randel , R. Ryf , A. Sierra , P. J. Winzer , A. H. Gnauck, C. A. Bolle, R.-J. Essiambre, D. W. Peckham, A. McCurdy, and R. Lingle, "6x56-Gb/s mode-division multiplexed transmission over 33-km few-mode fiber enabled by 6x6 MIMO equalization", *Optics Express*, vol. 19, no. 17 , pp. 16697-16707, 2011.

[50] S. Randel, R. Ryf, A. Gnauck, M.A. Mestre, C. Schmidt, R. Essiambre, P. Winzer, R. Delbue, P. Pupalaikis, A. Sureka, Y. Sun, X. Jiang, and R. Lingle, "Mode-multiplexed 6x20-GBd QPSK Transmission over 1200-km DGD-Compensated Few-Mode Fiber," in *OSA Optical Fiber Communication Conference*, 2012, p. PDP5C.5.

[51] P. Kaur, V.K.Jain and S.Kar, " Performance analysis of free space optical links using multi-input multi-output and perture averaging in presence of turbulence and various weather conditions," IET Communications, vol. 9, o. 8, pp. 1104-1109, 2015.

[52] A. Al Amin, A. Li, S. Chen, X. Chen, G. Gao, and W. Shieh, "Dual-LP11 mode 4x4 MIMO-OFDM transmission over a two-mode fiber," *Optics Express*, vol. 19, no. 17, pp. 16672- 16679, 2011.

[53] N. K. Fontaine, C. R. Doerr, M. A. Mestre, R. Ryf, P. Winzer, L. Buhl, Y. Sun, X. Jiang, and R. Lingle, "Space-division multiplexing and all-optical MIMO demultiplexing using a photonic integrated circuit," in *OSA Optical Fiber Communication Conference*, 2012, Paper PDP5B.1.

[54] P. Boffi, P. Martelli, A. Gatto, and M. Martinelli, "Mode-division multiplexing in fibre-optic communications based on orbital angular momentum," *Journal of Optics*, vol. 15, no. 7, p. 075403, 2013.

[55] D. John, and B. Culshaw, *Optical Fiber Sensors: Principles and components*. Boston, USA: Artech House, 1988.

[56] D. A. Krohn, *Fibre optic sensors: fundamentals and applications*, 3rd ed. USA, 2000.

[57] J. P. Dakin and B. Culshaw, *Optical Fiber Sensors: Principles and Components*. Boston, USA: Artech House, 1988.

[58] K. Fidanboylu and H. S. Efendioglu, "Fiber Optic Sensors and Their Applications," in 5th*International Advanced Technologies Symposium (IATS'09)*, Karabuk, Turkey, May 13-15, 2009.

[59] S. Yin, P. B. Ruffin, and F. T. S. Yu, *Fiber Optic Sensors*. 2nd ed. Boca Raton: Taylor & Francis Group, 2008, pp. 54-72.

[60] F. J. Arregui, Y. Liu, I. R. Matias, and R. O. Claus, "Optical fiber humidity sensor using a nano Fabry–Perot cavity formed by the ionic self-assembly method," *Sensors and Actuators B: Chemical*, vol. 59, no. 1, pp. 54-59, 1999.

[61] N.-K. Chen and G.-L. Cheng, "High sensitivity micro Sagnac loop interferometer based on tightly twisted micro fiber tapers," in *Optical Fiber Communication Conference/National Fiber Optic Engineers Conference*, Anaheim, California, 2013, Paper JW2A.28.

[62] E. M. Dianov, S. A. Vasiliev, A. S. Kurkov, O. I. Medvedkov, and V. N. Protopopov, "In-fiber Mach-Zehnder interferometer based on a pair of long period gratings," in *Proceedings of* 22nd *European Conference on Optical CommunicationECOC 96*, vol. 1, pp. 65-68, 1996.

[63] C. Graf, A. Thuring, H. Vahlbruch, K. Danzmann, and R. Schnabel, "Length sensing and control of a Michelson interferometer with power recycling and twin signal recycling cavities," *Optics Express*, vol. 21, no. 5, pp. 5287-5299, 2013.

[64] T. Woo-Hu and L. Chun-Jung, "A novel structure for the intrinsic Fabry-Perot fiber-optic temperature sensor," *Journal of Lightwave Technology*, vol. 19, no. 5, pp. 682-686, 2001.

[65] M. Sumetsky, "Optimization of optical ring resonator devices for sensing applications," *Optics Letters*, vol. 32, no. 17, pp. 2577-2579, 2007.

[66] Y. Verbandt, B. Verwilghen, P. Cloetens, L. Kempen, H. Thienpont, I. Veretennicoff, G. Vinckenroy, W. P. Wilde, and M. H. Voet, "Polarimetric optical fiber sensors: aspects of sensitivity and practical implementation," *Optical Review*, vol. 4, 1997, Paper A75-A79,.

[67] S. Ghetia, R. Gajjar, and P. Trivedi, "Classification of Fiber Optical Sensors," *International Journal of Electronics Communication and Computer Technology*, vol.3, no. 4, pp. 442-445, 2013.

[68] P. Rajeev, J. Kodikara, W.K.Chiu, and T. Kuen, "Distributed Optical Fibre Sensors and Their Applications in Pipeline Monitoring", *Key Engineering Materials,* vol. 558, pp. 424-434, 2013.

[69] A. Iadicicco, A. Cusano, G. V. Persiano, A. Cutolo, R. Bernini, and M. Giordano, "Refractive index measurements by fiber Bragg grating sensor," in *Proceedings of IEEE Sensors*, vol. 1, pp. 101-105, 2003.

[70] D. Inaudi, and S. Vurpillot, "Monitoring of concrete bridges with long-gage fiber optic sensors," *Journal of Intelligent Material Systems and Structures*, vol. 10, no. 4, pp. 280–292, 1999.

[71] L. Zou, and T. Landolsi, "Pipeline Leakage Detection using Fiber-Optic Distributed Strain and Temperature Sensors," White Paper, 2014.

[72] S. Singh, B. Raj, and S. K. Vishvakarma, "Analytical modeling of split-gate junction-less transistor for a biosensor application," *Sensing and bio-sensing research*, vol. 18, pp. 31-36, 2018.

[73] X. Z. Gao, S. J. Ovaska, X. Wang, and M. Y. Chow, "Multi-level optimization of negative selection algorithm detectors with application in motor fault detection," *Intelligent Automation & Soft Computing*, vol.16, no. 3, pp. 353-375, 2010.

[74] M. Tavakoli, L. Marques, and A. Almeida, "Development of an industrial pipeline inspection robot," *Industrial Robot: An International Journal*, vol. 37, no. 3, pp. 309–322, 2010.

[75] Y. Kwon, and B. Yi, "Design and motion planning of a two-module collaborative indoor pipeline inspection robot," IEEE Transactions on *Robotics*, vol. 28, no. 3, pp. 681–696, 2012.

[76] R. Murayama, S. Makiyama, M. Kodama, and Y. Taniguchi, "Development of an ultrasonic inspection robot using an electromagnetic acoustic transducer for a Lamb wave and an SH-plate wave," *Ultrasonics*, vol. 42, no. 1-9, pp. 825–829, 2004.

[77] V. Gopal, and M. Annamdas, "Review on Developments in Fiber Optical Sensors and Applications," *International Journal of Materials Engineering*, vol. 1, no. 1, pp. 1-16, 2011.

[78] W. Johstone, G. Thursby, B. Culshaw, S. Murray, M. Gill, A. Mc Donavh, D.

Moodie, G. Fawcett, G. Stewart, and K. Mccallion, "A Mutimode approch to optical fiber componebts and sensors," in *Proceedings of SPIE conference on Micro-optics II*, , vol. 1506, pp. 145, 1991.

[79] M. Attygalle, C. Lim, G. J. Pendock, A. Nirmalathas, and G. Edvell, "Transmission improvement in fiber wireless links using fiber Bragg gratings," *IEEE Photonics Technology Letters*, vol. 17, no. 1, pp. 190-192, 2005.

[80] V. H. Pham, H. Bui, T. V. Nguyen, T. S. Pham, T. C. Tran, T. T. Hoang, and Q. M. Ngo, "Progress in the research and development of photonic structure devices," *Advances in Natural Sciences: Nanoscience and Nanotechnology*, vol. 7, no.1, pp. 015003, 2016.

[81] X. Qiao, and M. A. Fiddy, "Distributed optical fiber Bragg grating sensor for simultaneous measurement of pressure and temperature in the oil and gas downhole," *Proceedings of SPIE - The International Society for Optical Engineering*, vol. 4870, 2002.

[82] A. M. Vengsarkar, P. J. Lemaire, J. B. Judkins, V. Bhatia, T. Erdogan, and J. E. Sipe, "Long-period fiber gratings as band-rejection filters," *Journal of Lightwave Technology,* vol. 14, no. 1, pp. 58-65, 1996.

[83] V. Rastogi, and K. S. Chiang, "Long-period gratings in planar optical waveguides," *Applied Optics,* vol. 41, no. 30, pp. 6351-6355, 2002.

[84] T. Erdogan, "Cladding-mode resonances in short- and long-period fiber grating filters," *Journal of the Optical Society of America A,* vol. 14, no. 8, pp. 1760-1773, 1997.

[85] J. E. Lee, "A quantitative analysis of tunable long period grating and its application," Ph.D Dissertation, Electrical Engineering, The Pennsylvania State University, 2007.

[86] R. Kashyap, Fiber Bragg Gratings: Academic Press, 1999.

[87] T. Mizunami, T. V. Djambova, T. Niiho, and S. Gupta, "Bragg gratings in multimode and few-mode optical fibers," *Journal of Lightwave Technology*, vol.18, no. 2, pp. 230-235, 2000.

[88] A. Ivanov, "Multi-parameter fiber optic sensors for structural health monitoring," Master Dissertation, Department of Electronics, Ottawa-Carleton Institute for Electrical and Computer Engineering, Carleton University, Canada, 2008.

[89] S. Singh, and R. S. Kaler, "Novel Optical Flat-Gain Hybrid Amplifier for Dense Wavelength Division Multiplexed System," *IEEE Photonic Technology Letters*,

vol. 26, no. 2, pp. 173-176, 2014.

[90] H. Monga, and R. S. Kaler, "Performance Comparison of Proposed 3D Coherent Spatial-Phase-Time Coding/Decoding with Super Structured Fiber Bragg Grating Based Optical CDMA Systems," *Journal of Communication Technology and Electronics*, vol. 59, no. 11, pp. 1169–1179, 2014.

[91] S. Huang, S. Xie, B. Zhou and Y. Gao, "Crosstalk of WDM Optical Communication Systems using Fabry-Perot Demodulators," *Journal of Optical Communications,* vol. 15, no. 3, pp. 101-103, 1994.

[92] H. Toba, K. Oda, K. Nosu and N. Takato, "Factors Affecting the Design of Optical FDM Information Distribution Systems," *IEEE Journal on Selected Areas in Communications,* vol.8, no.6, pp.965-972, 1990.

[93] A. D. Ellis, K. Smith, and D. M. Patrick, "All Optical Clock Recovery at Bit Rates upto 40 Gbit/sec," *Electronics Letters,* vol. 29, no.15, pp.1323-1324, 1993.

[94] H. Monga, and R. S. Kaler, "Spectrally Efficient 3D Optical CDMA using Coherent Spatial Phase–Time Coding/Decoding," *Journal Of Russian Laser Research*, vol. 35, no. 4, pp. 391-400, 2014.

[95] S. Z. M. Hasan, V. Kalavally, R. Parthiban, T. Win, and M. Premaratne, "Economic and system impact of hybrid Raman-EDFA amplification in a 40 X 40 Gbps optical transmission network with DPSK modulation," *Optical Fiber Technology,* vol. 19, no. 1, pp. 10-15, 2013.

[96] H. S. Chung, J. Han, S. H. Chang and K. Kim, "A Raman plus linear optical amplifier as an inline amplifier in a long-haul transmission of 16 channels X 10 Gbit/s over single-mode fiber of 1040 km," *Optics Communications,* vol. 244, no. 1-6, pp. 141-145, 2005.

[97] P. J. Winzer, "Energy-efficient optical transport capacity scaling through spatial multiplexing," *IEEE Photonics Technol. Letters*, vol. 23, no. 13, pp. 851-853, 2011.

[98] P. J. Winzer, "Optical networking beyond WDM," *IEEE Photonics Journal*, vol. 4, no. 2, pp. 647–651, 2012.

[99] C. Koebele, M. Salsi, L. Milord, R. Ryf, C. A. Bolle, P. Sillard, S. Bigo, and G. Charlet, "40 km transmission of five mode division multiplexed data streams at 100 Gb⁄s with low MIMO-DSP complexity," in *Proceedings of 37th European Conference and Exhibition on Optical Communication ECOC*, 2011, Paper Th.13.C.3.

[100] E. Desurvire, and M. N. Zervas, “Erbium-Doped Fiber Amplifiers: Principles and Applications,” *Physics Today*, vol. 48, no. 2, pp. 53, 1995.

[101] M. Gong, Y. Yuan, C. Li, P. Yan, H. Zhang, and S. Liao, “Numerical modeling of transverse mode competition in strongly pumped multimode fiber lasers and amplifiers,” *Optics Express*, vol. 15, no. 6, pp. 3236-3246, 2007.

[102] E. Ip, “Gain equalization for few-mode fiber amplifiers beyond two propagating mode groups,” *IEEE Photonics Technology Letters*, vol. 24, no. 21, pp. 1933-1936, 2012.

[103] A. Amphawan, Y. Fazeal, and H. Ibrahim, “ Investigation of channel spacing for Hermite-Guassian mode division multiplexing in multimode fiber,” *IEEE 11th International Colloquium on Signal Processing & its Applications (CSPA 2015)*, Kuala Lumpur, Malaysia, pp. 34-39, 2015.

[104] F. Schmidt, and K. Petermann, “Investigation of LP- and Vector-Modes for the Analysis of Space-Division Multiplexed Systems in the Nonlinear Regime,” *Journal Of Lightwave Technology*, vol. 35, no. 22, pp. 4859-4864, 2017.

[105] G. Rademacher, and K. Petermann, “Nonlinear Gaussian Noise Model for Multimode Fibers With Space-Division Multiplexing,” *Journal of Lightwave Technology*, vol. 34, no. 9, pp. 2280-2287, 2016.

[106] C. Antonelli, A. Mecozzi, and M. Shtaif, “Nonlinear propagation in Space-Division Multiplexed fiber-optic transmission,” in *IEEE Photonics Conference IPC*, pp. 256-258, 2015.

[107] K.-Po Ho, and J. M. Kahn, “Mode-dependent loss and gain: statistics and effect on mode-division multiplexing,” *Optics Express*, vol. 19, no. 17, pp. 16612-16635, 2011.

[108] A. Mecozzi,C. Antonelli, and M. Shtaif, “Nonlinear propagation in multi-mode fibers in the strong coupling regime,” *Optics Express*, vol. 20, no. 11, pp. 11673-11678, 2012.

[109] C. Antonelli, M. Shtaif, and A. Mecozzi, “Modeling of Nonlinear Propagation in Space-Division Multiplexed Fiber-Optic Transmission,” *Journal of Lightwave Technology*, vol. 34, no. 1, pp. 36-54, 2016.

[110] S. Mumtaz, R.-J. Essiambreand G. P. Agrawal, “Nonlinear Propagation in Multimode and Multicore Fibers: Generalization of the Manakov Equations,” *Journal of Lightwave Technology*, vol. 31, no. 3, pp. 398-406, 2013.

[111] J. E. Prilepsky, S. A. Derevyanko, K. J. Blow, I. Gabitov, and S. K. Turitsyn,

"Nonlinear inverse synthesis and eigenvalue division multiplexing in optical fiber channels," *Physical Review Letters*, vol. 113, no. 1, pp. 013901(1-5), 2014.

[112] S. Mumtaz, R.-J. Essiambre, and G. P. Agrawal, "Reduction of Nonlinear Penalties Due to Linear Coupling in Multicore Optical Fibers," *IEEE Photonics Technology Letters*, vol. 24, no. 18, pp. 1574-1576, 2012.

[113] D. Askarov, and J. M. Kahn, "Design of Transmission Fibers and Doped Fiber Amplifiers for Mode-Division Multiplexing," *IEEE Photonics Technology Letters*, vol. 24, no. 21, pp. 1945-1948, 2012.

[114] B. Franz, and H. Bulow, "Experimental Evaluation of Principal Mode Groups as High-Speed Transmission Channels in Spatial Multiplex Systems," *IEEE Photonics Technology Letters*, vol. 24, no. 16, pp. 1363-1365, 2012.

[115] R. E. Freund, "High Capacity and Reach in Multimode Fibers," in *23rd Annual Meeting of the IEEE Photonics Society*, Denver, pp. 553-554, 2010.

[116] J. M. Kahn, and K.-Po Ho, "Mode Coupling Effects in Multi-Mode Fibers," *IEEE Photonics Technology Letter*, vol. 14, pp. 187-193, 2010.

[117] D. R. Song, H. S. Park, B. Y. Kim, and K. Y. Song, "Acoustooptic Generation and Characterization of the Higher Order Modes in a Four-Mode Fiber for Mode-Division Multiplexed Transmission," *Journal of Lightwave Technology*, vol. 32, no. 23, pp. 4534-4538, 2014.

[118] S. O. Arik, D. Askarov, and J. M. Kahn, "Adaptive Frequency-Domain Equalization in Mode-Division Multiplexing Systems," *Journal of Lightwave Technology*, vol. 32, no. 10, pp. 1841-1852, 2014.

[119] K.-Po Ho, and J. M. Kahn, " Delay-Spread Distribution for Multimode Fiber with Strong Mode Coupling," *IEEE Photonics Technology Letters*, vol. 24, no. 21, pp. 1906-1909, 2012.

[120] K.-Po Ho,and J. M. Kahn, "Statistics of Group Delays in Multimode Fiber With Strong Mode Coupling," *Journal of Lightwave Technology*, vol. 29, no. 21, pp. 3119-3128, 2011.

[121] M. B. Shemirani, and J. M. Kahn, "Higher-Order Modal Dispersion in Graded Index Multimode Fiber," *Journal of Lightwave Technology*, vol. 27, no. 23, pp. 5461-5468, 2009.

[122] R. A. Panicker, and J. M. Kahn, "Algorithms for Compensation of Multimode Fiber Dispersion Using Adaptive Optics," *Journal of Lightwave Technology*, vol. 27, no. 24, pp. 5790-5799, 2009.

[123] S. O. Arik, and J. M. Kahn, "Coupled-Core Multi-Core Fibers for Spatial Multiplexing," *IEEE Photonics Technology Letters*, vol. 25, no. 21, pp. 2054-2057, 2013.

[124] D. H. Sim, and Y. Takushima, "High-Speed Multimode Fiber Transmission by using Mode-Field Matched Center-Launching Technique," *Journal of Lightwave Technology*, vol. 27, no. 8, pp.1018-1026, 2009.

[125] H. S. Chen, H. P. A. van den Boom and A. M. J. Koonen, "30-Gbit/s 3 x 3 Optical Mode Group-Division-Multiplexing System with Optimized Joint Detection," *IEEE Photonics Technology Letters*, vol. 23, no. 18, 2011.

[126] A. Adrian, S. Warm, C. A. Bunge, and K. Petermann "Number of usable Principal Modes in a Mode Division Multiplexing transmission for different Multi-mode fiber," in*Optical Society of America Optical Fiber Communication Conference/ National Fiber Optic Engineers Conference*, 2011, Paper JThA034.

[127] H. S. Chen, H. P. A. Boom, and A. M. J. Koonen, "30-Gbit/s 3 x 3 Optical Mode Group-Division-Multiplexing System with Mode-Selective Spatial Filtering," OSA *Optical Fiber Communication*, vol. 10, no. 1364, 2011, Paper owb1.

[128] A. Amphawan, S. Chaudhary, and V. W. S. Chan, "2 x 20Gbps - 40GHz OFDM Ro-FSO transmission with mode division multiplexing," *Journal of European Optical Society Rapid Publications,* vol. 9, p. 14041, 2014.

[129] R. Ryf, N. K. Fontaine, H. Chen, B. Guan, B. Huang, M. Esmaeelpour, A. H. Gnauck, S. Randel, S.J.B. Y, A. M. J. Koonen, R. Shubochkin, Y. Sun, and R. Lingle, "Mode-Multiplexed Transmission over Conventional Graded-Index Multimode Fibers," *Optics Express*, vol. 23, no. 1, pp. 235–246, 2015.

[130] D. K. Tripathi, P. Singh, N. K. Shukla, and H. K. Dixit, "Investigations with Mode Division Multiplexed Transmission," *Electrical and Electronics Engineering International Journal*, vol. 3, no. 3, pp. 43-51, 2014.

[131] R. Ryf, S. Randel, N. K. Fontaine, M. Montoliu, E. Burrows, S. Chandrasekhar, A. H. Gnauck, C. Xie, R. Essiambre, P. Winzer, R. Delbue, P. Pupalaikis, A. Sureka, Y. Sun, L. Gruner-Nielsen, R. V. Jensen, and R. Lingle, "32-bit/s/Hz spectral efficiency WDM transmission over 177-km few-mode fiber," in *OSA Optical Fiber Communication Conference/National Fiber Optic Engineers Conference*, 2013, Paper PDP5A.1. R.

[132] D. Inaudi, N. Casanova, B. Glisic, S. Vurpillot, P. Kronenberg, and S. Loret, "Lessons learned in the use of fiber optic sensor for civil structural monitoring,"

International Journal for Restoration of Buildings and Monuments, vol. 7*,* no. 3-4, pp. 301-320, 2001.

[133] L. Zhou, O. Sezerman, and W. Revie, "Pipeline corrosion monitoring by fiber optic distributed strain and temperature sensors," in *Proceedings of the NACE International Corrosion Conference and Expo*, New Orleans, LA, USA, pp. 16-20, 2008.

[134] G. Kister, "Structural health monitoring of a composite bridge using Bragg grating sensors. Part 1: Evaluation of adhesives and protection systems for the optical sensors," *Engineering Structures*, vol. 29, no. 3, pp. 440–448, 2007.

[135] K. Alhandawi, N. Vahdati, O. Shiryayev, and L. Lawand, "Corrosion monitoring along infrastructures using distributed fiber optic sensing," in *Proceedings of Sensors and Smart Structures Technologies for Civil, Mechanical, and Aerospace Systems*, vol. 9803, pp. 980340, 2016.

[136] H. Lee, and H. Sohn, "Damage detection for pipeline structures using optic-based active sensing," *SmartStructures and Systems*, vol. 9, no. 5, pp. 461–472, 2012.

[137] S. K. Sinha, S. R. Lyer, and M. C. Bhardwaj, "Non-Contact ultrasonic sensor and state-of-the-art camera for automated pipe inspection", in *Sensors IEEE*, vol. 1, pp. 493-498, 2003.

[138] L. Rena, T. Jianga, Zi-G. Jiab, Duang-S. Lia, Chao-L. Yuana and Hong-N. Lia, "Pipeline corrosion and leakage monitoring based on the distributed optical fiber sensing technology," *Elsevier Measurement*, vol. 122, pp. 57–65, 2018.

[139] L. Wong, S. Rathnayaka, W.K. Chiu, and J. Kodikara, "Fatigue damage monitoring of a cast iron pipeline using distributed optical fibre sensors," *Procedia Engineering*, vol. 188, pp. 293 – 300, 2017.

[140] J. W. Arkwright, I. D. Underhill, S. A. Maunder, A. Jafari, N. Cartwright, and C. Lemckert, "Fiber Optic Pressure Sensing Arrays for Monitoring Horizontal and Vertical Pressures Generated by Traveling Water Waves," *IEEE Sensors Journal*, vol. 14, no. 8, pp. 2739-2742, 2014.

[141] A. Gautam, A. Kumar, R. R. Singh, and V. Priye, "Optical sensing and monitoring architectures for pipelines using optical heterodyning and FBG filter," *Elsevier Optik*, vol. 127, pp. 9161-9166, 2016.

[142] E. Ip, N. Bai, Y.-K. Huang, E. Mateo, F. Yaman, S. Bickham, H.-Y. Tam, C. Lu, M.-J. Li, S. Ten, A. P. T. Lau, V. Tse, G.-D. Peng, C. Montero, X. Prieto, and G.

Li, “88 × 3 × 112-Gb/s WDM transmission over 50-km of three-mode fiber with inline multimode fiber amplifier”, in *37th European Conference and Exposition on Optical Communications*, OSA Technical Digest, 2011, Paper Th.13.C.2.

[143] N. Hanzawa, K. Saitoh, T. Sakamoto, T. Matsui, S. Tomita, and M. Koshiba, “Demonstration of mode-division multiplexing transmission over 10 km two-mode fiber with mode coupler”, *Optical Fiber Communication Conference,* OSA Technical Digest, 2011, Paper OWA 4.

[144] J. Sakaguchi, Y. Awaji, N. Wada, A. Kanno, T. Kawanishi, and T. Hayashi, “109- Tb/s (7x97x172- Gb/s SDM/ WDM/ PDM) QPSK transmission through 16.8 km homogenous multi-core fiber,” *Optical Fiber Communication Conference/ National Fiber Optic Engineers Conference*, 2011, Paper PDPB6.

[145] B. Zhu, T. Taunay, M. Fishteyn, X. Liu, S. Chandrasekhar, M. Yan, J. Fini, E. Monberg, F. Dimarcello, “Space-Wavelength-Polarization-Division Multiplexed Transmission of 56-Tb/s over a 76.8-km Seven-Core Fiber”, *Optical Fiber Communication Conference/National Fiber Optic Engineers Conference*, OSA, 2011, Paper PDPB7.

[146] B. Zhu, T. Taunay, M. Fishteyn, X. Liu, S. Chandrasekhar, M. Yan, J. Fini, E. Monberg, and F. Dimarcello, “112-Tb/s space-division multiplexed DWDM transmission with 14-b/s/Hz aggregate spectral efficiency over a 76.8-km seven-core fiber,” *Optics Express*, vol. 19, pp. 16665–16671, 2011.

[147] R. Ryf, A. Sierra, R. Essiambre, A. Gnauck, S. Randel, M. Esmaeelpour, S. Mumtaz, P. J. Winzer, R. Delbue, P. Pupalaikis, A. Sureka, T. Hayashi, T. Taru, and T. Sasaki, “Coherent 1200-km 6 × 6 MIMO mode-multiplexed transmission over 3-core microstructured fiber,” in *37th European Conference and Exposition on Optical Communications*, OSA Technical Digest, 2011, Paper Th.13.C.1.

[148] X. Liu, S. Chandrasekhar, X. Chen, P. Winzer, Y. Pan, B. Zhu, T. Taunay, M. Fishteyn, M. Yan, J. M. Fini, E. Monberg, and F. Dimarcello, “1.12- Tb/s 32-QAM-OFDM superchannel with 8.6-b/s/Hz intrachannel spectral efficiency and space-division multiplexing with 60-b/s/Hz aggregate spectral efficiency,” in *37th European Conference and Exposition on Optical Communications*, OSA Technical Digest, 2011, Paper Th.13.B.1.

[149] R. Ryf, N. K. Fontaine, M. A. Mestre, S. Randel, X. Palou, C. Bolle, A. H. Gnauck, S. Chandrasekhar, X. Liu, B. Guan, R. Essiambre, P. J. Winzer, S. Leon-Saval, J. Bland-Hawthorn, R. Delbue, P. Pupalaikis, A. Sureka, Y. Sun, L.

Grüner-Nielsen, R. V. Jensen, and R. Lingle, “12 × 12 MIMO transmission over 130-km few-mode fiber”, in Frontiers *in Optics 2012*, OSA Technical Digest, 2012, Paper FW6C.4.

[150] D. Qian, E. Ip, M.-F. Huang, M.-J. Li, A. Dogariu, S. Zhang, Y. Shao, Y.-K. Huang, Y. Zhang, X. Cheng, Y. Tian, P. Ji, A. Collier, Y. Geng, J. Linares, C. Montero, V. Moreno, X. Prieto, and T. Wang, “1.05 Pb/s transmission with 109 b/s/Hz spectral efficiency using hybrid singleand few-mode cores”, in Frontiers *in Optics 2012*, OSA Technical Digest, 2012, Paper FW6C.3.

[151] J. Sakaguchi, B. J. Puttnam, W. Klaus, Y. Awaji, N. Wada, A. Kanno, T. Kawanishi, K. Imamura, H. Inaba, K. Mukasa, R. Sugizaki, T. Kobayashi, and M. Watanabe, “305 Tb/s space division multiplexed transmission using homogeneous 19-core fiber,” *Journal of Lightwave Technology*, vol. 31, no. 4, pp. 554–562, 2013.

[152] A. H. Gnauck, S. Chandrasekhar, X. Liu, S. Randel, S. Corteselli, T. Taunay, B. Zhu, and M. Fishteyn, “WDM transmission of 603-Gb/s superchannels over 845 km of 7-core fiber with 42.2 b/s/Hz spectral efficiency,” in *European Conference and Exhibition on Optical Communication*, OSA Technical Digest, 2012, Paper Th.2.C.2.

[153] H. Takahashi, T. Tsuritani, E. L. T. de Gabory, T. Ito, W. R. Peng, K. Igarashi, K. Takeshima, Y. Kawaguchi, I. Morita, Y. Tsuchida, Y. Mimura, K. Maeda, T. Saito, K. Watanabe, K. Imamura, R. Sugizaki, and M. Suzuki, “First demonstration of MC-EDFA-repeatered SDM transmission of 40 × 128-Gbit/s PDM-QPSK signals per core over 6,160-km 7-core MCF,” *Optics Express*, vol. 21, no. 1, pp. 789–795, 2013.

[154] E. Ip, M.-J. Li, Y.-K. Huang, A. Tanaka, E. Mateo, W. Wood, J. Hu, Y. Yano, and K. Koreshkov, “146 × 6 × 19-Gbaud wavelength-and mode division multiplexed transmission over 10 × 50-km spans of few-mode fiber with a gain-equalized few-mode EDFA”, in *Optical Fiber Communication Conference/National Fiber Optic Engineers Conference*, OSA Tech. Digest, 2013, Paper PDP5A.2.

[155] H. Takara, A. Sano, T. Kobayashi, H. Kubota, H. Kawakami, A. Matsuura, Y. Miyamoto, Y. Abe, H. Ono, K. Shikama, Y. Goto, K. Tsujikawa, Y. Sasaki, I. Ishida, K. Takenaga, S. Matsuo, K. Saitoh, M. Koshiba, and T. Morioka, “1.01-Pb/s (12 SDM/222 WDM/456 Gb/s) crosstalk-managed transmission with 91.4-

b/s/Hz aggregate spectral efficiency", in *European Conference and Exhibition on Optical Communication*, OSA Technical Digest, 2012, Paper Th.3.C.1.

[156] T. Kobayashi, H. Takara, A. Sano, T. Mizuno, H. Kawakami, Y. Miyamoto, K. Hiraga, Y. Abe, H. Ono, M. Wada, Y. Sasaki, I. Ishida, K. Takenaga, S. Matsuo, K. Saitoh, M. Yamada, H. Masuda, and T. Morioka, "2 × 344 Tb/s propagation-direction interleaved transmission over 1500-km MCF enhanced by multicarrier full electric-field digital back propagation", in *39th European Conference and Exhibition on Optical Communication* ECOC, 2013, pp. 1-3.

[157] R. Ryf, N. K. Fontaine, H. Chen, B. Guan, S. Randel, N. Sauer, S. J. B. Yoo, A. Koonen, R. Delbue, P. Pupalaikis, A. Sureka, R. Shubochkin, Y. Sun, and R. Lingle, "23 Tbit/s transmission over 17-km conventional 50 μm graded-index multimode fiber", in *Optical Fiber Communication Conference*, Postdeadline Papers, 2014, Paper Th5B.1.

[158] T. Mizuno, T. Kobayashi, H. Takara, A. Sano, H. Kawakami, T. Nakagawa, Y. Miyamoto, Y. Abe, T. Goh, M. Oguma, T. Sakamoto, Y. Sasaki, I. Ishida, K. Takenaga, S. Matsuo, K.Saitoh, and T. Morioka, "12-core×3-mode dense space division multiplexed transmission over 40 km employing multi-carrier signals with parallel MIMO equalization," in *Optical Fiber Communication Conference*, Postdeadline Papers, OSA, 2014, Paper Th5B.2.

[159] D. Molia, M. Bigot, F. Achten, A. A Correa and P. Sillard, "850-950 nm Wideband OM4 Multimode Fiber for Next-Generation WDM Systems," in *Optical Fiber Communication Conference,* OSA, 2015,Paper M3B.1.

[160] A. Amphawan, and Y. Fazea, "Laguerre-Gaussian mode division multiplexing in multimode fiber using SLMs in VCSEL arrays," *Journal of the European Optical Society-Rapid Publications*, vol. 12, no.12, pp. 1-11, 2016.

[161] P. Sillard, D. Molin, M. B.-Astruc, K. Jongh, and F. Achten, "Multimode Fibers for Mode Division Multiplexing," *Conference on Laser and Electro-optics*, OSA, 2017, Paper STu4K.7.

[162] B. J. Puttnam, R. S. Luís, G. Rademacher, A. Alfredsson, W. Klaus, J. Sakaguchi, Y. Awaji, E. Agrell, and N. Wada, "Characteristics of homogeneous multi-core fibers for SDM transmission," *APL Photonics*, vol. 4, no. 2, pp. 022804 (1-10), 2019.

[163] Y. Jung, A. Wood, S. Jain, Y. Sasaki, S. Alam, and D. J. Richardson, "Fully integrated optical isolators for space division multiplexed (SDM) transmission,"

APL Photonics, vol. 4, pp. 022801 (1-7), 2019.

[164] P. J. Ryf, "Spatial multiplexing: The next frontier in network capacity scaling," in Proceedings *39th European Conference and Exhibitionn on Optical Communication ECOC*, 2013, pp. 372–374.

[165] R. H. Stolen, J. E. Bjorkholm, and A. Ashkin, "Phase-matched three wave mixing in silica fiber optical waveguides," *Applied Physics Letters*, vol. 24, no. 7, pp. 308–310, 1974.

[166] G. Rademacher, S. Warm, and K. Petermann, "Analytical description of cross-modal nonlinear interaction in mode-multiplexed multi-mode fibers," *IEEE Photonics Technology Letters*, vol. 24, no. 21, pp. 1929–1932, 2012.

[167] S. M. M. Friis, I. Begleris, Y. Jung, K. Rottwitt, P. Petropoulos, D. J. Richardson, P. Horak, and F. Parmigiani, "Inter-modal four-wave mixing study in a two-mode fiber", *Optics Express*, vol. 24, no. 26, pp. 30338-30349, 2016.

[168] R.-J. Essiambre, M. A. Mestre, R. Ryf, A. H. Gnauck, R.W. Tkach, A.R. Chraplyvy, Y. Sun, X. Jiang, and R. Lingle, "Demonstration of broadband inter-modal four wave mixing in graded-index few-mode fibers," in *Proceedings ofOptical Fiber Communication Conference*, OSA, pp. 1–3, 2013, Paper OM3B.2.

[169] M. S. Ismail, "Numerical solution of coupled nonlinear Schrödinger equation by Galerkin method," *Mathematics and Computer in Simulation*, vol. 78, no. 4, pp. 532–547, 2008.

[170] A. Mecozzi, C. Antonelli, and M. Shtaif, "Coupled Manakov equations in multimode fibers with strongly coupled groups of modes," *Optics Express*, vol. 20, no. 21, pp. 23436-23441, 2012.

[171] D. Marcuse, C. R. Menyuk, and P. K. A. Wai, "Application of the Manakov-PMD equation to studies of signal propagation in optical fibers with randomly varying birefringence," *Journal of Lightwave Technology*, vol. 15, no. 9, , pp. 1735-1746, 1997.

[172] R.-J. Essiambre, M. A. Mestre, R. Ryf, A. H. Gnauck, R. W. Tkach, A. R. Chraplyvy, Y. Sun, X. Jiang, and R. Lingle, "Experimental Investigation of Inter-Modal Four-Wave Mixing in Few-Mode Fibers," *IEEE Photonics Technology Letters*, vol. 25, no. 6, pp. 539-542, 2013.

[173] F. Poletti, and P. Horak, "Description of ultrashort pulse propagation in multimode optical fibers," *Journal Optical Society of America B*, vol. 25, no. 10,

pp. 1645-1654, 2008.

[174] R. Olshansky, "Propagation in glass optical waveguides," *Reviews of Modern Physics*, vol. 51, no. 2, pp. 341–367, 1979.

[175] I. Aavatsmark, T. Barkve, O. Boe, and T. Mannseth, "Discretization on unstructured grids for inhomogeneous, anisotropic media. Part I: Derivation of the methods," *SIAM Journal on Scientific Computing*, vol. 19, no. 5, pp. 1700-1716, 1998.

[176] P. Sillard, M. B. Astuc, D. Boivin, H. Maerten and L. Provost, " Few-Mode Fiber for Uncoupled Mode Division Multiplexing Transmissions," in Proceedings of *37th European Conference and Exhibition on Optical CommunicationECOC*, Geneva, Switzerland, 2011,Paper Tu.5.

[177] Sillard, P., Bigot-Astruc, M., Boivin, D., Maerten, H., & Provost, L. (2011, September). Few-mode fiber for uncoupled mode-division multiplexing transmissions. inProceedings of *37th European Conference and Exhibition on Optical CommunicationECOC*, pp. 1-3, 2011.

[178] R. Olshanky, "Mode Coupling Effects in Graded-Index Optical Fibers," *Applied Optics*, vol. 14, no. 4, pp. 935-945, 1975.

[179] P. J. Winzer, A. H. Gnauck, A. Konczykowska, F. Jorge, and J.-Y. Dupuy, "Penalities from in-band crosstalk for advanced optical modulation formats," in Proceedings of *37th European Conference and Exhibition on Optical CommunicationECOC*,Geneva, Switzerland, 2011, Paper Tu-5.

[180] N. Bai, and G. Li, "Adaptive Frequency-Domain Equalization for Mode-Division Multiplexed Transmission," *Photonics Technology Letters*, vol. 24, pp. 1918-1921, 2012.

[181] M. S. Faruk, and K. Kikuchi, "Adaptive frequency-domain equalization in digital coherent optical receivers," *Optics Express*, vol. 19, pp. 12789-12798, 2011.

[182] G. Li, N. Bai, N. Zhao, and C. Xia, "Space-division multiplexing: the next frontier in optical communication," *Advances in Optics and Photonics*, vol. 6, no. 4, pp. 413–487, 2014.

[183] R. Goyal, and R. S. Kaler, "A novel architecture of hybrid (WDM/TDM) passive opti-cal networks with suitable modulation format", *Optical Fiber Technology,* vol. 18, no. 6, pp. 518–522, 2012.

[184] N. Bai, E. Ip, Y. K. Huang, E. Mateo, F. Yaman, M. J. Li, S. Bickham, S. Ten, C. Montero, and V. Moreno, "Mode-division multiplexed transmission with

inline few mode fiber amplifier," *Optics Express*, vol. 20, no. 3, pp. 2668–2680, 2012.

[185] A. Amphawan, B. Nedniyom, and N. M. Al Samman, "Selective excitation of LP0l mode in multimode fiber using solid-core photonic crystal fiber," *Journal of Modern Optics*, vol. 60, pp. 1675-1683, 2013.

[186] H. Kogelnik, and T. Tamir, "Theory of Optical Waveguides," in *Guided-Wave Optoelectronics*. Springer Berlin Heidelberg, vol. 26, pp. 7-88, 1988.

[187] T. Erdogan, "Fiber grating spectra," *Journal of Lightwave Technology,* vol. 15, pp. 1277-1294, 1997.

[188] R. Sing, Sunanda, and E. K. Sharma, "Propagation characteristics of single-mode optical fibers with arbitrary complex index profiles: a direct numerical approach,"*IEEE Journal of Quantum Electronics,* vol. 37, pp. 635-640, 2001.

[189] A. Kersey, M. A. Davis, H. J. Patrick, M. Leblanc, K. P. Koo, C. G. Askins, M. A. Putnam, and E. J. Friebele, "Fiber grating sensors," *Lightwave Technology Journal* , vol. 15, pp. 1442-1463, 1997.

[190] M. Ramakrishnan, "Hybrid fiber optic sensor system for measuring the strain, temperature, and thermal strain of composite materials," *IEEE Sensors Journal*, vol. 14, no. 8, pp. 2571–2578, 2014.

[191] Y.-G. Liu, F.-L. Che, Z.-A. Jia, H.-W. Fu, H.-L. Wang, and M. Shao, "Investigation on the characteristics of micro/nanofiber Bragg grating for refractive index sensing," *Acta Physica Sinica,* vol. 62, no. 10, pp. 1128–1133, 2013.

[192] R. Hou, Z. Ghassemlooy, A. Hassan, C. Lu, & K. P. Dowker, "Modelling of long-period fibre grating response to refractive index higher than that of cladding," *Measurement Science and Technology*, vol. 12, no.10, pp. 1709, 2001.